

5 Cooling and Trimming the Part

- 5.1 Introduction
- 5.2 Overall Cooling Heat Balance
- 5.3 Cooling the Formed Shape
- 5.4 Steady State Heat Balance
 - Interfacial Resistance
 - Shape Factor
 - Convection Heat Transfer Coefficient
- 5.5 Cyclic Heat Balance
 - Cooling the Free Surface of the Sheet
 - Cooling Thin Sheet in Ambient Air
 - Transient Heat Removal From the Sheet
 - Quiescent Ambient Air
 - Moving Ambient Air
 - Cooling on Nonmetallic Molds
- 5.6 Transient Heat Transfer During Sheet Cooling on the Mold Surface—Computer Models
 - Interfacial Air
- 5.7 Shrinkage
 - Unconstrained Shrinkage
 - Constrained Shrinkage
- 5.8 Trimming
 - Trimming Heavy-Gage Parts
 - Trimming Thin-Gage Parts
- 5.9 Mechanics of Cutting
 - The Trim Region
 - Registering the Trim Site
 - The Nature of the Cut
 - Fracture Mechanics
 - Mechanical Chipping
 - Multiple-Edged Tool or Toothed Saw Performance
 - Abrasive Cut-Off Wheel
 - Toothless or Shear and Compression Cutting
 - Fracture Mechanics in Trimming
 - Nibbling
 - Brittleness, Orientation and Trim Temperature
- 5.10 Steel Rule Die
 - Resharpener
 - Tabbing and Notching
- 5.11 Punch and Die Trimming
 - Forged and Machined Dies
- 5.12 Drilling
- 5.13 Other Cutting Techniques
 - Thermal Cutting
 - Water Jet Cutting
- 5.14 Trimming—A Summary
- 5.15 References

5.1 Introduction

Once the part has been heated and formed to shape by contact with the cool mold surface, it must be cooled and rigidified. Then the part and its web must be separated by trimming. When thermoforming a reactive polymer such as thermosetting polyurethane or a crystallizing one such as nucleated CPET¹, the formed shape is rigidified by holding it against a heated mold to continue the crosslinking reaction or crystallization. In most cases, rigidifying implies cooling while in contact with a colder mold. For automatic thin-gage formers, the molds are usually actively cooled with water flowing through channels. Free surfaces of medium- and heavy-gage sheet are frequently cooled with forced air, water mist or water spray. For amorphous polymers, cooling of the formed part against a near-isothermal mold rarely controls the overall thermoforming cycle. For crystalline and crystallizing polymers such as PET, PP and HDPE, the cooling cycle can be long and can govern overall cycle time.

When the sheet has cooled sufficiently to retain its shape and, to a large extent, its dimension, it is stripped from the mold and transferred to a trimming station, where the web is separated from the product. Requisite holes, slots and cut-outs are drilled, milled or burned into the part at this time. Thin-gage roll-fed sheet can be either trimmed on the mold surface immediately after forming or on an in-line mechanical trimming press. Heavier-gage formed sheet is usually removed from the mold and manually or mechanically trimmed on a remote station. Trimming is really a solid phase mechanical process of crack propagation by brittle or ductile fracture. Care is taken when trimming brittle polymers such as PS or PMMA to minimize microcracks. With brittle polymers, the very fine sander, saw or microcrack dust generated by mechanical fracture can be a serious problem. Other polymers such as PP and PET are quite tough and require special cutting dies. Dull steel-rule dies cause fibers or hairs at the cutting edge of thin-gage fiber-forming polymers such as PET and PP. Slowly crystallizing polymers pose registry problems when in-line trimming presses are used. The speed of trim cutting and the nature of the cutting surface control the rate of crack propagation through the plastic. There are no exhaustive studies of the unique trimming and cutting characteristics of thermoformed polymers and so much information must be inferred from other sources including extensive studies on the machining of plastics.

5.2 Overall Cooling Heat Balance

As a first approximation, as the sheet touches the mold, it is assumed to be at an average, equilibrated temperature, T_{equil} , as described in Section 3.13. When the

¹ The unique processing conditions for crystallizing polyethylene terephthalate (CPET) are described in detail in Chapter 9, Advanced Thermoforming Processes.

average sheet temperature reaches the set temperature, T_{set} , as given in Table 2.5, the sheet is assumed to be sufficiently rigid to be removed from the mold surface. Typically, the amorphous polymer set temperature is about 20°C or 40°F below its glass transition temperature, T_g . The crystalline polymer set temperature is about 20°C or 40°F below its melting temperature, T_{melt} . During the cooling time, the mold temperature is assumed to be essentially constant at T_{mold} . The amount of heat to be removed by the coolant flowing through the mold is given as:

$$\begin{aligned} Q_{\text{polymer}} &= V^* \cdot \rho c_p (T_{\text{equil}} - T_{\text{set}}) \\ &= V^* \cdot \rho c_p \cdot \Delta T = V^* \cdot \rho \Delta H \end{aligned} \quad (5.1)$$

where V^* is the volume of plastic, ρ is its density and c_p is its heat capacity¹. Heat is removed from the free sheet surface by convection to the environmental air. Heat is removed from the sheet surface against the mold surface by conduction through the mold to the coolant. The coolant fluid removes the heat by convection. The heat load at any point on the mold surface depends on the sheet thickness, t_{local} , at that point. Sheet thickness, as noted in Chapter 4, is not uniform across the mold surface. The heat load at any point is given as:

$$q'_{\text{local}} = \rho \cdot c_p \cdot t_{\text{local}} \cdot \Delta T \quad (5.2)$$

This is the heat to be removed from a given region during the cooling portion of the total cycle, θ_{cool} . The local heat flux then is:

$$q''_{\text{local}} = \frac{q'_{\text{local}}}{\theta_{\text{local}}} = \rho \cdot c_p \cdot t_{\text{local}} \cdot \frac{\Delta T}{\theta_{\text{local}}} \quad (5.3)$$

The units on q''_{local} are kW/m² or Btu/ft² · h · °F. The total heat load during this time is given as:

$$Q_{\text{total}} = \int q''_{\text{local}} dA \quad (5.4)$$

The total heat load per unit time on a steady-state process is given as:

$$Q_{\text{steady state}} = Q_{\text{total}} \cdot N \quad (5.5)$$

where N is the number of parts produced per unit time. The units on $Q_{\text{steady state}}$ are kW or Btu/h.

At steady-state conditions, this energy is removed by the coolant system and by convection to the environmental air. Mold, coolant and air temperatures increase until the steady state is reached.

¹ The last equality relates the amount of heat removed to the differential enthalpy, ΔH , of the polymer. This expression should be used if the polymer is crystalline and molten during the forming step and is solidifying during the cooling step.

5.3 Cooling the Formed Shape

Consider a typical cooling step. The sheet of variable thickness but known temperature is pressed against a slightly irregular surface of a mold. The properties of the mold material are known and uniform throughout its volume, Chapter 6. Coolant of known properties flows through uniformly spaced channels in the mold. The free surface of the part is also cooled. At any instant, the temperature profile through the various layers of material is as shown in schematic in Fig. 5.1. The rate at which the energy is removed from the plastic to ambient air and coolant depends on the sum of resistances to heat transfer through each of these layers. Heat removal by the coolant is the primary way of cooling the formed part. Transfer to the environmental air is a secondary method but it can be quite important when trying to optimize cycle time. There are two aspects to heat removal from the formed polymer sheet to the coolant. The first deals with the overall heat transfer at steady state conditions. The second focuses on certain aspects of cyclical transient heat transfer.

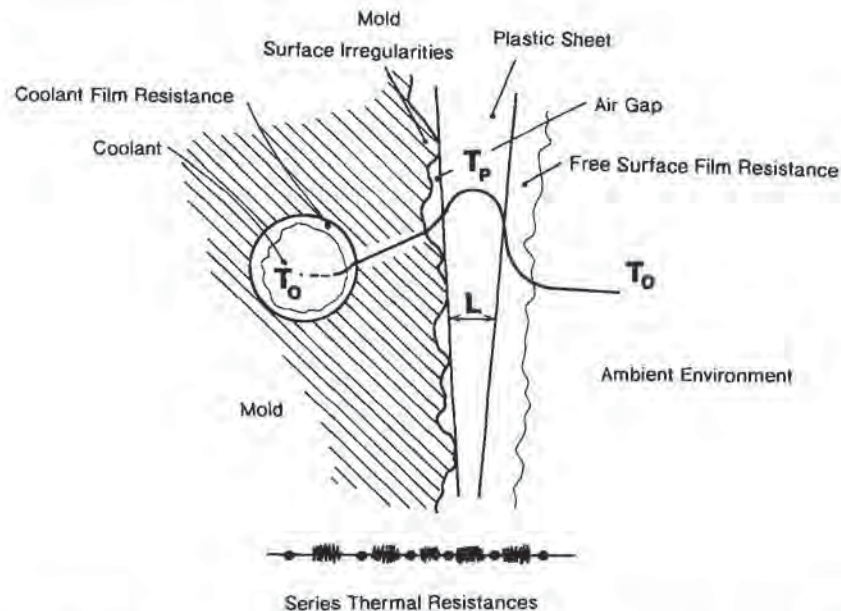


Figure 5.1 Schematic of various thermal resistances for sheet cooling against thermoforming mold

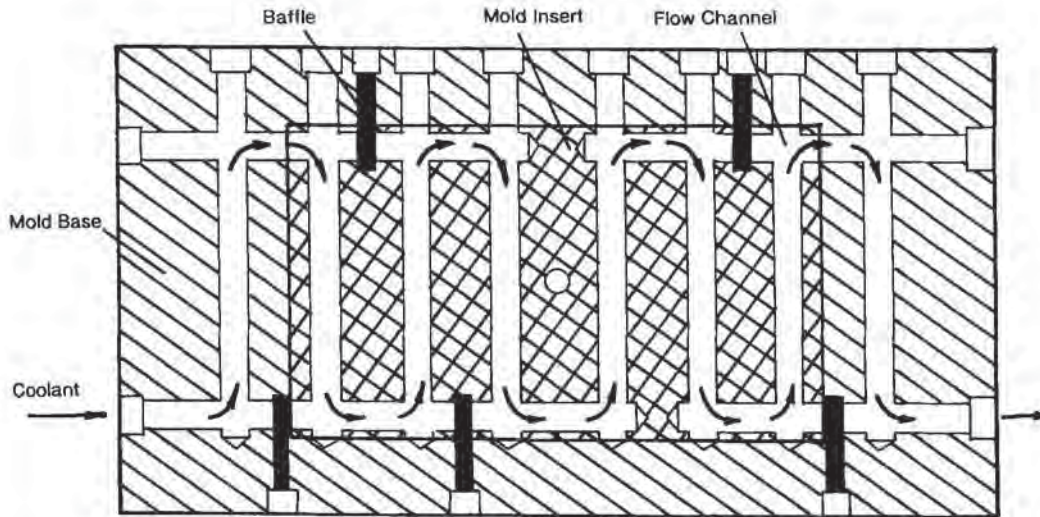


Figure 5.2 Typical serpentine coolant flow channel through thermoforming mold

5.4 Steady State Heat Balance

Consider the limiting case where all the energy is transferred directly to the mold and thence to the coolant. Typically, coolant lines are drilled or cast on a discrete, regular basis parallel to the mold surface (Fig. 5.2). Heat removal by coolant depends on convection heat transfer, or fluid motion¹. The total amount of energy removed by the coolant embedded in the mold is given as:

$$Q = UA \Delta T \quad (5.6)$$

where U is the overall heat transfer coefficient, A is the coolant surface area and ΔT is the increase in coolant temperature between inlet and outlet portions of the flow channel. The overall heat transfer coefficient includes all flow resistances between the sheet and the coolant. It is usually written as:

$$\frac{1}{U} = \sum R_i \quad (5.7)$$

where R_i represents the i th resistance to heat transfer. As seen in Fig. 5.1, for flowing fluids, there is a convective film resistance at the conduit surface, $1/\pi Dh_c$, where πD is the circumference of the conduit. If the coolant fluid is not kept clean, the coolant channel can become coated with residue, thus increasing thermal resistance. This

¹ This section deals only with the convection heat transfer coefficient of coolant flowing through lines in the mold. Section 6.4 considers coolant pressure drop-flow rate relationships for the specification of coolant line size.

Table 5.1 Fouling Factors for Coolant Lines¹

| Coolant | Condition | Fouling factor (Btu/ft · h · °F) ⁻¹ | Velocity > 3 ft/s |
|--|---------------------|---|-------------------|
| | | Velocity < 3 ft/s | |
| Treated make-up cooling tower water | Water < 125°F | 0.001 | 0.001 |
| Treated make-up cooling tower water | Water > 125°F | 0.002 | 0.002 |
| City water | Water < 125°F | 0.001 | 0.001 |
| City water | Water > 125°F | 0.002 | 0.002 |
| River water | Water < 125°F | 0.002 | 0.001 |
| River water | Water > 125°F | 0.003 | 0.002 |
| Treated boiler feedwater | Water < 125°F | 0.001 | 0.0005 |
| Treated boiler feedwater | Water > 125°F | 0.001 | 0.001 |
| Industrial heat transfer oil | | 0.001 | 0.001 |
| Ethylene glycol | | 0.001 | 0.001 |
| Glycerine-water | | 0.002 | 0.001 |
| Brine | Temperature < 125°F | 0.002 | 0.001 |
| Brine | Temperature > 125°F | 0.003 | 0.002 |
| Steam | | 0.001 | 0 |

¹ Information extracted from [1] by permission of copyright holder

resistance is called a fouling factor, ff . Fouling factors are given in Table 5.1 [1]. The resistance through the mold depends on the relative shapes of the mold surface and the coolant channels, and is usually described as $1/Sk_m$, where S is a shape factor and k_m is the thermal conductivity of the mold material. Since polymer sheet does not press tightly against the mold surface, there is a conductive resistance owing to trapped air, $1/h_a$. Although there may be other thermal resistances, these are the primary ones. So the overall heat transfer coefficient, U , is written as:

$$\frac{1}{U} = \frac{1}{\pi Dh_c} + \frac{1}{Sk_m} + \frac{1}{h_a} + ff \quad (5.8)$$

Interfacial Resistance

In most heat transfer processes, intimate or perfect contact between the hot and cold solids is assumed. Imperfect contact causes resistance to heat flow. Mold surface waviness and microscopic roughness or asperities reduce physical contact (Fig. 5.3). Increasing pressure against the sheet increases physical contact and reduces the resistance to heat transfer. In general, energy is transmitted across the interstices by a combination of:

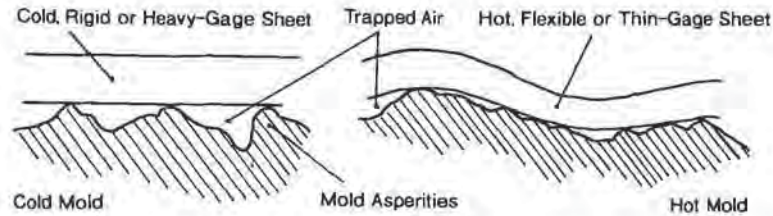


Figure 5.3 Interfacial resistance between sheet and thermoforming mold surface. Left shows substantial thermal resistance owing to large air gap. Right shows reduced thermal resistance

- Conduction at the asperities,
- Conduction through the interstitial fluid, and
- Radiation.

The resistance is thus a function of:

- The contacting material properties such as
 - Relative hardness,
 - Thermal conductivity,
 - Surface roughness and
 - Flatness,
- The conductivity and pressure of the interstitial fluid, and
- The pressure applied against the free surface of the sheet.

The interface coefficient, h_a , is a measure of thermal resistance across the gap. It is similar in concept to the convection heat transfer in that resistance to heat flow decreases with increasing value of h_a . For perfect contact, $h_a \rightarrow \infty$.

In thermoforming, the interstitial fluid is air, perhaps at a substantially reduced pressure. If the interface is a uniform air gap of $\delta = 0.025$ cm or 0.010 in and air thermal conductivity is $k_{\text{air}} = 0.029$ W/m \cdot °C or 0.0167 Btu/ft \cdot h \cdot °F, the value for h_a is about 114 W/m 2 \cdot °C or 20 Btu/ft 2 \cdot h \cdot °F. Contact heat transfer coefficient values between flowing polymer melts and mold surfaces of about $h_a = 568$ W/m 2 \cdot °C or 100 Btu/ft 2 \cdot h \cdot °F have been reported in injection molding [2-4]. Similar values are expected here. For two surfaces in contact, $h_a = h_{a0}P^n$, where P is the applied pressure and h_{a0} depends on the relative waviness and roughness of the two surfaces, Table 5.2 [5]. As seen, n has a value of about 2/3 for both rigid-rigid and rigid-flexible material contact in vacuum. Values for h_{a0} are typically 50 times greater in air than in hard vacuum.

There are no available data for interfacial resistance during thermoforming of softened plastic sheet against various types of mold surfaces. For hot sheet pressed against a relatively smooth, heated mold surface at a relatively high differential pressure, it is expected that an appropriate value for h_a would be about 568 W/m 2 \cdot °C or 100 Btu/ft 2 \cdot h \cdot °F. For rapidly cooling and rigidizing plastic sheet pressing against a highly textured, cold mold surface with a modest differential pressure, an appropriate value range for h_a of 114 to 284 W/m 2 \cdot °C or 20 to

Table 5.2 Contact Resistance and Conductance [5] $h_c = h_{c0} p^n$
 (Units on $h_c = \text{W/m}^2 \cdot ^\circ\text{C}$ or $\text{Btu/ft}^2 \cdot \text{h} \cdot ^\circ\text{F}$)
 (Units on p are MPa or lb_f/in^2)

| Material contact | Inner layer | Contact coefficient, h_c | | n |
|----------------------------|-------------|-----------------------------------|---|-----|
| | | ($\text{W/m}^2 \cdot \text{C}$) | ($\text{Btu/ft}^2 \cdot \text{h} \cdot ^\circ\text{F}$) | |
| Elastic deformation theory | None | 35.8 | 6.3 | 2/3 |
| Hard-to-hard | Vacuum | 113.6 | 20 | 2/3 |
| Hard-to-hard | Air | 5680 | 1000 | 1/6 |
| Hard-to-soft | Vacuum | 170 | 30 | 2/3 |

50 $\text{Btu/ft}^2 \cdot \text{h} \cdot ^\circ\text{F}$ should be considered for first cooling time estimates. Section 5.6 on computer simulation of the cooling process explores the relative effect of interfacial resistance on time-dependent sheet cooling.

Shape Factor

For thin metal molds, heat is conducted very rapidly from the plastic to the coolant. For relatively thick molds of:

- Plaster,
- Wood,
- Epoxy,
- Glass fiber-reinforced unsaturated polyester resin (FRP),
- Pressed fiberboard, or
- Any other nonmetallic material,

heat transfer is slowed by low mold material thermal conductivity. If the coolant system is considered to be coplanar with the mold surface (Fig. 5.4), the resistance to heat transfer per unit length ($L = 1$), across a mold D units thick is given as:

$$R_m = \frac{D}{k_m} \quad (5.9)$$

where k_m is the mold material thermal conductivity. Thermal conductivity values for many mold materials are given in Table 2.7. For round discrete conduits (Fig. 5.5) [6], a shape factor, S , is used:

$$R_m = \frac{1}{S k_m} \quad (5.10)$$

where S is given by:

$$S = \frac{2\pi}{\ln \left[\frac{2P}{D} \sinh \left(\frac{2\pi D}{P} \right) \right]} \quad (5.11)$$

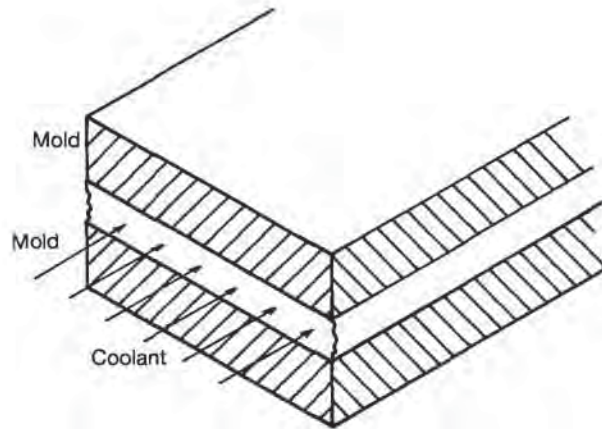


Figure 5.4 Schematic of coplanar coolant flow channel and mold surface, concept frequently called flooded cooling

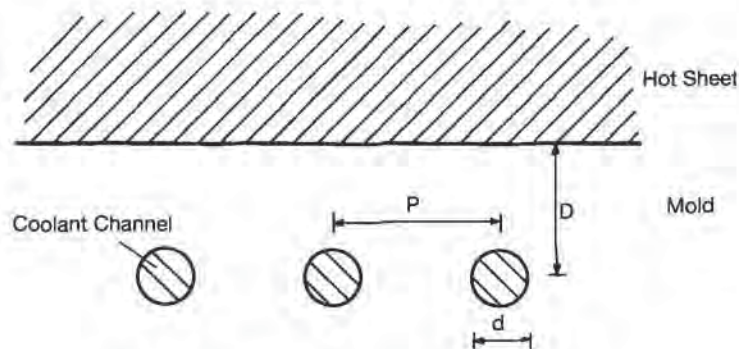


Figure 5.5 Geometric factors for mold shape factor analysis

Figure 5.6 gives this equation in graphic form. It is apparent that the thermal resistance of the mold decreases with increasing value of S , which is achieved with many large-diameter coolant lines placed relatively close to the mold surface. The typical value range for S is $2 \leq S \leq 3$. Example 5.1 illustrates the relative effects of these parameters on mold thermal resistance.

Example 5.1 Shape Factors and Mold Thermal Resistance

Determine the relative thermal resistances for the following two molds:

Mold 1: Thin-walled aluminum mold with $k_m = 131 \text{ Btu/ft h } ^\circ\text{F}$, having $d = 1/2\text{-in}$ water lines on $P = 2 \text{ in}$ centers, with the centerline being $D = 1 \text{ in}$ from the mold surface.

Mold 2: Thick-walled plaster mold with $k_m = 1.0 \text{ Btu/ft h } ^\circ\text{F}$, having $d = 1/2$ -in water lines on $P = 4$ in centers, with the centerline being $D = 2$ in from the mold surface.

Mold 1

$P/d = 4$, $D/d = 2$. From Fig. 5.6, $S = 2$.

$$R_m = \frac{1}{Sk_m} = \frac{1}{2 \cdot 1.0} = 0.0038$$

Mold 2

$P/d = 8$, $D/d = 4$. From Fig. 5.6, $S = 1.6$.

$$R_m = \frac{1}{Sk_m} = \frac{1}{1.6 \cdot 1.0} = 0.625$$

The plaster mold has more than 160 times the thermal resistance to heat transfer than the aluminum mold.

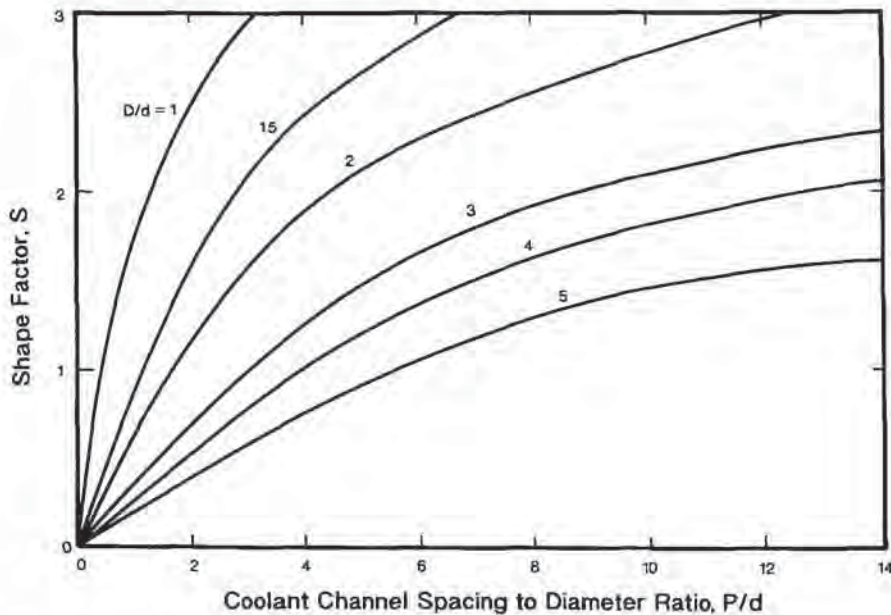


Figure 5.6 Effect of coolant line location on mold shape factor

Convection Heat Transfer Coefficient

The metal molds on automatic, roll-fed thin-gage thermoformers and on many heavy-gage forming operations are actively cooled, with water being the primary

coolant. There is a thermal resistance between the cool bulk flowing fluid and the warmer tube wall (Fig. 5.1). The primary dimensionless group used in fluid mechanics is the Reynolds number, Re :

$$Re = \frac{Dv\rho}{\mu} \quad (5.12)$$

where D is the tube diameter, v is the fluid velocity, ρ is the density of the fluid and μ is its Newtonian viscosity [7]. The Reynolds number is the ratio of inertial to viscous forces for the fluid. Slowly moving fluids are laminar when $Re < 2000$. Convection heat transfer to slowly moving fluids is poor. Rapidly flowing fluids are fully turbulent when $Re > 10,000$ and heat transfer is very rapid. Example 5.2 illustrates the interaction between flow rate and Reynolds number.

Example 5.2 Water as Coolant—Flow Rates

Consider 21°C or 70°F water flowing through 0.5-in or 1.27-cm diameter coolant channels. Determine the Reynolds number and the flow characteristic if the velocity is a) 0.52 ft/s or 0.16 m/s and b) 2.6 ft/s or 0.79 m/s. What are the volumetric flow rates at these velocities?

The water density is 62.4 lb/ft³. The viscosity is 0.658×10^{-3} lb_m/ft · s. The Reynolds number is:

$$Re = \frac{Dv\rho}{\mu} = \frac{0.5}{12} \text{ ft} \cdot v \cdot \frac{\text{ft}}{\text{s}} \cdot 62.4 \frac{\text{lb}_m}{\text{ft}^3} \cdot \frac{1}{0.658 \times 10^{-3} \text{ lb}_m/\text{ft} \cdot \text{s}} = 3951 \cdot v$$

For $v = 0.52$ ft/s: $Re = 2050$ and the water is laminar.

For $v = 2.6$ ft/s: $Re = 10,300$ and the water is turbulent.

The volumetric flow rate is given as:

$$V = \frac{\pi D^2}{4} \cdot v = 0.00136 \cdot v \frac{\text{ft}^3}{\text{s}} = 0.612 \cdot v \frac{\text{gal}}{\text{min}}$$

For $v = 0.52$ ft/s, the flow rate is 0.32 GPM.

For $v = 2.6$ ft/s, the flow rate is 1.6 GPM.

As discussed in Section 3.6, energy interchange between solid surfaces and flowing fluids is by convection. The proportionality between heat flux and thermal driving force is the convection heat transfer coefficient. The convection heat transfer coefficient is obtained from standard heat transfer theory and experiments. There are many methods for calculating values of h_c . In general, however, the Chilton-Colburn analogy between resistance to fluid flow and resistance to thermal energy flow yields adequate results [8]. The analogy states:

$$St \cdot Pr^{2/3} = f/8 \quad (5.13)$$

where St is the Stanton number, Pr is the Prandtl number and f is the coefficient of friction or friction factor. The Stanton and Prandtl numbers are:

Table 5.3 Prandtl Number Values For Several Coolants [9,10]

| Coolant | Temperature | | Prandtl no. |
|------------|-------------|------|-------------|
| | (°F) | (°C) | |
| Air | 32 | 0 | 0.72 |
| Air | 100 | 38 | 0.72 |
| Steam | 212 | 100 | 0.96 |
| Steam | 400 | 204 | 0.94 |
| Water | 32 | 0 | 13.7 |
| Water | 70 | 21 | 6.82 |
| Water | 100 | 38 | 4.52 |
| Water | 150 | 66 | 2.74 |
| Water | 200 | 93 | 1.88 |
| SAE 30 Oil | 60 | 16 | 1170 |
| SAE 30 Oil | 100 | 38 | 340 |
| SAE 30 Oil | 150 | 66 | 122 |
| SAE 30 Oil | 200 | 93 | 62 |
| SAE 30 Oil | 250 | 121 | 35 |
| SAE 30 Oil | 300 | 149 | 22 |
| Glycerine | 50 | 10 | 31,000 |
| Glycerine | 70 | 21 | 12,500 |
| Glycerine | 85 | 29 | 5,400 |
| Glycerine | 100 | 38 | 2,500 |
| Glycerine | 120 | 49 | 1,600 |
| Air | 32 | 0 | 0.72 |
| Air | 300 | 150 | 0.71 |
| Air | 600 | 315 | 0.685 |
| Light Oil | 105 | 40 | 340 |
| Light Oil | 150 | 65 | 62 |
| Light Oil | 250 | 120 | 35 |
| Light Oil | 300 | 150 | 22 |

$$St = \frac{h}{\rho c_p v} \quad (5.14)$$

$$Pr = \frac{v}{\alpha} \quad (5.15)$$

where h is the convective heat transfer coefficient, ρ is the fluid density at the appropriate temperature, c_p is the fluid heat capacity, v is the average fluid velocity, $\nu = \mu/\rho$, is the kinematic viscosity, and $\alpha = k/\rho c_p$, is the fluid thermal diffusivity. In essence, Pr is the ratio of inertial to thermal properties and St is the ratio of fluid to thermal resistances. Table 5.3 gives appropriate Prandtl number values for several coolants [9,10]. As examples, $Pr \approx 7$ for room temperature water and $Pr \approx 300$ for

100°C oil coolant. Examples 5.3 and 5.4 show the relative effectiveness of convection heat transfer to water and oil, respectively, as coolants¹.

Example 5.3 Water as Coolant—Temperature Increase

A 3 ft × 3 ft × 0.125-in thick plastic sheet is initially at 375°F and is to be cooled to 200°F. The sheet specific heat is 0.5 Btu/lb · °F and the density is 70 lb/ft³. Twelve sheets are thermoformed per hour. Determine the increase in coolant temperature.

Heat load from sheet:

$$Q \text{ (per cycle)} = \rho c_p V \Delta T = 574 \text{ Btu/cycle}$$

$$Q = 574 \cdot 12 = 6888 \text{ Btu/h to be removed by coolant.}$$

Consider 70°F water flowing through a 3/4-in diameter coolant channel at $v = 4$ ft/s. From Example 6.1, the $Re = 50,000$. The flow is turbulent and $f = 0.0248$. $Pr = 7.02$.

$$St \cdot Pr^{2/3} = f/8$$

$$h_c = \frac{(\rho c_p v) f}{8 \cdot (7.02)^{2/3}} = 770 \text{ Btu/ft}^2 \cdot \text{h} \cdot \text{°F}$$

Consider a 3 ft × 3 ft aluminum mold containing four waterlines spaced evenly. Consider the water lines to be 1½ in from the mold surface. Thus $P/d = 12$ and $D/d = 2$. From Fig. 5.6, the shape factor, $S \approx 3$. The thermal conductivity of aluminum, from Table 2.12, $k_m = 72.5$ Btu/ft · h · °F. Consider $h_a = \infty$. As a result, the total thermal resistance, U is given as:

$$\frac{1}{U} = \frac{12}{0.75\pi \cdot 770} + \frac{1}{3 \cdot 72.5} = 0.0112$$

or: $U = 89.3$ Btu/ft² · h · °F.

Surface area of coolant channels, $A = \pi DLN$, where D is the coolant diameter ($= 3/4$ -in), L is the channel length ($= 10$ ft), and N is the number of channels ($= 4$). $A = 7.85$ ft².

The increase in coolant temperature is given as:

$$\Delta T = \frac{Q}{UA} = \frac{6888}{89.3 \cdot 7.85} \approx 10^\circ\text{F}$$

This is considered to be a typical temperature increase for turbulent coolant flow.

¹ These examples use fluid flow data of Examples 6.1 and 6.2 discussed in detail in Chapter 6 on mold design.

Example 5.4 Oil as Coolant—Temperature Increase

A 3 ft × 3 ft × 0.125-in thick plastic sheet is initially at 375°F and is to be cooled to 200°F. The sheet specific heat is 0.5 Btu/lb · °F and the density is 70 lb/ft³. Twelve sheets are thermoformed per hour. Determine the increase in coolant temperature. Comment on the results.

Heat load from sheet:

$$Q \text{ (per cycle)} = \rho c_p V \Delta T = 574 \text{ Btu/cycle}$$

$$Q = 574 \cdot 12 = 6888 \text{ Btu/h to be removed by coolant.}$$

Consider 150°F SAE 10-like oil flowing through a 3/4-in diameter coolant channel at $v = 4$ ft/s. From Example 5.2, the Reynolds number, $Re = Dv\rho = 1925$. The flow is laminar and $f = 0.0333$. From Table 5.3, the Prandtl number, $Pr = 290$ and $Pr^{2/3} = 44$.

$$St \cdot Pr^{2/3} = f/8$$

$$h_c = \frac{(\rho c_p v) f}{8 \cdot (290)^{2/3}} = 38 \text{ Btu/ft}^2 \cdot \text{h} \cdot \text{°F}$$

Consider a 3 ft × 3 ft aluminum mold containing four waterlines spaced evenly. Consider the water lines to be 1½ in from the mold surface. Thus $P/d = 12$ and $D/d = 2$. From Fig. 5.6, the shape factor, $S \approx 3$. The thermal conductivity of aluminum, from Table 2.12, $k_m = 72.5$ Btu/ft · h · °F. Consider $h_a = \infty$. As a result, the total thermal resistance, U is given as:

$$\frac{1}{U} = \frac{12}{0.75\pi \cdot 38} + \frac{1}{3 \cdot 72.5} = 0.139$$

or: $U = 7.22$ Btu/ft² · h · °F.

Note that this value is less than one tenth that of water flowing at the same velocity. Surface area of coolant channels, $A = \pi DLN$, where D is the coolant diameter (=3/4-in), L is the channel length (=10 ft), and N is the number of channels (=4). $A = 7.85$ ft².

The increase in coolant temperature is given as:

$$\Delta T = \frac{Q}{UA} = \frac{6888}{7.22 \cdot 7.85} \approx 122^\circ\text{F}$$

Since the sheet must be cooled to 200°F, this is an unacceptable increase in oil temperature. One solution is to increase the oil flow rate. Doubling the flow rate will increase the pressure drop by a factor of just less than four. A second alternative is to increase the number of coolant lines. Doubling the number of coolant lines will increase the coolant surface area but the oil velocity will drop to half its current value, thus driving the flow even deeper into the laminar region. Since the friction factor is inversely proportional to the fluid velocity, the friction factor will double. However, since the heat transfer coefficient is essentially independent of velocity, the heat transfer coefficient will not be affected. In addition, the decreased spacing will

increase the shape factor value, S . As a result, doubling the number of coolant lines results in a more than double increase in the overall heat transfer coefficient and a resulting more than halving of the increase in oil temperature.

More exact calculations require knowledge of the roughness and geometric characteristics of the flow channel. In general, the Nusselt number, Nu , a dimensionless convective heat transfer coefficient is a product of the Reynolds number and the Prandtl number, as:

$$Nu = \frac{hD}{k} = C Re^m Pr^n \quad (5.16)$$

For fully developed turbulent flow in very smooth tubes, $C = 0.023$, $m = 0.8$ and $n = 0.4$, and the equation is called the Dittus-Boelter equation. For developing turbulent flow in smooth tubes, $m = 0.8$, $n = 0.33$ and C is given as:

$$C = 0.036 \left(\frac{D}{L} \right)^{0.055} \quad (5.17)$$

where D is the channel diameter, L is the channel length and $10 < L/D < 400$. This equation is usually called the Nusselt equation.

For laminar flow in smooth tubes, the Sieder-Tate version is frequently used. It is much more dependent on entrance length effects and so has $m = 1/3$, $n = 1/3$ and C as:

$$C = 1.86 \left(\frac{D}{L} \right)^{1/3} \quad (5.18)$$

where $Re \cdot Pr \cdot (d/L) > 10$. Example 5.5 illustrates heat transfer coefficient values obtained from these equations for a relatively simple flow channel design. For noncircular channels, the diameter is replaced with the hydraulic diameter, D_h , given as:

$$D_h = \frac{4A}{P} \quad (5.19)$$

where A is the cross-sectional area of the flow channel and P is the wetted perimeter.

Example 5.5 Convective Heat Transfer Coefficients for Serpentine Mold Channel

Figure 5.7 shows an example of a serpentine mold channel that has a roughness value, $\epsilon = 0.001 D$. Two coolants are to be evaluated—water at $70^\circ F$ and oil at $150^\circ F$. Determine the relative heat transfer effectiveness of these coolants in this flow channel.

Water as a coolant

$$\begin{aligned} \nu, \text{ kinematic viscosity} &= 1.06 \times 10^{-5} \text{ ft}^2/\text{s} \\ \rho, \text{ density} &= 62.4 \text{ lb}/\text{ft}^3 \end{aligned}$$

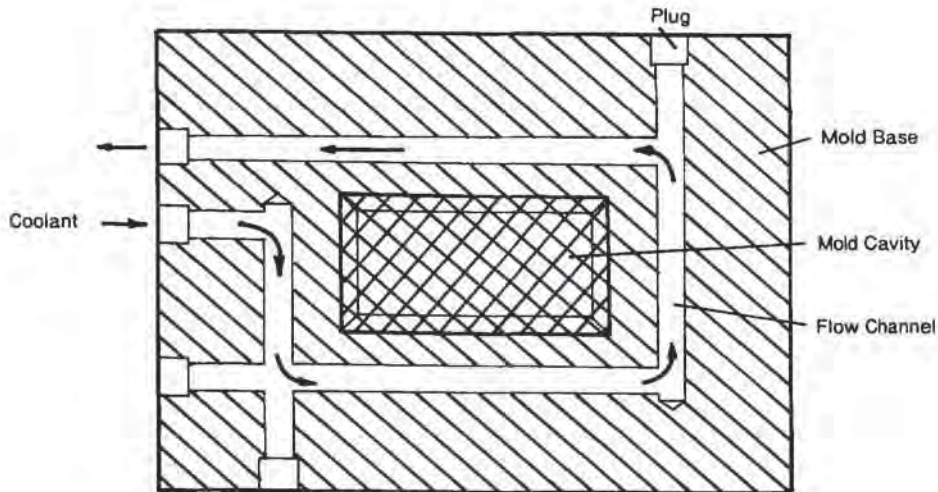


Figure 5.7 Coolant flow channel around mold insert

k , thermal conductivity = 0.35 Btu/ft · h · °F

v , average velocity = 4 ft/s

Prandtl number = 7

Reynolds number, $Re = 15,700$

Flow is turbulent

The friction factor-Reynolds number equation is:

$$f = 0.0204 + 4.212 \cdot Re^{-0.642} = 0.0289$$

- Stanton/Colburn analogy:

$$h = \frac{(\rho c_p v) f}{8} Pr^{2/3}$$

h , convective heat transfer coefficient = 886 Btu/ft² · h · °F

Nu , Nusselt number = $hD/k = 106$

- Dittus-Boelter fully developed flow:

$$Nu = 0.023 \cdot Re^{0.8} \cdot Pr^{0.4} = 114.$$

$h = 958$ Btu/ft² · h · °F

- Nusselt developing flow ($L = 20$):

$$Nu = 0.036 \cdot Re^{0.8} \cdot Pr^{0.33} \cdot \left(\frac{L}{40}\right)^{0.055} = 127.$$

$h = 1061$ Btu/ft² · h · °F

- Nusselt developing flow ($L = 6$):

$$Nu = 136, h = 1137 \text{ Btu/ft}^2 \cdot \text{h} \cdot \text{°F}$$

- Weighted average:

$$Nu = 131, h = 1095 \text{ Btu/ft}^2 \cdot \text{h} \cdot \text{°F}$$

The effect of developing flow is higher convective heat transfer.

Oil as a coolant

ν , kinematic viscosity = 1.35×10^{-4} ft²/s
 ρ , density = 54.5 lb/ft³
 k , thermal conductivity = 0.082 Btu/ft · h · °F
 v , average velocity = 4 ft/s

Prandtl number, $Pr = 290$

Reynolds number, $Re = 1235$

Flow is laminar

The friction factor-Reynolds number equation is:

$$f = 16/Re = 0.0518$$

- Stanton/Colburn analogy:

$$h = \frac{(\rho c_p v) f}{8} Pr^{2/3}$$

h , convective heat transfer coefficient = 58 Btu/ft² · h · °F
 Nu , Nusselt number = $hD/k = 29.5$

- Sieder-Tate for developing flow ($L = 20$):
 $Nu = 1.86 \cdot [Re \cdot Pr \cdot (D/L)]^{2/3} = 20.8$
 $h = 41$ Btu/ft² · h · °F
- Sieder-Tate for developing flow ($L = 6$):
 $Nu = 46.4$, $h = 91$ Btu/ft² · h · °F
- Averaged developing flow:
 $Nu = 32.1$, $h = 63$ Btu/ft² · h · °F

Again, convective heat transfer in developing flow is higher than with fully developed flow.

The arithmetic is considerably simplified for water at 21°C or 70°F. For laminar flow, the heat transfer coefficient is obtained from [11]:

$$h_{lam} = 3.52 \left(\frac{k}{D} \right) Re^{1/2} \left(\frac{D}{L} \right)^{1/3} \quad (5.20)$$

where k is the thermal conductivity of the fluid, and D and L are the diameter and length of the flow channel, respectively. For turbulent flow in water at 21°C or 70°F, the heat transfer coefficient is:

$$h_{turb} = 0.068 \left(\frac{k}{D} \right) Re^{0.8} \left(\frac{D}{L} \right)^{0.055} \quad (5.21)$$

The relative values for laminar and turbulent water flow in a typical mold are given in Example 5.6.

Example 5.6 Laminar and Turbulent Heat Transfer

Determine the relative effect on heat transfer coefficient when the flow rate is increased so that flow moves from laminar to turbulent flow. Consider a serpentine coil imbedded in an epoxy mold, where $L/d = 100$. From Equations 5.20 and 5.21, determine the relative effect on the Biot number, the relative heat transfer coefficient. Then determine the actual heat transfer coefficients for water flowing in a 0.500-in or 1.27 cm diameter coil. The thermal conductivity of water is $0.35 \text{ Btu/ft} \cdot \text{h} \cdot ^\circ\text{F}$. Then, determine the heat transfer coefficient in the transition region, $2000 < Re < 10,000$.

For laminar flow, $Re \leq 2000$. Consider $Re = 2000$. From Equation 5.20, the Biot number, $Bi = hD/k$ is given as:

$$Bi = \frac{hD}{k} = 3.52 \cdot Re^{1/2} \cdot \left(\frac{D}{L}\right)^{1/2} = 3.52 \cdot 2000^{1/2} \cdot (0.01)^{1/2} = 15.7$$

For fully turbulent flow, $Re \geq 10,000$. Consider $Re = 10,000$. From Equation 5.21, the Biot number is:

$$Bi = \frac{hD}{k} = 0.068 \cdot Re^{0.8} \cdot \left(\frac{D}{L}\right)^{0.055} = 0.068 \cdot 10000^{0.8} \cdot (0.01)^{0.055} = 83.7$$

Note that increasing the flow rate by a factor of five increases the relative heat transfer coefficient by a factor of $83.7/15.7 = 5.3$. The dimensional convection heat transfer coefficient for the coolant is given as:

$$h_{\text{water, lam}} = 15.7 \cdot 0.35 \frac{\text{Btu}}{\text{ft} \cdot \text{h} \cdot ^\circ\text{F}} \cdot \frac{12}{0.5 \text{ ft}} = 132 \frac{\text{Btu}}{\text{ft}^2 \cdot \text{h} \cdot ^\circ\text{F}} = 750 \frac{\text{W}}{\text{m}^2 \cdot ^\circ\text{C}}$$

$$h_{\text{water, turb}} = 83.7 \cdot 0.35 \cdot 12 = 700 \frac{\text{Btu}}{\text{ft}^2 \cdot \text{h} \cdot ^\circ\text{F}} = 4000 \frac{\text{W}}{\text{m}^2 \cdot ^\circ\text{C}}$$

Approximate values for heat transfer coefficients in the transition region, $2000 < Re < 10,000$ are obtained by averaging. For example, for $Re = 5000$, the approximate heat transfer coefficient is:

$$h_{\text{water, trans}} = (700 - 132) \cdot \frac{(5000 - 2000)}{(10000 - 2000)} + 132 = 345 \frac{\text{Btu}}{\text{ft}^2 \cdot \text{h} \cdot ^\circ\text{F}} = 2000 \frac{\text{W}}{\text{m}^2 \cdot ^\circ\text{C}}$$

Since the heat is conducted perpendicular to the mold plane, the fluid resistance must be corrected for the flow channel diameter and the number of flow channels in a given mold area (Fig. 5.1). If there are N flow channels of diameter d , then the area ratio is $\pi DNL/L^2$, and the effective resistance is:

$$R_h = \frac{L}{\pi D N h_{\text{conv}}} \quad (5.22)$$

or $(1/\pi D N h_{\text{conv}})$ per unit area. This resistance is small for turbulent water flowing in many closely-spaced large-diameter flow channels. It is quite significant for laminar oil flowing in widely-spaced small-diameter flow channels.

5.5 Cyclic Heat Balance

The total amount of energy to be removed from the plastic sheet by the coolant is easily determined for any given cycle from Equation 5.1. At steady state, this energy is usually transferred to:

- The metal mold, and thence to the coolant,
- Cooler metal surfaces such as stripper bars and sheet clamps, and thence to surrounding air,
- Surrounding air, and/or
- Sprayed liquids such as water mist that then evaporate.

Consider the limiting case where a plastic sheet of uniform temperature T_p and uniform thickness t_p is brought in contact with a mold having an initially uniform temperature T_m and thickness t_m . Consider the mold to be made of a high thermal conductivity metal that is in contact with a coolant having a uniform temperature T_m . The free surface of the plastic sheet is insulated. The time-dependent temperature profile through the mold and the plastic sheet are shown in schematic in Fig. 5.8. Typically, the initial interfacial temperature between the sheet and the mold is much closer to that for the mold than that for the plastic. As cooling proceeds, the interfacial temperature falls.

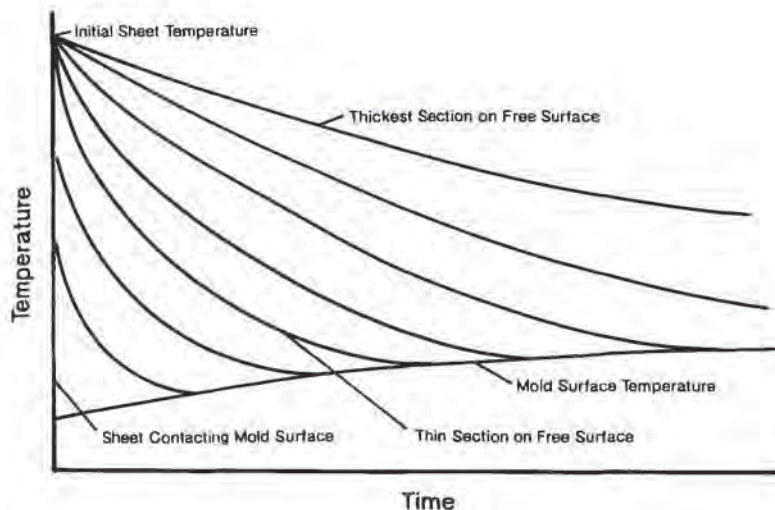


Figure 5.8 Characteristic time-dependent temperature profiles of thermoformed part cooling against a metal mold

Cooling the Free Surface of the Sheet

There are four general methods for cooling the free surface of the sheet:

- *No cooling.* In this case, the surface is essentially insulated from the environment.
- *Natural air cooling.* That is, no fans or forced air cooling methods are used.
- *Forced air cooling.* This can be as simple as clock-timer actuated shop floor fans or as complex as special-purpose high-velocity blowers, and
- *Water fog or mist cooling.* The mist is usually clock-timer controlled to shut off some time prior to sheet removal from the mold surface. This allows the fine water drops to evaporate before the part is removed.

Free surface cooling effectiveness increases as one progresses down this list. The measure of effectiveness of heat removal is the convective heat transfer coefficient, h . Table 5.4 summarizes the relative values of convective heat transfer coefficients for the last three free surface cooling methods. The convective heat transfer coefficient for an insulated surface is $h = 0$. Matched metal molds are used if the sheet is foam, reinforced or highly filled, or if close tolerance is needed in certain regions. In this case, the effective heat transfer coefficient, $h_{\text{eff}} = \infty$. These methods are shown in schematic in Fig. 5.9.

Cooling Thin Sheet in Ambient Air

When a thin sheet of plastic is heated to the forming condition, it must be quickly transferred to the mold surface to minimize heat loss to the surrounding air. For very thin sheet, less than 0.005 in or 0.01 cm in thickness, the sheet is usually heated by

Table 5.4 Cooling a Part on the Mold—Relative Values of Thermal Resistance

| Physical resistance | Form for resistance | Typical reciprocal value | |
|---|---------------------|--------------------------|--------------------------------|
| | | (W/m ² · °C) | (Btu/ft ² · h · °F) |
| Free surface cooling | | | |
| Ambient air | $1/h_{\text{air}}$ | 2.84 to 5.68 | 0.5 to 1 |
| Forced air | $1/h_{\text{air}}$ | 28.4 to 56.8 | 5 to 10 |
| Water spray | $1/h_{\text{mist}}$ | 284 to 568 | 50 to 100 |
| Interface gap** | $1/h_c$ | 114 to 284 | 20 to 50 |
| Mold | | | |
| Aluminum | D^*/k_m | 34,330 | 6000 |
| Plaster | d/t_0 | 21 | 3.7 |
| Coolant | | | |
| Laminar water ($L/\pi d N h_{\text{cool}}$) | | 454 | 80 |
| Turbulent water ($L/\pi d N h_{\text{cool}}$) | | 4000 | 700 |

D^* is the effective mold thickness and includes shape factor

** See Table 5.2 for these values

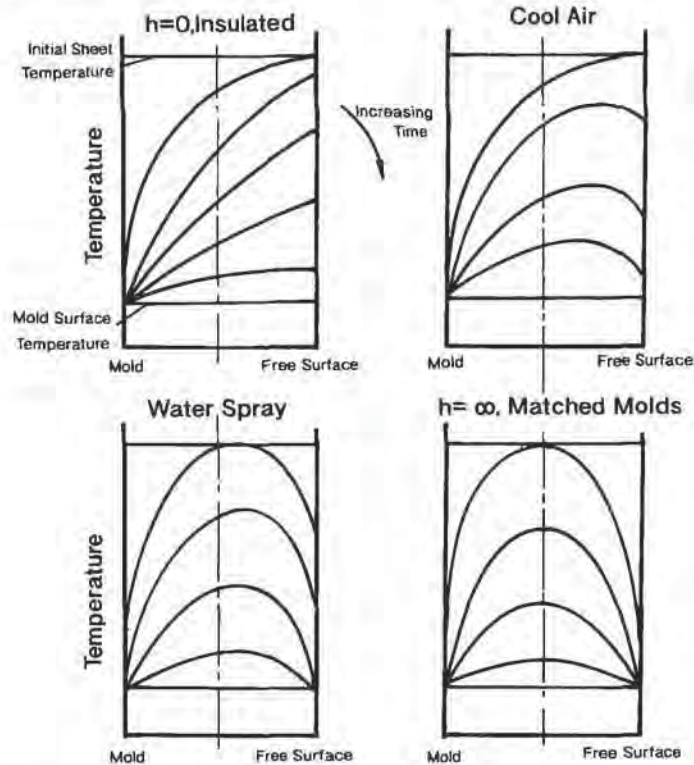


Figure 5.9 The effect of various free-surface cooling techniques on time-dependent temperature profiles of thermoformed part cooling against a metal mold

contact heat transfer, then blown from the heater directly onto the mold surface. There is an extensive discussion of transient heat transfer to thin sheet in Chapter 3. This lumped-parameter analysis is directly applicable to the cooling of thin sheet in ambient air. The dimensionless temperature, Y , is given as:

$$Y = \frac{(T - T_{\text{air}})}{(T_i - T_{\text{air}})} = e^{-Bi \cdot Fo} = e^{(-\alpha\theta/kL)} \quad (5.23)$$

where T_i is the initial sheet temperature, T_{air} is the air temperature, θ is time, α is thermal diffusivity, k is thermal conductivity, h is convection heat transfer coefficient between the sheet and the ambient air, and L is the sheet thickness. Note that the cooling time, θ is proportional to the sheet thickness to the first power. In contrast, for conduction-controlled heat transfer, the cooling time is proportional to the square of sheet thickness. The lumped parameter cooling time curves for various film thicknesses are compared with experimental data in Fig. 5.10. Since nothing is known about the experimental processing conditions or sheet material parameters, the curves are fit at $L = 0.15$ cm or 0.060 in by selecting values for the convection

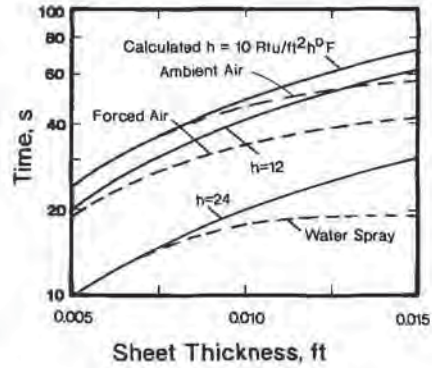


Figure 5.10 Effect of sheet thickness on cooling time for convection-controlled thin sheet. Solid lines are calculated. Dashed lines are experimental

heat transfer coefficient, h . The shapes of these convection-controlled curves agree better with the data than do the conduction-controlled curves.

Transient Heat Removal From the Sheet

The energy in the sheet is removed by conduction to the mold and free surfaces. The transient one-dimensional conduction heat transfer equation, Equation 3.4, applies:

$$\rho c_p \left(\frac{\partial T}{\partial \theta} \right) = k \left(\frac{\partial^2 T}{\partial x^2} \right) \tag{5.24}$$

subject to the following boundary conditions:

$$-k \left. \frac{\partial T}{\partial x} \right|_{x=L} = h_{conv}(T - T_{air}) \tag{5.25}$$

$$T(0,x) = T_i(x) \tag{5.26}$$

$$T(\theta,0) = T_{mold} \tag{5.27}$$

Equation 5.25 is the heat flux from the free sheet surface to the ambient air, with h_{conv} as the convection heat transfer coefficient, Table 3.2. T_i is the initial sheet temperature at the time of contact with the mold surface. If draw-down onto the sheet surface is very rapid, $T_i(x)$ is represented by the equilibration temperature profile discussed in Section 3.13. As a first approximation, $T_i(x) = T_i$, an average sheet temperature. Two limiting conditions bound the solution of this equation and its attendant boundary conditions.

Quiescent Ambient Air

When heat transfer to air is very small relative to the rate of energy conducted to the mold, $h \rightarrow 0$, the free surface is approximated by an insulated surface. This is usually the case for natural convection of heat to quiescent air. Figure 5.11 is used

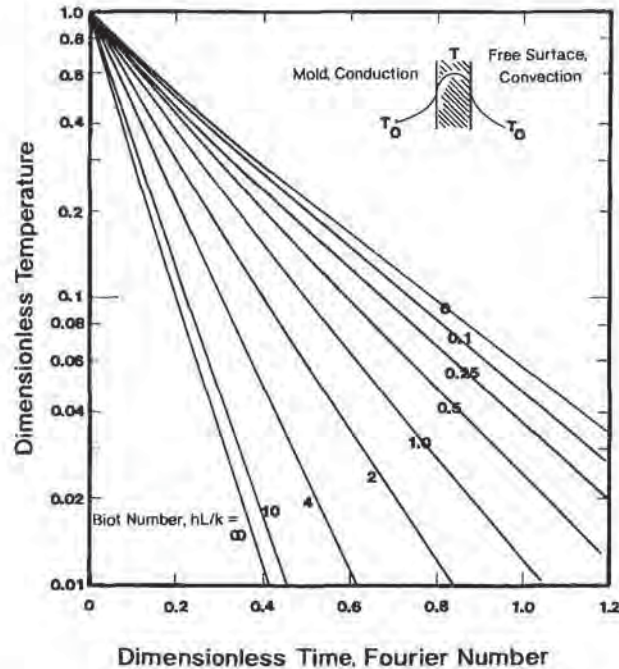


Figure 5.11 Time-dependent average sheet temperature as a function of the rate of heat loss from the free surface. Dimensionless temperature, $Y = (T - T_o)/(T_i - T_o)$ where T_i is the initial sheet temperature and T_o is the mold surface temperature and ambient air temperature. Biot number, $Bi = hL/k$, where h is the convection heat transfer coefficient and k is polymer thermal conductivity. Fourier number, $Fo = \alpha\theta/L^2$ where α is the thermal diffusivity, θ is time and L is sheet thickness

to obtain the dimensionless time, $Fo = \alpha\theta/L^2$, with the dimensionless temperature, Y , given as:

$$Y = \frac{(T - T_{\text{mold}})}{(T_i - T_{\text{mold}})} \quad (5.28)$$

where T_i is the average sheet temperature. Since $h_{\text{conv}} = 0$, $Bi = hL/k$, the Biot number is zero. L is the actual thickness of the sheet. This is illustrated in Example 5.7.

Example 5.7 Cooling Time for Heavy-Gage PS Sheet—I

A polystyrene sheet 0.438 in or 1.11 cm thick initially at 375°F or 191°C is cooled by pressing it against a mold at 75°F or 24°C. Determine the time required to cool the sheet to an average temperature of 175°F or 79°C. PS thermal conductivity is 0.073 Btu/ft · h · °F or 0.0003 cal/g · s · °C. PS density is 65.5 lb/ft³ or 1.05 g/cm³. PS specific heat is 0.5 Btu/lb · °F = 0.5 cal/g · °C. The free surface is exposed only to ambient air. Assume $h_{\infty} = 0$.

The dimensionless average temperature, Y is given as:

$$Y = \frac{(175 - 75)}{(375 - 75)} = 0.333$$

From Fig. 5.11, the Fourier number at this value of Y for $Bi = 0$ is $Fo = 0.345$. The polymer thermal diffusivity is given as:

$$\alpha = \frac{k}{\rho \cdot c_p} = 5.7 \times 10^{-4} \frac{\text{cm}^2}{\text{s}} = 2.2 \times 10^{-3} \frac{\text{ft}^2}{\text{h}}$$

The cycle time is given as:

$$Fo = \frac{\alpha \theta}{L^2} = 5.7 \times 10^{-4} \cdot \frac{1}{(1.11)^2} \cdot \theta[\text{s}] = 0.345$$

or $\theta = 746$ s. This is shown as the top line of Table 5.5.

Moving Ambient Air

Figure 5.11 is also used to approximate the relative effect of air movement on the cooling time, so long as $T_{\text{air}} \approx T_{\text{mold}}$. Now the dimensionless temperature, Y , is given as:

$$Y = \frac{(T - T_{\text{mold}})}{(T_i - T_{\text{mold}})} \approx \frac{(T - T_{\text{air}})}{(T_i - T_{\text{air}})} \quad (5.29)$$

Note that as Bi increases, through increase in the value for the convection heat transfer coefficient, the cooling time drops rapidly. When $Bi = \infty$, the dimensionless time to reach the same dimensionless temperature drops to one-fourth that for the quiescent case ($Bi = 0$). This directly supports the discussion in Chapter 3 that the value of L should be half the actual sheet thickness when energy interchange is symmetric across the sheet. Example 5.8 illustrates the effect of heat transfer coefficient value on cooling time.

Example 5.8 Cooling Time for Heavy-Gage Polystyrene Sheet—II

Using the data from Example 5.7, determine the reduction in cooling time if the following free surface coolants are used:

a) Ambient air with a heat transfer coefficient of

$$h = 1 \text{ Btu/ft}^2 \cdot \text{h} \cdot ^\circ\text{F} \text{ or } 5.68 \text{ W/m}^2 \cdot ^\circ\text{C},$$

b) Forced air with a heat transfer coefficient of

$$h = 10 \text{ Btu/ft}^2 \cdot \text{h} \cdot ^\circ\text{F} \text{ or } 57 \text{ W/m}^2 \cdot ^\circ\text{C}, \text{ and}$$

c) Water mist with a heat transfer coefficient of

$$h = 100 \text{ Btu/ft}^2 \cdot \text{h} \cdot ^\circ\text{F} \text{ or } 570 \text{ W/m}^2 \cdot ^\circ\text{C}.$$

For each case, the Biot number $Bi = hL/k$.

$$a) Bi = \frac{1 \text{ Btu}}{\text{ft}^2 \cdot \text{h} \cdot ^\circ\text{F}} \frac{0.438}{12} \text{ ft} \cdot \frac{1}{0.073} \frac{\text{ft} \cdot \text{h} \cdot ^\circ\text{F}}{\text{Btu}} = 0.5$$

The value of Fo for $Y = 0.333$ and $Bi = 0.5$ from Fig. 5.11 is $Fo = 0.256$ or $\theta = 554$ s. This is about 26% reduction in cycle time from the insulated example, $Bi = 0$ of Example 5.7.

b) $Bi = 5$. The value of Fo from Fig. 5.11 is 0.123 and the cycle time $\theta = 266$ s. This is a 64% reduction in cycle time.

c) $Bi = 50$. The value of Fo from Fig. 5.11 for $Bi = \infty$ is 0.086. The best cycle time possible is $\theta = 187$ s. This is a 75% reduction in cycle time from the insulated example.

These values are tabulated in Table 5.5.

The effect of altering free surface cooling conditions is seen in Fig. 5.12 [12]. The nature of the polymer and the details about the processing conditions are unknown. For $L = 0.15$ cm or 0.060 in sheet, water spray reduces the cooling time by about 60%. For thicker sheet, $L = 0.45$ cm or 0.180 in, water spray reduces the cooling time by about 65%. As expected, the cooling time increases with increasing sheet thickness. As expected, the effect is most obvious with ambient air cooling.

On the other hand, if conduction heat transfer through the plastic sheet controls the cooling time, the effect of sheet thickness is easily determined. At any given average sheet temperature, the dimensionless time, Fo , is a simple function of the Biot number:

$$Fo = f(Bi) \quad (Y \text{ fixed}) \quad (5.30)$$

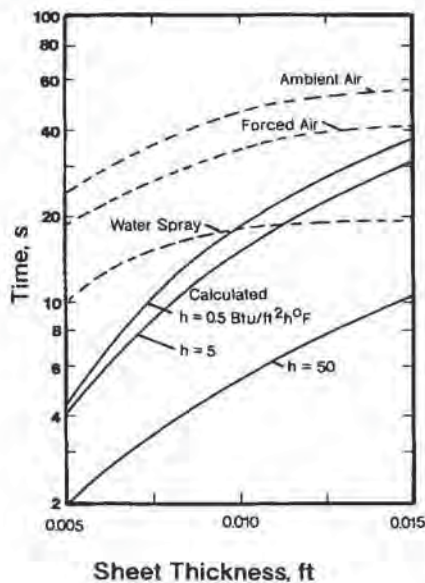


Figure 5.12 The effect of various cooling techniques on cooling time as function of sheet thickness, theory from Fig. 5.11. Experimental data from [12]

Table 5.5 Calculated Cooling Times for Polystyrene Sheet (Combined Convection/Conduction Heat Transfer)

| Type of free surface cooling | Convection heat transfer coefficient | | Thin-gage sheet | | | Heavy-gage sheet | | |
|-------------------------------|--------------------------------------|--------------------------------|--------------------------|-------------|----------------|------------------------|-------------|----------------|
| | (W/m ² · °C) | (Btu/ft ² · h · °F) | L = 0.111 cm = 0.0438 in | | | L = 1.11 cm = 0.438 in | | |
| | | | Biot no. | Fourier no. | Cycle time (s) | Biot no. | Fourier no. | Cycle time (s) |
| Insulated | 0 | 0 | 0 | 0.345 | 7.46 | 0 | 0.345 | 746 |
| Ambient air | 5.7 | 1 | 0.05 | 0.323 | 6.98 | 0.5 | 0.256 | 554 |
| Forced air | 57 | 10 | 0.5 | 0.256 | 5.54 | 5.0 | 0.123 | 266 |
| Water spray | 570 | 100 | 5.0 | 0.123 | 2.66 | 50 | 0.086 | 187 |
| Direct contact or matched die | ∞ | ∞ | ∞ | 0.086 | 1.87 | ∞ | 0.086 | 187 |

Initial sheet temperature, $T_i = 190.6^\circ\text{C}$ or 375°F

Mold ambient temperature, $T_o = 23.9^\circ\text{C}$ or 75°F

Final average temperature, $T_a = 79.4^\circ\text{C}$ or 175°F

Thermal conductivity = $0.0003 \text{ cal/gm} \cdot \text{s} \cdot ^\circ\text{C}$ or $0.073 \text{ Btu/ft} \cdot \text{h} \cdot ^\circ\text{F}$

Thermal diffusivity = $0.00057 \text{ cm}^2/\text{s}$ or $0.0022 \text{ ft}^2/\text{h}$

From these values, the following are found:

$$Y = 0.333$$

$$Bi = hL/k$$

$$Fo = \alpha\theta/L^2 = 0.0863[1 + 3 \exp(-0.667 Bi^{0.667})]$$

As seen in Fig. 5.11, the approximate form for Equation 5.30 is:

$$Fo = Fo_\infty[1 + \beta \exp(-aBi^a)] \quad (5.31)$$

Fo_∞ is the value of Fo when $Bi = \infty$, the limiting case where both sides of the sheet contact solid surfaces. When $Bi = 0$, $Fo = 4Fo_\infty$. Since $Fo = \alpha\theta/L^2$, the cooling time θ is proportional to the square of the sheet thickness *for both limiting cases*. It is apparent then, that when conduction from the plastic sheet controls heat transfer, doubling the sheet thickness always increases the cooling time by a factor of four. See also Table 5.5 where Equation 5.31 is used to compare cycle times for various free surface cooling modes.

As seen in Fig. 5.13, actual cooling times show a relationship that is more linear with thickness. The observed values are substantially higher than the values obtained from Fig. 5.12. This indicates that, at least in this case, the experimental sheet is *not* being cooled in a conduction-controlled environment. Again, the exact conditions used to obtain the experimental data of Fig. 5.13 are unknown.

Cooling on Nonmetallic Molds

For metal molds, the time-dependent conduction resistance through the mold during the heat removal process from the sheet is usually negligible. Heavy-walled, non-

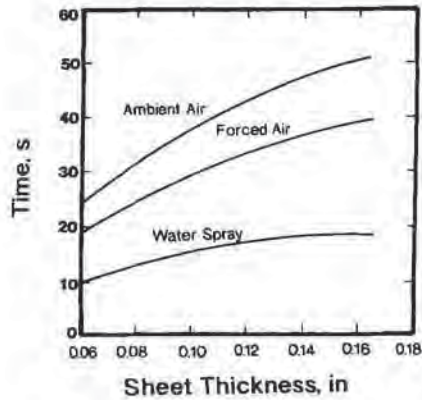


Figure 5.13 Measured sheet thickness-dependent cooling times for various cooling techniques. Figure adapted from [23]

metallic molds alternately store and liberate heat during each forming cycle. An estimate of the rate at which heat penetrates the mold is obtained by integrating the time-dependent heat conduction equation, as discussed below. As with energy input to plastic sheet, Chapter 3, there are two limiting conditions that are important. If the energy transfer is constant heat flux and the mold is considered as a semi-infinite slab of thermal diffusivity, α , the depth of penetration of energy, δ , is approximately:

$$\text{(Constant Heat Flux)} \quad \delta = \sqrt{6\alpha\theta} \quad (5.32)$$

The penetration dimensionless time, $Fo = \alpha\theta/L^2 = 1/6$ [13]. If the surface is raised instantaneously to a constant temperature, the depth of penetration of energy, δ , is approximately:

$$\text{(Constant Surface Temperature)} \quad \delta = \sqrt{24\alpha\theta} \quad (5.33)$$

and the penetration dimensionless time, $Fo = \alpha\theta/L^2 = 1/24$. In thermoforming, the actual condition is closer to the constant flux approximation. If D is the effective thickness of the mold, then the time for the heat to be felt at the coolant interface is:

$$\frac{D^2}{24\alpha} < \theta < \frac{D^2}{6\alpha} \quad (5.34)$$

Example 5.9 illustrates how the type of mold material dictates the penetration time of heat into the mold. For many thermoforming operations where actively cooled nonmetallic molds are used, the coolant probably would not see all the energy removed from the sheet until after the sheet had been removed from the mold. The mold, in effect, is storing the sheet thermal energy during the cooling cycle, then transferring it to the coolant after the cycle. The heat is also being convected away from the mold surface during the times when no sheet contacts the mold surface, as shown in Fig. 5.14. The approximate increase in mold temperature during the cooling cycle and the approximate time required to return the mold to within 2% of its initial temperature are illustrated in Example 5.10. For all practical cases where low-conductivity molds made of wood, plaster, fiberglass and even certain metal-filled epoxies are used, the average mold temperature continues to increase in value during the forming process

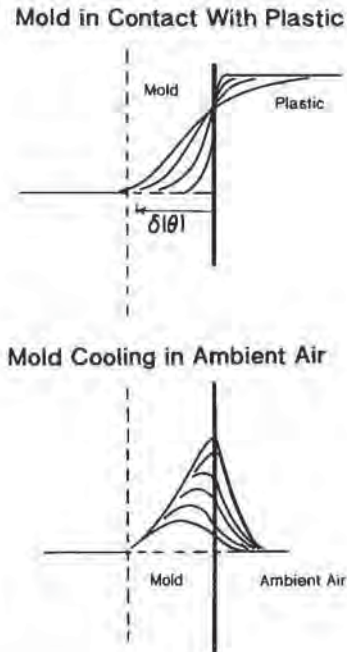


Figure 5.14 Schematic thermoforming mold temperature profiles when mold is in contact with hot polymer [top] and with ambient air [bottom]

until the energy added during the cooling portion of the cycle just equals that extracted during the entire cycle time. From Equation 5.2, the amount of heat added per unit area of the mold for a given cycle is:

$$q'' = \rho c_p \cdot t_{avg}(T_i - T_f) \quad (5.35)$$

Example 5.9 Transient Heat Penetration into Molds

Consider two molds, a prototype plaster mold with a relative thickness $D = 2$ cm or 5.1 cm, and a production aluminum mold with a relative thickness $D = 0.2$ in or 0.51 cm. Determine the elapsed time for a heat pulse to travel to the reverse side of each of these mold materials. The thermal diffusivity for aluminum is $0.49 \text{ cm}^2/\text{s} = 1.9 \text{ ft}^2/\text{h}$ and for plaster is $30 \times 10^{-4} \text{ cm}^2/\text{s}$ or $11.6 \times 10^{-3} \text{ ft}^2/\text{h}$.

From Equation 5.34, the penetration time is bracketed by $D^2/c \cdot \alpha$, where $c = 24$ for constant surface temperature and $c = 6$ for constant heat flux. For aluminum, $D^2/\alpha = 0.0816$ s. For plaster, $D^2/\alpha = 1333$ s. Thus the penetration time for aluminum is:

$$0.0034 \text{ s} < \theta < 0.0136 \text{ s}$$

The penetration time for plaster is:

$$55.5 \text{ s} < \theta < 222 \text{ s}$$

For aluminum, it is apparent that energy transfer is almost immediate, within milliseconds. For plaster, there is a substantial lag in energy transfer.

Example 5.10 Approximate Increases in Cycle Time for Prototype Molds

Consider the case where a prototype plaster mold heats during contact with the formed sheet. If the initial mold temperature is 75°F or 24°C and the final mold temperature is 125°F or 52°C, estimate the average sheet temperature at 746 s (see Example 5.7) for an insulated free surface. Then estimate the time required to cool the sheet to an average temperature of 175°F or 79°C. Then determine the approximate time required to cool the mold back to its initial temperature.

The correct approach to this problem is to solve the transient heat conduction equations for the cooling sheet and the heating mold, as done in Section 5.6. The bounds on the answer are obtained by assuming an *initial* mold temperature of 125°F or 52°C. At $Fo = 0.345$ and $Bi = 0$, $Y = 0.333$.

$$Y = \frac{(T - T_o)}{(T_i - T_o)} = \frac{(T - 125)}{(375 - 125)} = 0.333$$

$$T_{ave} = 208^\circ\text{F} = 98^\circ\text{C}$$

In other words, the average sheet temperature is somewhere between 175°F or 79°C as determined with an isothermal mold and 208°F or 98°C as determined by an artificially high mold temperature of 125°F or 52°C. The time needed to attain an average sheet temperature of 175°F or 79°C is obtained as follows:

$$Y = \frac{(175 - 125)}{(375 - 125)} = 0.200$$

For $Bi = 0$, $Fo = 0.53$ from Fig. 5.11. Therefore $\theta = 1145$ s. The actual time is somewhere between 746 s for 75°F or 52°C mold temperature and 1145 s for 125°F or 52°C mold temperature. The increase of more than 50% in cycle time is a strong indication of the importance of maintaining constant mold surface temperature.

Figure 5.11 is used to determine the cooling rate of the prototype mold. Consider cooling the mold to within 2% of its initial temperature. That is $T_{mold,final} = 76^\circ\text{F}$ or 24°C . Now:

$$Y = \frac{(76 - 75)}{(125 - 75)} = 0.02$$

For $Bi = 0$, $Fo = 1.4$. The cooling time is given as:

$$\frac{\alpha\theta}{D^2} = 1.4$$

For plaster, $\alpha = 30 \times 10^{-4}$ cm²/s and $D = 2$ cm. Therefore the cooling time is given as $\theta = 1870$ s. It is apparent that temperatures in prototype molds increase with the number of parts molded.

where t_{avg} is the average sheet thickness, for this illustration. T_i is the initial sheet temperature, T_f is the final sheet temperature and T_a^* is the time-average sheet temperature, such as $T_a^* = (T_i + T_{avg})/2$. This amount of heat is to be removed in the cooling time, θ_c . There are N forming cycles in the total time θ_T . The total amount of heat to be removed from the sheet in the time θ_T is thus given as:

$$Q_{total} = N \cdot \rho c_p \cdot t_{avg} (T_i - T_f) \quad (5.36)$$

The heat convected away by the cooled air in contact with the sheet in the time θ_T is:

$$Q_{conv} = h_{air} (T_a^* - T_{air}) \frac{\theta_{cool}}{\theta_T} \quad (5.37)$$

The time when no sheet contacts the mold surface is given as $(1 - \theta_{cool}/\theta_T)$. During this time, energy is being transferred from the mold surface to the cooling air:

$$Q_{conv} = h_{air} (T_{mold,avg} - T_{air}) \frac{(1 - \theta_{cool})}{\theta_T} \quad (5.38)$$

That absorbed by the mold is given as:

$$Q_{mold} = Q_{avg} - Q_{conv} \quad (5.39)$$

The amount of heat transferred to the coolant during the entire cooling portion of the cycle is:

$$Q_{cool} = h_{cool} (T_{mold,avg} - T_{cool}) \quad (5.40)$$

The overall heat balance is then given as:

$$\begin{aligned} Q_{cool} &= h_{cool} (T_{mold,avg} - T_{cool}) \\ &= N \cdot \rho c_p \cdot t_{avg} (T_i - T_f) - h_{air} (T_a^* - T_{air}) \frac{\theta_{cool}}{\theta_T} - h_{air} (T_{mold,avg} - T_{air}) \frac{(1 - \theta_{cool})}{\theta_T} \end{aligned} \quad (5.41)$$

As is apparent, $T_{mold,avg}$ is the only unknown temperature. Example 5.11 illustrates the relative temperature increase for cyclic cooling on a plaster mold. As expected, average equilibrium mold temperature values increase with decreased time between forming steps and decrease with higher coolant flow rates, lower coolant temperatures and more efficient convection cooling at the free surface. A more exact analysis is presented below when all aspects of transient heat removal from plastic sheet are incorporated in a general computer program in the next section.

Example 5.11 Equilibrium Mold Temperature

Make a steady-state heat balance on a plaster mold to determine its equilibrium mold temperature. The mold is cooling a 0.060 in or 1.5 mm PS part in 20 s. There is a 20 s delay for part removal, insertion and draw-down of the next part. The initial average sheet temperature is 375°F or 190°C. The final average sheet temperature is 175°F or 79°C. The initial mold temperature is 75°F or 24°C. The PS specific heat is 0.45 cal/g · °C or 0.45 Btu/lb · °F. The PS density is 1.05 g/cm³

or 65.5 lb/ft^3 . The convection heat transfer coefficient to forced air is $h_{\text{air}} = 28.4 \text{ W/m}^2 \cdot ^\circ\text{C}$ or $5 \text{ Btu/ft}^2 \cdot \text{h} \cdot ^\circ\text{F}$. The air temperature is 75°F or 24°C . The heat transfer coefficient to the coolant is $h_{\text{cool}} = 284 \text{ W/m}^2 \cdot ^\circ\text{C}$ or $50 \text{ Btu/ft}^2 \cdot \text{h} \cdot ^\circ\text{F}$. The coolant temperature is 75°F or 24°C .

All the values for Equation 5.41 are known except the equilibrium mold temperature, $T_{\text{mold,avg}}$. The first term on the right is:

$$N \cdot \rho_p \cdot t_{\text{avg}}(T_i - T_f) = 90 \cdot 65.5 \cdot 0.45 \cdot \frac{0.060}{12} \cdot (375 - 175) = 2650 \frac{\text{Btu}}{\text{ft}^2 \cdot \text{h}}$$

This is the heat that must be removed from the sheet. The second term on the right is the amount of heat convected from the sheet to the air. Here $\theta_{\text{cool}}/\theta_T = 0.5$. The average sheet temperature is $T_{\text{avg}} = 375 - 175 = 275^\circ\text{F}$.

$$h_{\text{air}}(T_{\text{avg}} - T_{\text{air}}) \cdot 0.5 = 500 \frac{\text{Btu}}{\text{ft}^2 \cdot \text{h}}$$

The average heat loss from the uncovered mold is given as the third part of the right side of Equation 5.41:

$$h_{\text{air}}(T_{\text{mold,avg}} - T_{\text{air}})(1 - 0.5) = 5 \cdot 0.5 \cdot (T_{\text{mold,avg}} - 75)$$

And the average heat loss to the coolant is given as the term on the left in Equation 5.41:

$$h_{\text{cool}} \cdot (T_{\text{mold,avg}} - T_{\text{cool}}) = 50 \cdot (T_{\text{mold,avg}} - 75)$$

The mold temperature is then obtained from:

$$(50 + 2.5) \cdot (T_{\text{mold,avg}} - 75) = 2650 - 500 = 2150 \frac{\text{Btu}}{\text{ft}^2 \cdot \text{h}}$$

Or $T_{\text{mold,avg}} = 116^\circ\text{F}$ or 46.6°C .

5.6 Transient Heat Transfer During Sheet Cooling on the Mold Surface—Computer Models

As shown in Fig. 5.1, the convective and conductive elements discussed above represent resistances to heat removal from the sheet. Time-dependent sheet temperature is determined by simultaneously solving the transient heat conduction equations for both the formed plastic sheet and the mold¹:

$$\rho_p \cdot c_{p,p} \left(\frac{\partial T}{\partial t} \right) = k_p \left(\frac{\partial^2 T}{\partial x^2} \right) \quad (5.42)$$

$$\rho_m \cdot c_{p,m} \left(\frac{\partial T}{\partial t} \right) = k_m \left(\frac{\partial^2 T}{\partial x^2} \right) \quad (5.43)$$

¹ The general transient one-dimensional heat conduction equation was described in detail in Chapter 3.

where ρ , c_p and k are the density, heat capacity and thermal conductivity values and "p" and "m" are for polymer and mold, respectively. Thermal diffusivity, α is defined as $k/\rho \cdot c_p$. The boundary conditions needed to solve these equations are:

$$-k_p \left. \frac{\partial T}{\partial x} \right|_{x=0} = h_a(T_p - T_a) \quad (5.44)$$

$$-k_m \left. \frac{\partial T}{\partial x} \right|_{x=L_m} = h_w(T_m - T_w) \quad (5.45)$$

$$q = -\frac{k_p}{dx_p}(T - T_{i1}) = -\frac{k_a}{dx_i}(T_{i1} - T_{i2}) = -\frac{k_m}{dx_m}(T_{i2} - T_m) \quad (5.46)$$

$$T_p(t=0) = T_{o,p} \quad (5.47)$$

$$T_m(t=0) = T_{o,m} \quad (5.48)$$

The first two equations represent convection conditions at the free surface and the mold/coolant interface, respectively. The third set of three equations represents the heat conduction across the interfacial air trapped between the plastic sheet and the mold surface. The last two equations represent the initial sheet and mold temperatures, respectively. The solution to these equations uses finite difference [14,15]. The explicit method uses a time step defined as:

$$\Delta t = Fo \cdot \Delta x^2 / \alpha \quad (5.49)$$

where Fo is the Fourier number. For mathematical stability, $Fo < \frac{1}{2}$ ¹. Once the time step is determined, the temperatures at $t + \Delta t$ are obtained from:

$$T_{p,n}(t + \Delta t) = Fo_p [T_{p,n-1}(t) + T_{p,n+1}(t) - (2 - 1/Fo_p)T_{p,n}] \quad (5.50)$$

$$T_{m,n}(t + \Delta t) = Fo_m [T_{m,n-1}(t) + T_{m,n+1}(t) - (2 - 1/Fo_m)T_{m,n}] \quad (5.51)$$

$$T_{p,1}(T + \Delta t) = Fo_p [T_{p,2}(t) + Bi_a \cdot T_a + (1/2 \cdot Fo_p - 1 - Bi_a)T_{p,1}(t)] \quad (5.52)$$

$$T_{m,m}(T + \Delta t) = Fo_m [T_{m,m-1}(t) + Bi_w \cdot T_w + (1/2 \cdot Fo_m - 1 - Bi_w)T_{m,m}(t)] \quad (5.53)$$

Bi is the Biot number, given as:

$$Bi_a = h_a \cdot \frac{\Delta x_p}{k_p}; \quad Bi_w = h_w \cdot \frac{\Delta x_m}{k_m}$$

The proper value of h_w , the effective convective heat transfer coefficient for the coolant, must include the film heat transfer coefficient for the coolant, the shape factor discussed in Section 5.4 and any fouling factor.

The time-dependent temperature profile depends on relative material and geometric values of the plastic sheet and the mold. Figure 5.15 gives one example of the coupled temperature profiles with no interstitial air layer, that is $T_{i1} = T_{i2} \equiv T_i$. Table 5.6 is a parametric study of some of the parameters. In this study, it is apparent in the first block of data that the total cooling time is strongly affected by mold materials from aluminum to plaster. As expected, the effect of coolant methods on

¹ Since there are two Fourier numbers, one for the plastic and one for the mold, stability is achieved by selecting the smaller time step that satisfies the $Fo < \frac{1}{2}$ criterion.

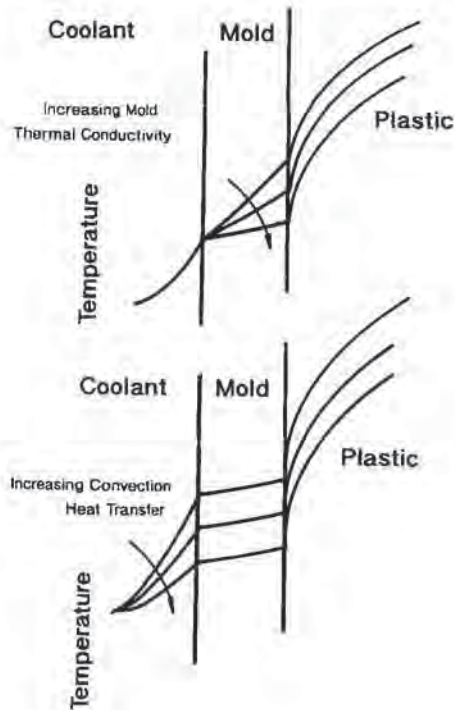


Figure 5.15 Schematic temperature profiles through coolant, mold and polymer with increasing mold thermal conductivity [top] and increasing coolant convection heat transfer [bottom]

cooling time is less important for prototype materials such as plaster than for production materials such as aluminum. The effect of mold thickness for production mold materials such as aluminum is essentially nil.

In all conduction heat transfer models, such as that used to produce Fig. 5.12, the unaccomplished temperature change, Y , is shown to be proportional to the Fourier number of the polymer, $Fo = \alpha\theta/L^2$, where α is the polymer thermal diffusivity, θ is time and L is the thickness of the polymer sheet. If the average sheet temperature at removal from the mold surface is fixed, the unaccomplished temperature change, Y , is fixed and so is the Fourier number. The time required to cool the sheet to that temperature should then be proportional to the *square* of the sheet thickness:

$$\theta_{\text{cool}} = (Fo_{\text{fixed}}/\alpha) \cdot L^2 \quad (5.54)$$

Doubling the sheet thickness should increase the cooling time by a factor of four. This concept is confounded in practice by the presence of the mold and the attendant transient heat conduction to the coolant. Figure 5.16 shows that the effective cooling time of a polymeric sheet in contact with a mold having finite thermal conductivity is not in proportion to the square of the sheet thickness, but rather to a power somewhat less than 2¹. The heat conduction square law, Equation 5.54, is therefore conservative.

¹ For the example shown, θ is proportional to $L^{1.7}$.

Table 5.6 Parametric Study of Cooling of Polystyrene Sheet to an Average Temperature of 150°F Against a Mold of Various Materials

| Mold material | Coolant type | Surface cooling | Plastic thickness (in) | Mold thickness (in) | Time to cool (s) | Interface temperature* (°F) | Surface temperature* (°F) |
|---------------|--------------|-----------------|------------------------|---------------------|------------------|-----------------------------|---------------------------|
| Aluminum | Water | Forced air | 0.100 | 0.500 | 19.4 | 77.7 | 171.1 |
| Aluminum | Water | Natural air | 0.100 | 0.500 | 26.4 | 77.1 | 187.6 |
| Steel | Oil | Natural air | 0.100 | 0.500 | 28.3 | 86.2 | 182.3 |
| Cu/bronze | Oil | Natural air | 0.100 | 0.500 | 28.8 | 85.6 | 183.5 |
| Zn alloy | Oil | Natural air | 0.100 | 0.500 | 28.5 | 88.1 | 182.2 |
| Al-epoxy | Oil | Natural air | 0.100 | 0.500 | 45.5 | 117.6 | 162.8 |
| Maple | Oil | Natural air | 0.100 | 0.500 | 236.4 | 149.5 | 146.9 |
| Plaster | Oil | Natural air | 0.100 | 0.500 | 116.9 | 144.1 | 149.2 |
| Plaster | None | Natural air | 0.100 | 0.500 | 116.9 | 144.4 | 149.3 |
| Plaster | None | None | 0.100 | 0.500 | 200.0 | 145.0 | 152.6 |
| Aluminum | Water | None | 0.100 | 0.500 | 29.7 | 76.8 | 192.4 |
| Aluminum | Water | Natural air | 0.100 | 0.500 | 26.4 | 77.1 | 187.6 |
| Aluminum | Water | Forced air | 0.100 | 0.500 | 19.4 | 77.7 | 171.1 |
| Aluminum | Water | Water spray | 0.100 | 0.500 | 7.4 | 78.1 | 78.5 |
| Aluminum | Water | Forced air | 0.100 | 0.500 | 19.4 | 77.7 | 171.1 |
| Aluminum | Water | Forced air | 0.100 | 1.000 | 19.2 | 77.1 | 171.3 |
| Aluminum | Water | Forced air | 0.100 | 2.000 | 19.1 | 76.1 | 170.9 |
| Aluminum | Water | Forced air | 0.100 | 4.000 | 19.5 | 76.1 | 167.8 |
| Aluminum | Water | Forced air | 0.050 | 1.000 | 5.7 | 76.5 | 180.7 |
| Aluminum | Water | Forced air | 0.100 | 1.000 | 19.2 | 77.1 | 171.3 |
| Aluminum | Water | Forced air | 0.200 | 1.000 | 61.1 | 75.2 | 156.1 |
| Aluminum | Water | Forced air | 0.400 | 1.000 | 190.5 | 72.6 | 135.2 |

* When average sheet temperature $\leq 150^\circ\text{F}$

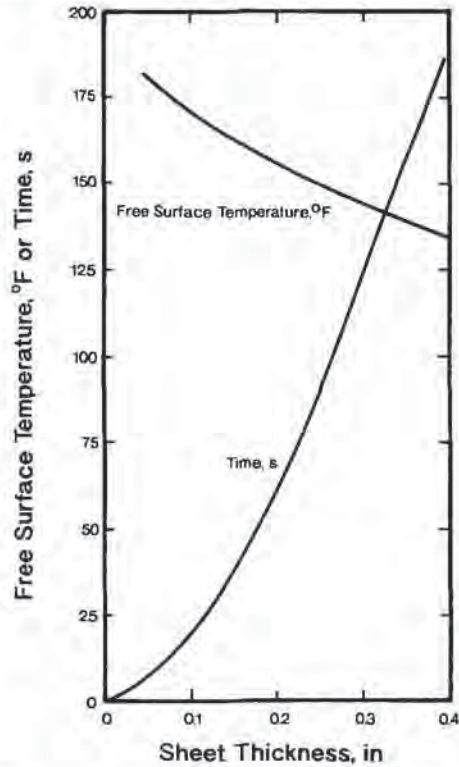


Figure 5.16 Calculated sheet thickness-dependent cooling time and free surface temperature—parametric study

Interfacial Air

The actual thickness of the interstitial air layer between the polymer sheet and the mold is unknown. Arithmetically, Equation 5.44 is used with two interfacial temperatures, T_{i1} being the polymer surface temperature at the polymer/air interface and T_{i2} being the mold surface temperature at the air/mold interface. With some manipulation, these interfacial temperatures are related to the interior plastic and mold temperatures, T_p and T_m , respectively.

$$k'_p = k_p/\Delta x_p; k'_i = k_i/\Delta x_i; k'_m = k_m/\Delta x_m \quad (5.55)$$

$$k''_i = k'_i/(k'_i + k'_p); k''_p = k'_p/(k'_i + k'_p) \quad (5.56)$$

$$k''_m = k'_m/(k'_m + k'_i); k''_{i,m} = k'_i/(k'_i + k'_m) \quad (5.57)$$

$$T_{i1} = \frac{k''_p \cdot k''_m}{(1 - k''_i \cdot k''_{i,m})} \cdot T_m + \frac{k''_p}{(1 - k''_i \cdot k''_{i,m})} \cdot T_p \quad (5.58)$$

$$T_{i2} = \frac{k''_m}{(1 - k''_i \cdot k''_{i,m})} \cdot T_m + \frac{k''_{i,m} \cdot k''_p}{(1 - k''_i \cdot k''_{i,m})} \cdot T_p \quad (5.59)$$

Table 5.7 Parametric Study of Cooling of Polystyrene Sheet to an Average Temperature of 150°F Against an Aluminum Mold Using Forced Air and Water as Coolants With an Air Interstitial Layer

(Plastic sheet thickness = 0.100 in)
(Mold thickness = 1.00 in)

| Interfacial air layer thickness (in) | Surface temperature (°F) | Plastic/air interfacial temperature (°F) | Time to cool (s) |
|--------------------------------------|--------------------------|--|------------------|
| 0 | 171.2 | 77.1 | 19.2 |
| 0.0001 | 170.4 | 78.2 | 19.5 |
| 0.0010 | 165.8 | 86.9 | 21.9 |
| 0.0020 | 162.1 | 94.9 | 24.2 |
| 0.0030 | 158.8 | 101.2 | 26.5 |
| 0.0050 | 153.8 | 110.7 | 30.8 |
| 0.0080 | 149.4 | 120.5 | 36.3 |
| 0.0100 | 147.2 | 124.9 | 39.7 |

The numerical solution to the coupled transient heat transfer equations proceeds as before, using standard finite difference equations. Table 5.7 shows the results of one parametric study. As redone in Fig. 5.17 for this specific study, the overall cycle time

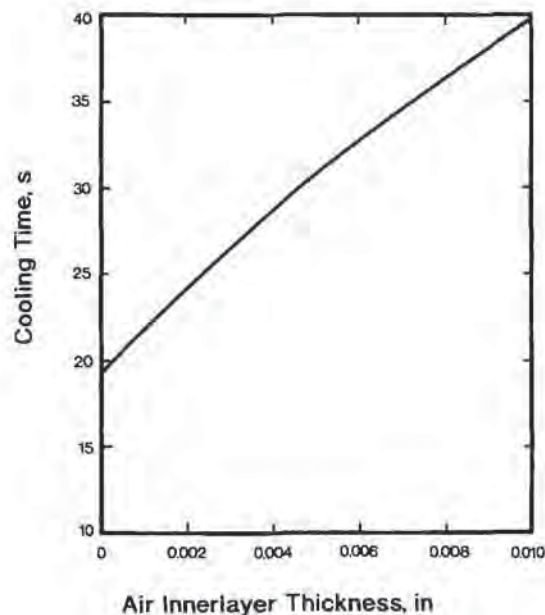


Figure 5.17 The effect of trapped air gap thickness on cooling time—parametric study

increases with interstitial layer thickness in a power-law fashion. Example 5.12 shows another way in which this arithmetic can be used in thermoforming.

Example 5.12 Finding Air Bubbles

Can infrared scanning detect an air bubble in an opaque plastic sheet while it is in contact with the mold surface?

Consider the database used in the parametric study of Table 5.7. Assume the gap between the plastic and the mold in the air bubble is 0.005 in, Fig. 5.18. The bulk of the plastic, in intimate contact with the mold surface, reaches an average sheet temperature of 150°F in 19.2 s. At that time, the free sheet surface temperature is 171°F. From the computer model at 19.2 s, the average temperature in the plastic over the air bubble is 185°F, the temperature of the polymer/air bubble interface is 128°F and the surface temperature of the plastic over the air bubble is 191°F. The 20°F temperature difference in plastic free surface temperature should be easily detected with a standard infrared scanning device.

5.7 Shrinkage

As with all materials, plastics increase in specific volume or decrease in density with increasing temperature¹. The specific volume of any polymer changes in slope with temperature at the glass transition temperature (Fig. 5.19). The specific volume of a crystalline polymer shows a distinct discontinuity in slope during melting. The

¹ Volumetric change at thermodynamic equilibrium, V_e , the result of increased molecular motion, such as rotation and reptation, is related to the coefficient of thermal expansion, COE, in the following way. Volumetric change is a function of temperature and pressure, according to:

$$dV = \left(\frac{\partial V}{\partial T} \right)_P dT + \left(\frac{\partial V}{\partial P} \right)_T dP \quad (5.60)$$

Rearranging:

$$\frac{dV}{V} = k dT - \beta dP \quad (5.61)$$

$$k = \left(\frac{\partial \ln V}{\partial T} \right)_P; \quad \beta = - \left(\frac{\partial \ln V}{\partial P} \right)_T \quad (5.62)$$

where k is the volume expansivity or coefficient of thermal expansion, $k \equiv \text{COE}$, with units of temperature⁻¹, and β is the isothermal or bulk compressibility, with units of pressure⁻¹. Thermal expansion is usually restricted to dimensional changes of the polymer over a temperature range in which the polymer has no thermodynamic transitions. Typical values for coefficients of thermal expansion of many polymers and some mold materials are given in Table 5.8.

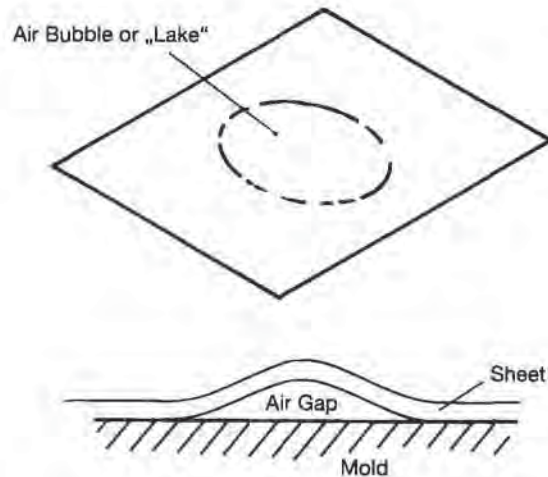


Figure 5.18 Schematic of air bubble or lake in molded part

volumetric change in the polymer during cooling from the forming temperature to room temperature is called “shrinkage”. All polymers shrink when cooled, regardless of the process. Shrinkage occurs in thermoforming when the hot polymer sheet is cooled against a rigid mold. There are two general types of shrinkage:

- Unconstrained shrinkage, sometimes called isotropic shrinkage. The formed part decreases uniformly in dimension to the densities shown in Fig. 5.19. The final part is said to be in thermodynamic equilibrium.
- Constrained shrinkage. The formed part is constrained from shrinking in at least one direction. The final part density may not achieve the thermodynamically equilibrated value until some time after the part has been removed from the mold and trimmed from its web.

Unconstrained Shrinkage

Crystalline polymers heated above their melt temperatures typically have greater unconstrained shrinkage values than amorphous polymer, as seen in Fig. 5.19 and Table 5.9 [16]. This figure shows the difference in volumetric change between an amorphous and a crystalline polypropylene. The volumetric change is converted to isotropic linear dimensional change as follows. Volumetric shrinkage, S_v , is defined as [17]:

$$S_v = \frac{(V_m - V_r)}{V_m} = 1 - \frac{V_r}{V_m} \quad (5.63)$$

Table 5.8 Coefficients of Thermal Expansion For Plastics
[ASTM D 696]

| Material | Thermal expansion (solid) | |
|----------------------------|---------------------------|--------------------|
| | (°F) ⁻¹ | (°C) ⁻¹ |
| ABS | 60–130 | 35–70 |
| ABS/PVC | 50–90 | 30–50 |
| ABS/PC | 70 | 40 |
| 20% GR ABS | 20 | 10 |
| POM acetal copolymer | 60–85 | 35–45 |
| Cast PMMA | 50–90 | 30–50 |
| Extruded PMMA | 50–90 | 30–90 |
| Ethyl cellulose | 100–200 | 55–110 |
| Cellulose acetate | 80–180 | 45–100 |
| Cellulose butyrate | 110–170 | 60–95 |
| Cellulose propionate | 80–120 | 45–65 |
| PCTFE | 35–70 | 20–40 |
| PVDF | 70–140 | 40–80 |
| PTFE | 70–120 | 40–65 |
| Polyamide 6 (PA 6) | 80 | 45 |
| Polyamide 66 (PA 66) | 80 | 45 |
| Polybutylene | 125–150 | 70–85 |
| Polycarbonate | 70 | 40 |
| Polybutylene terephthalate | 60–95 | 35–55 |
| Polyethylene terephthalate | 65 | 35 |
| PETG | 50–70 | 30–40 |
| Polyetherimide | 50–55 | 30 |
| LDPE | 100–220 | 55–120 |
| HDPE | 60–110 | 35–60 |
| Polyimide | 45–55 | 25–30 |
| Polymethyl pentene | 65 | 35 |
| mPPO | 40–70 | 20–40 |
| PPS | 25–50 | 15–30 |
| PP homopolymer | 80–100 | 45–55 |
| PP copolymer | 70–95 | 40–55 |
| PS—unmodified | 50–80 | 30–45 |
| FR PS—rubberized | 45 | 25 |
| SAN | 65–70 | 35–40 |
| SMA | 80 | 45 |
| Thermoplastic polyurethane | 100–200 | 55–110 |
| Polysulfone | 55 | 30 |
| Polyether sulfone | 55 | 30 |
| Thermoplastic elastomer | 85–190 | 50–105 |
| PVC—rigid | 70 | 40 |
| PVC—flexible | 70–250 | 40–140 |

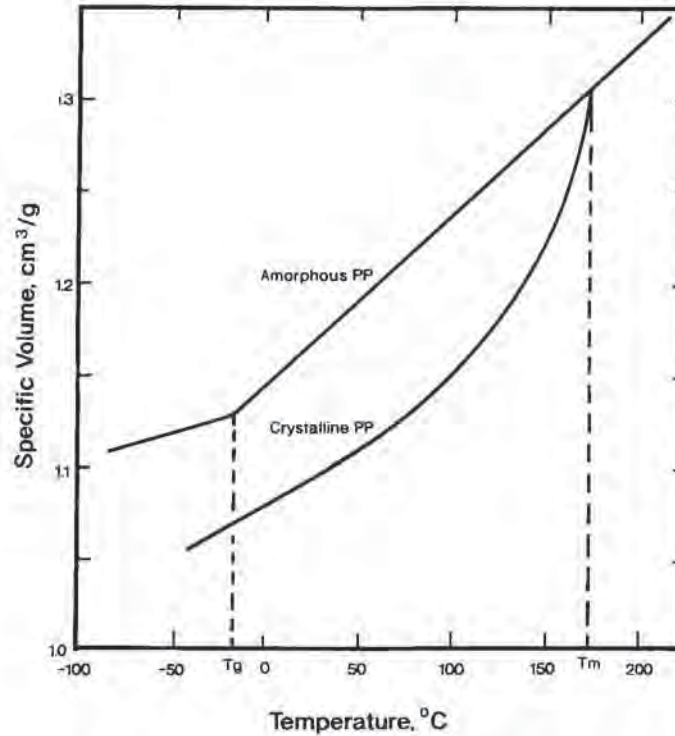


Figure 5.19 Temperature-dependent specific volume of amorphous and crystalline polypropylene, PP homopolymer [16]. Figure used with permission of copyright owner

where V_m and V_r are the specific volumes of the polymer at room temperature and the forming temperature, respectively. Linear shrinkage, S_l , is given as:

$$S_l = 1 - \frac{L_r}{L_m} = 1 - \left(\frac{V_r}{V_m} \right)^{1/3} = 1 - (1 - S_v)^{1/3} \quad (5.64)$$

When the cube root is expanded in series form, the linear shrinkage is approximated as:

$$S_l \approx \frac{S_v}{3} + \text{higher order terms} \quad (5.65)$$

Shrinkage values are usually given as ranges. The actual values depend on the temperature difference between forming temperature and room temperature. Table 5.9 gives representative shrinkage ranges for thermoformed polymers. The recommended shrinkage values are used when actual experience with shrinkage of a specific polymer is unknown. The following processing aspects influence the extent of shrinkage [18]:

- *Part Design.* Draft on both female and male surfaces influence the extent of constraint on the sheet as it cools. This is discussed below and again in the

Table 5.9 Shrinkage Values for Thermoformable Polymers

| Polymer | Shrinkage range (%) | Recommended shrinkage (%) |
|------------------------------|---------------------|---------------------------|
| ABS—Medium impact | 0.6–0.9 | 0.7 |
| ABS—Heat resistant | 0.5–0.8 | 0.7 |
| ABS—Flame retarded | 0.5–0.8 | 0.7 |
| Cellulose acetate | 0.4–0.9 | 0.5 |
| Cellulose butyrate | 0.3–0.9 | 0.4 |
| Cellulose propionate | 0.3–0.9 | 0.5 |
| Ethylene vinyl acetate (20%) | 0.3–0.8 | 0.6 |
| FEP fluoropolymer | 1.5–4.5 | 3.0 |
| PTFE fluoropolymer | 5.0–10.0 | 7.0 |
| Polycarbonate | 0.5–0.7 | 0.6 |
| Polyetherimide | 0.6–0.8 | 0.7 |
| PEEK | 0.8–1.0 | 0.8 |
| Polyethersulfone | 0.6–0.8 | 0.7 |
| LDPE | 1.5–4.5 | 3.0 |
| HDPE | 2.0–4.5 | 2.5 |
| PMMA | 0.2–0.8 | 0.6 |
| mPPO | 0.5–0.7 | 0.7 |
| PP | 1.0–2.5 | 2.0 |
| HIPS | 0.5–0.8 | 0.6 |
| PS | 0.5–0.7 | 0.6 |
| Polysulfone | 0.7–0.9 | 0.8 |
| Thermoplastic urethane | 0.5–1.0 | 0.8 |
| Flexible PVC | 10.0–15.0 | 12.0 |
| Flexible PVC (filled) | 2.0–3.5 | 3.0 |
| Rigid PVC | 0.1–0.5 | 0.3 |
| PVDC | 0.5–2.5 | 1.5 |
| Rubberized styrene (Kraton) | 0.1–0.5 | 0.3 |
| SMA | 0.5–0.9 | 0.7 |
| SAN | 0.3–0.5 | 0.5 |
| K-Resin | 0.4–0.8 | 0.7 |
| PBT | 0.2–0.4 | 0.4 |
| Amorphous PET | 0.3–0.6 | 0.5 |
| Crystallized PET | 10.0–18.0 | 12.0 |
| XT Polymer | 0.4–0.8 | 0.7 |

chapter on mold design. Male elements such as posts, bosses, partitions and gussets in female molds also influence shrinkage.

- *Part Wall Thickness Uniformity.* Thin sections cool more rapidly than heavy sections and as a result differential shrinkage will result when part wall thicknesses are not very uniform.
- *Mold Temperature.* A 10°C or 18°F difference in mold surface temperature may change shrinkage values by as much as 0.1%.
- *Depth of Draw.* Deeply drawn parts are usually characterized by nonuniform wall thickness, part regions that are formed at lower temperatures than others, and

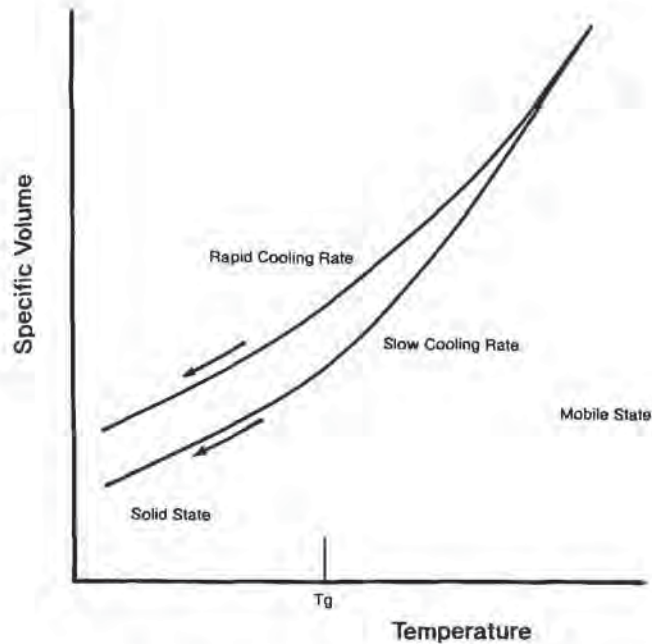


Figure 5.20 The schematic effect of cooling rate on specific volume of an amorphous polymer

regions that have contacted lower temperature plugs. All these aspects influence local shrinkage.

- *Initial Sheet Forming Temperature.* Lower forming temperatures result in lower shrinkage.

Constrained Shrinkage

Applied stresses inhibit shrinkage. When the plastic sheet is constrained against the mold surface by part design, mold temperature or applied force, complete isotropic shrinkage may be inhibited. Even if mold design and processing conditions are ideal, differential shrinkage may result due to differences in part wall thickness. When the stresses holding the sheet against the mold surface are removed, shrinkage continues. As noted, volumetric change is temperature dependent. Rapid cooling of the plastic sheet forces the polymer into a thermodynamically non-equilibrium state since there is insufficient time for molecular relaxation before the molecular mobility is inhibited. Consider the temperature-dependent volumetric change schematic of Fig. 5.20. The specific volume of the polymer is written as:

$$V = V(T;\theta) \quad (5.66)$$

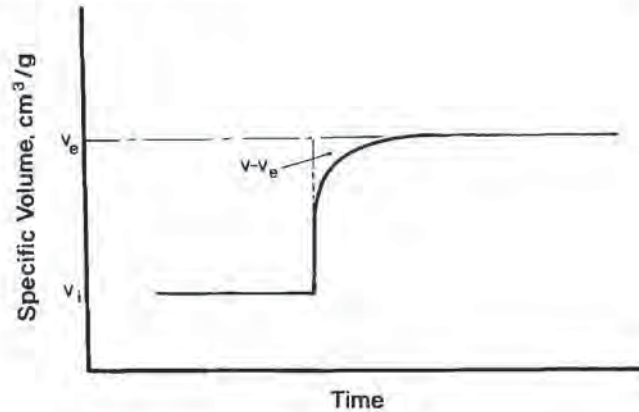


Figure 5.21 Characteristic time-dependent change in specific volume of an amorphous polymer to a step change in environmental temperature [19]. Figure used with permission of copyright owner. V_i is the initial volume. V_e is the final volume of the polymer

where T is temperature and θ is time. The differential form for the volume is:

$$dV = \left(\frac{\partial V}{\partial \theta} \right)_{\tau} d\theta + \left(\frac{\partial V}{\partial T} \right)_{\theta} dT \quad (5.67)$$

The temperature-dependent volumetric change is given as:

$$\frac{dV}{dT} = \left(\frac{\partial V}{\partial T} \right)_{\theta} + \left(\frac{\partial V}{\partial \theta} \right)_{\tau} \left(\frac{1}{r} \right) \quad (5.68)$$

where $r = dT/d\theta$, the rate of cooling. Consider a time-dependent change in specific volume in response to a step change in environmental temperature for an amorphous polymer such as polystyrene (Fig. 5.21) [19]. The initial change in specific volume is given as V_i and the time-dependent change is:

$$\left(\frac{\partial V}{\partial \theta} \right)_{\tau} = \tau(V_e - V) \quad (5.69)$$

where V_e is the equilibrium value of the specific volume and τ is the isothermal rate constant. If the constant pressure temperature-dependent equilibrium volume is written as:

$$V_e = aT + b \quad (5.70)$$

the rate of change of actual volume with temperature is given as:

$$\frac{dV}{dT} = x + \left(\frac{\tau}{r} \right) (aT + b - V) \quad (5.71)$$

Equation 5.71 shows that the maximum amount of shrinkage owing to a step change in sheet temperature for an amorphous polymer is a function of the isothermal rate constant, τ , and the degree of quench, r . The isothermal rate constant, τ , is related to material relaxation once applied stresses are removed. Stress relaxation time, λ ,

at the glass transition temperature, T_g , for most polymers is about 1000 s [20]. The stress relaxation time, λ , usually increases exponentially with increasing temperature:

$$\lambda = A \exp(\Delta E/RT) \quad (5.72)$$

where A is a pre-exponential constant and ΔE is the energy of activation. Values for ΔE are predicted for amorphous and some crystalline polymers for temperatures above T_g [21]. Extrapolation to most crystalline polymers and to temperatures below T_g is unwarranted. The isothermal rate constant, τ , mirrors the stress relaxation time constant, λ :

$$\tau = K e^{-C/T} \quad (5.73)$$

where K has the units of time⁻¹ and C has the units of temperature. The solution to Equation 5.71 with Equation 5.73 substituted for τ is not available in closed form. For intense quenching, $r \rightarrow -\infty$. Thus:

$$\frac{dV}{dT} \rightarrow x \quad (5.74)$$

That is, the final specific volume change simply equals the initial instantaneous volume change. When $r \rightarrow 0$, $V \equiv V_e$. Figure 5.22 shows the effect of quenching on the final specific volume of polystyrene. Example 5.13 illustrates the time-dependency of specific volume as determined through stress relaxation. As a practical example, the effect of mold temperature on HDPE shrinkage is seen in Table 5.10 [22].

Example 5.13 Temperature-Dependent Stress Relaxation

Consider a polymer with $\Delta E \approx 40 \text{ kcal/g mol} \cdot K$. Its glass transition temperature $T_g = 100^\circ C = 210^\circ F$. Determine the stress relaxation time at $T = 80^\circ C = 176^\circ F$ relative to that at the glass transition temperature.

Taking the logarithm of Equation 5.72 yields:

$$\ln(\lambda) = \ln A + \frac{\Delta E}{RT}$$

For the two temperatures:

$$\ln(\lambda_{100}) - \ln(\lambda_{80}) = \frac{\Delta E}{1.987} \left(\frac{1}{373} - \frac{1}{353} \right) = \frac{40}{1.987} (2.681 - 2.833) = -3.058$$

$$\lambda_{80} = 21.3 \text{ times that of } \lambda_{100}$$

As noted for most polymers, $\lambda_{T_g} \approx 1000 \text{ s}$. As a result, the approximate relaxation time for PS at $80^\circ C$ is 5.9 h.

About 70% to 80% of the dimensional change due to shrinkage occurs as the sheet cools from the forming temperature to the set temperature or the heat distortion temperature at 455 kPa or 66 lb_f/in² [23]. Stabilization to final dimension may take several hours, however. Strain recovery is one of the major causes of the

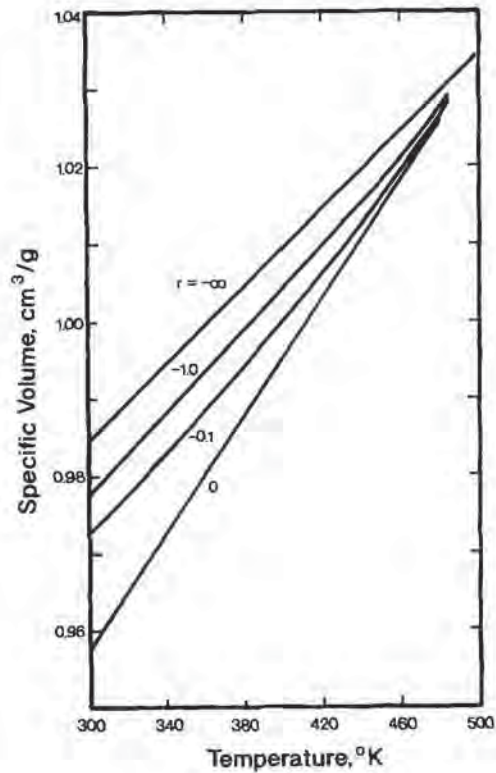


Figure 5.22 Temperature-dependent specific volume of amorphous polystyrene, PS. r is the rate of quenching. Figure used with permission of copyright owner

Table 5.10 Effect of Mold Temperature on HDPE Shrinkage Drawn into a H:D = 1 Symmetric Mold [22]

| Mold temperature (°C) | Shrinkage (%) |
|-----------------------|---------------|
| 40 | 1.8 |
| 65 | 1.9 |
| 75 | 1.9 |
| 90 | 2.4 |

long times needed to achieve stable part dimensions. Uneven strain recovery caused by nonuniform orientation in the trim area, as an example, is the major cause of long-term part distortion and warping [18]. In difficult cases, 24 h annealing at temperatures approaching mold temperature or maximum part use temperature prior to trimming can reduce warping.

Shrinkage can cause serious part removal problems when forming onto male molds. Draft angles are estimated from:

$$\theta_{\text{draft}} = \tan^{-1} (2 \times \text{shrinkage fraction}) \quad (5.75)$$

Example 5.14 shows the difference in recommended draft angles for amorphous and crystalline polymers [24]. For amorphous plastics, draft angles can be as small as $\frac{1}{2}$ degree to 1 degree. For crystalline polymers, it should be greater than 2 degree to 3 degrees. Female portions of molds require no draft if smooth and $\frac{1}{2}$ degree if textured. Draft angles are also discussed in Chapter 6 on mold design.

Example 5.14 Draft Angles for Amorphous and Crystalline Polymers

A mold designed for PS has recently been used to run PC. Are the draft angles correct? Can this mold be used to run POM, acetal? POM has a recommended shrinkage value of 3.0%.

From Table 5.9, the recommended shrinkage values for both PS and PC are 0.6%. Therefore if the draft angles for PS were initially correct, they are correct for PC.

To estimate draft angles for POM, consider Equation 5.75:

$$\theta_{\text{draft}} = \tan^{-1} (2 \times \text{shrinkage fraction})$$

For PS and PC, the recommended draft angle is:

$$\theta_{\text{draft}} = \tan^{-1} (2 \times 0.006) = 0.7 \text{ degrees}$$

For POM:

$$\theta_{\text{draft}} = \tan^{-1} (2 \times 0.03) = 3.4 \text{ degrees}$$

The original draft angles are too small for POM.

5.8 Trimming

There are many acceptable ways of efficiently separating formed parts from the surrounding plastic. Thin-gage parts are usually trimmed automatically. Very heavy-gage parts are trimmed manually. Medium-gage and heavy-gage parts are usually fixtured and trimmed manually or with computer-aided robots. Routers, water-jets and lasers are used for automatic trimming. As discussed below, the cutting surface must be fed at a fixed rate in a plane perpendicular to the cutting direction. Prototype parts are usually trimmed manually with routers and bandsaws. Very thin parts can be trimmed with a paper cutter or hand scissors.

Typical trimming devices are shown in schematic in Fig. 5.23. The trimming devices include:

- Manual knives, including
 - Bread knives for low-density foams,

- Linoleum knives or knives with recurving blades,
Knives with replaceable blades,
- Routers, such as
 - Hand-held, high-speed routers at 20,000 RPM with carbide router tips,
 - Table-mounted fixed-position routers,
 - Multi-axis routers,
 - Band saws,
 - Circular saws, including
 - Stationary saws,
 - Hand-held, small diameter saws,
 - Saws with toothless blades for foams,
 - Abrasive wheels,

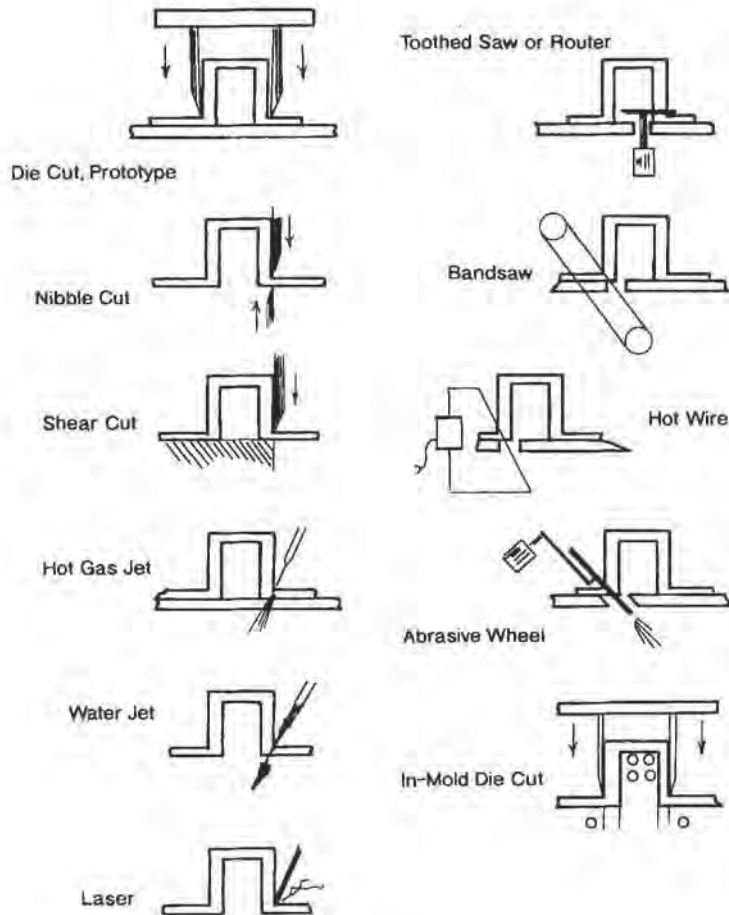


Figure 5.23 Schematic examples of various trimming methods

- Sharp-edged compression blades, including
 - Steel-rule dies,
 - Ground forged dies,
 - Machined dies,
- Guillotines, including
 - One-sided linear shear,
 - Two-sided linear shear,
- Flames,
- Lasers,
- Water jets, and
- So on.

Trimming Heavy-Gage Parts

Heavy-gage parts are usually removed from the molds with the web attached, then placed on trimming fixtures and trimmed with manual or computer-aided trimming devices. For prototype parts and a few hundred parts, hand operated routers, saws and bandsaws are commonly used. For parts having a planar trim path, simple compression or dinking presses are used (Fig. 5.24). The press consists of a steel rule die mounted in a wooden frame and mounted to the movable top platen and a ductile cutting surface mounted to the stationary bottom platen. The part and web is registered against stops on the bottom platen cutting surface and the press is closed pneumatically, mechanically or hydromechanically.

For production runs, steel rule dies are mounted in rigid steel or aluminum frames (Fig. 5.25). The trim is removed by compression. Specifications for the steel rule die are given below. For very heavy-gage plastic where the trim surface is

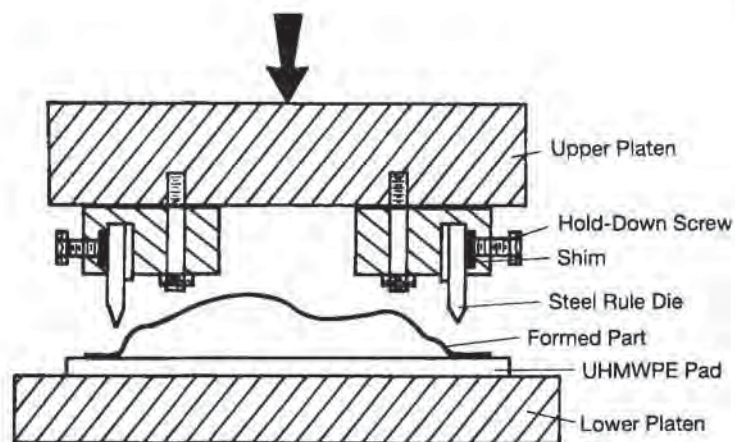


Figure 5.24 Schematic of steel rule die prototype trim or dink station

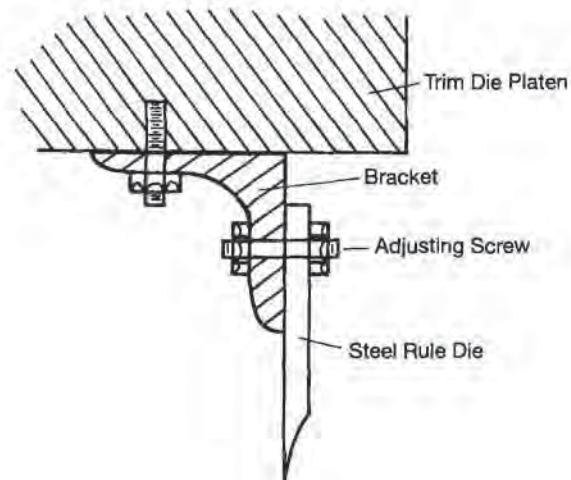


Figure 5.25 Characteristic steel rule die mounting assembly

piecewise linear, a standard sheet guillotine is used. Forged and machined dies are also growing in popularity. For longer production runs, computer-driven multi-axis routers and saws are used. Figure 5.26 shows a typical five-axis table used to drive a multiple router head. When using a multi-axis trimmer, the part to be trimmed is fastened tightly against a fixture using clips or vacuum. The cut is initially programmed by leading the router head manually around the fixture. The computer

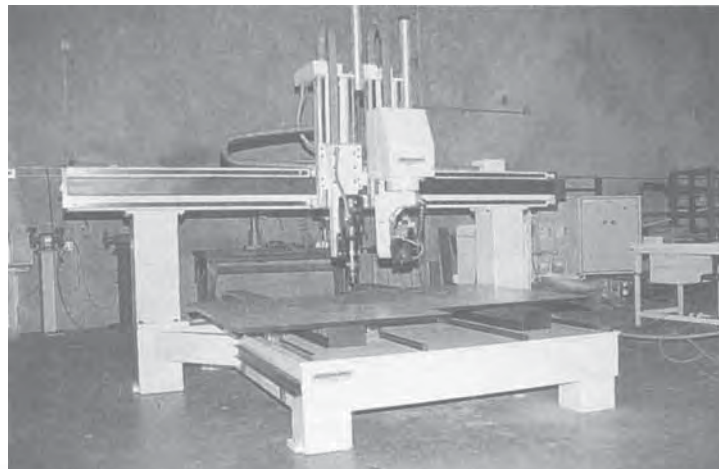


Figure 5.26 Multiple-axis computer-driven router trimmer. Figure used with permission of Thermwood Corporation

learns the correct path in this manner. Minor changes in the cutting path are usually incorporated in this first-pass program in order to fine tune the trim path.

For heavy-gage parts, trimming can also involve other post-molding operations such as:

- Drilling,
- Slotting,
- Grooving,
- Ultrasonic welding,
- Solvent welding or other forms of gluing,
- Ultrasonic insertion of fasteners,
- Grinding or milling local wall thickness to tolerance, and
- So on.

Trimming Thin-Gage Parts

Typically, many parts are simultaneously formed on roll-fed presses. Thin-gage, roll-fed parts are typically trimmed either:

- After forming but while the sheet and web are still on the mold, usually referred to as “trim in place”, or
- After the sheet and web are stripped from the mold, in a separate in-line mechanical or hydromechanical press.

These trimming systems are quite different and represent a major early decision when choosing a thermoforming line. Trim-in-place punch-and-die systems are usually considered as part of the mold design (Fig. 5.27). If the parts are completely punched from the web, methods must be used to remove the parts from the mold region as quickly and thoroughly as possible. Common methods are vacuum suction, mechanical part removal and mold rotation [25]. For vacuum suction, a vacuum tube is used for each cavity. The parts adhering to the tubes are shuttled from the press to a drop box. The drop box feeds an orienting and stacking device. In mold rotation, the mold containing the parts drops free of the web plane, then rotates to dump the parts into the drop box (Fig. 5.28). Frequently, air assist blows the parts free of the cavity. Frequently, the trim die is tabbed so that a small portion of the part remains attached to the web. As a result, the parts are not quite separated from the web in the mold. However, once the tabbed part-web structure is free of the mold, air or mechanical assists punch the parts from the web. The primary concerns with on-mold trimming are:

- Incomplete separation of all parts from the web. The parts that are still attached to the web as it exits the mold area may foul downstream machinery or web wind-up equipment. In addition, these good parts are not saleable,
- Parts that remain in some mold cavities after the removal process, due to undercuts, poor mechanical or vacuum picking, or static charge between the part and the mold cavity,

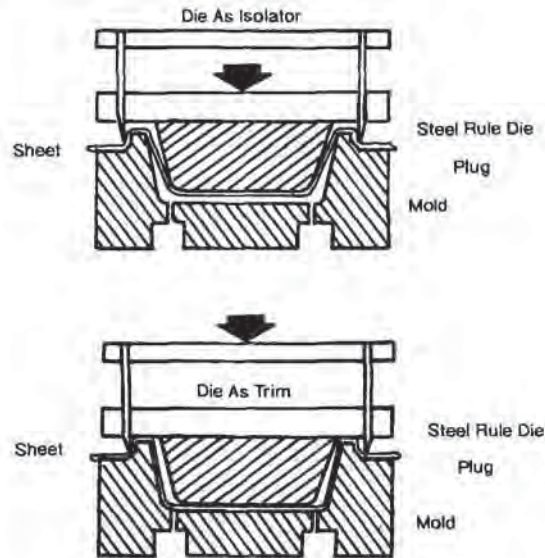


Figure 5.27 Trim-in-place or in-situ trim die. As shown, trimming is by compression

- Parts that accidentally drop back into the cavity plane after picking, and
- Dust and microfibers that remain on the mold surface. This detritus is usually transferred to as-molded parts.

Punch-and-die design and tabbing are discussed in detail below.

In most thin-gage forming operations, the web and formed part sheet is removed from the mold to an in-line trimming press. Usually the sheet is held in a vertical plane while being trimmed. As a result, the sheet is brought from the horizontal position to the vertical position by means of a hump-back or camel-back arch (Fig. 5.29). The hump-back trimming press allows the punched out parts to be collected on horizontal tables, thus simplifying the counting and bagging process. The die used in in-line trimming can be steel rule die, but is usually machined or forged. Again, punch and die design is discussed in detail below. Technically, punch and die trimming uses the shear mechanism of cutting, as described below.

5.9 Mechanics of Cutting

There are five general mechanisms of cutting (Fig. 5.30) [26]. They are:

- In-plane uniaxial compression or die-cutting,
- Mode III antiplane pure shear or nibbling and shear cutting,

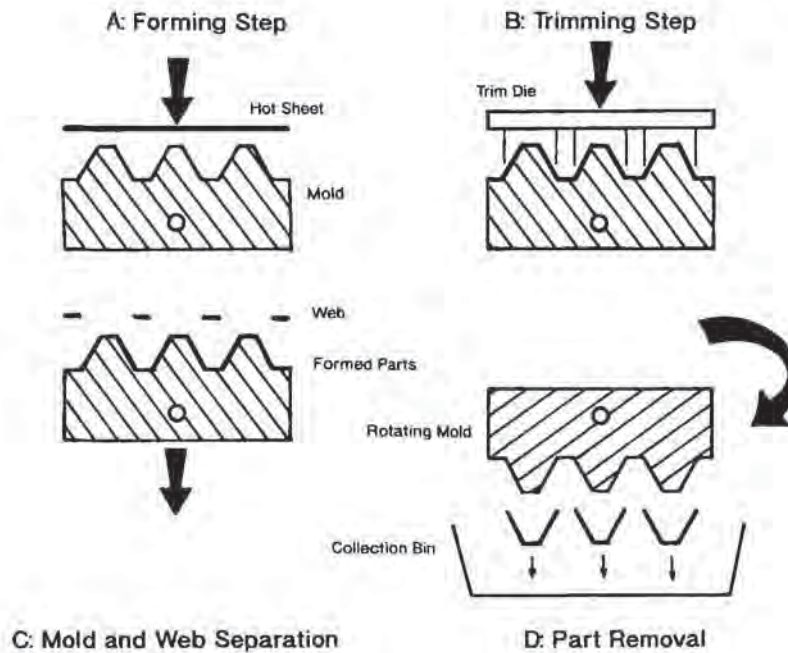


Figure 5.28 In-mold trimming with part removal by mold rotation

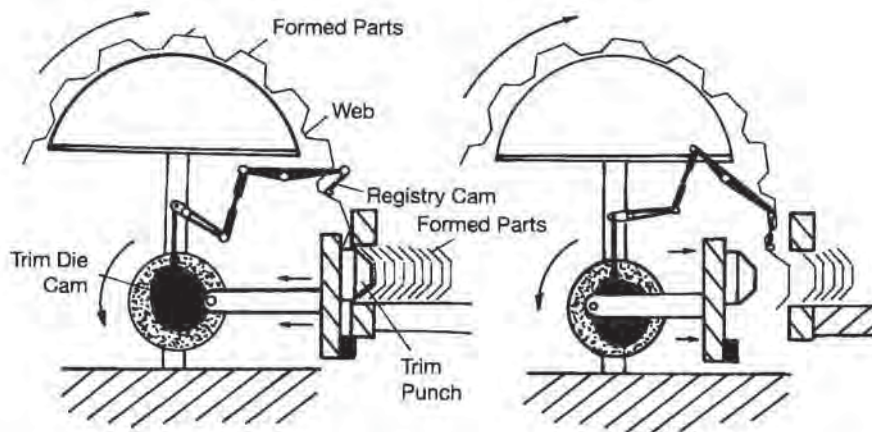


Figure 5.29 Camel-back or hump-back in-line roll-fed former trimming press with cam-operated punch-and-die trimmer. Figure redrawn from [27]

- Abrasion or abrasive cutting, grinding, filing, buffing and water jet cutting,
- Brittle tensile fracture or routing, drilling and sawing, and
- Thermal or hot knife, hot wire and laser cutting.

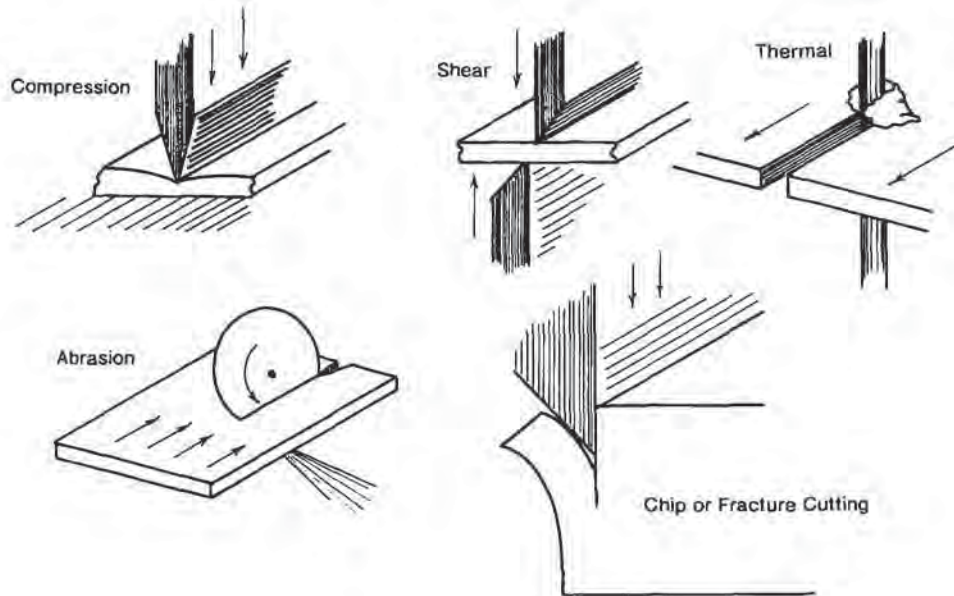


Figure 5.30 Five characteristic cutting mechanisms. Figure redrawn from [26]

Mechanical compression and shear cutting dominate the trimming industry. The characteristics of some of these mechanisms are detailed below.

The Trim Region

Typically, the trim region is relatively well-defined as the linear edge where the part ends. In certain cases, the region is demarked in the forming process as a trim channel (Fig. 5.31). The accuracy of trimming to tolerance depends on several elements:

- Local polymer shrinkage at the trim line,
- Whether the polymer is crystalline or amorphous,
- Whether the polymer continues to shrink for some time after forming but before trimming,
- Whether the polymer is tough or brittle at the trim temperature,
- The tightness of the fixture to the formed part,
- The allowable variation in part temperature at the trim station,
- The presence of registry or locating cones,
- The trim die temperature and its variation with time,
- The thickness and thickness variation of the part at the trim line,
- The allowable variation in local part wall thickness,

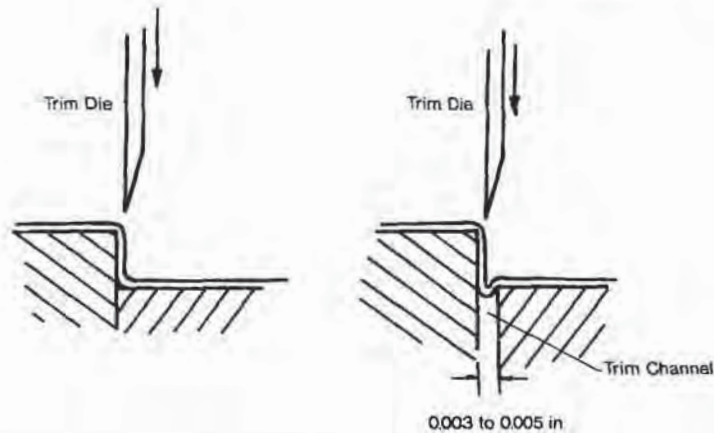


Figure 5.31 Compression (left) and shear or pinch trimming (right) configurations

- The increase in trim die temperature from the temperature at which the die gaps were set,
- The strength of the die clamping frames, and
- The amount of flexure in the die during cutting.

Registering the Trim Site

Trim registers or locators are usually designed into the mold. These are cones or truncated pyramidal structures, as shown in schematic in Fig. 5.32. For heavy-gage sheet, risers or indentations are used by the operator to positively position the sheet against the trim fixture prior to trimming. For thin-gage sheet, the locators catch indexing lugs ahead of the in-line trim die. For thin-gage sheet, peripheral locators are located on the four corners of the multicavity mold and interstitial locators are

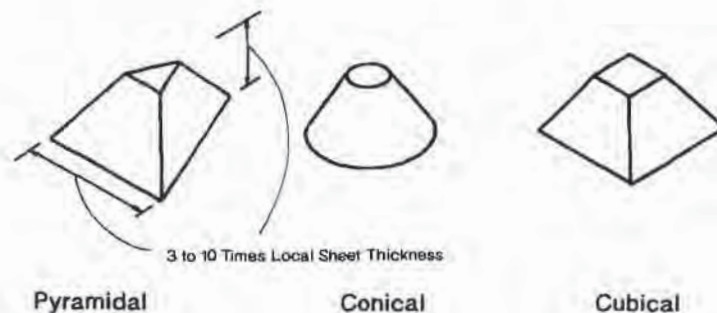


Figure 5.32 Various shapes for sheet registry on punch station

located on at least a few of the web regions between cavities. The indexing lugs on the trim press are usually adjusted to ensure full engagement of all locators on the sheet surface prior to start-up and then once or twice a shift as the various elements of the forming and trimming presses warm to equilibrium. During long production runs, periodic examination of locators after contact with trimming lugs may indicate if long-term forming problems are developing.

The actual number of trim locators is not as important as the shape. Typically, the locator riser should have substantial draft of at least 15 degrees. Truncated cones are frequently used. Truncated boxes, wedges and pyramids are used, albeit with very generous vertical side radii, where trimming tolerance is critical and where the polymer may move locally between the forming and trimming stations.

The Nature of the Cut

The toughness of the polymer at the time of trimming dictates the nature of the fracture, as discussed below. The polymer toughness is best demonstrated by the polymer resistance to applied compression stress, as delivered by a toothless trim die (Fig. 5.33). As seen, for tough, ductile or hot polymers such as HDPE, PC and FPVC, the cutting blade forces the polymer to essentially flow away from the blade tip. The tip of the cut is therefore just ahead of the blade tip. For brittle polymers such as PS, APET and PMMA, the crack propagates very quickly from the initial point of blade tip insertion. For rubber-modified polymers such as HIPS and ABS, the crack propagation is arrested by the rubber particles. Microscopic examination of

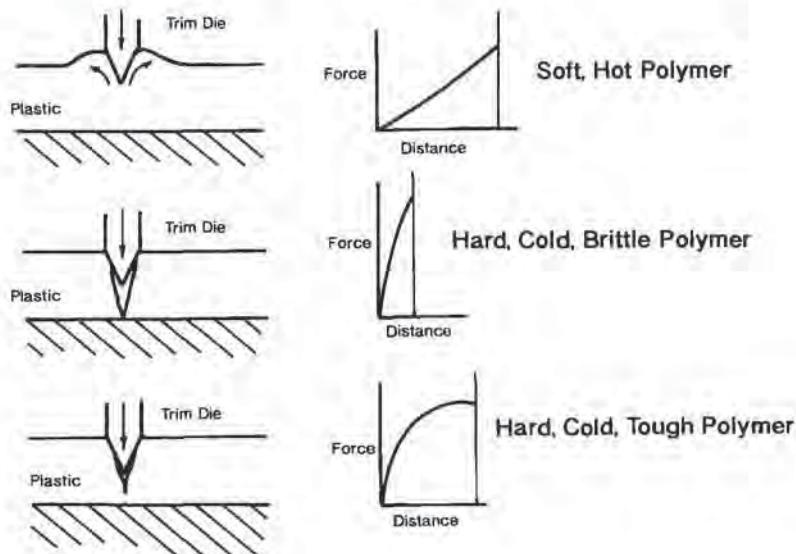


Figure 5.33 Characteristic polymer response to trim die penetration

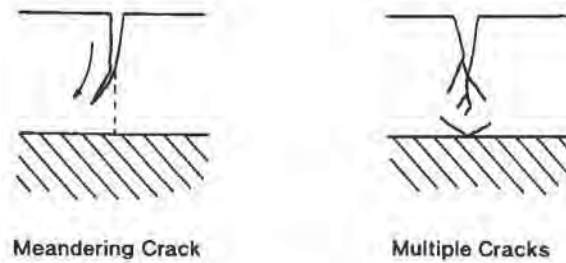


Figure 5.34 Characteristic problems in trimming of brittle polymers

the trim surface of rubber-modified polymers shows fragments of rubber and holes where the rubber particles have been torn from the crack surface. Since the crack propagates very rapidly during compression cutting of brittle polymers, the crack path can meander (Fig. 5.34). Multiple cracks can occur as the cutting blade passes through the cutting zone. These cracks generate discrete particles, which are typically called *trim dust*. Microscopic examination of these particles reveals chunky, sharp-edged particles of 1 to 50 μm in dimension. The high surface area of these high-surface energy particles implies high static attraction to surrounding ungrounded surfaces, such as the plastic parts and web structure. Although PS has the most tenacious trim dust, adhering trim dust is a problem with PMMA, APET, CPET, PC and other brittle and tough-brittle polymers. In addition to the production of micron-sized particles, edge microcracks are also formed perpendicular to the cutting plane during trimming of brittle plastics. These microcracks produce near-serrated edges under 30-power optical

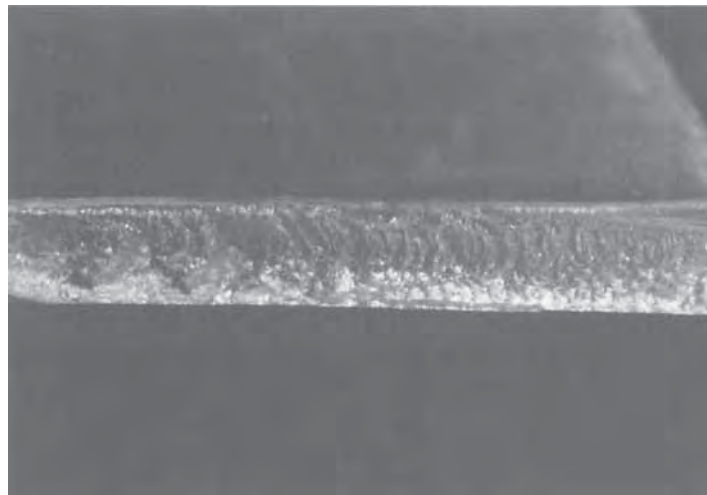


Figure 5.35 Optical microphotograph of compression cut of polystyrene, PS

micrography (Fig. 5.35). In addition to yielding an undesirable rough lip, these microcracks are sources for crack propagation or splitting into the part.

For certain ductile polymers such as PP, HDPE and CPET under certain cutting conditions, microfibers are formed. These microfibers are usually called *angel hair* or *fuzz*, are typically 50 to 150 μm in cross-sectional dimension and can be 50 mm long. Although there is no consensus as to the primary cause of microfibers [27,28], they usually occur when trimming fiber-forming or crystalline polymers. Some of the conditions that are thought to minimize microfibers include:

- Reducing the polymer temperature prior to trimming,
- Resharpener the cutting blade,
- Using a single-sided honed blade with a hardened tip,
- Increasing the rate of travel of the blade into the sheet,
- Ensuring that the cutter blade fully contacts the cutting anvil for steel rule dies,
- Ensuring that the steel rule die does not move out of plane during its travel through the sheet,
- Reducing the gap between the punch and die for in-line trimming,
- Ensuring that the blade engages the sheet at all places on the trim line simultaneously, and
- Ensuring that the only mode of cutting is compression cutting.

The dulled cutting tip is probably the most common cause of microfiber generation. Like cutter dust, microfibers are tenacious, particularly on PP and CPET. Since food containers are the primary products of these polymers, microfibers are unacceptable both from an appearance viewpoint, as they resemble human hair, and a health viewpoint, since these polymers are not approved as “food additives” [29].

Fracture Mechanics

Trimming is semi-controlled fracture mechanics. The purpose of the trimming process is to separate one piece of plastic into at least two pieces. Mechanical chipping such as drilling, abrasive sanding, multi-tooth cutting and routing, results in many granular pieces of plastic, in addition to the desired part and the web. Ideally, compression and shear cutting with toothless blades should result only in the desired part and the web. Unfortunately, such is not the case. The toughness of the polymer at the time of trimming dictates the nature of the fracture, as discussed above. The mechanics of multi-tooth and toothless cutting are relatively well known. Kobayashi [30] considers all mechanical cutting as controlled tensile fracture of the plastic. This section develops the mechanics of fracture as it pertains to trimming.

Mechanical Chipping

As a first step to understanding trimming parameters, examine the interaction of a single cutting-edge tool with the polymer (Fig. 5.36). A single cutting-edge tool is

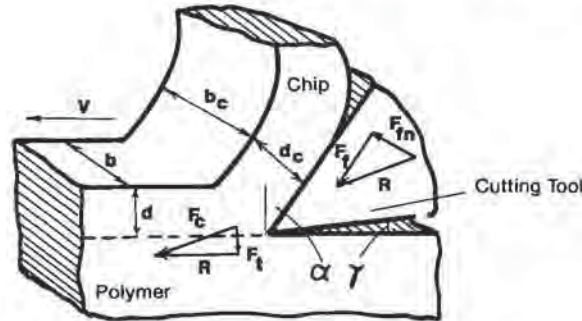


Figure 5.36 Orthogonal single-edge cutting geometry [30]. Figure used with permission of copyright owner

used in machining, turning and shaping but not in trimming of thermoformed parts. But the cutting actions of tools having multiple edges, such as saws, drills, routers and mills represent the sum of cutting actions of many single-edged tools. The physical factors affecting cutting actions on plastics are summarized in Table 5.11. Tool geometry factors are more complex for multiple-edged tools. The nature of the

Table 5.11 Factors Affecting Cutting Characteristics of Plastics¹

X = Major effect
x = Minor effect

| Factor | Effect | | | | |
|-----------------------|----------------|-----------------------|-----------|----------------|------------------|
| | Chip formation | Cut surface roughness | Tool wear | Heat generated | Gumming, burning |
| Tool design: | | | | | |
| Tool geometry*: | | | | | |
| Rake angle | X | | | | |
| Relief angle | | X | | | |
| Point radius | | | X | x | |
| Tool material | | X | | | |
| Machining conditions: | | | | | |
| Depth of cut** | X | | X | x | x |
| Cutting speed | X | | X | x | x |
| Feeding speed | X | | X | | |
| Ambient work | x | | | X | X |
| Temperature: | | | | | |
| Cooling system | | | | X | X |

¹ Adapted from [26], with permission of the author

* For single-edged cutting tools. Tool geometry effects are more complicated for multiple-edged cutting tools

** Tooth depth of cut

chip formed in cutting is used as a guide cutting tool selection, and as an indication of how cutting is proceeding (Table 5.12). For example, PS chips in multiple-edge saw cutting should be discrete and separate easily, with no evidence of softening, gumming, or threadlines.

Multiple-Edged Tool or Toothed Saw Performance

Kobayashi [26] presents extensive experimental results for plastics performance when cut with single-edge tools. A cutting force balance is shown in Fig. 5.36. When the perpendicular cutting-force component F_t is zero, the cutting tool obtains the maximum cut surface accuracy. The cutting tool rake angle at this condition is known as the *critical rake angle*. All tools should have cutting angles equal to or greater than this value. The optimum cutting conditions for nearly all polymers should produce continuous chips of uniform thickness. If the cutting depth or tooth depth is too large, discontinuous chips are produced and the cutting surface has many microcracks. If the cutting depth is too small, the plastic will heat from friction and may burn or gum the cutting tool.

Multiple-edged tool performance is determined by comparing the tooth depth of cut and the cutting speeds with single-edged tool performance. For a circular saw (Fig. 5.37), the tooth depth of cut, g , is:

$$g = \frac{v \cdot p \sin \phi}{U} \quad (5.76)$$

where U is the peripheral speed of the blade [m/min], $U = \pi DN$, D is its outside diameter [m], $D = 2R$, N is the blade speed [RPM], v is the cut-off speed or the work feed rate [m/min], and p is the tooth spacing [mm]. The angle ϕ is given as:

$$\phi = \cos^{-1} \frac{(h - b/2)}{R} \quad (5.77)$$

where h is the cut-off height or the distance between the saw centerline and the bottom of the plastic sheet [m], and b is the sheet thickness [m]. Example 5.15 illustrates these relationships.

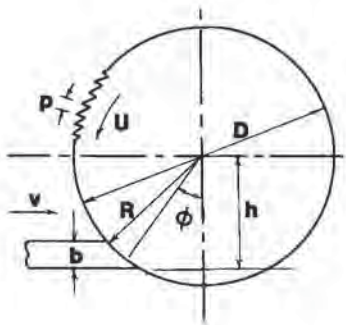


Figure 5.37 Toothed saw trimming geometry [30]. Figure used with permission of copyright owner

Table 5.12 Classification of Plastic Machining Chips¹

| Classification | Nature of chip | Thickness-to-cut depth | Cutting force fluctuation | Surface roughness | Nature of deformation | Material type | Cutting speed | Typical plastics | Comments on cause |
|---|----------------|--------------------------|---------------------------|------------------------|---------------------------|------------------------------|---------------|------------------------------|--|
| Continuous-flow | Continuous | ≈ 1 | Small | Small | Elastic | High elongation, rubber-like | Slow | PE, PTFE, FEP, PP | High elastic deformation |
| Continuous-shear | Continuous | > 1 | Small | Irregular, shear marks | Plastic | Brittle | Medium-high | PS, ABS | Slippage continuously by shear stress |
| Discontinuous-simple shear | Discontinuous | > 1 Irregular | Moderate | Irregular | Plastic | Brittle | Medium | PMMA | Plastic fracture by simple shear |
| Discontinuous-complex | Discontinuous | ≈ 1 Irregular | Large | Very irregular, wavy | Elastic | Brittle | High, sticky | PMMA, PS | Plastic fracture by shear with compressive and/or tensile stress |
| Discontinuous-crack | Discontinuous | > 1 Irregular | Very large | Hackle marks | Brittle, elastic fracture | Brittle | High | PMMA, PS | Elastic fracture, brittle fracture |
| Discontinuous-complex (shear with cracks) | Discontinuous | Chips | Very large | Gouges | Brittle fracture | Brittle | High | High modulus, Low-elongation | Plastic fracture by shear with compressive and/or tensile stress |

¹ Adapted from [26], with permission of author

Example 5.15 Cutting with a Saw

Consider a $D = 15.2$ cm or 6 in diameter saw having four teeth per in. The blade revolves at 1000 RPM. The sheet is 0.100 in or 0.254 cm thick. The cut-off height is 2 in or 5.1 cm. A minimum tooth depth, g , is selected to be 0.004 in or 0.1 mm to minimize gumming or burning. Determine the maximum feed rate.

From Equation 5.76:

$$v = \frac{U \cdot g}{p \sin \phi}$$

p is the tooth spacing or 1/4 (teeth/in) = 0.25 in or 0.637 cm. The peripheral speed of the blade, $U = \pi DN$. For this example:

$$U = \pi \cdot 15.2 \text{ cm} \cdot \frac{1000}{\text{min}} = 47,750 \text{ cm/min}$$

The angle is given from Equation 5.77 as:

$$\phi = \cos^{-1} \frac{(h - b/2)}{D/2} = \cos^{-1} \frac{(5.1 - 0.254/2)}{15.2/2}$$

$$\phi = 49 \text{ degrees}$$

Therefore:

$$v = \frac{47,750 \cdot 0.01 \text{ cm}^2/\text{min}}{0.637 \text{ cm} \cdot 0.756} = 990 \text{ cm/min} = 16.5 \text{ cm/s} = 6.5 \text{ in/s}$$

This is the maximum feed rate of this stock into the saw.

Note that the feed rate is proportional to blade speed and diameter and inversely proportional to tooth spacing. Thermal damage to the plastic is minimized by:

- Wide tooth spacing,
- Coarse toothed blades,
- Small blades,
- Low speed blades, and
- High feed rates.

However wide tooth spacing causes relatively rough cut edges with many brittle polymers such as PS, ABS, SAN, PMMA, and RPVC. Hollow-ground blades with no tooth set and wide-kerf carbide blades yield smooth cut edges. Spring-set and swag-set teeth also produce quality cut edges (Fig. 5.38).

Abrasive Cut-Off Wheel

Abrasive wheels with 30- to 200-grit surfaces produce relatively smooth cut surfaces at high cut-off rates with about one-half to one-third the heat generated by toothed

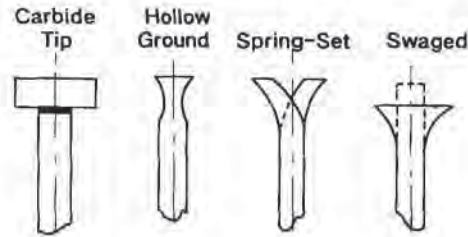


Figure 5.38 Typical saw tooth designs

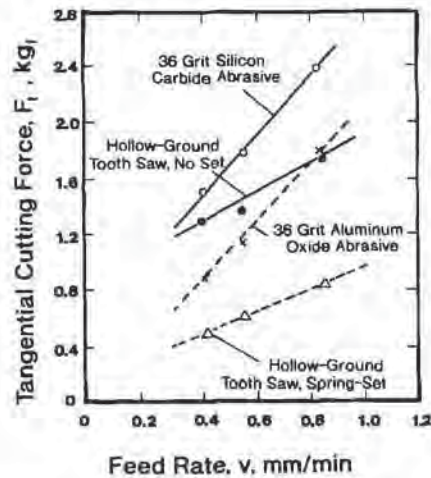


Figure 5.39 Comparison of abrasive disk and toothed saw trimming forces as function of polymer feed rate [30]. Figure used with permission of copyright owner

saws [26]. Typical abrasives include aluminum oxide or alumina, silicon carbide, tungsten carbide and diamond. Diamond abrasive wheels are the most expensive but last longest. Abrasives are held together with thermosetting binders such as phenolics, ureas and epoxies. Cutting forces are usually higher for abrasive wheels than for toothed wheels at the same feed rate (Fig. 5.39). Abrasive wheel cut surface roughness is usually smaller (Table 5.13). Finer grit wheels produce smoother surfaces but at reduced cut-off rates (Table 5.14).

The machinability of a plastic, η , is written as [26]:

$$\eta = \frac{V_m}{V_w \cdot HP \cdot S_r} \quad (5.78)$$

where V_m is the volume of polymer cut per unit time [mm^3/min], V_w is the amount of tool wear per unit time [mm^3/min], HP is power consumption [$\text{kg} \cdot \text{m}/\text{min}$], and S_r is the cut surface roughness [μm]. For properly selected cutting wheels, the amount of tool wear is essentially negligible, and machinability is redefined as:

Table 5.13 Cutting-Off Operation¹

Peripheral speed 2500 m/min

| Polymer | Surface roughness (μm) | | | |
|------------------|-------------------------------------|----|--------------|-----|
| | Abrasive wheel | | Circular saw | |
| | A | B | C | D |
| SAN | 32 | 23 | 8 | 200 |
| ABS | 28 | 16 | 10 | 200 |
| PA-610 (a nylon) | 34 | 16 | 6 | 36 |
| PC | 8 | 6 | 5 | 25 |

¹ After [26], with permission of author

Key:

A: 36 Grit silicon carbide, resinoid—medium grade

B: 36 Grit aluminum oxide, resinoid—medium grade

C: Saw, hollow-ground, zero-set teeth, 300 mm, diameter, 2 mm thick, 2.3 teeth/cm or 5.8 teeth/in, 0° rake-angle, 60° relief angle

D: Saw same as C except 0.2 mm set to teeth

Table 5.14 Finishing Operations Sanding Belt Surface Roughness¹Silicon carbide sanding belt
2000 m/min, 0.5 kg/cm² applied force, 20 min

| Polymer | Surface roughness (μm) | | Amount removed (g) | | Removal rate (mg/s) | |
|---------|-------------------------------------|----------|--------------------|----------|---------------------|----------|
| | 60 Grit | 240 Grit | 60 Grit | 240 Grit | 60 Grit | 240 Grit |
| PMMA | 36 | 2 | 295 | 28 | 246 | 23.3 |
| RPVC | 39 | 2 | 360 | 8 | 300 | 6.7 |
| PC | 41 | 2 | 235 | 9 | 196 | 7.5 |

¹ Adapted from [26], with permission of author

$$\eta^* = \frac{V_m}{HP \cdot S_f} \quad (5.79)$$

For cutting wheels:

$$\eta = \frac{v \cdot b \cdot B}{F_t \cdot U \cdot S_f} \quad (5.80)$$

where b is the sheet thickness, B is the wheel thickness and F_t is the tangential component of the cutting force. The ratio of efficiencies of abrasive and toothed wheels operating at the same feed rates and peripheral speeds is written as:

$$\eta_{\text{ratio}} = \frac{\eta_{\text{abrasive}}}{\eta_{\text{toothed}}} = \frac{B_a F_{tt} S_{ft}}{B_t F_{ta} S_{fa}} \quad (5.81)$$

Abrasive wheels are typically 2 to 5 times thicker than toothed wheels. Both produce about the same surface roughness on the cut edge at the same cut-off speeds (Table 5.13). The cut-off forces for abrasive wheels are about 2 to 5 times those for toothed wheels. Therefore:

$$\eta_{\text{ratio}} = \frac{(2 \text{ to } 5)}{(2 \text{ to } 5)} \approx 1 \quad (5.82)$$

Although the cut-off efficiencies of abrasive and toothed wheels are about the same, the cost of operating abrasive wheels is about 5 to 10% that of toothed wheels. When loaded, abrasive wheels are redressed with a gum block or a wire brush. Toothed wheels require resharpener and tooth resetting.

Toothless or Shear and Compression Cutting

Saw cutting depends on brittle tensile fracture of the plastic under the force of the tooth. In solids, Young's modulus, E , is the proportionality between pure elastic tensile stress and strain:

$$\sigma = E \cdot \epsilon \quad (5.83)$$

When a solid is sheared, the proportionality between pure shear stress and strain is the modulus of rigidity or shear modulus, G :

$$\sigma_s = G \cdot \epsilon_s \quad (5.84)$$

The bulk modulus, B , is the ratio of hydrostatic pressure to solid volume change per unit volume. Solid compressibility is the reciprocal of the bulk modulus. These moduli are related through Poisson's ratio, ν , the ratio of unit width change to unit length change [31]:

$$E = 2G \cdot (1 + \nu) = 3B \cdot (1 - 2 \cdot \nu) \quad (5.85)$$

Poisson's ratio, $\nu = 0.5$ for a material with constant volume under stress. For most plastics, $0.3 < \nu < 0.4$. Table 5.15 gives representative values for Poisson's ratio. A value of $\nu = 0.35$ is used if none is available for a given polymer. At this value, $E/G = 2.7$ and $E/B = 0.9$. Thus the expected resistance to shearing forces is only about 40% of the resistance to stretching or tensile forces. When this is applied to traditional thermoform trimming operations, shear cutting should require lower specific energy than, say, saw cutting.

Fracture Mechanics in Trimming

Fracture mechanics is the study of crack propagation in plastics under stress. There are three general types of fracture, as shown in Fig. 5.40 [32,52]. Mode I is a tensile mode where fracture surfaces are spread apart by the stress. Mode II is a shear mode, where stress forces the fracture surfaces to slide perpendicular to the advancing crack. Mode III is a tearing mode, where the fracture surfaces are forced apart

Table 5.15 Poisson's Ratio for Several Thermoformable Polymers [50]

| Polymer | Poisson's ratio |
|-------------|-----------------|
| LDPE | 0.49 |
| HDPE | 0.47 |
| PP | 0.43 |
| PIB | 0.47 |
| PS | 0.38 |
| Rigid PVC | 0.42 |
| PCTFE | 0.44 |
| PTFE | 0.46 |
| PMMA | 0.40 |
| mPPO | 0.41 |
| PPS | 0.42 |
| PET | 0.43 |
| PBT | 0.44 |
| PA 66 | 0.46 |
| PA 6 | 0.44 |
| PC | 0.42 |
| Polysulfone | 0.42 |
| Polyimide | 0.42 |

by the stress in the direction parallel to the crack [32]. Shear cutting is considered as Mode III, antiplane shear. This fracture mode is also found in torsion of notched rods. Mode I fracture, cleavage or tensile-opening, dominates classical fracture analysis since it is the most common form of material failure and since it is the easiest to study in the laboratory.

If the plastic is not held tightly, Mode III crack propagation control is difficult to maintain. The advancing crack tends to meander uncontrollably, and secondly, tangent cracks can form. The amount of force required to propagate a crack in any mode and the rate at which a stable crack is propagated can only be estimated from the extensive studies of Mode I failures. The amount of energy needed to *initiate* a crack in any polymer is substantially less than its theoretical cohesive strength. Cracks begin at flaws or defects in the polymer. They propagate when the decrease in elastic strain energy equals or exceeds the energy needed to create a new crack surface. When a tensile specimen with a small horizontal crack, a in length, is stressed, it is in plane stress. The stress needed to propagate that crack is:

$$\sigma = \sqrt{\frac{E \cdot G^*}{\pi a}} = \frac{K_c}{\sqrt{\pi a}} \quad (5.86)$$

where E is Young's modulus and G^* is the fracture energy:

$$G^* = 2(P + \gamma) \quad (5.87)$$

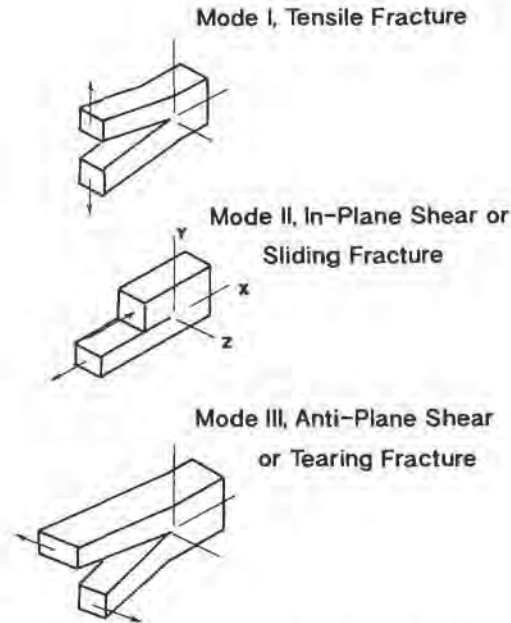


Figure 5.40 Characteristic fracture modes [32]. Redrawn Figure used with permission of Prentice-Hall Publications, Inc.

where P is the plastic work done during yielding and γ is the surface energy of the polymer. In Equation 5.86, K_c is the fracture toughness. The stress needed to *initiate* a crack is frequently far greater than that needed to *sustain* crack propagation [33]. For PMMA for example, the ratio of stress levels is about 1000. For vulcanized natural rubber, it is about 325. The plastic deformation stretching energy is usually much greater than the surface energy. For ductile plastics such as PTFE, PP, PET and TPO, $P \gg \gamma$. Even for very brittle plastics such as PS and PMMA, $P > 2 \cdot \gamma$. Example 5.16 illustrates these relative values. One measure of the fracture toughness of a polymer is the area under its tensile stress-strain curve. If the area is large, the polymer is tough. Polymers that show great plastic flow after yielding, such as HDPE, PP and PET, have high fracture toughness. If the area under the tensile stress-strain curve is small, as with PS and PMMA, the polymer is brittle. The stress level that produces fracture is analogous to the crack tip *stress intensity level* that produces sustained fracture. As noted in the second part of Equation 5.86, fracture toughness or stress intensity factor, K_c is written as:

$$K_c = f(\sigma, a) \quad (5.88)$$

Characteristically, the stress intensity factor is written as:

$$K_c = C\sigma \cdot \sqrt{\pi a} \quad (5.89)$$

Example 5.16 Fracture Energies for Ductile and Brittle Polymers

Consider vulcanized rubber and PMMA as typical of ductile and brittle polymers, respectively. Determine the relative ratio of yielding work to surface energy of each of these polymers.

The plastic work during yielding of PMMA is $P = 0.185 \text{ ft-lb}_f/\text{in}^2 = 0.211 \text{ kJ/m}^2$. The surface energy for PMMA is about $\gamma = 0.039 \text{ kJ/m}^2 = 0.0342 \text{ ft-lb}_f/\text{in}^2$. The fracture energy is given as:

$$G^* = 2(P + \gamma) = 2(0.211 + 0.039) = 0.5 \text{ kJ/m}^2 = 0.44 \text{ ft-lb}_f/\text{in}^2$$

The ratio of plastic work to surface energy, $P/\gamma = 0.211/0.039 = 5.4$. This is a strong indication of a very brittle polymer.

The plastic work for vulcanized rubber, P , is unknown. However, the fracture energy, $G^* = 13 \text{ kJ/m}^2 = 11.4 \text{ ft-lb}_f/\text{in}^2$ and the surface energy for vulcanized rubber is about $\gamma = 0.012 \text{ kJ/m}^2 = 0.010 \text{ ft-lb}_f/\text{in}^2$. The calculated value of plastic work is:

$$P = \frac{G^*}{2} - \gamma = \frac{13}{2} - 0.012 = 6.49 \text{ kJ/m}^2 = 5.67 \text{ ft-lb}_f/\text{in}^2$$

Thus the ratio of plastic work to surface energy, $P/\gamma \approx 6.49/0.012 = 567$. This is a strong indication of a very ductile polymer.

The coefficient C depends on the geometry of the crack and the surface being fractured. One example of C is given in Fig. 5.41 [32], for an edge crack of length a in a sheet of width W under uniaxial tension. For unreinforced polymers, values for K_c range from about 0.5 to 10. Typical values for K_c for a few polymers are given in Table 5.16. The fracture stress given in Equation 5.88 is written symbolically as:

$$\sigma = \frac{\text{Material Parameter}}{\text{Geometric Parameter}} \quad (5.90)$$

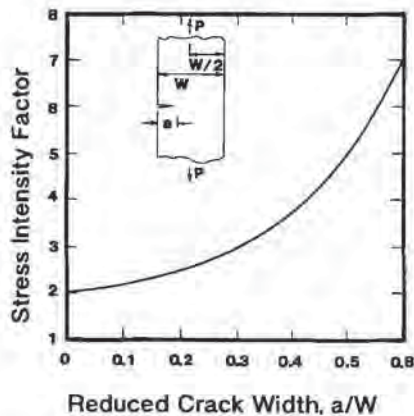


Figure 5.41 Geometric parameters for stress concentration factor for mode I, tensile fracture [32]. Redrawn Figure used with permission of Prentice-Hall Publications, Inc.

Table 5.16 Stress Intensity Factors for Some Plastics and Other Materials¹Values in parentheses obtained from $K_c = \sqrt{E \cdot G^*}$

| Materials | Young's modulus, E | | Fracture energy, G* | | Stress intensity factor, K | |
|-----------------------|--------------------|--|----------------------|--------------------------|----------------------------|------------------------------|
| | (GPa) | (1000 lb _f /in ²) | (kJ/m ²) | (ft-lb/in ²) | (MN/m ^{3/2}) | (1000 lb/in ^{3/2}) |
| Vulcanized rubber | 0.001 | 0.145 | 13 | 11.4 | (0.114) | (2.05) |
| Polyethylene | 0.15 | 21.8 | 20* | 17.5 | (1.73) | (31.2) |
| PS | 3.0 | 435 | 0.4 | 0.35 | 1.1) | 19.8 |
| HIPS | 2.1 | 305 | 15.8* | 13.8 | (5.76) | (104) |
| PMMA | 2.5 | 363 | 0.5 | 0.48 | 1.1 | 19.8 |
| Epoxy | 2.8 | 406 | 0.1 | 0.087 | 0.5 | 9.0 |
| Rubber-modified epoxy | 2.4 | 348 | 2 | 1.75 | 2.2 | 39.8 |
| FRP | 7 | 1,015 | 7 | 6.12 | 7 | 126 |
| Glass | 70 | 10,150 | 0.007 | 0.0061 | 0.7 | 12.6 |
| Wood | 2.1 | 305 | 0.12 | 0.105 | 0.5 | 9.0 |
| Aluminum | 69 | 10,000 | 20 | 17.5 | 37 | 666 |

¹ Adapted from [33], with permission of copyright holder

* J-Contour Integral. See [33: p. 82]

In the tensile Mode I, an infinite stress is needed to initiate a crack of zero length. Once the crack is propagating, the stress diminishes rapidly.

The rate of crack propagation is also important. For fatigue failure where the load is applied in cyclic fashion, the following relationship is used:

$$\frac{da}{dN} = A_f \cdot \Delta K^m \quad (5.91)$$

where N is the number of cycles, ΔK is the stress intensity factor range, $\Delta K = K^{\max} - K^{\min}$, and m and A_f are polymer material properties [33]. Some values for A_f and m are given in Table 5.17. ΔK is proportional to K_{Ic} , the fracture toughness. For many polymers [33,34], $0.5 < [\Delta K/K_{Ic}] < 0.67$. Cyclic crack propagation rate is used only as a guide to determine crack speed in Mode I tensile fracture. Cyclic fatigue crack growth occurs at substantially lower stress levels than those needed to sustain crack growth in continuous loading. In turn, this guideline can be used only as an estimate of the shear stress needed to control crack propagation in Mode III antiplane shear fracture. As noted, Mode III fracture is the apparent mode occurring during shear cutting of plastics such as guillotining, diagonal brake cutting, nibbling and paper cutting. An appropriate relationship for the rate of crack propagation, $\dot{a} = da/d\theta$ is:

$$\dot{a} = \frac{da}{d\theta} = \beta \cdot \sigma^m \cdot \alpha^{m/2} \quad (5.92)$$

where σ is the shear stress and β includes geometric factors and material constants. If the crack length ahead of the shear is to remain stable, or \dot{a} is to be constant, the

Table 5.17 Crack Propagation Parameters

$$da/dN = A_r \cdot \Delta K^m$$

da/dN units are mm/cycle
 ΔK units are $\text{MN}/\text{m}^{3/2}$
 A_r units are $[\text{MN}/\text{m}^{1/2}]^{-m}$

Note: For crystalline polymers, the general relationship is:

$$da/dN = A^* \cdot (\Delta K/E)^7 \text{ where } 0.5 < A^* < 3$$

($\Delta K/E$) units are $\text{m}^{1/2}$

| Polymer | $A_r \times 1000$ | m | Range of ΔK |
|---------|-------------------|------|---------------------|
| PS | 2.65 | 3.73 | 0.5 to 1.2 |
| PMMA | 99 | 10.0 | 0.4 to 1.0 |
| PES | 1.5 | 9.5 | 0.6 to 1.2 |
| HDPE | 0.35 | 5.22 | 1.0 to 2.5 |
| PC | 0.118 | 4.81 | 1.0 to 3.0 |
| mPPO | 0.0365 | 6.2 | 1.0 to 3.0 |
| RPVC | 0.164 | 2.2 | 0.5 to 1.0 |
| PA 66 | 0.00728 | 3.63 | 1.5 to 8.0 |
| PVF | 0.0087 | 3.2 | 1.5 to 8.0 |

rate of shear is approximately proportional to the applied force to the m th power. For RPVC in Table 5.17, $m = 2.2$ and the shear rate should increase about four times when the applied load is doubled. On the other hand, for PMMA, $m = 10$ and the shear rate should increase about four times with only a 15% increase in applied load.

Compression cutting occurs when the steel rule die is pressed perpendicularly into plastic sheet that is resting on an unyielding surface. Load compression follows the true material stress-strain curve. A modification of compression molding that employs uniaxial plane-strain compression is used to determine stress-strain curves for polymers that neck or fracture easily [35]. Compression cutting is particularly useful when the polymer yields in compression but fractures brittlely in tension or shear. RPVC, PC and PMMA are typical polymers that lend themselves well to compression cutting. Compression yield stresses are usually higher than tensile or shear yield stresses (Table 5.18). Thus more force per unit cutting area is required to die cut a plastic than to shear cut it. Comparison of typical stress-deformation curves, Fig. 5.42 [35], shows that the area under the compression curve continues to increase with increasing strain. As a result, crack propagation in compression is more stable for polymers that are brittle or neck badly. Compression cutting is the preferred method for cutting LDPE and should be considered for trimming PET, PA or nylon, POM or acetal, low-density foams and thin-gage OPS and PMMA.

For a very brittle polymer being trimmed with a very sharp, wide die, a perpendicular crack is created ahead of the blade. The crack can propagate as a Mode I fracture, as shown in schematic in Fig. 5.43. The crack can be uncontrollable with an irregular reverse side cut surface, microcracking and crazing. The stress required to cut through the material is given in terms of the stress intensity factor,

Table 5.18 Yield Stresses and Cutting Shear Stresses

| Polymer | Tensile yield stress | | Compressive stress (yield) | | Flexure stress (yield) | | Sharp knife cutting stress | |
|---------|----------------------|--|----------------------------|--|------------------------|--|----------------------------|--|
| | (MPa) | (1000 lb _f /in ²) | (MPa) | (1000 lb _f /in ²) | (MPa) | (1000 lb _f /in ²) | (MPa) | (1000 lb _f /in ²) |
| HDPE | 28 | 4 | 20 | 3 | - | - | - | - |
| LDPE | 10 | 1.5 | - | - | - | - | - | - |
| PP | 34 | 5 | 41 | 6 | 45 | 6.5 | - | - |
| PET | - | - | 83 | 12 | 98 | 14 | - | - |
| PC | 62 | 9 | 86 | 12.5 | 94 | 13.5 | - | - |
| RPVC | 41 | 6 | 69 | 10 | 77 | 11 | 91-126 | 13-18 |
| PS | - | - | 83 | 12 | 77 | 11 | 110 | 15.8 |
| HIPS | 21 | 3 | - | - | 35 | 5 | - | - |
| ABS | 34 | 5 | 41 | 6 | 35 | 5 | - | - |
| mPPO | 48 | 7 | 76 | 11 | 84 | 12 | - | - |
| PA 66* | 55 | 8 | 103 | 15 | 119 | 17 | - | - |
| CA | - | - | - | - | 42 | 6 | 60 | 8.6 |
| CAB | - | - | - | - | 35 | 5 | 45-50 | 6.4-7.1 |
| CAP | - | - | 21 | 3 | 28 | 4 | - | - |
| PMMA | - | - | 83 | 12 | 91 | 13 | - | - |
| POM** | 69 | 10 | 110 | 16 | 98 | 14 | - | - |

* Dry nylon

** Polyoxymethylene, acetal homopolymer

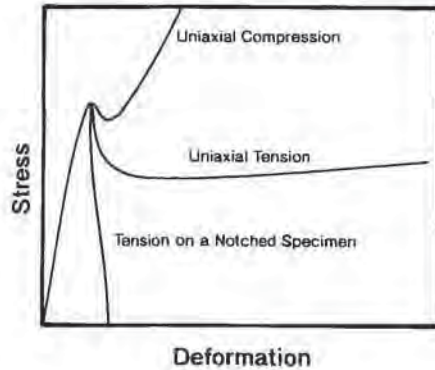


Figure 5.42 Stress-strain curves for various types of fracture in a notch-sensitive ductile polymer [35]. Figure used with permission of John Wiley & Sons, Inc.

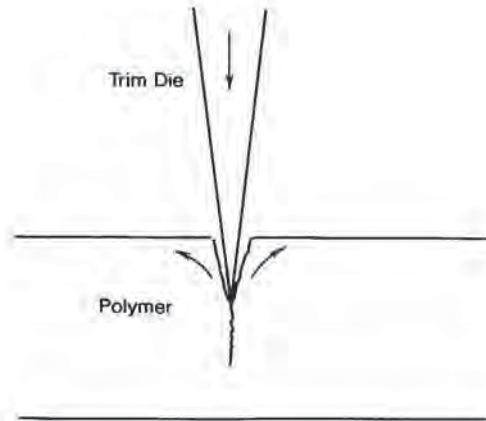


Figure 5.43 Characteristic mode I fracture with wedge effect of trim die into brittle polymer sheet

Equation 5.89, and is frequently much less than the compression yield strength. One way of partially controlling crack propagation in very brittle polymers such as PS and PMMA is to place a very slightly resilient mat between the plastic sheet and the table. Very hard rubber or heavy-gage UHMWPE works well. If the plastic or rubber is too soft, the plastic may bind the cutting blade and chipping, splitting and uncontrolled fracture may be aggravated.

Typically the force required to cut through a polymer sheet is proportional to the cut length and the sheet thickness to some power a ,

$$\text{Force} \propto (\text{cut length}) \times (\text{sheet thickness})^a \quad (5.93)$$

Since the crack proceeds the cutting blade tip, the force required to cut through a brittle polymer may be only weakly dependent on sheet thickness.

For a ductile polymer and a blunt die, the deformation stress is obtained directly from the stress-strain curve. Since most polymers strain harden to some extent in

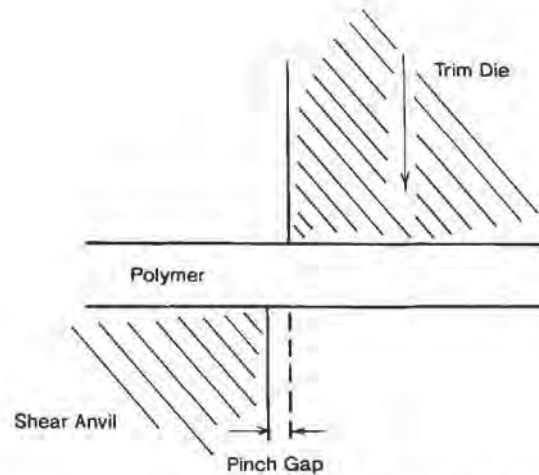


Figure 5.44 Characteristic combined shear and compression punch- and die-cutting of tough or ductile polymer

compression, the force required to cut through a tough polymer increases with the depth of cut [36] and $a \approx 1$:

$$\text{Force} \propto (\text{cut length}) \times (\text{sheet thickness})^1 \quad (5.94)$$

For ductile polymers, a combination shear and compression die cut is used (Fig. 5.44). With this type of cut, the lower force of a shear cut is combined with the stable crack propagation at increasing stress-strain of a compression cut. Heavy-gage plasticized PVC or FPVC, HDPE and PP are cut in this way. Combination shear cutting forces for several cutter blade designs are shown in Figs. 5.45 and 5.46 [37] for RPVC and PS, respectively. It is apparent that cutter force is proportional to sheet thickness, or $a = 1$ in Equation 5.93. Cutting forces for dull knives at 20°C or 68°F are measurably higher for polymers that yield, such as PVC, as seen in Table 5.19. These values compare well with blanking force guidelines for thin-gage sheet (Table 5.20) [38]. Values for effective shear stress or cutting force per unit thickness and cutter length are about the same as compressive yield stress values in Table 5.18. Cutting forces at 60°C or 140°F are about 10% lower than those at 20°C or 68°F.

Nibbling

Nibbling is a cyclic trimming process. An estimate of nibbling force is made from Mode I tensile fracture crack propagation. Example 5.17 illustrates this. As noted earlier, the force required to initiate a crack is as much as 1000 times greater than that needed to sustain it. Nibbling is a process requiring crack initiation at each stroke. Further additional force is required to overcome friction between the nibbler

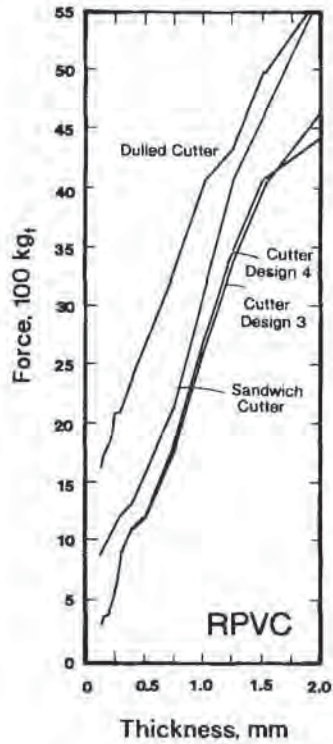


Figure 5.45 Experimental sheet thickness-dependent shear cutting force for rigid polyvinyl chloride, RPVC, for several trim dies [37]

Table 5.19 Shear Cutting Forces Data from Figs. 5.45 and 5.46 [37]

Blade length = 10 in or 250 mm
Sheet thickness = 0.039 in or 1 mm

| Polymer | Blade design | Total force | | Cutting stress | |
|---------|--------------|--------------------|------|----------------|--|
| | | (kg _f) | (lb) | (MPa) | (1000 lb _f /in ²) |
| PVC | # 3 | 2600 | 5720 | 104 | 15.1 |
| | # 4 | 2710 | 5960 | 108 | 15.8 |
| | Sandwich | 3100 | 6820 | 124 | 18.0 |
| | Dull* | 3900 | 8580 | 156 | 22.6 |
| PS | # 3 | 2680 | 5900 | 107 | 15.5 |
| | # 4 | 2680 | 5900 | 107 | 15.5 |
| | Sandwich | 2680 | 5900 | 107 | 15.5 |
| | Dull** | 2900 | 6380 | 116 | 16.8 |

* Exhibits a "zero thickness" resistance of 1360 kg_f or 2990 lb_f, or an equivalent shear stress of 54 MPa or 7900 lb_f/in²

** Exhibits a "zero thickness" resistance of 460 kg_f or 1000 lb_f, or an equivalent shear stress of 18 MPa or 2700 lb_f/in². In addition, the force-thickness curve is nonlinear

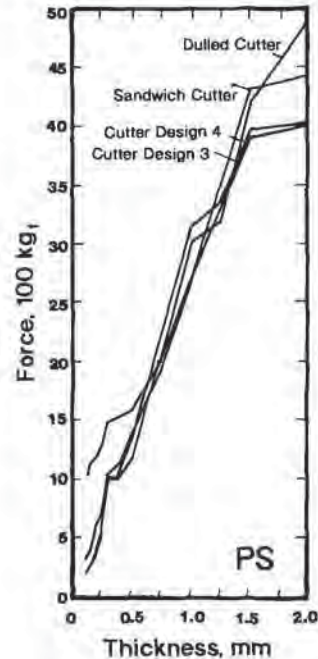


Figure 5.46 Experimental sheet thickness-dependent shear cutting force for polystyrene, PS, for several trim dies [37]

Table 5.20 Blanking Force Guidelines for 0.25 mm or 0.010 in Sheet [38]

| Nature of polymer | Type of polymer | Force | | Total force in 10 in or 25 cm | |
|-------------------|--------------------------|-----------------------|-----------------------|-------------------------------|--------------------|
| | | (kg _f /cm) | (lb _f /in) | (kg _f) | (lb _f) |
| Soft | Polyolefins, cellulose | 27 | 150 | 680 | 1500 |
| Medium | Flexible PVC | 46 | 250 | 1140 | 2500 |
| Hard, Tough | OPS, PET, PS, PMMA, RPVC | 91 | 500 | 2280 | 5000 |

blade and the plastic and to push the cut-off plastic piece from the kerf. As with compression cutters, a good first approximation of the value of the cutting-off shear stress is the yield strength value of the plastic (Table 5.18).

Example 5.17 Nibbling Force for PMMA

Thin-gage PMMA sheet, 0.025 in or 0.1 cm thick, is to be cut in one cycle. Determine the force needed to sustain a crack. For PMMA, $A_r = 0.1$ (MN/m^{1/2})^{-m} and $m = 10$.

From Equation 5.91, the stress intensity factor range is obtained:

$$\Delta K = (da/dN)^{1/m} \cdot A_r^{-1/m}$$

Now $da/dN \geq 0.1$ cm. Assume $da/dN \equiv 1$. Then $\Delta K = 1.26 \text{ MN/m}^{1/2}$. If $\Delta K = 0.5 K_c$, the critical stress intensity factor for crack propagation and $C = 2$, the tensile stress needed to sustain the crack is given as:

$$\sigma = \frac{K_c}{C} \cdot \sqrt{\pi a} = \frac{1.26 \cdot \sqrt{\pi \cdot 0.001}}{0.5 \cdot 2} = 0.071 \text{ MN/m}^2 = 10.3 \text{ lb}_f/\text{in}^2$$

This is the tensile stress needed to propagate the crack. The tensile yield stress of PMMA is about 45 MN/m^2 or $8500 \text{ lb}_f/\text{in}^2$. Since nibble-cutting should require about the same expenditure of force as compression-shear cutting, the apparent force needed to sustain a crack in PMMA is only about 0.1% of the total force needed to cut the plastic.

Brittleness, Orientation and Trimming Temperature

Many brittle plastics exhibit uncontrolled fracture, secondary crack propagation, reverse-side chipping, crazing and splitting when compression or shear cut. Brittle fracture occurs when the *brittle strength* of the polymer is less than its yield strength. The brittle strength of a polymer below its glass transition temperature, T_g , is weakly dependent on temperature over a wide range of temperature, 100°C or more. On the other hand, polymer yield stress is essentially a linearly decreasing function of temperature (Table 5.21) [35]. As the polymer temperature increases, the probability of fracture at stresses below the yield stress decreases. The problems associated with brittle fracture trimming diminish as well. At elevated temperatures approaching T_g , the polymer is ductile and high-speed cutting-off techniques that depend on brittle fracture crack propagation such as routing and sawing, become inefficient.

Table 5.21 Temperature Effect on Yield Stress For Various Polymers¹

| Polymer | Linear region | | Temperature coefficient of yield stress | |
|---------|---------------|--------------|---|---|
| | (°C) | (°F) | (MPa/°C) | (lb _f /in ² · °F) |
| PMMA | 50 to 100 | 122 to 212 | 0.97 | 78.2 |
| PTFE | -250 to -140 | -420 to -220 | 0.85 | 68.5 |
| PE* | -60 to 20 | -76 to 68 | 0.82 | 66.1 |
| RPVC | -80 to 60 | -112 to 140 | 0.80 | 64.5 |
| PP | -40 to 20 | -40 to 68 | 0.74 | 59.6 |
| PA 66 | -100 to 60 | -150 to 140 | 0.74 | 59.6 |
| APET | -20 to 60 | -4 to 140 | 0.49 | 39.5 |
| PC | -40 to 120 | -40 to 250 | 0.32 | 25.8 |

¹ Adapted from [35], with permission of copyright owner

* Chlorinated polyethylene

Thermoformed shapes frequently have high degrees of orientation in the trim areas. Part shape can enhance nonuniform orientation. Cutting relieves local stresses. Although this aids crack propagation to some degree, particularly in shear cutting, it can also cause:

- Nonuniform part dimensions,
- Binding of the cutting tools,
- Part warping, and
- Part distortion.

Secondary fracture effects such as crazing can result. Uncontrolled crack propagation can proceed in the orientation direction rather than in the desired cut path, or the crack can meander. This results in splitting and splintering, dust and angel hair. Highly nonuniformly oriented parts of brittle polymers are frequently formed on hot molds and then the parts with the trim attached are partially annealed prior to trimming. The trim is then cut away while the parts are still warm. Heavy-gage amorphous polymers such as RPVC and ABS and easily oriented crystalline polymers such as PA 66 and PP benefit by this trimming approach.

As a general rule for all polymers, dust and angel hair problems and part warpage and distortion may be minimized by increasing the part temperature at the time of trimming. Increasing trim die temperature is usually ineffective. Part of the difficulty in trimming with hot dies is in conduction heat transfer from the heating source to the cutting tip. The die is envisioned as a metal fin. The effectiveness of conduction heat transfer to fins decreases rapidly with the length-to-thickness ratio of the fin [39]. This is due primarily to convection heat transfer to the cool ambient air:

$$\eta_r = \frac{\tanh mL}{mL} \quad (5.95)$$

where mL is given as:

$$mL = \sqrt{\frac{2h}{kt}} L \quad (5.96)$$

where h is the convection heat transfer coefficient between the heated trim die and the ambient air (Table 5.4), k is the thermal conductivity of the trim die steel, L is the distance between the heater and the cutting tip and t is the thickness of the trim die. As is apparent in Fig. 5.47 [40], the energy efficiency of heated dies decreases rapidly with L/t ratio, for both rectangular and tapered dies. In words, since heated dies are very inefficient heat transfer devices, it is usually difficult to maintain cutting tips at the proper temperature.

5.10 Steel Rule Die

As noted, the steel rule die is the most common method of cutting prototype sheet having thickness less than about 0.100 in or 2.5 mm. Steel rule dies are most effective

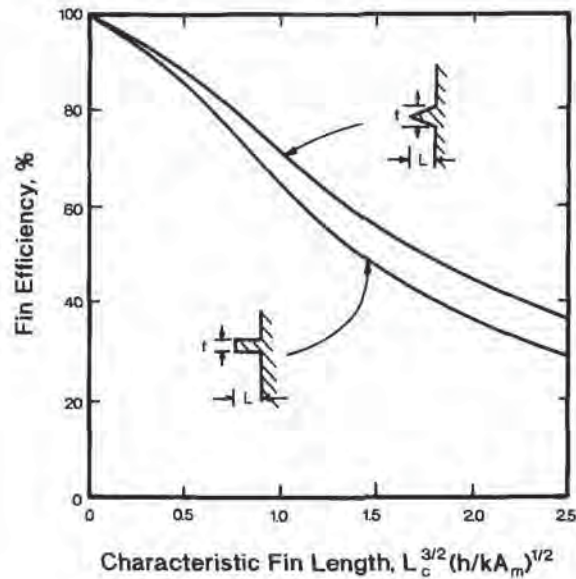


Figure 5.47 Heat transfer efficiency for heated dies with rectangular and triangular cross-sections. L is the length of the die from the heating source and A is its cross-sectional area. Redrawn from [40]

if the sheet thickness at the point of trimming is less than about 0.025 in or 0.64 mm. Typically, the steel used in thermoforming trim dies is A2D2. Depending on the method of hardening, this steel has a hardness of 48 to 52 Rc. It is considered a hard steel. The steel hardness range depends on the particular application, the polymer and the ease of sharpening the die:

- Steels with 45 to 48 Rc hardness are considered maleable or peenable. They are easily bent and sharpened and are easily dulled by cutting against compression plates having equal hardness.
- Steels with 48 to 52 Rc hardness hold excellent edge but are not normally honed. They form the base stock for advanced hardening techniques. Steels with this hardness dull when cutting toughened polymers.
- Steels with 52 to 56 Rc hardness are considered hardened steels. They hold excellent edge even when single- and double-honed, as described below. If they are chipped or dulled, they are difficult to resharpen but can be honed.
- Steels with 56 Rc and higher hardness are usually produced by locally hardening lower Rockwell steels. Dies with 60 Rc hardness are used to trim filled, reinforced, and composite thermoformed parts.

Although there are many ways of hardening steel, steel rule dies are usually hardened by:

- Case hardening,
- Induction hardening,

- Shot peening, particularly the cut edge, and
- Cubic boron nitriding.

Nitriding yields the hardest cut edge. Typically, nitrided dies are rarely resharpened at the thermoforming press.

Steel rule dies are usually 1 in or 25 mm to 2 in or 50 mm in depth. The die thickness depends on the sheet thickness, its toughness and the depth of draw of the part. Although dies are standardized in the following thicknesses:

- Thin-gage die with 0.028 in or 0.71 mm thickness,
- Medium-gage die with 0.042 in or 1.07 mm thickness, and
- Heavy-gage die with 0.056 in or 1.42 mm thickness,

steel rule dies are fabricated from sheet steel of any thickness if necessary. The die steel is available in strip form or in continuous roll. The cutting edge shape is ground in one of several configurations shown in Fig. 5.48. The single-sided cutting edge is most common, since it is inexpensive to grind and to resharpen. The double-sided cutting edge is recommended if the die is quite long, since the forces are centered directly over the fracture zone. The double-sided cutting edge is more difficult to align for trim line accuracy than the single-sided cutting edge. Honed cutting edges are used when a very sharp, very hard cutting edge is needed. These edges tend to feather and nick easily however. Recently, there has been interest in the single-sided double bevel cutting edge, which requires less frequent sharpening than the single bevel cutting edge.

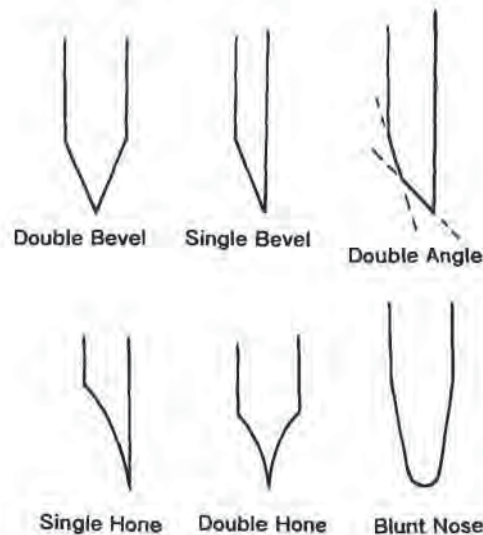


Figure 5.48 Characteristic cutting edges on trim dies

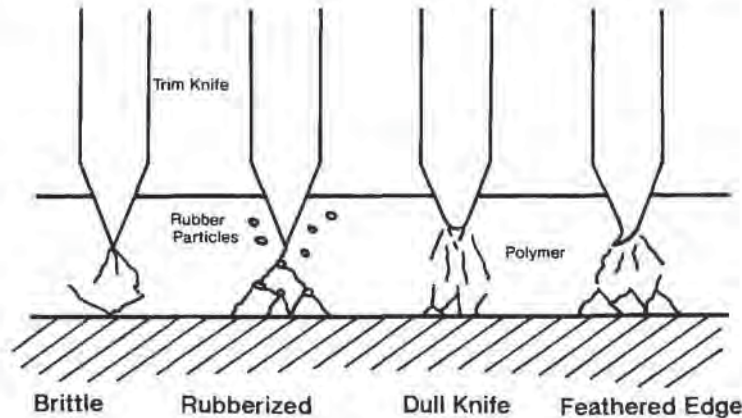


Figure 5.49 Generation of dust and angel hair from various trim die cutting edges

Resharpenering

In time, all steel rule dies dull. The edge either flattens from repeated contact with the compression plate or the edge rolls or feathers (Fig. 5.49). As noted, blunt dies require greater force to penetrate the plastic than sharp dies. Blunt dies are considered to be the primary source of dust, microcracks, crazing and angel hair. With the possible exception of nitrided dies and dies having hardness values in excess of 56 Rc, all dies can be resharpened. Usually the die must be removed from the trim press for resharpening. There are several ways to resharpen the dies:

- *Stropping*, or smoothing the cutting edge with a leather strap. Stropping is most effective when the cutting edge shows a very light feather. The technique removes very little if any steel, typically <0.0005 in or <12 μm . In fact, stropping is recommended prior to installing a newly ground die.
- *Honing*, or smoothing the cutting edge with a ceramic or Arizona stone. Honing removes up to 0.0015 in or 40 μm steel from the edge. The die can probably be placed in the trim press without additional shimming to compensate for metal loss.
- *Peening* or 200 grit glass sphere blasting. This is most effective with medium-hardened dies where microscopic nicks have occurred in the cutting edge. Again, only about 0.002 in or 50 μm are removed. These dies should be shimmed before reinitiating trimming.
- *Chemical etching*. Again, this is effective with medium-hardened dies. Although the chemical etch can remove substantial amounts of metal, usually less than 0.005 in or 125 μm of metal are removed. These dies should be shimmed before reinitiating trimming.
- *Grinding*. This is effective with hardened dies. Usually less than 0.010 in or 250 μm metal is removed. If more than this must be removed owing to nicks or breaks in the die cutting edge, the die is usually scrapped.

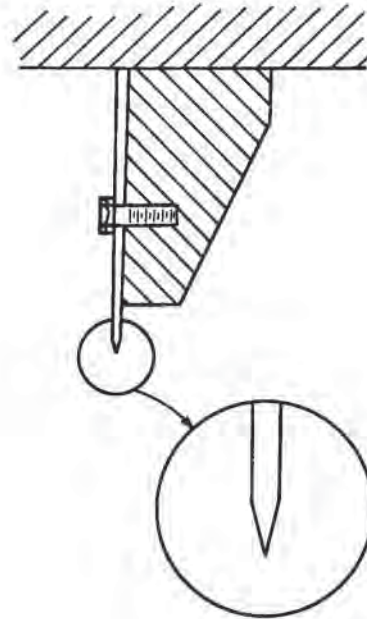


Figure 5.50 Characteristic steel rule die mounting configuration that allows for adjustments after resharpening. Redrawn from [41]

There are two general ways of fabricating a trim die. If the die has relatively few bends, it is fabricated of one or two strips of die steel, with all radiuses carefully bent such that the die lays flat to within $\frac{1}{4}$ degree. Bend radiuses for thin-gage die steel should not be less than $\frac{1}{8}$ in or 3.2 mm. The desired radius is $\frac{1}{4}$ in or 6.4 mm. If the required trim line is very complex, the die is constructed of many strips of die steel, with the intersections being welded and hand ground.

As noted, for simple parts and prototype parts trimmed on a manual compression press, the trim die is mounted in a simple wood framework. For production presses, the trim die has adjusting slots drilled at 1 in or 25 mm spaces about 0.5 in or 12 mm above the cutting edge. This allows the die to be mounted in a metal bracket that acts to reinforce the blade and allow blade adjustment (Fig. 5.50) [41]. The trim die bracket is usually aluminum.

Tabbing and Notching

In many cases with thin-gage roll-fed forming, there are many parts formed simultaneously. As noted in Section 5.7, if these parts are completely separated from the web, the many parts must be collected, oriented and stacked. In certain instances, depending on the gage of the sheet, the brittleness and tear resistance of the polymer and the specific part design, the parts are only partially punched from the sheet. The die is tabbed or notched so that the parts remain with the web until manually removed. Figure 5.51 shows two examples of tabbing dies. The frequency and dimension of tabs remain an art form dictated in part by the notch sensitivity of the plastics and

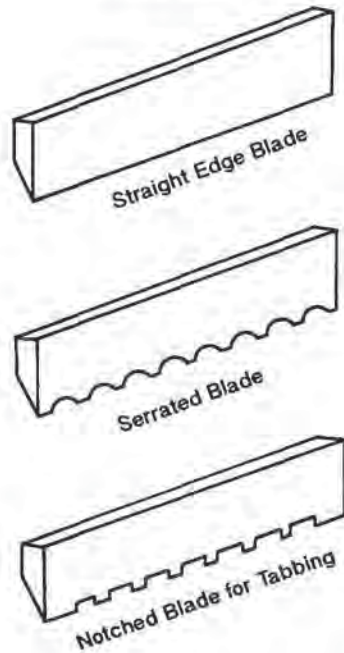


Figure 5.51 Characteristic die cutting edge configurations. The notched blade is used for tabbing

its resistance to tear. One measure of tear resistance is obtained from ASTM D 1004, known as the Graves tear initiation test or from ASTM D 1922, known as the Elmendorf tear test. Although these tests are designed for ranking the tear resistance of films (Table 5.22) [42], the results are useful in ranking the tab strength of thermoformed sheet. As is apparent, the tear strengths of polyolefins and flexible PVC are substantially greater than that of PS. As a result, the lengths of the tear tabs for polyolefins need to be substantially shorter than those for PS. If the tear tab is too long, part removal from the web will be inhibited and the torn edge may be unsightly.

5.11 Punch and Die Trimming

Figure 5.52 [43] shows a typical punch and die arrangement. Punch and die trimming is common for in-mold and in-line trimming of thin-gage roll-fed formed parts. The key to successful punch and die trimming lies in the accuracy with which the punch is aligned with the die. As discussed earlier, the tolerance between the punch and the die is critical to the minimization of dust, angel hair and microcracks (Fig. 5.45). The gap width is usually set with feeler gages at about 0.0015 in or 37.5 μm when the set is cold. The gap width when the cutting surfaces are hot and at steady temperature should not exceed 0.001 in or 25 μm . The punch is harder than the die, with the punch steel being hardened to 60 Rc to 65 Rc. The punch is usually ground after

Table 5.22 Tear Strength of Films [42](ASTM D1004 Graves initiation tear strength, all films 0.001 in or 25 μm thick)

| Polymer | Tear strength | |
|---------------------------|---------------|----------|
| | (gr/mil) | (mN/m) |
| Cellulosic (Cellophane) | 0.8–3.9 | 0.3–1.5 |
| Cellulose acetate | 1.6–3.9 | 0.6–1.5 |
| Low density polyethylene | 8 | 3.1 |
| Copolymer polyethylene | 7 | 2.7 |
| High-density polyethylene | 20 | 7.7 |
| Unoriented polypropylene | 25 | 9.7 |
| Oriented polypropylene | 4–6 | 1.5–2.3 |
| PA 6 | 7.8–20 | 3.0–7.8 |
| Polycarbonate | 7.8–9.5 | 3.0–3.7 |
| Ionomer | 5.9–9.8 | 2.3–3.8 |
| APET | 10–60 | 3.9–23.2 |
| Polyimide | 3.1 | 1.2 |
| FPVC | 24–39 | 9.3–15 |
| Polystyrene | 2 | 0.78 |
| PVDC (Saran) | 3.9–39 | 1.5–15 |

being hardened. The die steel hardness is about 45 Rc to 50 Rc. As a result, the die wears in and the punch wears out. The cut surfaces of the web and part are good indicators of die misalignment or wear:

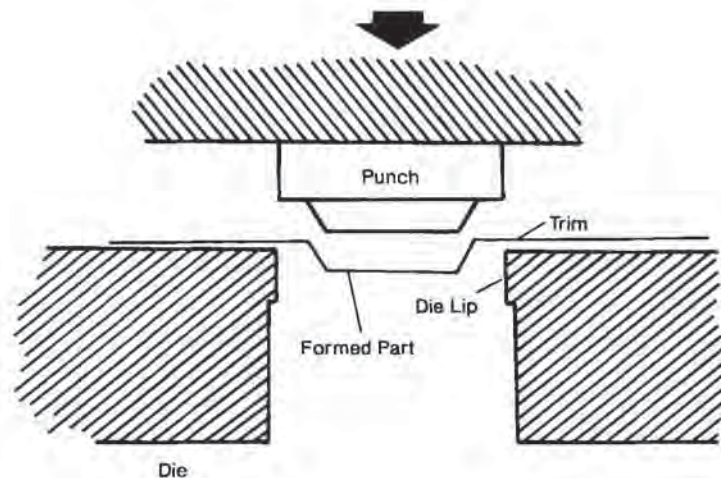


Figure 5.52 Schematic of punch-and-die arrangement yielding a pinch-type compression cut

- If the plastic is soft or warm, the cut edge may appear smeared or feathered,
- If the plastic is a fiber former, the cut edge may show microfibers at 30-power magnification,
- If the plastic is ductile or ductile-brittle, the cut edge may appear lacy, and
- If the plastic is brittle, the cut edge may appear jagged with many microcracks at 30-power magnification.

For accurate compression-shear cutting, it is necessary for the cutting edge of the die to mate with the punch simultaneously everywhere. Frequently, an intense light is shone behind the die as the punch advances. The point of peripheral extinguishment should occur simultaneously everywhere.

Punches and dies wear and the gap width increases. To regap, the die lips are usually shot- or grit-peened. The punch and the newly peened die are slowly brought together and any interference is pressed out by the press action [44]. If the punch shows erosion or microscopic galling, the punch edge is also stropped.

Although punch and die sets are designed to mate in a planar fashion, there are occasions when this is not desirable. For example, when very heavy sheet is being

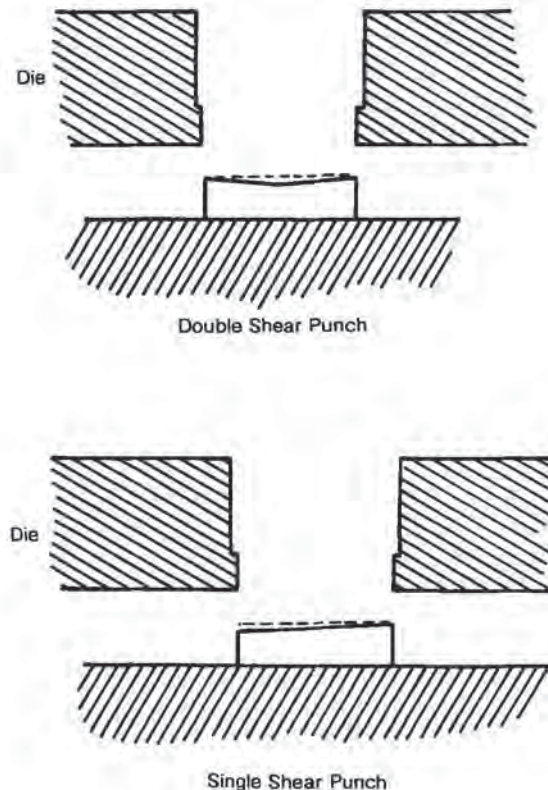


Figure 5.53 Punch geometries that yield a pinch-type shearing cut

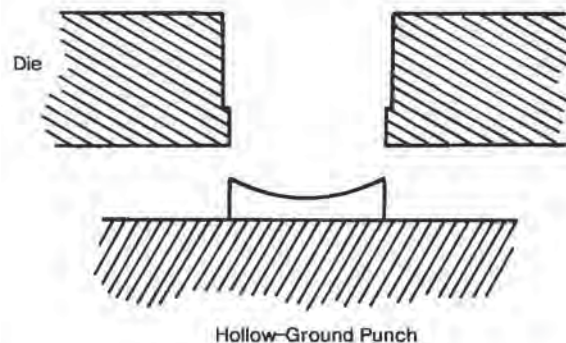


Figure 5.54 Hollow-ground punch that yields a combination of compression and shear cutting

trimmed in place on the forming press, the punch is altered to a single shearing punch (Fig. 5.53). The shearing action reduces the load on the hydraulic system driving the punch. If the sheet is not tightly held during shearing, it may move and the trim line may move away from the desired line. To minimize this effect, the punch is altered to a double-shearing punch (Fig. 5.53). The initial punch penetration at two points acts to stabilize the sheet against lateral movement. Shear and compression cutting is sometimes combined when the punch is dished or hollowed (Fig. 5.54).

Forged and Machined Dies

Steel rule dies are not normally used for sheet with thickness greater than 0.050 in or 1.3 mm in the trim area and for parts deeper than about $1\frac{1}{2}$ in or 38 mm. Machinable tool steel such as P7 or H20 is used to manufacture heavy duty dies. These dies are first oil or air annealed, then sharpened. For tough polymers, the dies are hardened to about 50 Rc. These dies are assembled into easily aligned fixtures and are nearly always removed for resharpening. Although forged and machined dies are more expensive than steel rule dies, they are the dies of choice for tough, filled or reinforced polymers formed into heavy-gage parts. The causes of dust and angel hair with forged dies are similar to those with steel rule dies. Similarly, forged dies wear, chip and dull in ways similar to steel rule dies. Chipped dies are rewelded and worn dies are resharpened rather than discarded [45].

5.12 Drilling

Drilling, slotting and grooving are mechanical operations similar to trimming. These operations are frequently done while the thermoformed shape is still held in the

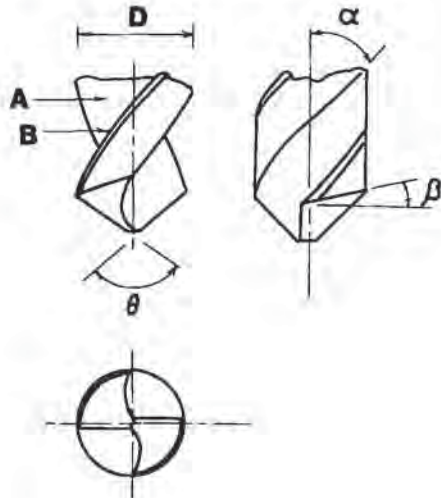


Figure 5.55 Two-tooth twist drill geometry [26].
Figure used with permission of author

trimming fixture. Plastics are quite difficult to drill without some damage to the surrounding area. Friction between the drill flutes and the drilled hole heats and expands the plastic inward, burning it or gumming the drill. Continuous chips from polyphenylene sulfide or PPS, PC and other high performance plastics can spiral around the drill, binding and stalling it. With olefins, thermal distortion at the hole inlet can cone the hole. For PMMA, PS and SAN, the hole exit can be chipped as the drill tip breaks through. Nevertheless, most plastics are drilled with conventional two-tooth twist drills (Fig. 5.55) [26]. Single-edged tool cutting guidelines are used for drilling. The depth of cut per drill tooth, d , is given as:

$$d = \frac{s}{n} \cdot \sin \frac{\theta}{2} = \frac{v}{nN} \sin \frac{\theta}{2} \quad (5.97)$$

where n is the number of teeth on the drill (usually two), N is the rotational drill speed [RPM], v is the axial feed rate [mm/min], and θ is the point tooth angle [deg]. The drill feed speed, $s = v/n$ [mm/rev].

A large depth of cut produces cut surface fracture and fracture around the hole as the drill exits. A small depth of cut enhances friction and can result in gumming and hole distortion. Example 5.18 illustrates the manner in which Equation 5.97 is applied to the drilling of PMMA.

Example 5.18 Drilling PMMA

Experimentally, the drill feed rate, v_g , below which PMMA will gum the drill is given as:

$$v_g = 25 \times 10^{-6} N^2 \text{ [mm/min]}$$

where N is the rotational drill speed, [RPM]. At high drill feed rate, v_c , PMMA will crack, producing hackle marks in the drilled hole. Experimentally:

$$v_c = 0.28N - 20 \times 10^{-6} N^2 \text{ [mm/min]}$$

Determine the acceptable drill feed rate range for $N = 2000$ RPM, 4000 RPM and 6000 RPM.

At $N = 2000$, the drill feed rate range from Equation 5.97 is given as:

$$100 \text{ [mm/min]} < v < 480 \text{ [mm/min]}$$

At $N = 4000$, the range is:

$$400 \text{ [mm/min]} < v < 800 \text{ [mm/min]}$$

At $N = 6000$, the range is:

$$900 \text{ [mm/min]} < v < 960 \text{ [mm/min]}$$

Above $N = 6000$ RPM, there is no acceptable value for v .

Table 5.23 Effect of Drill Geometry on Drilling Conditions in Plastics¹

| Drill parameter | Drilling condition |
|-----------------|------------------------|
| Point angle | Rotational drill speed |
| Rake angle | Drill feeding speed |
| Relief angle | Work temperature |
| Helix angle | Cooling provisions |
| Shape of flutes | Nature of the hole |

¹ Adapted from [26], with permission of author

Drilling conditions for many plastics are given in Tables 5.23 and 5.24. For many polymers, high elastic deformation and recovery can wear drill, gum drill surfaces and distort the drilled hole. The drills for plastics such as PS, RPVC, and PC should be air- or liquid-cooled. An air jet on the drill shank during drilling of most plastics is beneficial [46]. Water is sometimes used for PS and RPVC. Rapeseed oil produces optimum cooling for PC. Nylons or polyamides must be moisture-controlled or drilled hole dimensions will change. In crystalline and tough, amorphous polymers such as HDPE, PP, and high-rubber content ABS, nonuniform biaxial orientation in the plastic may cause the hole to become elliptical. Excess friction during drilling aids in this distortion. In highly elastic plastics such as HDPE, UHMWPE and PTFE, the drilled holes are always smaller than the drill. Tapered, highly polished, widely-spaced flutes on the drill are desired. Further, for tough, highly elastic polymers or for critical hole dimensions, holes should first be drilled undersized. Then the hole should be enlarged to the desired diameter.

Table 5.24 Drilling Conditions for Plastics¹

| Polymer | Point angle (deg) | Helix angle (deg) | Lip relief angle (deg) | Rake angle (deg) | Feeding speed (mm/rev) | Drill speed (rpm) ² | Wet/dry | Flute condition | Degree of difficulty in drilling ³ | Comments |
|-----------------|-------------------|-------------------|------------------------|------------------|----------------------------|--------------------------------|-----------|-----------------------|---|--|
| PE | 70-90 | 10-20 | 9-15 | 0 | 0.18-0.25 | 2000-4000 | Dry OK | 3 point drill pref. | 0 | High plasticity |
| RPVC | ≈120 | ≈27 | NA | NA | ≈0.3 | 2000 | Wet pref. | Extra-large flutes | 6 | Inlet hole poorer than exit hole |
| PMMA | 55-140 | NA | 12-20 | NA | ≈0.05 | 2000 | Water/oil | Polished | 3 | Some gummy inner surfaces. Extract drill frequently |
| PS | 60-90 | 40-50 | 12-15 | 0 | 0 (dry) 0.025-0.4 (wet) | 4000 500-2000 | Wet only | Wide, highly polished | 8+ | Easy to gum. Inlet holes can come at low feed rates |
| ABS-low rubber | 70-90 | 10-20 | 9-15 | 0 | 0.025-0.4 | 500 | NA | Polished | 4 | Can gum at inlet |
| ABS-med. rubber | 70-90 | 10-20 | 9-15 | 0 | 0.05-0.4 | 500-1000 | NA | Polished | 4 | Can gum at inlet |
| ABS-high rubber | 70-90 | 10-20 | 9-15 | 0 | 0.05-0.4 | 500-1000 | NA | Polished | 5 | |
| SAN | 70-90 | 10-20 | 9-15 | 0 | 0.2-0.4 | 500 | Wet perf. | Polished | 5 | More elastic than ABS. Hole smaller than drill |
| PTFE | 70-90 | 10-20 | 9-15 | 0 | 0.025-0.1 | 500-2000 | Dry OK | Deep, highly polished | 1 | Very high elasticity, hole always smaller than drill |
| PA 6 | 70-90 | * | 9-15 | * | 0.1-0.4 | 500-2000 | Dry OK | Polished | 3 | Carbide drills preferred |

| | | | | | | | | | | |
|--------------|-------|-------|-------|----|----------|----------|-----------------|-----------------------|---|---|
| PA 66 | 70-90 | * | 9-15 | * | 0.2-0.4 | 500-1000 | Dry OK | Special drill useful | 3 | Dimensions can change if not properly dried |
| PA 610 | 70-90 | * | 9-15 | * | 0.2-0.4 | 500-4000 | Dry OK | Special drill useful | 3 | Pull drill out frequently in deep holes |
| PC | 70-90 | 10-20 | 9-15 | 0 | 0.05-0.2 | 500 | Correct Wet/Oil | NA | 2 | Some gumming, chips very tough, can blind drill. Rapeseed oil |
| POM (Acetal) | 60-90 | NA | 10-15 | NA | 0.05-0.4 | 500-4000 | Dry OK | Wide, highly polished | 2 | Some exit cracks at low drill speeds |
| PP | * | * | * | * | 0.2-0.4 | 500-4000 | Dry OK | NA | 1 | High elasticity gumming at low speeds |

¹ Adapted from [26], with permission of author

² On 8.1 mm diameter drill

³ 0 = Easy, 9 = Very difficult

* Conventional twist drill angles

5.13 Other Cutting Techniques

Nearly every way of separating one portion of a material from another has been attempted with plastics. Some of the more successful methods include:

- Hot wire cutting or thermal cutting,
- Laser beam cutting, in essence an advanced form of thermal cutting,
- Water jet cutting, and
- Flame or thermal cutting.

Thermal Cutting

Most plastics can be trimmed thermally by simply locally melting the plastic. The cutter can be a hot wire or blade, requiring direct contact of a hot solid with the plastic at the trim point. Or it can be non-contact trimming with hot air, a combustion flame or a thermal laser. In addition to being energy inefficient, hot jet cutting torches are difficult to maintain. Typical problems include:

- Cut surface scorching,
- Local degradation or discoloration at the parting line,
- Kerf width variability,
- Hot gas temperature variability,
- Polymer slag spatter,
- Slag deposition and dripping,
- Slag threadlines,
- Local polymer ignition, including drips,
- Potentially noxious gas generation from combustion, and
- Obnoxious smoke, particularly from fire-retarded styrenics.

When the cutting shape does not need to be precise and the polymer is easily melted, direct contact flame cutting works well. For example, it is used to produce drain holes in polyolefin disposable plant trays in an in-line process. In laser cutting, the polymer is vaporized by the intense focused energy beam. Laser cutting is slower than hot gas cutting but is more accurate and cleaner. A typical cutting rate for a 50W laser through 0.500 in or 12.7 mm PMMA is about 1 ft/min or 300 mm/min.

In contact melting, the heated wire is typically only a few degrees above the polymer melt or flow temperature [47,48]. Wires are electrically heated, rheostatically controlled, and PTFE-coated nichrome resistant. Heated blades are frequently resistance tapes or plates adhered to steel saw blades. The plastic melting rate per unit width of heating surface, \dot{m} [kg/m · s or lb/ft · h], is given in terms of a convective heat transfer coefficient, h_p , for flowing plastic melt. Approximate values of $h_p = 200 \text{ W/m}^2 \cdot ^\circ\text{C}$, $0.00475 \text{ cal/cm}^2 \cdot \text{s} \cdot ^\circ\text{C}$ or $35 \text{ Btu/ft}^2 \cdot \text{h} \cdot ^\circ\text{F}$ are reported. The melting rate is:

$$\dot{m} = \frac{\pi D h_p}{2 c_p} \left(\frac{\text{Nu}}{\text{Pe}} \right) \quad (5.98)$$

where c_p is the polymer heat capacity and D is the heated wire diameter. For a heated blade, $\pi D \rightarrow L^*$, the width of the heated blade. Nu is the Nusselt number, the ratio of conduction to convection heat transfer:

$$Nu = \frac{hL}{k} \quad (5.99)$$

where h is a convection heat transfer coefficient, L is a characteristic fluid film thickness and k is the thermal conductivity of the polymer. Pe is the Peclet number, the product of two other dimensionless groups. $Pe = Re \cdot Pr$, where Re is the Reynolds number, a ratio of inertial to viscous forces, and Pr is the Prandtl number, a ratio of thermal to viscous resistance:

$$Pr = \frac{\mu c_p}{k} \quad (5.100)$$

where μ is the polymer Newtonian viscosity. The ratio, Nu/Pe , occurs frequently in heat transfer to flowing fluids. For melting polymers, the ratio is a function of two material parameters:

$$\frac{Nu}{Pe} \approx \frac{2}{A} (B)^{0.26} \quad (5.101)$$

where A is a fluid film parameter having a range of $0.5 < A < 3$ for crystalline polymers and B is a solid parameter having a range of $0.1 < B < 1$ for crystalline polymers [47]. Example 5.19 illustrates how these relationships are used to predict cutting rates for HDPE.

Example 5.19 Trimming HDPE With a Heated Wire

Consider trimming 0.250 in or 6.35 mm thick HDPE using a 0.030 in or 0.76 mm diameter nichrome wire. Determine the maximum trimming speed. For this example, $A = 3$ and $B = 0.1$ in Equation 5.101. The specific heat of HDPE is 1.0 Btu/lb · °F or 1.0 cal/g · °C.

The appropriate values for Nu/Pe needed in Equation 5.98 are obtained from Equation 5.101:

$$\frac{Nu}{Pe} = \frac{2}{A} (B)^{0.26} = \frac{2}{3} (0.1)^{0.26} = 0.167$$

The melting rate, \dot{m} , is obtained from Equation 5.101:

$$\dot{m} = \frac{\pi D \cdot t \cdot h_p}{2 \cdot c_p} \cdot (Nu/Pe) = \frac{\pi \cdot 6.35 \cdot 0.076 \cdot 0.00475 \cdot 0.167}{2 \cdot 1} = 0.00060 \text{ g/s}$$

where $h_p = 0.00475 \text{ cal/cm}^2 \cdot \text{s} \cdot \text{°C}$. The melting rate of 0.6 mg/s or 0.001 lb/h is the maximum cutting speed. The volume rate of plastic melted is given as:

$$\dot{V} = \frac{\dot{m}}{\rho} = \frac{0.0006 \text{ g/s}}{0.96 \text{ g/cm}^3} = 0.000625 \text{ cm}^3/\text{s}$$

The projected cutting surface is:

$$\frac{\pi Dt}{2} = \frac{\pi \cdot 0.076 \cdot 6.35}{2} = 0.76 \text{ cm}^2$$

As a result, the maximum cutting rate, v , is:

$$v = \frac{0.000625 \text{ cm}^3/\text{s}}{0.76 \text{ cm}^2} = 0.00082 \text{ cm/s} = 14 \text{ ft/h}$$

A is a melt shielding parameter, the ratio of melt sensible heat to latent heat of fusion. B is the equivalent ratio for the solid phase. For high latent heat crystalline polymers, a substantial fraction of heat is carried away by the melt. A and B are small and the ratio, Nu/Pe , is relatively large. As a result, the cutting rate can be high. For polymers with low latent heats, the ratio, Nu/Pe , is small and the cutting rate is low. The Griffin melting model [48] is truly not applicable to amorphous polymers since they have no latent heats. Increasing the hot wire temperature increases the relative values of A and B . This effectively decreases the melting rate, since some cutting energy must now be used to heat the polymer to a higher temperature. As noted, the cutting rate is inversely proportional to the sheet thickness.

Water Jet Cutting

Water jet cutting and abrasive water jet cutting are new techniques developed for trimming high-modulus, low elongation to break polymers. The techniques have found greatest application in trimming composite thermoplastic and thermosetting structures. The typical water jet uses ultra-filtered water that is delivered to the cutting jet at pressures up to 690 MPa or 100,000 lb_f/in^2 . Typical water jet pressures are about 345 MPa or 50,000 lb_f/in^2 . The water is directed through a sapphire orifice having a diameter of about 0.5 to 2.5 mm or 0.020 to 0.100 in. The jet velocity near-sonic is about 1000 m/s or 3300 ft/s. For tough polymers and composites, abrasive garnet grit of 100 to 500 μm diameter is added to the water stream at about 5% (volume). A schematic of an abrasive water jet cutting head is shown in Fig. 5.56 [49]. Water jet cutting works well when polymers have yield stresses of 80 MPa or 12,000 lb_f/in^2 or less. For polymers with higher yield stresses or for composites, abrasive water jet cutting is recommended. The kerf produced is typically about 5% wider than the diameter of the jet at jet entrance to the sheet. It is recommended that the jet-to-sheet distance be no more than 5 mm or 0.200 in.

Water jet cutting has several advantages over thermal cutting:

- The process is dustless,
- The process does not generate noxious gases,
- The jet can be stopped or slowed without any damage to the part being cut and without widening of the cutting kerf,

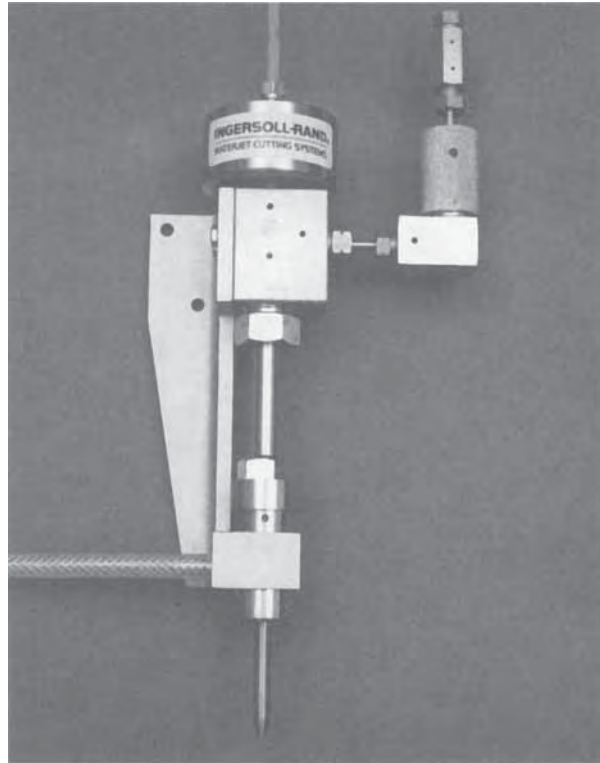


Figure 5.56 Water jet cutting device for thermoformed composites and laminates

- The cutting process can be started at any point on the part, and
- The cutting process is essentially isothermal and low temperature.

There are several disadvantages to water jet and abrasive water jet cutting:

- There is substantial noise owing to air coupling at the impingement point,
- The jet nozzle tip wears rapidly when abrasives are used,
- Abrasives are relatively expensive and not easily recovered,
- Water cleanliness is extremely important. Fouled water will result in erratic cutting,
- At high feed rates, the water jet can be diverted by irregularities in the polymer or variations in polymer thickness or when very heavy-gage ductile plastics are cut. This causes the kerf to meander, and
- The kerf tends to be wider at the entrance to the piece. This is particularly noticeable with heavy-gage ductile plastics such as HDPE and when abrasives are used.

Table 5.25 gives some cutting speeds for abrasive and nonabrasive water jets.

Table 5.25 Water Jet Cutting Speeds for Polymers and Composites [49]

| Material class | Thickness | | Cutting speed | |
|---|-----------|-------|---------------|----------|
| | (mm) | (in) | (m/min) | (in/min) |
| <i>Water Jet at 360 MPa or 52,000 lb_f/in² and 20 HP</i> | | | | |
| Polyurethane, } Polyethylene, } Rubber (30+ } Durometer) } | 6.4 | 0.250 | 6 | 225 |
| | 12.7 | 0.500 | 3 | 100 |
| | 25.4 | 1.000 | 1 | 40 |
| Rubber (30- } Durometer), } Paper, fabric, } Corrugated } cardboard } | 0.13 | 0.005 | 15 | 600+ |
| | 0.38 | 0.015 | 8 | 300+ |
| | 0.81 | 0.032 | 8 | 300+ |
| | 1.6 | 0.063 | 8 | 300+ |
| | 3.2 | 0.125 | 8 | 300+ |
| | 6.4 | 0.250 | 8 | 300+ |
| EPS, foam rubber, } Foam PUR, } Balsa wood } | 1.6 | 0.063 | 15 | 600+ |
| | 12.7 | 0.500 | 12 | 450 |
| | 25.4 | 1.000 | 7 | 275 |
| <i>Abrasive Jet at 240 MPa or 35,000 lb_f/in², 150 μm Garnet and 20 HP</i> | | | | |
| Epoxy-graphite, } Epoxy-aramid, } Polyester-glass } | 3.2 | 0.125 | 1.60 | 63 |
| | 6.4 | 0.250 | 0.75 | 30 |
| | 12.7 | 0.500 | 0.46 | 18 |
| | 19.1 | 0.750 | 0.30 | 12 |
| | 25.4 | 1.000 | 0.13 | 5 |

5.14 Trimming—A Summary

The selection of a trimming technique depends primarily on the stress-strain nature of the polymer at its trimming temperature. However many processing elements influence the choice including:

- The gage of the sheet,
- The part size,
- The overall draw ratio,
- The nonplanar nature of the trim line,
- The complexity of the trim line,
- The acceptable level of cut surface roughness,
- The required dimensional tolerance,
- The economically required speed of trimming,
- The extent of fixturing or hold down,
- The number of secondary or ancillary piercing steps required,
- The skill of the operator or pressman,
- The availability of the desired trim equipment,

Table 5.26 Suitability of Trimming Techniques

(Heavy-gage in parentheses)
 0 = Unsuitable 9 = Preferred, best

| Type of polymer | Typical polymer | Trim category | | | | | | | | | | | |
|------------------|---|---------------|-----------|------------|--------|--------------|----------------|----------|----------|-------------|-----------|------------|-----------|
| | | Die cut | Shear cut | Nibble cut | Router | Circular saw | Abrasive wheel | Band saw | Hot wire | Hot gas jet | Water Jet | Grit blast | Laser cut |
| Very brittle | PS, PMMA, SAN | 9(0) | 6(2) | 4(4) | 0(4) | 2(6) | 2(9) | 3(4) | 6(7) | 4(6) | 5(2) | 8(8) | 7(8) |
| Brittle | ABS, RPVC, CA, CPET, CAB | 9(0) | 7(2) | 5(4) | 2(5) | 3(7) | 4(9) | 3(4) | 4(7) | 5(4) | 6(2) | 8(8) | 7(8) |
| Tough | mPPO, CAP, PPS, PA 6, PA 66, PET OPS | 5(2) | 9(6) | 6(8) | 3(8) | 5(9) | 5(7) | 4(7) | 3(8) | 7(6) | 5(2) | 8(2) | 7(8) |
| Ductile, rubbery | LDPE, PP, HDPE, FPVC, TPE, TPO, PTFE, FEP | 8(2) | 9(8) | 7(8) | 5(3) | 7(6) | 7(5) | 2(3) | 2(8) | 3(6) | 3(5) | 0(0) | 7(9) |

Table 5.27 Trim Quality—Thin Gage

| Process | Trimming type | Tooling type | Pressure/vacuum | Parts per shift | Quality A = highest | Scrap rate | Time for delivery of tooling—weeks |
|---------------------------------|----------------------|---------------------|-----------------|-----------------|---------------------|---|---|
| Roll-fed/Cut sheet | Manual/Steel rule | Epoxy | Vacuum | Lowest | D | High | 3-4 |
| Roll-fed/Cut sheet | Manual/Steel rule | Aluminum | Pressure | Medium | D | Low | 5-6 |
| Roll-fed | In-line/Steel rule | Aluminum | Both | High | C | Low | 5-6 |
| Roll-fed | Off-line/Punch & die | Aluminum | Both | Highest | B | Low | 12-15 |
| Roll-fed/Contact heat | Trim-in-place | Aluminum | Pressure | Medium | B | Low | 5-6 |
| Roll-fed | Trim-in-place | Aluminum | Pressure | Low | A | Low | 15-20 |
| Process type | Setup time | Tooling cost/cavity | Skill required | Machine cost | Per Part cost | Number formed parts per shift—comparative | Comments |
| Roll-fed/Cut sheet | Lowest | Lowest | Lowest | Lowest | Highest | 800 | Manual die cut |
| Epoxy tool | Low | Low | Low | Low | High | 4000 | Manual die cut |
| Roll-fed/Cut sheet Aluminum | Medium | Medium | Medium | Medium | Low | 4000 | |
| Roll-fed/In-line Trim | High | High | High | High | Lowest | 8000 | Large number of cavities, maximum number of parts |
| Form-trim-in-place—Contact heat | Low | Medium | Low | Medium | Low | 5000 | Female, nonplugged molds |
| Form-trim-in-place—Oven heat | Medium | Highest | Medium | Highest | Low | 8000 | Fewer cavities, fewer formed parts |

¹ Adapted from [51], with permission of copyright owner

- The availability of resharpening methods,
- Among others.

As noted, not all trimming devices are suitable for all types of plastics in all thicknesses. For example, automatic programmed laser cutting is clean and accurate but is impractical for trimming thin-gage roll-fed APET. Die cutting is quicker, cheaper and can be installed as part of the in-mold forming process and therefore becomes the trimming process of choice. Some techniques such as abrasive grit cutting are dusty and work best on high modulus, brittle polymers. Abrasive and toothed wheel cutting and routing generate dust. Heavy-gage parts of PMMA, ABS and PS should be sprayed with an antistat prior to trimming to minimize the almost-impossible-to-remove cutter dust. The rank of trimming techniques in Table 5.26 is meant only as a guideline, in terms of matching the intrinsic natures of the cuts and the material stress-strain behavior. Economics and availability may dictate a less-than-optimum choice for trimming. Table 5.27 illustrates some of the economic considerations needed for thin-gage trimming [51].

5.15 References

1. D.Q. Kern, *Process Heat Transfer*, McGraw-Hill Book Co., New York (1950), Table 12 of Appendix, p. 845.
2. M.R. Kamal and S. Kenig, "The Injection Molding of Thermoplastics. Part II: Experimental Test of the Model", *Polym. Eng. Sci.*, 12 (1972), pp. 302-308.
3. M.K. Liao and C.S. Li, "Investigation of Thermal Conduction Between Mold and Melt During Injection Molding Process", *SPE ANTEC Tech. Papers 40* (1994), pp. 501-505.
4. B.O. Rhee, C.A. Hieber and K.K. Wang, "Experimental Investigation of Thermal Contact Resistance in Injection Molding", *SPE ANTEC Tech. Papers 40* (1994), pp. 496-500.
5. J. Schneider, "Conduction", in W.M. Rohsenow and J.P. Hartnett, Eds., *Handbook of Heat Transfer*, McGraw-Hill Book Co., New York (1973), Section 3, pp. 3-14 to 3-16.
6. J.L. Throne, *Plastics Process Engineering*, Marcel Dekker, Inc., New York (1979), Figure 10.5-6A, p. 518.
7. S.W. Churchill, *Viscous Flows: The Practical Use of Theory*, Butterworths, Boston (1988), pp. 12-13.
8. R.B. Bird, W.E. Stewart and E.N. Lightfoot, *Transport Phenomena*, John Wiley & Sons, Inc., New York (1960), pp. 401-404.
9. C.P. Kothandaraman and S. Subramanyan, *Heat and Mass Transfer Data Book*, 3rd Ed., John Wiley & Sons, Inc., New York (1977), pp. 13-16.
10. F. Kreith, *Principles of Heat Transfer*, 2nd Ed., International Textbook Company, Scranton PA (1965), Appendix II.
11. J.P. Holman, *Heat Transfer*, 4th Edition, McGraw-Hill Book Co., New York (1976), p. 207.
12. W.K. McConnell, Jr., Handout, SPE Industrial Thermoforming Symposium and Workshop, Arlington TX, 12-14 March 1985.
13. T.R. Goodman, "Application of Integral Methods to Transient Nonlinear Heat Transfer", in T.F. Irvine, Jr., and J.P. Hartnett, Eds., *Advances in Heat Transfer*, Vol. 1, Academic Press, New York (1964), p. 54, p. 59.
14. D.R. Croft and D.G. Lilley, *Heat Transfer Calculations Using Finite Difference Equations*, Applied Science Publishers, London (1977).

15. G.M. Dusenberre, *Heat-Transfer Calculations by Finite Differences*, International Textbook Co., Scranton PA (1961).
16. P.C. Powell, *Engineering with Polymers*, Chapman & Hall Ltd., London (1983), pp. 254-257.
17. R.C. Progelhof and J.L. Throne, *Polymer Engineering Principles: Properties, Processes, Tests for Design*, Hanser Publishers, New York (1993), p. 342.
18. G. Gruenwald, *Thermoforming: A Plastics Processing Guide*, Technomic Publishing Co., Inc., Lancaster PA (1987), pp. 34-36.
19. R.C. Progelhof and J.L. Throne, *Polymer Engineering Principles: Properties, Processes, Tests for Design*, Hanser Publishers, New York (1993), Figure 4.34.
20. G.L.F. Ehlers, "Thermal Stability", in E. Baer, Ed., *Engineering Design for Plastics*, Reinhold, New York (1964), p. 402.
21. Z. Tadmor and C.G. Gogos, *Principles of Polymer Processing*, John Wiley & Sons, New York (1979), p. 163.
22. D. Burgess, "Vacuum Forming of High-Density Polythene", *British Plast.*, 32 (1959), pp. 195-6, 223.
23. W.K. McConnell, Jr., "Thermoforming Plastic Sheet and Film", from *Tool and Manufacturing Engineers Handbook*, Vol. 2., 4th Ed., Part of handout at SPE Industrial Thermoforming Symposium and Workshop, Arlington TX, 12-14 March 1985.
24. G. Beall, *Glenn Beall's Design Guide II for Pressure Formed Plastic Parts*, Arrem Plastics Inc., Addison IL (1985), pp. 11-12.
25. J.H. Schut, "Make Way for Lots of Firsts", *Plast. World*, 52:6 (Jun 1994), pp. 57-61.
26. A. Kobayashi, *Machining of Plastics*, McGraw-Hill Book Co., New York (1967), Chapter 1, "Fundamental Considerations".
27. J. Florian, *Practical Thermoforming: Principles and Applications*, Marcel Dekker, Inc., New York (1987), pp. 112-113.
28. G. Gruenwald, *Thermoforming: A Plastics Processing Guide*, Technomic Publishing Co., Inc., Lancaster PA (1987), p. 57.
29. J. Florian, *Practical Thermoforming: Principles and Applications*, Marcel Dekker, Inc., New York (1987), p. 112.
30. A. Kobayashi, *Machining of Plastics*, McGraw-Hill Book Co., New York (1967), p. 32.
31. L.E. Nielsen, *Mechanical Properties of Polymers*, Reinhold, New York (1962), p. 6.
32. R.W. Hertzberg, *Deformation and Fracture Mechanics of Engineering Materials*, John Wiley & Sons, New York (1976), p. 262.
33. A.J. Kinloch and R.J. Young, *Fracture Behaviour of Polymers*, Applied Science Publishers, London (1983), p. 87.
34. R.W. Hertzberg and J.A. Manson, *Fatigue of Engineering Plastics*, Academic Press, New York (1980), p. 136.
35. P.I. Vincent, "Fracture—Short-Term Phenomena", in N.M. Bikales, Ed., *Mechanical Properties of Polymers*, Wiley-Interscience, New York (1971), p. 125.
36. J. Florian, *Practical Thermoforming: Principles and Applications*, Marcel Dekker, Inc., New York (1987), pp. 103-106.
37. H. Voigt, *Lehrgang für Thermoformung*, Paul Kiefel Thermoformmaschinen GmbH, Freilassing, Germany, undated, p. 1.4.2.
38. G. Gruenwald, *Thermoforming: A Plastics Processing Guide*, Technomic Publishing Co., Inc., Lancaster PA (1987), p. 59.
39. J.P. Holman, *Heat Transfer*, 4th Edition, McGraw-Hill Book Company, New York (1976), pp. 38-39.
40. J.P. Holman, *Heat Transfer*, 4th Edition, McGraw-Hill Book Company, New York (1976), p. 40.
41. J. Florian, *Practical Thermoforming: Principles and Applications*, Marcel Dekker, Inc., New York (1987), pp. 106-112.
42. M. Bakker, Ed., *The Wiley Encyclopedia of Packaging Technology*, John Wiley & Sons, New York (1986).
43. J. Florian, *Practical Thermoforming: Principles and Applications*, Marcel Dekker, Inc., New York (1987), Figure 31-1.

44. J. Florian, *Practical Thermoforming: Principles and Applications*, Marcel Dekker, Inc., New York (1987), p. 116.
45. J. Florian, *Practical Thermoforming: Principles and Applications*, Marcel Dekker, Inc., New York (1987), p. 114.
46. J. Frados, Ed., *Plastics Engineering Handbook*, 4th Ed., Van Nostrand Reinhold, New York (1976), p. 701.
47. O.M. Griffin, "Thermal Transport in the Contract Melting of Solids", *Polym. Eng. Sci.*, 12 (1972), pp. 265-271.
48. J.L. Throne, *Plastics Process Engineering*, Marcel Dekker, Inc., New York (1979), p. 824.
49. J. Korican, "Water-Jet and Abrasive Water-Jet Cutting", in C.A. Dostal, Ed., *Composites*, Volume I, *Engineered Materials Handbook*, ASM International, Metals Park OH, 1987, pp. 673-675.
50. R.C. Progelhof and J.L. Throne, *Polymer Engineering Principles: Properties, Processes, Tests for Design*, Hanser Publishers, New York (1993), p. 551.
51. S.R. Rosen, "Trimming Basics", paper presented at SPE Thermoforming Conference, Midland MI (Sept. 1992).
52. R.M. Caddell, *Deformation and Fracture of Solids*, Prentice-Hall, New York (1980), p. 209.

6 Thermoforming Molds

- 6.1 Introduction
- 6.2 Prototype Molds
 - Wood
 - Fiberboard
 - Plaster
 - Plastic
 - White Metal
 - Nickel
- 6.3 Production Molds
 - Aluminum
 - Steel
 - Other Metals
- 6.4 Mold Coolant Channels
 - Mold Channel Flow
 - Expansion
 - Contraction
 - Sharp-Edged Orifice
- 6.5 Vent Holes
 - Sizing Vacuum Systems—Steady State
 - Sizing Vacuum Systems—Dynamic
 - Solenoid Valve Flow Resistance
 - Vent Hole Resistance to Flow
 - Vent Hole Diameter
 - Other Types of Vents
 - Vent Hole Placement
- 6.6 Surface Treatments
 - Surface Texture
- 6.7 Plug Design Considerations
 - Plug Materials
 - Wood Plugs
 - Plastic Plugs
 - Metal Plugs
 - Plug Design Concepts
- 6.8 Sheet Clamping
- 6.9 Sag Bands and Sheet Supports
- 6.10 Other Aspects of Mold Design
 - Undercuts
 - Encapsulation
 - Moving Elements
 - Stripper Plates/Bars
 - Mold Releases
 - Web Breakers, Catchers and Chasers
 - Moats, Dams and Double Steps
 - Chamfers and Radii
 - Prestretching Restraints
- 6.11 Efficient Use of Sheet
 - Heavy-Gage Sheet
 - Thin-Gage Sheet
- 6.12 References

6.1 Introduction

The thermoforming mold can be as simple as a smoothed block of wood over which a heated sheet is draped. Many production molds may be as complicated as injection molds and may include:

- Moving elements,
- Articulated plugs,
- Sophisticated means for isolating sheet over multicavities,
- Means for ejecting formed sheet from mold cavities,
- In-mold trimming of formed sheet,
- Means for retrieving trimmed parts, and
- Down-stream filling and sealing means.

Selection of suitable mold materials depends to a great degree on the severity and length of service. If only a few parts are to be made and the hot plastic sheet is deformed at relatively low temperatures with vacuum alone, wood, plaster or reinforced or filled thermosetting resin is usually used as a mold material. On the other hand, if thousands of parts are needed and high temperatures and pressures are needed to achieve final part design criteria, durable mold materials such as aluminum and even steel are used.

Regardless of the materials used, every mold must meet specific criteria and must therefore have certain features:

- Provisions are needed for clamping the sheet against the mold surface,
- Vent or vacuum holes are needed in those areas into which the sheet is drawn last,
- The mold surface should be relatively nonadhesive during sheet contact and static-free after the sheet is removed,
- The mold surface must be sufficiently hard to retain its shape and texture for the lifetime of the part,
- The mold must not change in dimensions during fabrication through thermal expansion,
- The mold must not change in dimensions during storage through moisture absorption, and
- The mold material should be relatively free from chemical and moisture attack to minimize:
 - Swelling,
 - Cracking,
 - Rusting,
 - Corrosion, and
 - Patina development.

Appropriate mold material selection depends on economic considerations as well. Some of these are:

- Initial cost of the material,
- Ease of fabrication,

- Ease of repair,
- Ease of maintenance,
- Ease of serviceability,
- Quick-change suitability,
- Requirements for safe storage,
- Mold weight,
- Availability of mold materials,
- Shop personnel familiarity with the material, and
- Material toughness against accidental abuse while in use and in storage.

Some of these intrinsic factors frequently rule out an otherwise acceptable mold material [1].

In this chapter, prototype and production mold materials are discussed. Design of coolant flow channels and vacuum holes are then described. Some design features regarding surface treatment and surface texture are detailed. Plug design is described. Clamping methods, sheet supports, rapid mold change concepts and some aspects of break-away molds are discussed.

6.2 Prototype Molds

Strictly speaking, prototype molds are designed to produce a few parts. These parts may be used to demonstrate part design concepts that are to be subsequently either production thermoformed or injection or blow molded. The parts may be used for product testing and prototype assembly schemes. Frequently, however, prototype molds are used to produce tens to hundreds of parts in a classical production run. Some of the many heavy-gage sheet applications that are made exclusively on prototype molds include:

- Indoor and outdoor signs,
- Point-of-purchase displays,
- Horticultural pool shells,
- Swimming pools,
- Spas,
- Plant containers,
- Custom dunnage,
- Bathtubs,
- Equipment housings, and
- Medical furniture.

Wood, plaster, glass fiber-reinforced plastic, filled epoxy and zinc and white metal alloys are materials commonly used for prototype molds. Each has many advantages and some serious limitations. A review of each follows.

Table 6.1 Finishing Qualities of Selected Hardwoods Used in Prototype Thermoform Molds [2]

| Wood | Planing | Shaping | Drilling | Sanding | Resistance to splitting |
|------------|---------|---------|----------|---------|-------------------------|
| Ash | C | E | A | C | C |
| Hickory | C | H | A | B | D |
| Hard maple | E | C | A | G | E |
| Red oak | A | H | A | B | C |
| Walnut | D | G | A | G | E |
| White oak | D | G | A | G | E |
| Mahogany | C | F | A | E | F |

A = 90–100 C = 70–79 E = 50–59 G = 30–39 J = 10–19
 B = 80–89 D = 60–69 F = 40–49 H = 20–29 K = 0–9

Wood

Hardwoods are used for prototype and short production runs. The wood must be thoroughly kiln-dried before shaping to minimize stress relief in the form of warping, cracking and checking during fabrication, forming and storage. Properties of typical hardwoods used in thermoforming are shown in Tables 6.1 and 6.2 [2]. Woods such

Table 6.2 Minimum Mechanical Properties of Selected Hardwoods Used in Prototype Thermoform Molds [2]

| Property | Unit | Wood type | | | | | |
|---|--|-----------|------------------|-------------|----------------|-----------|--------|
| | | White ash | Shagbark hickory | Sugar maple | Pinoak red oak | White oak | Walnut |
| Density | lb/ft ³ | 34 | 40 | 35 | 36 | 37 | 32 |
| | kg/m ³ | 550 | 640 | 560 | 580 | 600 | 510 |
| Flexural modulus | $\times 10^6$ lb _f /in ² | 1.44 | 1.57 | 1.55 | 1.32 | 1.25 | 1.42 |
| | GPa | 9.93 | 10.8 | 10.7 | 9.10 | 8.62 | 9.79 |
| Work to maximum load | in-lb _f /in ³ | 16.6 | 23.7 | 13.3 | 14.0 | 11.6 | 14.6 |
| | cm-kg/cm ³ | 1.17 | 1.67 | 0.94 | 0.99 | 0.82 | 1.03 |
| Maximum crushing strength parallel to grain | lb _f /in ² | 3990 | 4580 | 4020 | 3680 | 3560 | 4300 |
| | MPa | 27.5 | 31.6 | 27.7 | 25.4 | 24.5 | 29.6 |
| Fiber stress at proportional limit | lb _f /in ² | 670 | 840 | 640 | 720 | 670 | 490 |
| | MPa | 4.62 | 5.79 | 4.41 | 4.96 | 4.62 | 3.38 |
| Parallel-to-perpendicular compression ratio | | 5.96 | 5.45 | 6.28 | 5.11 | 5.31 | 8.78 |
| Impact bending height to complete failure | in | 38 | 74 | 40 | 48 | 42 | 37 |
| | m | 0.97 | 1.88 | 1.02 | 1.22 | 1.02 | 0.94 |

as walnut or pecan are oily. The exuding oil may interfere with adhesives during fabrication and may be undesirable during forming. Wood such as balsa, boxwood and certain second-growth pines are too soft for mold materials. Repeated forming pressure crushes the cell structure, producing poor surfaces and loss of dimension. Conventional woodworking techniques are used to fabricate the molds. Wood sections are usually assembled with fluted dowels and resorcinol, hot melt or epoxy adhesives. Hot melt adhesives allow faster assembly but yield weaker joints than other adhesives. Standard wood-filling techniques are used to remove surface defects during mold fabrication. Vent holes are usually drilled through the primary surface first, then enlarged by drilling from the back of the mold. Final sanding to 200 grit is usually sufficient for most low-pressure forming techniques. It is very important that the assembled wood be carefully and thoroughly dried prior to finishing. During forming, the rapid, cyclical heating from contact with the hot plastic will pull moisture from the wood. If the wood is not thoroughly dried, the wood can crack or check. Wood grain is characterized by alternating hard and soft bands. Occasionally, the softer portions preferentially shrink. This leads to an unacceptable texture that is transferred to the formed shape.

After thorough drying, the surface may need to be sealed with temperature-resistant enamel or varnish¹. Recently, epoxy enamels and varnishes have been developed that protect wood surfaces for hundreds of cycles without refinishing. For low-temperature forming of polymers such as cellulose acetate, flexible PVC and PS foam, polyurethane varnishes work satisfactorily. If mold release is needed, paraffin wax, caruba wax, Treewax, Vaseline or a light coating of white grease is used. For food contact and medical parts, vegetable oil spray is used.

Wood is also used as a component in molds made of more permanent materials. For example, since wood is rapidly and easily shaped, temporary plugs, web catchers and web breakers can be formed during early mold shake-down trials to determine optimum material distribution. Owing to the high compression strength and low density of end-grain woods such as oak and walnut, these are used for permanent plugs in many production runs.

Fiberboard

Fiberboard is produced by mixing wood fibers with thermosetting resins such as urea or phenolic, then pressing the mass into sheets at elevated temperature to crosslink the resin. The sheet product so produced is typically 0.125 to 3 in or 3.2 to 75 mm in thickness and is available in at least three grades:

¹ It may not always be necessary or desirable to seal the wood surface. As an example, the mold is not usually sealed when it is used to produce parts of slightly different designs. When a wood that is not thoroughly dried is sealed, then cyclically heated, the moisture diffusing to the surface will crack or blister the sealant. Excessive blistering leads to unacceptable surface texture in the formed shape. Sometimes it is more feasible economically to rebuild the mold than to strip the sealant from the surface.

- Low-density fiberboard, with a density range of 0.1 to 0.4 g/cm³ or 6 to 25 lb/ft³. This product is used in construction as moderately good insulation sheathing. One brand is known in the US as Cellotextm,
- Medium-density fiberboard, with a density range of 0.5 to 0.7 g/cm³ or 30 to 45 lb/ft³. This product is relatively new and is produced by radio-frequency curing of the thermosetting resin. It finds use in the thermoforming industry as a mold material, as described below. One brand is known in the US as Moldboardtm [45], and
- High-density fiberboard, with a density range of 0.8 to 1.3 g/cm³ or 50 to 90 lb/ft³. This product is used in construction as grainless dense paneling. One brand is known in the US as Masonitetm.

Physical properties of medium-density fiberboard used as a mold material are given in Table 6.3 [44]. Pressure is not very high during fabrication of this density fiberboard. As a result, the board is somewhat porous. This allows vacuum to be drawn everywhere through the mold surface, as shown in schematic in Fig. 6.1. The fiberboard is worked using conventional woodworking saws and shapers. Overheating the cutting surface will result in gum deposit on the cutting surface, however. The porosity of the fiberboard is not exceptional. As a result, fiberboard molds work best for relatively shallow-draw male parts. Although primary surfaces are usually semi-gloss or matte, there are no vent hole nibs or nipples.

Plaster

Most commercial molding plasters are not strong or tough enough to be used for prototype molds. The properties of the few that are strong enough are given in Table 6.4 [3–5]. Plasters are inorganic calcicous materials that hydrolytically react and

Table 6.3 Medium-Density Pressed Fiber Board for Prototype Tooling [44]

| Property | Unit | Thickness | | |
|---|----------------------------------|-----------------|---------------|------------|
| | | 3/16 to 5/16 in | 3/8 to 7/8 in | 1 to 1¼ in |
| Density | lb/ft ³ | 50 | 48 | 47 |
| Internal bond | lb _r /in ² | 125 | 110 | 90 |
| Modulus of rupture | lb _r /in ² | 5,500 | 4,500 | 4,000 |
| Modulus of elasticity | lb _r /in ² | 500,000 | 450,000 | 400,000 |
| Linear expansion from 50% to 90% RH at room temperature | % | 40 | 30 | 30 |
| Moisture content | % wt | 5 to 7 | 5 to 7 | 6 to 8 |
| Thickness tolerance | in | ±0.005 | ±0.005 | ±0.005 |
| Length/width tolerance | in | ±0.0625 | ±0.0625 | ±0.0625 |
| Corner to corner tolerance | in/ft | ±0.0156 | ±0.0156 | ±0.0156 |

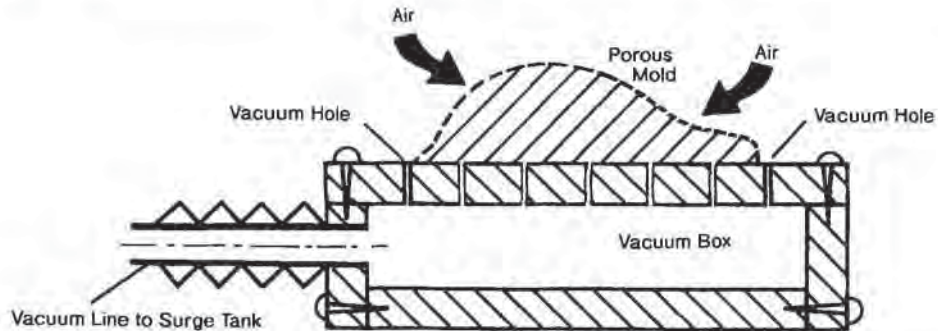


Figure 6.1 Schematic of mold, vacuum holes, vacuum box and corrugated line to surge tank. Mold material here is porous fiberboard through which air will pass

Table 6.4 Molding Plasters [3,4]

| Commercial | Source | Water ratio (pph) | Setting time (min) | Dry compressive strength | |
|--|--------------------|----------------------|--------------------------|-----------------------------|-------------------------------------|
| | | | | (MPa) | (lb _r /in ²) |
| Pattern shop hydrocal (Hydrocal A-11) | US Gypsum | 54-56 | 20-25 | 22.1 | 3,200 |
| Industrial white Hydrocal | US Gypsum | 40-43 | 20-30 | 37.9 | 5,500 |
| Ultracal 30 | US Gypsum | 35-38 | 25-35 | 50.3 | 7,300 |
| Densite K5 | Georgia Pacific | 27-34 | 15-20 | 65.5 | 9,500 |
| Super X Hydro-Stone | US Gypsum | 21-23 | 17-20 | 96.5 | 14,000 |

harden when mixed with water. Molds are formed by casting the newly prepared water-plaster mixture against a part pattern. Since the hydrolytic reaction is exothermic to 100°C or 200°F or so, the pattern should not be fragile. Typically, pattern surfaces are coated with a release agent such as a water soluble polyvinyl alcohol or PVOH. Soaps such as Murphy's oil soap are also used¹. Vents are designed in by placing release-agent-coated wires perpendicular to the pattern surfaces prior to casting. For very thick molds made in multiple pours, soda straws are placed over the wires after the first pour. This allows the wire to be easily extracted later and also provides for a modicum of "back-drafting". For very thick molds made in a single pour, release-agent-coated tapered pins should always be used.

¹ Murphy's oil soap is available in leather goods stores and laundry and cleaning areas of grocery stores. It is used primarily to clean porous surfaces such as wood and leather. To use it as a water-soluble release agent, coat the pattern with a generously thick coat and allow it to dry thoroughly. Add a second coat to those areas that are not at least semi-glossy.

A very hard void-free surface on the mold is achieved by “splating” a thin layer of relatively high water content plaster slurry against the pattern. This thin layer is allowed to harden before further casting continues. This technique is adapted from that used by artisans working in fine plaster art [3]. To ensure adequate dispersion, the plaster must be very carefully mixed into the water. Once the plaster and water are thoroughly mixed, the mass is vibrated for several seconds to dislodge large air bubbles. Sisal, straw and glass fibers are excellent reinforcing fibers for plaster¹. To ensure adequate wet-out and adhesion, the organic fibers are soaked in water for several minutes before being mixed into the water-plaster mixture. Typically, fiber reinforcement levels are 10% to 20% (vol). The mixture becomes harsh with higher reinforcement levels and air bubbles and voids are easily entrapped. Additional water reduces the strength of the plaster matrix. Typically, 35 parts water per hundred parts of plaster is a useful starting recipe [4].

Cure against the pattern usually takes about 30 min, although slower reacting plasters and those with fibers or fillers need as much as 1 h to reach demolding or green strength given in Table 6.4. While casting the primary mold, the moldmaker usually pours a simple test mold. This test mold is used to judge the level of exotherm and the degree of cure. After the pattern has been removed and the vent wires pulled, the mold is set aside in a dry, warm area for several days. This time is needed to develop the final properties and to stabilize the water content. The mold can crack if it is used before being thoroughly dried. The mold surface is then finished with open grit paper. Epoxy floor varnish is used if a smoother surface is needed. However, plaster molds are usually used for expediency and a fine surface is of secondary concern.

Plaster molds are surprisingly durable. They can withstand cyclic forming temperatures of most commercial plastics quite well. They are quite heavy however. The molds should never be subjected to flexural loading since failure is catastrophic. Plaster breaks are repaired with epoxy, as are spalled surfaces. Auto body putty also works well. However, broken molds are rarely repaired and so patterns are usually preserved to produce a new mold. Glass- and polymer-fiber reinforced plasters and cementitious products such as water-curing hydraulic cement are also prototype mold materials, but material costs are up to 5 times those of conventional molding plasters.

Plastic

Great advances have been made in the last few years in formulating thermosetting plastic resins for thermoforming mold. In particular, plastic molds are economically preferred for:

- Heavy-gage sheet forming,
- Part forming where heat buildup on the mold surface is intermittent,

¹ Other fibers are used to reinforce plaster. As an example, polypropylene and polyethylene fibers are used to produce impact-resistant construction grade plaster board. Normally, these fibers are too expensive to be used for prototype thermoforming tooling.

- Parts where the mold does not need to be heated to facilitate forming,
- Very large surface area parts such as,
 - Outdoor signs,
 - Camper tops,
 - Outdoor swimming pools,
- Drape and low-pressure vacuum forming, and
- Prototype forming for less than 100 parts.

For applications where mold surface temperatures do not exceed 60°C or 140°F and where drape and vacuum forming are used, epoxy and unsaturated polyester resin or UPE are materials of choice. These resins are usually combined with various forms of glass fibers. The exact manner of mold fabrication depends on the mold shop, but the general procedure usually followed is described below.

Since thermosetting resins usually cure most efficiently at relatively high temperatures of 100°C to 125°C or 200°F to 260°F, the pattern must be thoroughly dried before beginning mold fabrication. Plaster and wood patterns should be thoroughly air oven dried at 50°C or 120°F for at least 24 h [5]. The pattern surfaces are then sealed with at least two coats of air-sprayed thinned automotive lacquer or industrial polyurethane or PUR. The hard surfaces are then waxed twice with a hard paste wax such as carnuba or Treewax. The surfaces are power-buffed after each wax application. PVC plastisol is recommended as a release agent [5]. If the patterns are thoroughly dried, aqueous polyvinyl alcohol or PVOH can also be used. These release agents should be air-sprayed to ensure uniform coverage. Two coats are recommended.

Generally, epoxy and UPE molds are fabricated in similar ways, although UPE mold construction is more complex and requires more steps. For glass fiber-reinforced UPE or GR-UPE molds, a 0.3 to 0.4 mm or 0.010 to 0.015 in layer of special resin known as gel-coat is first sprayed against the prepared pattern. A typical gel-coat recipe is given in Table 6.5. This layer is allowed to air-cure, either at room temperature or under infrared lamps, until tacky. An optional second layer can then be applied. The surface should then be carefully inspected for bubbles or other defects. Care at this point can obviate expensive surface repairs later on. A layer of very fine glass fabric known as *C-veil* is then placed against the gel-coat. A thin layer of UPE laminating resin is sprayed over the fabric and gently squeegeed into it¹. Once the *C-veil* layer has cured to a tacky state, the first layers of reinforcing glass are laid. The glass fabric normally used is a plain weave of about 4 to 10 threads per cm or 10 to 25 threads per in [tpi]. The fabric weight is about 500 g/m² or 20 oz/yd². Plain weave is used because:

- It has good strength in both directions,
- It can be easily oriented and shifted to fit tight curves,
- It has an open weave to minimize air entrapment, and
- It is an expensive fabric structure.

¹ An alternate method involves dipping the *C-veil* in catalyzed resin and applying the wetted fabric to the gel-coated surface. Since the wet fabric is quite weak and the resin drains readily from it, this approach is quite messy and consumes more resin than spraying. However, it leads to far fewer dry pockets between the gel-coat and *C-veil*.

Table 6.5 Typical Recipe for Unsaturated Polyester Resin Gel-Coat for Prototype Thermoforming Molds

| Resin recipe | Molar ratio | |
|---|-----------------|--|
| Isophthalic acid | 1 | |
| Maleic anhydride | 1 | |
| Neopentyl glycol, glycol excess, 2% | 2.04 | |
| Acid number ≈ 18 Hydroxyl number ≈ 30 Gel time ≈ 5 min Peak exotherm $\approx 225^\circ\text{C}$ or 437°F | | |
| Formulation (polystyrene in polyester at 40 wt %) | Parts by weight | |
| Polyester, as above | 48 | |
| TiO ₂ pigment | 20 | |
| Styrene diluent | 32 | |
| Fumed silica | 1.5 | |
| Cobalt octoate promoter | 0.3 to 0.6 | |
| Methyl ethyl ketone peroxide catalyst | 0.2 to 0.3 | |
| Clear casting properties on 0.32 cm or 0.125 in thick sample | | |
| Flexural strength | 145 MPa | 21,000 lb _f /in ² |
| Flexural modulus | 3.9 GPa | 570,000 lb _f /in ² |
| Elongation | 1.9% | |
| Tensile strength | 65.5 MPa | 9,500 lb _f /in ² |
| Heat distortion temperature | 112°C | 234°F |

Strips are cut 50 mm by 500 mm or 2 in by 20 in, hand-dipped in catalyzed resin and hand-applied to critical high-stress areas of the mold such as corners and rim. The strips are then hand-rolled to express air and ensure intimate contact with the C-veil layer. Usually the resin bath is catalyzed for a 1 h gel time¹. The moldmaker needs to know approximately how much resin can be applied in that time. A typical resin recipe is given in Table 6.6. Since UPE resins exotherm when curing, the thickness of the built-up layer of uncured resin on the mold must be restricted to about 6 mm or 0.25 in. Excessive thickness will cause the resin to crack during curing. Thicker mold sections are fabricated by building atop the mostly cured mold substrate.

Once the critical stress areas on the mold have been constructed, reinforcing elements such as thoroughly dried, untreated wood or plaster are added. Scrap fully cured GR-UPE pieces are also used. These are held in place with resin and resin-wetted woven glass fabric. Automotive body putty, a filled UPE product, can also be pressed into irregular areas. These materials are then cured in place. The rest of the mold surface area is then built, either by hand dipping squares of fabric in catalyzed resin and hand applying, or by applying dry fabric to the surface and

¹ The gel time is that time when the resin becomes stringy and jelly-like. Beyond the gel time, no further manipulation such as rolling or expressing, is possible.

Table 6.6 Typical Recipe for Unsaturated Polyester Resin With Fiberglass Mat Reinforcing for Prototype Thermoforming Molds

| Resin recipe | Molar ratio | |
|--|-----------------|--|
| Isophthalic acid | 1 | |
| Maleic anhydride | 1 | |
| Propylene glycol | 2.2 | |
| Acid number ≈ 8 Hydroxyl number $\approx 45-50$ Gel time $\approx 8-12$ min Peak exotherm $\approx 225^\circ\text{C}$ or 437°F | | |
| Formulation (polystyrene in polyester at 40 wt %) [recipe depends on wet-out method, type of fabrication—hand layup, spray-up, etc.] | Parts by weight | |
| Polyester, as above | 42 | |
| TiO ₂ pigment | 28 | |
| Styrene diluent | 30 | |
| Cobalt octoate promoter | 0.3 | |
| Methyl ethyl ketone peroxide catalyst | 0.15 to 0.3 | |
| Total physical properties of fiberglass-reinforced polyester | | |
| Flexural strength | 138 MPa | 20,000 lb _f /in ² |
| Flexural modulus | 7.0 GPa | 1,000,000 lb _f /in ² |
| Elongation | 1.0% | |
| Tensile strength | 82.8 MPa | 12,000 lb _f /in ² |
| Heat distortion temperature | 190°C | 375°F |

squeegeeing resin into it. These layers are then cured to tackiness. Once the entire pattern surface has been covered with at least one layer of nearly-cured fabric and resin, additional layers are added in rapid succession. Wet fabric does not stick well to vertical surfaces. As a result, the mold orientation during fabrication usually dictates the total mold construction time.

After a solid reinforced layer is built over the entire mold surface to 3 mm or 0.125 in or so, chopped glass and reactive resin is sprayed onto it. Since the sprayed material resembles wet hay, it must be carefully rolled to express air. Rolling is done with special spaced-disk rollers. The reason for restricting spray-up techniques to supporting roles for hand lay-up is that spray-up laminates have only about 70% to 80% of the flexural strength and modulus of hand lay-up laminates [5]. The spray-up technique is much less labor intensive than hand lay-up and so mold costs are reduced by using it in a supporting role. Once the minimum mold thickness of about 6 mm or 0.25 in is reached, the inner mold structure is constructed. The moldmaker must keep in mind that molds built this way are very large. Even the low pressures used in vacuum forming generate substantial forces that can crush or buckle an unreinforced plastic mold. A standard inner structure is an egg-crate of 2 to 2.5 cm or 0.75 to 1 in thick exterior plywood or laminated wood having 10 to 15 cm or 4

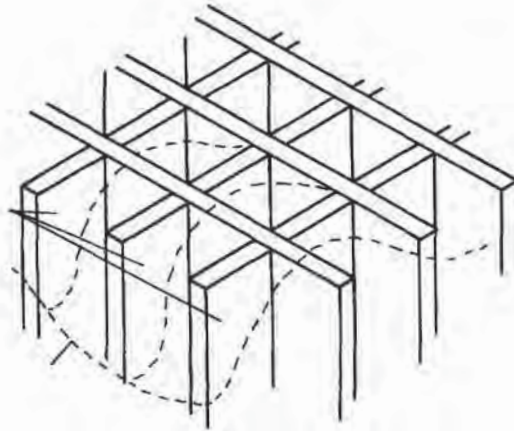


Figure 6.2 Egg-crate cradle that fits into male mold

to 6 in openings. For a male mold, the egg-crate is shaped to fit inside the formed mold structure (Fig. 6.2). For a female mold, the egg-crate is fashioned into a cradle to support the flat sides and bottom of the mold (Fig. 6.3). The plywood is held in place with reactive resin and glass fiber tape or automotive body putty. The plywood core allows for easy access to vent holes.

For additional reinforcement, aluminum or phenolic-impregnated paper honeycomb sheet up to 5 cm or 2 in thick is used. This is just laid into the wet resin against the mold back and held in place until the resin cures. PVC, aluminum or GR-UPE pipe is also used for reinforcing. Pipe sections are joined to each other and to the mold back with resin-wet fabric strips and held until the resin sets. The rim of a very

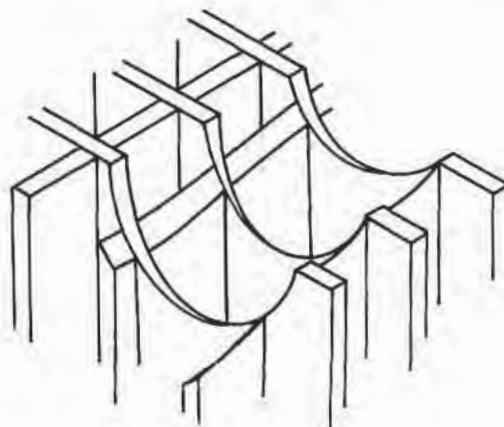


Figure 6.3 Egg-crate cradle into which female mold fits

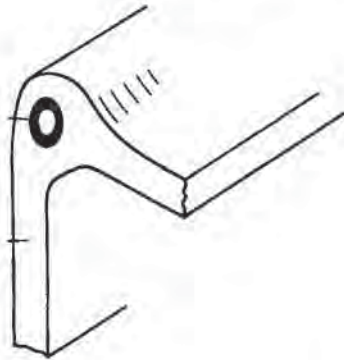


Figure 6.4 Pipe reinforcement in castable reinforced resin mold

large mold is commonly reinforced in this manner (Fig. 6.4). If the mold must withstand large buckling forces although not necessarily large pressures, lightweight organic cement can be cast against the mold back. Recently, many cements have been developed where a low density aggregate such as slag or Perlite expanded material is mixed with 5 to 10% (wt) UPE or epoxy resin as a binder, then troweled in place. Expanded polystyrene or EPS beads can be mixed with low viscosity epoxy resin as a low-density backing agent¹. It is necessary to ensure adequate vent hole placement *and access* before the mold back is sealed in several cm or inches of cement.

Once the mold construction is complete, it must be cured thoroughly, preferably at room temperature. Curing normally takes 24 to 48 h, although more time may be required if some areas are quite thick. To ensure a hard, thorough cure, the mold and pattern is placed in a warm air oven at 50°C or 120°F for an additional 24 to 48 h. It is difficult to cure UPE in thin cross-sections to a tack-free state at room temperature, however. Oxygen inhibits reactivity on exposed surfaces. One way around this is to spray a thin layer of air-drying, film-forming PVOH solution on the exposed curing UPE surface. Once the UPE is fully cured, the resulting thin film is then stripped from the mold. If the pattern has been properly prepared, it should release easily from the mold. UPEs and epoxies shrink on curing. If sufficient taper has not been provided on female molds and female portions of male molds, the mold and pattern can become locked together. Even with adequate pattern preparation, considerable manpower and time may be required to release very large molds from patterns. Mold release is best accomplished with combinations of air, water and weight. The entire assembly is suspended slightly above the shop floor with the heavier element nearest the floor. Air and water from separate sources are forced between the edges of the mold and the pattern at the interface. In desperate cases, the pattern must be destroyed to free the mold.

The mold surface is then adequately cleaned, waxed and buffed prior to use. Even though plastic molds can last for hundreds of cycles, surface deterioration can begin

¹ EPS cannot be used with unsaturated polyester resin, since UPE contains styrene monomer, a solvent for EPS.

in a very few cycles. The most common problem is pinholing, due to collapse of small bubbles trapped in and behind the gel-coat during fabrication. Some dimples and dents are caused by problems in applying the release coat to the pattern. Delamination and blistering are also problems. Usually surface repairs are straightforward. The defect area is sanded or ground down to good material. A patch of catalyzed resin containing a filler such as fumed silica is then troweled into the defect. Cure is by infrared lamp. The region is then finished by feathering into the surrounding good mold material. A cave-in, break-out or development of star cracks during forming require heroic repair efforts. Growing numbers of these usually indicate that the mold was improperly reinforced. Fabrication of a new mold is preferred over attempted repair.

Although this section has focused on UPE mold fabrication, epoxy molds are fabricated in a similar fashion [5]. Most epoxies are mineral- or aluminum-powder filled [6]. The extent of shrinkage varies with the filler content. There is very little exotherm generated with the higher loaded epoxies. Glass fabric is used with epoxies in a manner similar to that with UPE. Some molding epoxies have very high viscosities, however, and substantial effort is required to thoroughly wet out the glass fabric. Water lines are easily cast in place in molds made using either UPE or epoxy. GR-UPE is economically preferred for very large molds and water lines can be PVC pipe or aluminum electrical conduit. Epoxy is more expensive than GR-UPE and so is used for small molds where water lines are aluminum or copper tubing.

Filled thermosetting polyurethanes are now available for prototype tooling [46]. The PUR systems are typically two-part 1:1 mixtures. Most of the systems are heavily loaded, typically with calcium carbonate or other inorganics. By varying the catalyst concentration, prepared recipes have been developed that allow pot life times of a few minutes to several hours. Table 6.7 gives properties of some typical prototype PURs.

Two other approaches for producing prototype molds are being developed. The first uses the concepts of rapid prototyping, detailed in Section 7.3. Rapid prototyping or RP is the generic term used to describe several methods for producing prototype parts [47]. The process uses the mold shape as the computer-generated image. Stereolithography or SLA has been used to produce small prototype molds from UV-curable polyurethane. The cured SLA sheet was back-filled with aluminum-filled epoxy for rigidity [48]. Syntactic foams are also being used to produce prototype tools. The computer-generated mold image is fed to a multi-axis trimming station, Chapter 5. The syntactic foam is then machined into the prototype mold. Both techniques provide rapid turn-around times. These allow the designer to evaluate specific part details and to make necessary changes in a very short time. SLA and syntactic foam molds are not expected to produce more than a few parts.

Recently, aerospace applications have included thermoforming of high temperature polymers¹. The typical GR-UPE and GR-epoxy molds described above are restricted to about 60°C or 140°F use temperature. Higher temperature epoxies are

¹ Composite thermoforming is covered in detail in Chapter 9 on advanced thermoforming techniques.

used to produce molds with use temperatures to 150°C or 300°F. Molds of these materials require much high curing temperatures and much greater care in pattern making and preparation. One manufacturer [7] recommends graphite cloth with aerospace-grade epoxy for fabricating molds that see sheet temperatures of 200°C or 390°F or more. These molds are used to form reactive reinforced resin sheet at low temperatures with curing of the formed sheet against the heated mold at temperatures of 200°C or 390°F. These sophisticated molds include aluminum or copper pipe so that hot oil can be used as a coolant. A mold life of 500 parts is claimed.

White Metal

The metal welding industry relies on the establishment of an intensely hot arc that is drawn between electrically isolated metal surfaces energized with high amperage, low voltage DC power. The arc causes most common metals to melt. When high velocity air is blown into the arc, the molten metal breaks into very fine drops. The molten drops can be transported by the air for short distances before cooling below their fusion temperature. One system, the TAFE system, is shown in Fig. 6.5 [8,50]. The TAFE system establishes the electrical arc between metal wires that are fed in a controlled fashion into the spray zone. By accurate control of the metal wire speed, a uniformly fine metal spray issues. The spray is used to coat a surface. Although most metals can be sprayed, zinc and zinc-alloy metals offer good balances of:

- Flexibility in spraying,
- Relatively low molten metal temperatures, thus preserving pattern surfaces,
- Small drop sizes,
- Good densification and low porosity,
- Good hardness in the metal mold, and
- Good strength in the metal mold.

Typically, zinc has a spraying temperature of 410°C or 770°F and is dispensed at 5 kg/h or 10 lb/h at a power level of 50 to 150A, 20 V, 2 kW. A typical surface hardness is 70 Rb. Other physical properties are given in Table 6.8 [8].

The spraying process begins by securely fastening the pattern, if small, to a turntable and then coating it and the table edges with aqueous PVOH release agent. Once the pattern is secured and dry, the metal spray unit is activated and an arc established¹. The spraying rhythm is similar to paint spraying. The objective is to build up a uniform coat over the entire surface. It is necessary to begin spraying at the edges of the pattern. This ties the edges of the metal layer tightly to the edges of the turntable. If this is not done correctly, the air carrier can infiltrate a loose edge, lift the thin metal layer, and catastrophically tear it from the pattern. The process

¹ Care must be taken at this point. If the release coating is not dry, the hot metal will cause steam bubbles in the finished mold surface. If the metal is focused too long against one portion of the PVOH-coated mold, the PVOH may degrade and pits will form in the finished mold surface.

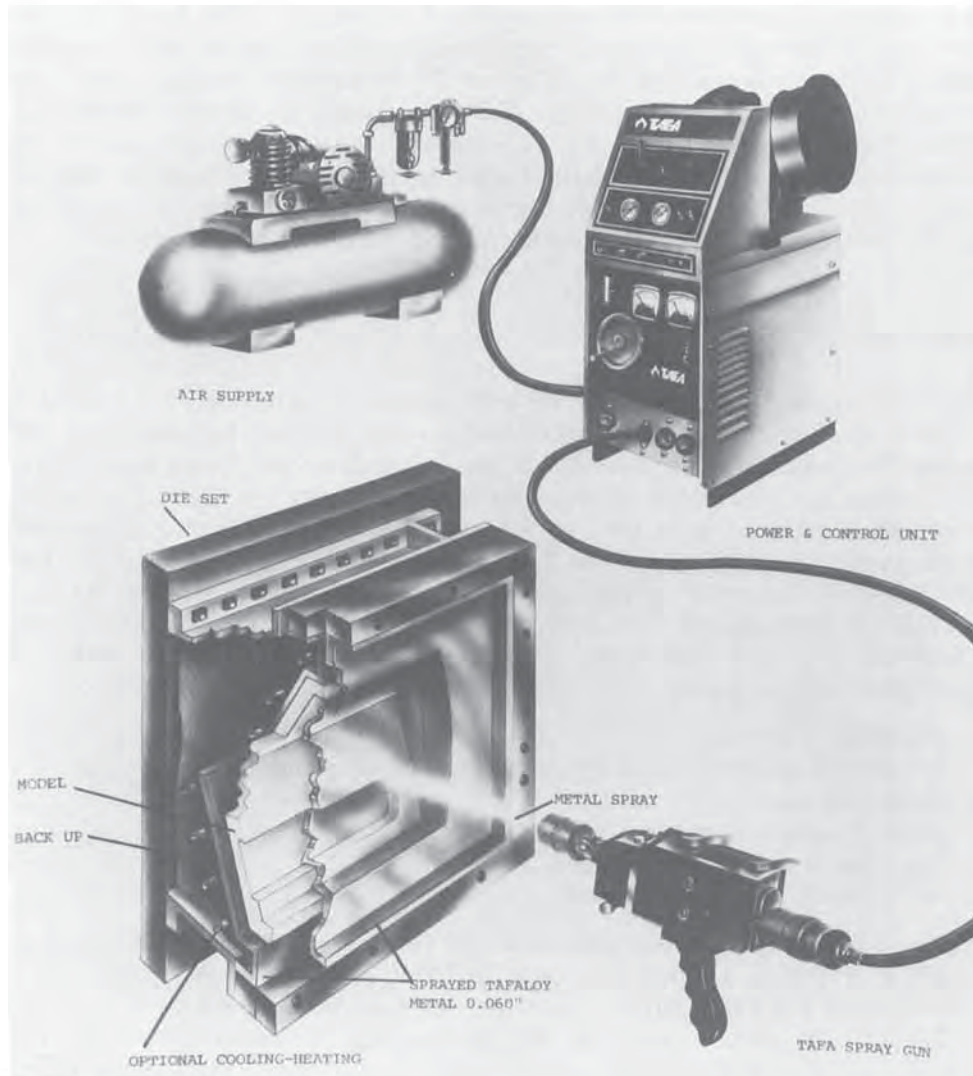


Figure 6.5 Rendering of tafa metal spray technique for thermoform mold fabrication. Photo by permission of Tafa Metallisation, Dow (Concord) NH

must then be restarted beginning with pattern preparation. It is recommended that spraying be done in a well-ventilated hood and the operator should wear a breathing helmet. The pattern can be made of temperature sensitive materials such as plastic, foam or paper. However, care must be taken to prevent concentrated hot metal spraying in a small area. If the pattern is small and spraying is continuous, the interfacial temperature between the pattern and the mold can easily exceed 100°C or

Table 6.8 Properties of Sprayed Zinc [8]

| | | |
|-------------------------------------|------------------------|---|
| Hardness | 70 Rc | |
| Tensile strength | 128 MPa | 18,500 lb _f /in ² |
| Melting point | 410°C | 770°F |
| Temperature on contact with pattern | 240°C | 650°F |
| Density, % theoretical | 92 to 95% | |
| Shrinkage | 0.1 to 0.2% | |
| Cost | \$102/m ² | \$9.50/ft ² |
| Weight | 24.3 kg/m ² | 5.0 lb/ft ² |
| Melting power | 0.44 kW/kg | 0.2 kW/lb |
| Spray droplet size | 50 to 150 μm | |

210°F. Temperatures to 200°C or 390°F have been measured. Typically, spraying continues until a uniform layer of metal of at least 1.5 mm or 0.060 in has been deposited. Reinforcing structures, copper water lines, and other features are then placed on the molded shell and these are encapsulated by spraying additional metal (Fig. 6.6). For greater metal rigidity in stress areas such as edges, corners, and deep recesses, the zinc layer is built to 6 mm or 0.25 in or more. To complete the mold fabrication, epoxy cements are cast behind the metal skin. If the mold needs to be a good heat sink, metal-filled epoxies of the types described above are used. These typically have continuous use temperatures to 120°C or 250°F. Note that certain epoxy formulations depolymerize at local temperatures of 200°C or 390°F or more.

Although spray metal molds have been used in production for vacuum forming for years without appreciable wear, pressure forming dramatically shortens mold life.

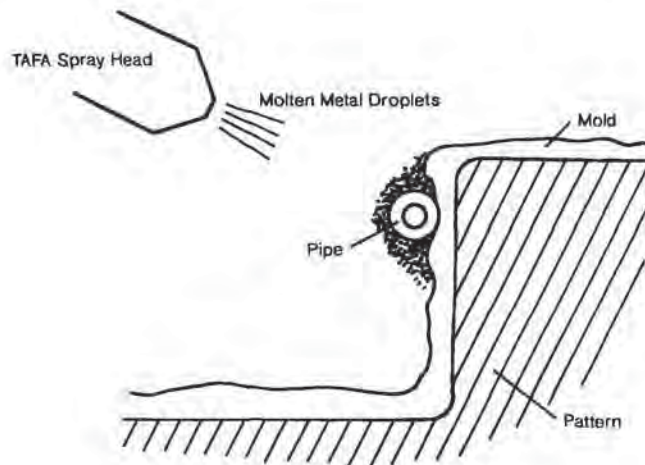


Figure 6.6 Schematic of metal coolant line or metal pipe reinforcement for spray-up white metal mold

When molding sheet molding compound or SMC for example, pressures to 1.5 MPa or 200 lb_f/in² and temperatures to 120°C or 250°F are common. For SMC, mold life is reduced to 100 pieces or so. The primary mode of failure is surface flaking or spalling. In SMC applications, chrome surface diffusion plating is used to harden the zinc surface. The chrome surface is 0.08 to 0.188 or 0.003 to 0.007 in thick and its hardness is 55 to 65 Rc. This treatment increases the cost and delivery time of the mold and should be used only when spray molds are used in pressure thermoforming.

Nickel

Nickel molds are also used for prototype thermoforming. A thin electroformed nickel surface is reinforced with sprayed zinc metal, cast white metal or cast aluminum- or nickel-filled epoxy. The nickel used is a very pure electroplating grade of 99.95% with a trace of cobalt. The pattern surface must be conductive. For wood, plaster, ceramic and plastic patterns, a coating of PUR varnish is sprayed over the pattern surface. While the varnish is still tacky, a very fine coating of powdered graphite is air-blown onto it. The PUR is then cured, either at room temperature or in a free convection oven at 50°C or 120°F. The pattern is then immersed in a cold plating bath. Nickel is laid against the surface at 4 μm/h until a uniform layer of about 1.5 mm or 0.060 in thick has been deposited over the entire pattern surface. The pattern and nickel layer assembly is then removed from the bath. The dried surface is then backed with sprayed white metal or cast epoxy. Alternately, the pattern and nickel assembly is immersed in a second plating bath where copper is added to a thickness of 10 mm or 0.400 in thick or so. Hot plating techniques lay nickel against the pattern surface at the rate of 10 to 20 μm/h, but may produce a coarse-grained porous surface. Normally this surface is dull and matte. It cannot be polished to semi-gloss. But the surface is quite satisfactory for production of non-appearance low-pressure thermoformed parts. Nickel produced by hot plating has about 50% of the toughness of cold plated electroformed nickel. It also costs about 50% of the cost of cold plated electroformed nickel. Recently, a vapor deposition technique has been developed that achieves dry nickel vapor deposition of 0.25 mm/h or 0.010 in/h. Thicknesses of 1 mm or 0.040 in to 25 mm or 1-in are possible without secondary backing. Surface hardness of 40 to 42 Rc with Class A and texture finishes are possible [9].

6.3 Production Molds

Roll-fed sheet forming economics dictate high production rates and long mold life. For this reason, metals yielding low maintenance, good surface hardness, reasonably low cost and low wear are selected. Aluminum has been the choice for many years for the following reasons:

- Aluminum molds wear well,
- Aluminum has outstanding heat transfer characteristics,
- Aluminum is relatively lightweight,
- Aluminum is easy to machine,
- Aluminum is easy to cast,
- Aluminum is moderate in cost, and
- Aluminum has excellent strength-to-weight ratio.

Of these, low cost, ease of fabrication and lightweight are most important. Aluminum molds do not appreciably increase the inertial factor of mechanically acting forming presses. More details are given below. Many newer forming processes involve increased pressures, temperatures and stresses. Processes such as:

- High speed forming,
- Matched die forming,
- In-mold punch-and-die trimming and cutting,
- Pressure forming,
- Heated mold forming for crystallizing polyethylene terephthalate (CPET), and
- Composite sheet forming,

are challenging the ability of aluminum to meet long-term high-production requirements. Steels that are normally used in injection molding are sometimes used in severe conditions in thermoforming. Molds for these high-demand applications may be quite expensive. The expense is justified only on the basis of faithfulness and accuracy over millions of cycles and other features, such as sliding action or in-mold punch-and-die trimming *and* only if these features cannot be achieved in any other mold material.

Aluminum

As noted, aluminum is the material of choice for nearly all thermoforming molds. It is easily fabricated, it has a very high thermal conductivity so sensible heat from the formed plastic sheet is rapidly removed and it is a lightweight, tough metal. Thermoforming molds can be made of either machined plate or cast metal. Typically, molds are fabricated from plates of either 2024-T4 or 6061-T651, aircraft grade. Table 6.9 gives the chemical analysis of these aluminums. Typical machined aluminum is 130 Brinnell. Since tool steel hardness is as high as 300 Brinnell, care must be taken during mold changing and alignment with steel members to avoid marring, gouging and dinging the softer aluminum. Aluminum also has a relatively high thermal expansion coefficient of $19 \times 10^{-6} \text{ } ^\circ\text{C}^{-1}$ when compared with steel at $11 \times 10^{-6} \text{ } ^\circ\text{C}^{-1}$. Care must be taken to minimize abnormal stress and potential buckling or bowing when heating large tightly clamped molds. Molten aluminum is cast at 550 to 600°C or 1000 to 1100°F against ceramic, dried and fired gypsum plaster or foundry sand patterns. Usually atmospheric casting is used to produce prototype or short production-run molds. Atmospheric or foundry casting yields molds that may have surface porosity and nonuniform surface hardness. Porosity

Table 6.9 Chemical Analysis of Machined Aluminum 2024-T4 or 6061-T651

| | |
|----|--------------|
| Cu | 1 to 2% |
| Mg | 0.5 to 1% |
| Mn | 0.5% |
| Si | 4 to 8% |
| Fe | 1% [maximum] |
| Ni | 1% |
| Ti | trace |
| Zn | trace |

can be a problem when pressure forming or if drilled coolant lines pass close to the mold surface. A uniformly high finish is very difficult with foundry cast molds. Pressure casting produces a much denser mold with much more uniform surface hardness, albeit at a higher cost. Patterns must be rugged enough to withstand the thermal shock of molten metal *and* 7 MPa or 1000 lb_f/in². Fired ceramic patterns are recommended. A casting ceramic of ethyl silicate and quartz powder can be fused into patterns that will withstand pressure casting conditions [10].

Steel

The most severe service of any thermoforming process cannot match, say, typical mold temperatures, pressures, erosiveness, or number of required parts of a standard injection molding using filled or reinforced thermoplastics. As a result, thermoforming molds do not need to be constructed of the same tool steel as that specified for injection molds. However, mold shops that specialize in injection molds are accustomed to working in specific types of steels. They will therefore frequently quote jobs in these materials. Prehardened steels such as AISI P20 are recommended for large molds and molds with low demands on wear resistance. P20 is more difficult to machine and polish than, say, S7 or H13 steels. Since the last two must be air-hardened after machining, the mold shop does not risk mold dimensional change or distortion with P20. The chemical analyses of H13 and P20 are given in Table 6.10. H13 hardness is 30 to 36 Rc. Sophisticated techniques have been developed for machining and hobbing molds and for hardening steel surfaces. Although these heroic methods are not really needed for the thermoforming mold itself, hardened steel is used for mold elements such as:

- Slides,
- Collapsing cores,
- Rails,
- Guides,
- Platen frames,
- Sheet clamps,

Table 6.10 Chemical Analysis of Tool Steels

| Air-hardened P13 tool steel | | Oil-hardened P20 tool steel | |
|-----------------------------|-------------|-----------------------------|-------------|
| C | 0.35% | C | 0.35% |
| Cr | 5.0% | Cr | 1.25% |
| Mo | 1.5% | Mo | 0.4% |
| V | 1.0% | | |
| Hardness | 50 to 54 Rc | Hardness | 30 to 36 Rc |

- Hold-downs,
- Pins, and
- Pin-chains.

Similarly, investment casting of molten steel against ceramic patterns is also not needed [11].

Other Metals

In injection molding, beryllium/copper and Kirksite are frequently used for prototype tooling [11,12]. Typically, molds of these materials yield more parts than aluminum, sprayed metal and plastic molds. Steel molds yield more parts than all other materials (Table 6.11). Low-pressure thermoforming molds see much less severe service than injection molds. As a result, these exotic materials are rarely used. Nevertheless, the service guides given in Table 6.11 hold for low-pressure forming molds as well, with mold lifetimes extended by a factor of at least 10. The mold

Table 6.11 Guide to Tooling Materials [12]

| Material | Delivery time, (weeks) | Number of parts, × 1000 | | Repairs ¹ | Changes, texture | Surface ² finish |
|------------------|------------------------|-------------------------|------------|----------------------|------------------|-----------------------------|
| | | Injection mold | Thermoform | | | |
| Epoxy | 2 to 4 | 0.1 | 0.1 to 10 | 3 | No | C/D |
| Sprayed metal | 2 to 4 | 0.05 | 0.1 | 3 | No | C/D |
| Kirksite | 4 to 20 | 100 | 1,000 | 1 | Yes | B |
| Beryllium/copper | 4 to 12 | 500 | 1,000 | 2 | Yes | A/B |
| Aluminum | | | | | | |
| Cast | 3 to 8 | 50 | 200 | 2 | Yes | A/B |
| Machined | 12 to 20 | 100 | 1,000 | 2 | Yes | B/C |
| Steel | 12 to 26 | 1,000 | 10,000 | 1 | Yes | A |

¹ 1 = Easy, 3 = Difficult

² A = Diamond, B = Buff polish, C = 400–600 Grit, D = 350–400 Grit

lifetimes for high-pressure pressure forming and composite forming at elevated temperatures are much closer to those for injection molding.

6.4 Mold Coolant Channels

Many prototype molds and all production molds are actively cooled. Recommended mold temperatures are given in Table 2.5. In production molds, the coolant lines are usually gun-bore drilled in a manner similar to those drilled in injection molds [13]. There are many ways of embedding coolant lines in prototype molds, as noted above. Plastic, aluminum or copper pipe is cast in place in spray-up GR-UPE molds and cast epoxy molds. Copper or aluminum tubing is fastened in place in spray-up white metal and electroformed nickel molds. The location, diameter and number of coolant lines depends on the size and complexity of the mold, and the heat removal potential of the mold material. The determination of heat removal rates is given below. It is recommended that a mold with a properly designed coolant channel pattern should exhibit no more than 3°C or 5°F temperature variation across its surface at steady-state production and that the coolant temperature increase is no more than 3°C or 5°F from inlet to outlet [14]. It is apparent from Table 2.5 that for most commodity polymers, the coolant of choice is hot water. Figure 6.7 shows a simple closed circulating system for treated water as a coolant in thermoforming. To cool polycarbonate, polysulfone and other engineering polymers, the water coolant system must be pressurized to 0.4 MPa or 50 lb_f/in² or more. Hot oil is recom-

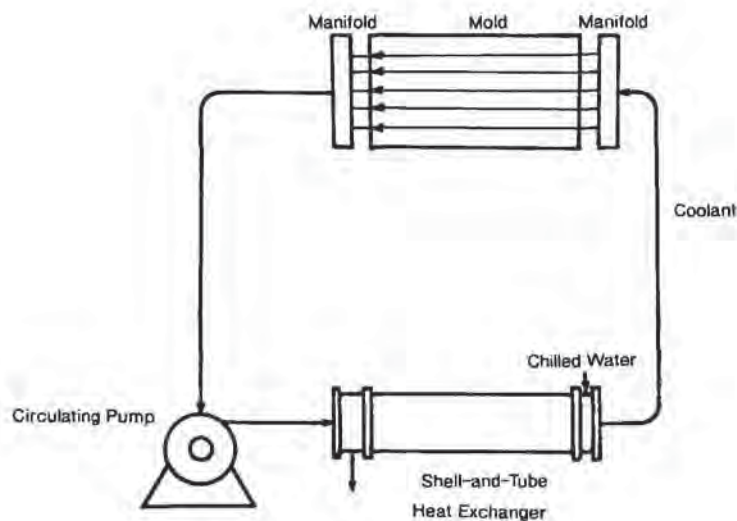


Figure 6.7 Mold coolant plumbing schematic

mended for filled and fiber-reinforced engineering polymers and for higher temperature polymers.

Mold Channel Flow

Figure 6.7 shows an example of a closed circuit coolant system for a thermoform mold assembly. Pressure losses in complex plumbing systems such as that shown in Fig. 6.7 are best analyzed in terms of Darcy-Weisbach “head losses” for each of the various elements in the system [15]. For simple flow in a constant-area pipe, the head loss is given as:

$$h = \left(\frac{fL}{D} \right) \frac{v^2}{2g_c} \quad (6.1)$$

where L/D is the pipe length-to-diameter ratio, v is the average fluid velocity, g_c is an appropriate conversion factor, and f is the *friction coefficient*. The value of f depends on the nature of fluid flow in the pipe. There are three types of fluid flow that can occur in mold channel flow. These are identified in terms of the fluid Reynolds number, defined as:

$$\text{Re, Reynolds number} = \frac{Dv \cdot \rho}{\mu} \quad (6.2)$$

where D is the pipe diameter, v is the average fluid velocity, ρ is the fluid density, and μ is the fluid viscosity. Re is dimensionless and the other variables are in appropriate units. The fluid is called *laminar* when $\text{Re} \leq 2000$. The friction factor for laminar flow is given as:

$$f = \frac{64}{\text{Re}} \quad (6.3)$$

The fluid is in *transition* when $2000 \leq \text{Re} \leq 10,000$ or so. And the fluid is considered to be *turbulent* when $\text{Re} \geq 10,000$. For transition and turbulent flow, the friction factor is given in terms of a relative pipe wall roughness factor, ϵ/D [16,17]. An approximate correlation for $\epsilon/D \leq 0.04$ and $\text{Re} \geq 10,000$ is [18,19]:

$$f = a + b \text{Re}^{-c} \quad (6.4)$$

where

$$a = 0.094 [\epsilon/D]^{0.225} + 0.53 [\epsilon/D]$$

$$b = 88 [\epsilon/D]^{0.44}$$

$$c = 1.62 [\epsilon/D]^{0.134}$$

For flow through non-constant area elements, the head loss equation is written as:

$$h = K \frac{v^2}{2g_c} \quad (6.5)$$

An appropriate value for K , the head loss coefficient, is needed for each flow area change. These are summarized as follows:

Expansion

For flow from a small diameter pipe, D_1 , to a large diameter pipe, D_2 , K is obtained from:

$$K = \left[1 - \left(\frac{D_1}{D_2} \right)^2 \right]^2 \quad (6.6)$$

When the pipe discharges into a reservoir, $K = 1$.

Contraction

For flow from a large diameter pipe to a small diameter pipe, the head loss coefficient is given as:

$$K = \left(\frac{1}{c} - 1 \right)^2 \quad (6.7)$$

where c , the contraction coefficient, is a function of the area ratio of the pipes (Fig. 6.8). Note that c asymptotically approaches $c = 0.61$. This value is frequently used when the exact area ratios are unknown, such as flow through pinched tubing.

Sharp-Edged Orifice

On occasion, short constrictions are used to control fluid flow. Approximate values for K for valves, elbows, tees and other constrictions are given in Table 6.12 [20,21]. In certain instances, quick-disconnects and other devices that allow for rapid

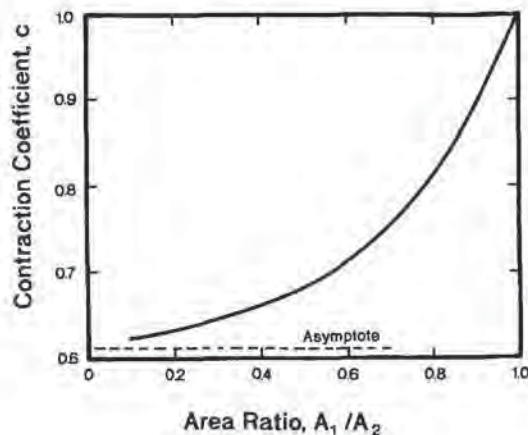


Figure 6.8 Head loss contraction coefficient for coolant flow

Table 6.12 Head Loss Coefficients for Various Plumbing Fittings
[20,21]

| Type of constriction | K, Head loss coefficient |
|---|--------------------------|
| Elbow | 0.9 |
| Tee | 1.8 |
| 180° bend | 2.2 |
| Globe valve fully open | 10.0 |
| Check valve fully open | 2.5 |
| Gate valve fully open | 0.19 |
| Gate valve 3/4 open | 1.15 |
| Gate valve 1/2 open | 5.6 |
| Gate valve 1/4 open | 24.0 |
| Diaphragm or butterfly valve fully open | 2.3 |
| Diaphragm or butterfly valve 3/4 open | 2.4 |
| Diaphragm or butterfly valve 1/2 open | 4.3 |
| Diaphragm or butterfly valve 1/4 open | 21.0 |

disassembly are employed. These devices can be considered as sharp-edged orifices and the head loss coefficients obtained from:

$$K = \left(\frac{1}{c_o^2} - 1 \right) \quad (6.8)$$

where c_o is obtained from Fig. 6.8, it is advisable to use a single velocity when making head loss calculations for complex systems. The complex system head loss equation would appear as:

$$h_{\text{total}} = \left[\sum \frac{fL}{D} + \sum K \right] \frac{v^2}{2g_c} \quad (6.9)$$

In certain cases, as with multiple flow channels in a conventional mold, head losses in the manifolded section should be calculated separately. Example 6.1 is an analysis for water as the coolant. Example 6.2 shows the effect of using oil as the coolant. In Section 5.5, heat transfer between the sheet, its ambient air environment and the coolant medium was considered in detail. As noted, heat transfer efficiency is highest when coolant flow is turbulent, that is, when $Re > 10,000$ or so. This is usually the case for most dedicated water coolant recirculating systems. High Reynolds number is achieved through high fluid velocity, small pipe dimension, and low fluid viscosity. Turbulent flow is best achieved by high volumetric flow rates although it is apparent from the head loss equation, Equation 6.9, that pressure drop increases roughly in proportion to the square of fluid velocity. Increasing coolant viscosity reduces coolant effectiveness. Thus, reducing coolant temperature, changing from water to brine, water-ethylene glycol, or water-glycerine, and changing to oil usually results in increased pressure drop and a reduction in heat transfer efficiency.

Example 6.1 Water as a Coolant

Consider the mold coolant system of Fig. 6.7 using water with the following dimensions:

Waterline diameter = $1\frac{1}{2}$ in
 Waterline length (total) = 100 ft
 Water temperature = 70°F
 Water kinematic viscosity = 1.06×10^{-5} ft²/s
 Water density = 62.4 lb/ft³
 Fluid velocity in $1\frac{1}{2}$ in water line is 4.1 ft/s.

Pipe and mold roughness ratio, $\epsilon/D = 6 \times 10^{-5}$. The friction factor, f , determined from empirical Equation 6.4, to be:

$$f = 0.01058 + 1.221 \text{Re}^{-0.44}$$

Plumbing to the mold includes:

6 elbows
 1 fully open gate valve
 $1\frac{1}{2}$ open gate valve
 1 expansion into a $2\frac{1}{2}$ in manifold
 1 contraction from a $2\frac{1}{2}$ in manifold

Consider pressure loss through manifold negligible.

Mold conditions include:

Coolant diameter = $3/4$ in
 Coolant length = 10 ft
 4 parallel coolant lines in mold
 Plumbing in mold includes:
 6 90° turns or elbows
 1 expansion into $2\frac{1}{2}$ in manifold
 1 contraction into $2\frac{1}{2}$ in manifold
 2 quick disconnects considered to be orifices

Determine pressure drop through plumbing complex.

Flow in $1\frac{1}{2}$ in waterline

Reynolds number, $\text{Re} = Dv\rho/\mu = 50,000$.
 Flow is turbulent.

Friction factor, $f = 0.021$.

| | |
|--|-----------------|
| Head loss coefficient, $fL/D =$ | 16.83 |
| Head loss for 6 elbows, $6 \times 0.9 =$ | 5.4 |
| Head loss for valves = | 5.79 |
| Head loss for expansion, contraction = | $\frac{1.5}{2}$ |
| Total head loss | 29.52 |

Total pressure drop in $1\frac{1}{2}$ in waterline:

$$P = 29.52 \frac{v^2}{2g_c} \times \rho = 3.31 \text{ lb}_f/\text{in}^2$$

Flow in mold channels

With 4 parallel lines, velocity in mold channels same as that in $1\frac{1}{2}$ waterline from pump. However, Re decreases:

Reynolds number, $Re = Dv\rho/\mu = 25,000$.

Flow is turbulent.

Friction factor, $f = 0.0248$.

Head loss coefficient, $fL/D = 3.96$

Head loss for 6 elbows, $6 \times 0.9 = 5.4$

Head loss for 2 sets of orifices = 3.374

Head loss for expansion, contraction = $\frac{1.5}{10.27}$

Total head loss

Total pressure drop in $3/4$ in mold coolant channel:

$$P = 10.27 \frac{v^2}{2g_c} \times \rho = 1.59 \text{ lb}_f/\text{in}^2$$

Thus the total pressure drop for the plumbing system of Fig. 6.7 is given as:

$$P_{\text{total}} = 3.31 + 1.59 = 4.9 \text{ lb}_f/\text{in}^2$$

Pumping rate:

$$Q = \frac{v \cdot \pi D^2}{4} \cdot \frac{\rho}{8.33} = 22.5 \text{ gal/min}$$

Example 6.2 Oil as a Coolant

Consider the mold coolant system of Fig. 6.7 using oil with the following dimensions:

Oil coolant line diameter = $1\frac{1}{2}$ in

Oil coolant line length (total) = 100 ft

Oil temperature = 150°F

Oil kinematic viscosity¹ = $1.3 \times 10^{-4} \text{ ft}^2/\text{s}$

Oil density = $54.5 \text{ lb}/\text{ft}^3$

Fluid velocity in $1\frac{1}{2}$ in oil coolant line is 4.1 ft/s.

Pipe and mold roughness ratio, $\epsilon/D = 6 \times 10^{-5}$. The friction factor, f , is determined from empirical Equation 6.4, to be:

$$f = 0.01058 + 1.221 Re^{-0.44}$$

¹ Equivalent to SAE 10 oil

Plumbing to the mold includes:

6 elbows

1 fully open gate valve

1 open gate valve

1 expansion into a $2\frac{1}{2}$ in manifold

1 contraction from a $2\frac{1}{2}$ in manifold

Consider pressure loss through manifold negligible.

Mold conditions include:

Coolant diameter = $3/4$ in

Coolant length = 10 ft

4 parallel coolant lines in mold

Plumbing in mold includes:

6 90 turns or elbows

1 expansion into $2\frac{1}{2}$ in manifold

1 contraction into $2\frac{1}{2}$ in manifold

2 quick disconnects considered to be orifices

Determine pressure drop through plumbing complex.

Flow in $1\frac{1}{2}$ in oil coolant line

Reynolds number, $Re = Dv\rho/\mu = 3850$.

Flow is in transition.

Friction factor, $f = 0.0429$.

Head loss coefficient, $fL/D = 34.31$

Head loss for 6 elbows, $6 \times 0.9 = 5.4$

Head loss for valves = 5.79

Head loss for expansion, contraction = $\frac{1.5}{47.00}$

Total head loss

Total pressure drop in $1\frac{1}{2}$ in oil coolant line:

$$P = 47.00 \frac{v^2}{2g_c} \times \rho = 4.60 \text{ lb}_f/\text{in}^2$$

Flow in mold channels

With four parallel lines, velocity in mold channels is same as that in $1\frac{1}{2}$ oil coolant line from pump. However, Re decreases:

Reynolds number, $Re = Dv\rho/\mu = 1925$.

Flow is laminar.

Friction factor, $f = 0.0333$.

Head loss coefficient, $fL/D = 5.33$

Head loss for 6 elbows, $6 \times 0.9 = 5.4$

Head loss for 2 sets of orifices = 3.374

Head loss for expansion, contraction = $\frac{1.5}{15.60}$

Total head loss

Total pressure drop in 3/4 in mold coolant channel:

$$P = 15.60 \frac{v^2}{2g_c} \times \rho = 1.52 \text{ lb}_f/\text{in}^2$$

Thus the total oil coolant pressure drop for the plumbing system of Fig. 6.7 is given as:

$$P_{\text{total}} = 4.60 + 1.52 = 6.12 \text{ lb}_f/\text{in}^2$$

6.5 Vent Holes

As the hot plastic sheet is drawn into the mold, the trapped air must be evacuated. Small holes are drilled into the mold surface in the regions where the last portion of the drawing sheet contacts the mold. The number and diameter of these vent or vacuum holes is determined prior to mold design. If the vent hole diameter is too large, hot plastic is drawn into it, producing an unsightly bump, nipple or nib on the finished part. If the nib is excessive, the sheet can rupture. If too few holes are provided or if the vent area is too small, the rate of draw-down will be controlled by the rate of air flowing from the cavity. If the rate is very slow, the sheet may cool so much during draw-down that it can no longer be stretched into the corners and full mold shape replication is not achieved.

Vent hole design is coupled to vacuum system design. Figure 6.9 shows a schematic of a typical thermoformer vacuum system. The basic system consists of:

- Vacuum pump, capable of achieving 28 to 28.5 in mercury (28 in Hg to 28.5 in Hg) vacuum,

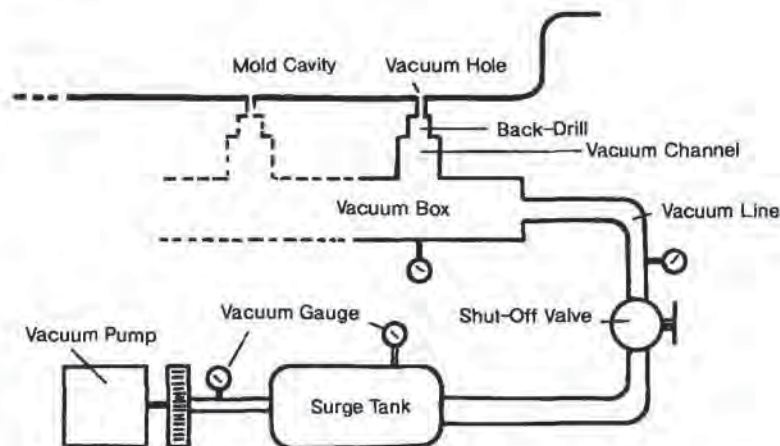


Figure 6.9 Typical plumbing between mold cavity and vacuum pump

- Vacuum surge tank, typically having 6 to 20 times the volume of the combined mold cavity volumes,
- A solenoid-actuated shut-off valve,
- A flow control valve,
- Large-diameter plumbing between the surge tank and the vacuum box,
- A vacuum box or chamber fixed between the mold platens,
- A mold or molds containing:
 - Vacuum or vent holes, and
 - Vacuum slots or drilled holes between the vent holes and the vacuum box, and
- A mold cavity or mold cavities.

As discussed in Chapter 1, two types of vacuum systems are currently used. For very large installations with many thermoforming machines and other uses for evacuated air such as vacuum-routing, a central vacuum system is used. Very large diameter (4 in minimum with 6 in typical) vacuum lines are plumbed to each application. This is shown in schematic in Fig. 6.10. For small installations, each thermoforming machine is equipped with a dedicated vacuum system. This is shown in schematic in Fig. 1.23 for a shuttle press¹.

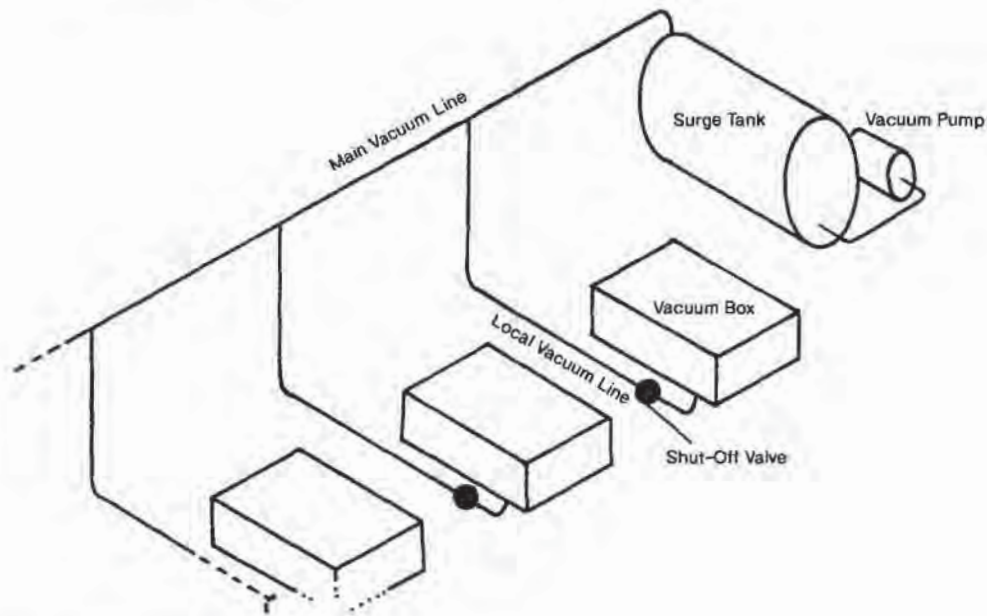


Figure 6.10 Central vacuum system schematic

¹ Even though a central vacuum system is preferred for a multiple former shop, it is important to reserve at least one, dedicated, working vacuum pump and surge tank for emergencies or for auxiliary evacuation for deep cavity jobs.

Table 6.13 Gas-Law Constant

| Numerical value | Units |
|-----------------|--|
| 1.987 | cal/g-mol · K |
| 1.987 | Btu/lb-mol · °R |
| 82.06 | cm ³ · atm/g-mol · K |
| 0.08205 | liter · atm/g-mol · K |
| 10.731 | ft ³ · lb _r /in ³ · lb-mol · °R |
| 0.7302 | ft ³ · atm/lb-mol · °R |

Sizing Vacuum Systems—Steady State

Low pressure air is compressible. As a result, the arithmetic needed to size vacuum lines and vent holes depends on compressible fluid flow. For all intents, air can be considered as an ideal gas. The ideal gas equation is:

$$PV = nRT \quad (6.10)$$

where P is pressure, V is volume, T is absolute temperature, n is a function of the molecular weight of the gas, and R is the gas constant (Table 6.13).

For most cases, air flow can be considered as isothermal. That is, the gas does not change in temperature as it flows through various constrictions in the piping system. In this case, the relationship between gas pressure and volume is given as:

$$P_o \cdot V_o = P_1 \cdot V_1 \quad (6.11)$$

where P is pressure (absolute), V is volume and “o” and “1” represent the various states of the air. Example 6.3 illustrates how this expression is used to size the surge tank. Typically, the minimum volume of any vacuum system, including the piping and vacuum box, should be 6 to 20 times that of the mold cavity.

Example 6.3 Surge Tank Volume

Determine the surge tank volume, V_s , needed to evacuate a mold of V_m ft³ volume initially at P_m pressure (absolute). The minimum desired pressure on the hot sheet against the mold is to be P_{min} . The vacuum pump is capable of achieving P_v pressure (absolute) and the air temperature is constant.

The working equation is:

$$V_s \cdot P_v + V_m \cdot P_m = (V_s + V_m) \cdot P_{min}$$

Consider the case where:

$$P_v = 28 \text{ in Hg} = 0.94 \text{ lb}_r/\text{in}^2 \text{ (absolute)}$$

$$P_{min} = 24 \text{ in Hg} = 2.9 \text{ lb}_r/\text{in}^2 \text{ (absolute)}$$

$$P_m = 14.7 \text{ lb}_f/\text{in}^2 \text{ (absolute) = atmospheric pressure}$$

$$V_s = V_m \cdot \frac{(14.7 - 2.9)}{(2.9 - 0.94)} = 6.0 V_m$$

In other words, the vacuum surge system, including all the piping and the vacuum box, should be at least six times the volume of the mold cavity.

Consider the case where blow air is used to prestretch the thermoformed sheet. For this case, P_m is greater than atmospheric pressure. The typical prestretching pressure for 10% talc-filled polypropylene from Table 6.13 is 8 to 10 lb_f/in^2 . Repeat the above calculation, using $P_m = 24.7 \text{ lb}_f/\text{in}^2$ to determine the minimum vacuum surge system volume.

$$V_s = V_m \cdot \frac{(24.7 - 2.9)}{(2.9 - 0.94)} = 11.1 V_m$$

Typically, vacuum tank volumes range from six to 20 times the expected cavity volume.

Sizing Vacuum Systems—Dynamic

The above discussion does not consider the time required to evacuate a mold cavity. The fundamentals of compressible fluid flow are given elsewhere [22,23]. As a first approximation, air flow in thermoforming vacuum systems can be considered as isothermal. Correctly, gas flow is adiabatic for high velocities through constrictions. That is, the pressure-volume relationship is:

$$P_o V_o^\gamma = P_i V_i^\gamma \quad (6.12)$$

where $\gamma = 1.4$ for air. The speed of an adiabatic compression wave moving through stagnant air is given as:

$$c^2 = \frac{\gamma \cdot P}{\rho} \quad (6.13)$$

where ρ is the density of the gas. c is usually called the velocity of sound. As shown in Example 6.4, the velocity of sound at 70°F and atmospheric pressure is about 1100 ft/s. The Mach number, Ma , is the ratio of gas velocity to sonic velocity:

$$Ma = \frac{V}{c} \quad (6.14)$$

Example 6.4 The Velocity of Sound in Air

Determine the velocity of sound at one atmosphere and 70°F and at 0.05 atmospheres and 70°F.

$$\rho = 0.082 \text{ lb}_m/\text{ft}^3$$

$$\gamma = 1.4 \text{ for air.}$$

$$c^2 = \gamma \cdot P/\rho = 1.414 \cdot 7144 \left(\frac{\text{lb}_f}{\text{ft}^2} \right) \cdot \frac{1}{0.082} \left(\frac{\text{ft}^3}{\text{lb}_m} \right) \cdot 32.2 \left(\frac{\text{ft} \cdot \text{lb}_m}{\text{lb}_m \cdot \text{s}^2} \right)$$

The velocity of sound, c , at $14.7 \text{ lb}_f/\text{in}^2$ is:

$$c = 1078 \text{ ft/s}$$

$$\rho = 0.05 \cdot 0.082 = 0.0041 \text{ lb}_m/\text{ft}^3$$

The velocity of sound, c , at $0.74 \text{ lb}_f/\text{in}^2$ is:

$$c = 241 \text{ ft/s}$$

Gas velocities equal to the velocity of sound are *sonic* and those less than the velocity of sound are *subsonic*. Usually, air flow in vacuum systems is always subsonic. However, sonic conditions can exist at the vent hole inlet, as discussed below. If the fluid velocity is low in certain portions of the vacuum system, that region can be considered as incompressible and traditional incompressible fluid mechanics can be used. If the velocity is high—that is, if the Mach number is on the order of 0.3 or more—the flow must be considered compressible. Sonic flow is established so long as the absolute pressure differential across the vent hole is less than 0.53.

For incompressible air flow in vacuum systems, as detailed in Section 6.4, an appropriate pressure drop-flow rate relationship is written in “head loss” terms:

$$h_{\text{total}} = \left(\sum \frac{fL}{D} + \sum K \right) \frac{V^2}{2g_c} \quad (6.15)$$

where f is the friction factor, L is the pipe length, D is the pipe diameter, V is average air velocity, g_c is a unit correction term, and K is the effective resistance through a specific constriction (Table 6.12). The pressure drop, dP_i , through the i th segment of the vacuum system is given as:

$$dP_i = h_i \cdot \rho_{i,\text{mean}} \quad (6.16)$$

where h_i is the head loss through the i th segment and $\rho_{i,\text{mean}}$ is the average or geometric mean air density through that segment. The total pressure drop is then:

$$dP_{\text{total}} = \sum_i dP_i \quad (6.17)$$

Another less accurate method is to obtain an effective pressure drop, given as:

$$dP = h_{\text{total}} \cdot \rho_{\text{mean}} \quad (6.18)$$

Note that ρ_{mean} is an appropriate mean value of the density of the air. It can be the simple geometric mean of the density of the inlet and exit gas stream or the average of the densities of the air at every segment.

Considering air as an incompressible gas in order to determine pressure drop is satisfactory for all the piping with the exceptions of:

- Flow through solenoid valves, and
- Flow through vent holes.

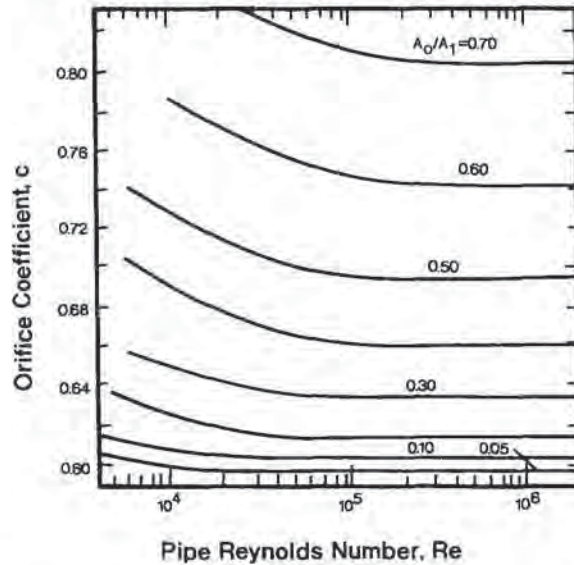


Figure 6.11 Flow rate-dependent orifice coefficient for compressible air in vacuum systems. Reynolds number, $Re = Dv \cdot \rho/\mu$ where D is pipe diameter, v is air velocity, ρ is air density and μ is air viscosity

Solenoid Valve Flow Resistance

Solenoid valves act to isolate the surge tank-vacuum pump system from the vacuum box-mold system. Although vacuum system solenoid valves are designed to offer minimum resistance to the flowing air, their shapes are such that the pressure loss is best considered as the result of compressible flow through a sharp-edged orifice. Figure 6.11 gives the orifice coefficient for incompressible flow. The pressure drop-flow rate equation is written as:

$$\dot{m} = c_o Y A_o (2\rho_1 dP)^{1/2} \quad (6.19)$$

where \dot{m} is the mass flow rate, c_o is the orifice coefficient, A_o is the minimum area of the orifice, $A_o = \pi D_o^2/4$, ρ_1 is the density of air in the pipe ahead of the orifice and dP is the pressure drop across the orifice. The compressibility correction factor, Y of Fig. 6.12, is dependent on the pressure drop across the orifice and the diameter ratio of the orifice and pipe. Example 6.5 illustrates the use of this equation.

Example 6.5 Compressible Air Pressure Drop Across Solenoid-Orifice

Air at 5 lb_f/in² (absolute) pressure and 70°F flows at 1 lb_m/s through a 2-in diameter pipe. A solenoid valve, acting as an orifice, has an internal constriction, $A_o/A_1 = 0.5$. What is the pressure drop across the valve?

$$\rho (14.7 \text{ \& } 70^\circ\text{F}) = 0.082 \text{ lb}_m/\text{ft}^3$$

$$Re > 100,000$$

From Fig. 6.11, $c(A_o/A_1 = 0.5) = 0.69$

$$D_o/D_1 = 0.707$$

Equation 6.19 is used to obtain the result:

$$\dot{m} = c_o Y A_o (2\rho_1 dP)^{1/2}$$

The air density at 5 lb_f/in² is:

$$\rho = 0.0812 \cdot \left(\frac{5}{14.7}\right) = 0.0276 \text{ lb/ft}^3$$

Since Y is a function of pressure drop, initially assume $Y = 0.9$ ($P_2/P_1 = 1$). Solving for ΔP :

$$\Delta P = \left[\frac{4}{0.695 \cdot 1.0 \cdot 4\pi} \right]^2 \frac{144}{2 \cdot 0.0276 \cdot 32.3^2} = 0.53 \text{ lb}_f/\text{in}^2$$

$P_2 = 5 - 0.52 = 4.48 \text{ lb}_f/\text{in}^2$. $P_2/P_1 = 0.89$. The value for Y is then iterated using this value of P_2/P_1 . When $Y = 0.96$, $\Delta P = 0.57$ and $P_2 = 5.43 \text{ lb}_f/\text{in}^2$.

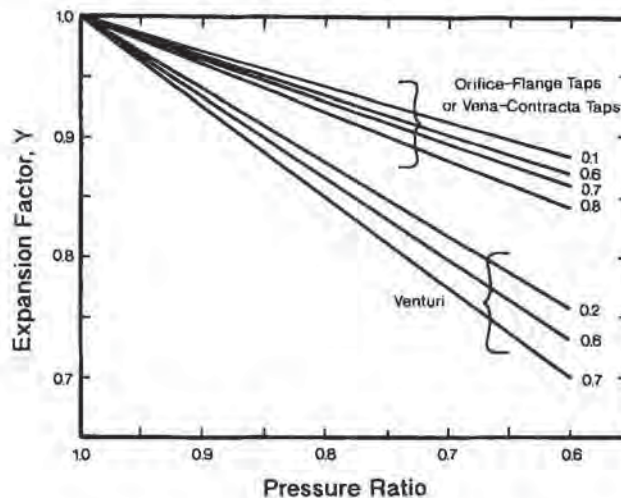


Figure 6.12 Expansion factor for vacuum system compressible air flowing through orifices and venturis

Vent Hole Resistance to Flow

When the solenoid is actuated to open the valve, the compression shock wave propagates from the valve upstream to the vent holes. Since the vent holes offer very high flow resistance, sonic velocity may be established at the entrances to the vent

holes. If this is the case, the maximum rate of evacuation of the mold cavity is calculated from:

$$\dot{m}_{\max} = NA_v \cdot c \cdot \rho \quad (6.20)$$

where A_v is the area of the vent hole, N is the number of vent holes, c is the sonic velocity and ρ is the density. If the evacuation time of a mold cavity having volume v_m is t , and the diameter of a given vent hole is D , the air velocity is:

$$v_{\text{air}} = \frac{v_m}{N(\pi D^2/4)t} \quad (6.21)$$

If the velocity of air through the hole is sonic, the number of vent holes of diameter D is given as:

$$N = \frac{v_m}{c(\pi D^2/4)t} \quad (6.22)$$

Example 6.6 illustrates the relationship between rate of cavity evacuation and the absolute minimum number of vent holes. The analysis above assumes that the vent hole has essentially zero length. As expected, the pressure drop increases with increasing vent hole length. The effect of vent hole length is determined from compressible "head loss" calculations. In essence, the friction factor is determined in standard fashion, as outlined earlier in this chapter. The head loss factor, fL/D , is calculated and the reductions in velocity and pressure are determined from Table 6.14. Example 6.7 illustrates the way in which this is determined.

Example 6.6 Vent Hole Sizing and Evacuation Rate

What is the absolute minimum number of vent holes needed to evacuate a 1 ft³ mold cavity in 10 s? $D = 1/32$ -in.

Individual vent hole area, $A = \pi D^2/4 = 0.000767 \text{ in}^2$

Mass flow rate = $1 \text{ ft}^3/10 \text{ s} = 0.1 \text{ ft}^3/\text{s}$.

Sonic velocity = 1000 ft/s

Mass flow rate, a single vent = $\frac{1000 \cdot 7 \cdot 67 \times 10^{-4}}{144} = 0.00533 \text{ ft}^3/\text{s}$

Total minimum number of vents, $N = 0.1/0.00533 = 18.8 \approx 20$

Example 6.7 Effect of Vent Hole Length on Pressure Drop and Air Velocity

Consider the case where 70°F air is exhausting at sonic velocity through a 0.0313-in diameter vent hole. Determine the pressure drop and velocity reduction for vent hole lengths of 0.125 in and 0.250 in. Consider the drilled hole to be smooth-bored. The kinematic viscosity of air is $2.15 \times 10^{-4} \text{ ft}^2/\text{s}$.

The Reynolds number is given as:

$$\text{Re} = \frac{Dv}{\nu} = \frac{1}{32 \cdot 12} (\text{ft}) \cdot 1000 \left(\frac{\text{ft}}{\text{s}} \right) \cdot \frac{1}{0.000215} \left(\frac{\text{s}}{\text{ft}^2} \right)$$

$$\text{Re} = 12,500.$$

From the Moody friction factor-Reynolds Number diagram, Fig. 6.13 (see Streeter, pp. 288-289), $f = 0.029$. Thus:

$$fL/D = 0.029 \cdot 0.125/0.0313 = 0.116$$

Interpolating from Table 6.14, $v/c = 0.789$ and $P/P_c = 1.365$. At the exit of the vent hole, the velocity is $1000 \times 0.789 = 789$ ft/s. And the pressure is $14.7/1.365 = 10.77$ psi.

For $L = 0.250$ in, $fL/D = 0.232$. Interpolating from Table 6.14, $v/c = 0.694$ and $P/P_c = 1.519$. At the exit of the longer vent hole, the velocity is 694 ft/s and the pressure is 9.69 psi.

Table 6.14 Effect of Vent Hole Length on Pressure Drop

| fL/D | V/c | P/P_c |
|--------|-------|---------|
| 0 | 1 | 1 |
| 0.0033 | 0.958 | 1.061 |
| 0.0145 | 0.915 | 1.129 |
| 0.0363 | 0.870 | 1.205 |
| 0.0723 | 0.825 | 1.289 |
| 0.1273 | 0.779 | 1.385 |
| 0.2081 | 0.732 | 1.493 |
| 0.3246 | 0.684 | 1.618 |
| 0.4908 | 0.635 | 1.783 |

Note that the Reynolds number through a vent hole is relatively small, even though the air velocity is sonic. This is due to the very small vent hole diameter. The volumetric flow rate through the piping between the vent holes and the vacuum surge tank is determined from:

$$\dot{V} = N \cdot c \cdot \frac{\pi D^2}{4} \quad (6.23)$$

where N is the number of vent holes and c is sonic velocity. As a first approximation, the air velocity everywhere else is given as:

$$v = \dot{V}/A_p = \frac{\dot{V} \cdot 4}{\pi D_p^2} = N \cdot c \cdot \left(\frac{D_v}{D_p} \right)^2 \quad (6.24)$$

Thus the Reynolds number in any pipe of diameter D_p is related, on first approximation, to the sonic velocity Reynolds number:

$$\frac{Re_p}{Re_v} = \frac{N \cdot D_v}{D_p} \quad (6.25)$$

Example 6.8 explores the relative values of these variables.

Example 6.8 Relative Velocities and Reynolds Numbers in Vacuum Pipe Flow

Assume the air velocity through a 0.0313-in diameter vent hole is 1000 ft/s¹. There are 100 vent holes. Calculate the volumetric flow rate, the Reynolds number through the vent hole, and the Reynolds number through the 2-in diameter pipe to the vacuum surge tank.

$$v = 2.15 \times 10^{-4} \text{ ft}^2/\text{s}$$

$$Re = \frac{0.0313}{12} (\text{ft}) \cdot 1000 \left(\frac{\text{ft}}{\text{s}} \right) \cdot \frac{1}{2.15 \times 10^{-4}} \left(\frac{\text{s}}{\text{ft}^2} \right) = 12,100$$

$$\text{Volumetric flow rate} = \frac{Nc \cdot \pi D_v^2}{4 \cdot 144} = 0.534 \text{ ft}^3/\text{s}$$

If the volumetric flow rate is constant, the Reynolds number in the 2-in diameter pipe is given as:

$$Re_p = Re_v \cdot \frac{N}{D_p} \cdot D_v = 12,100 \cdot 100 \cdot \frac{0.0313}{2} = 18,900$$

If the density is constant, the velocity in the 2-in diameter pipe is given as:

$$v_2 = \frac{\pi D^2}{4} \cdot \dot{V} = 24.5 \text{ ft/s}$$

¹ This assumes that the vent hole length is negligible. If it is not, it is necessary to reduce this value to the proper one as shown in Example 6.7.

It is apparent from the examples for flow through the solenoid valve and the vent holes that such constrictions can severely restrict the rate at which air is exhausted from the mold cavity. Before summarizing the evacuation flow characteristics, consider the replacement of traditional hard piping for vacuum lines with corrugated flexible tubing. Corrugations act as localized expansions and contractions along the entire length of the tubing. The worst case scenario is obtained by multiplying the orifice head loss coefficient K by the number of corrugations in the tubing length. The best case scenario assumes that the pipe has great roughness. As seen in Fig. 6.13, the friction factor approaches a constant value at relatively low Reynolds numbers for very rough pipe. For a pipe of $\epsilon/D = 0.05$, for example, the friction factor approximates 0.072 for $Re > 30,000$ or so.

Computation of flow rate-pressure drop through the vacuum system requires trial-and-error. The following protocol will enable rapid iteration:

1. Assume the air pressure in the mold cavity to be atmospheric.
2. Assume sonic velocity at the inlet to the vent holes.

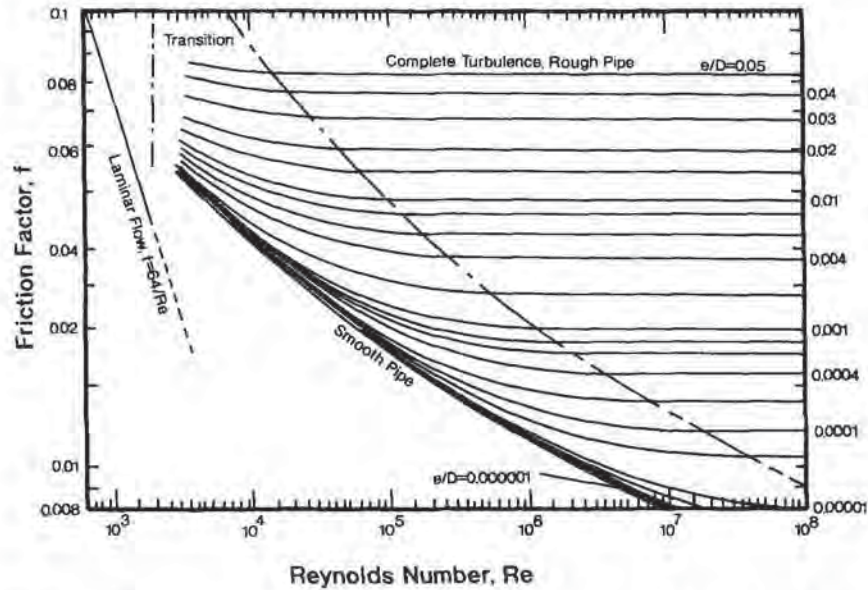


Figure 6.13 Flow rate-dependent friction factor for flow in a pipe. e/D is measure of roughness, Reynolds number, $Re = Dv \cdot \rho/\mu$ where D is pipe diameter, v is fluid velocity, ρ is fluid density and μ is fluid viscosity

3. Determine the velocity, density, and pressure at the exit of the vent holes.
4. Calculate the Reynolds number for air flow in the vent hole.
5. Estimate the practical number of vent holes to be used¹.
6. If a solenoid valve is used, estimate the pressure loss from the orifice equation.
7. Using the "head loss" approach, calculate the total head losses for the piping, elbows, vacuum box, back-drilled region on the mold, expansion loss into the surge tank and the pressure loss across the solenoid.
8. Add to this the pressure loss across the vent hole.
9. If the calculated pressure loss is greater than that determined from the available pressure differential between the surge tank and atmosphere, the assumed flow rate is too great. In other words, there is too much resistance to flow for the chosen velocity. Since the controlling factor is the assumption of sonic flow at the inlet to the vent hole, it is necessary to reduce this velocity to a value below the velocity of sound. Estimate this velocity by multiplying the ratio of available to calculated pressure drops by the velocity of sound. Continue to iterate until there is reasonable agreement on pressure drop values.
10. If the calculated pressure loss is less than that determined from the available pressure differential between the surge tank and atmosphere, the assumed flow

¹ This number is usually 3 to 5 times greater than the minimum number of vent holes calculated. One method is to assume that the Reynolds number in the vacuum pipe equals that in the vent hole. From this, the number of vent holes can be estimated.

rate is too small. Unfortunately, the greatest flow rate that can be assumed is sonic flow. This means that the cavity volume could be evacuated even faster than the current mold design allows. One way of increasing evacuation rate is to increase the number of vent holes. Another is to increase the diameter of the vent holes. Both of these options can lead to part design problems, as detailed later.

Example 6.9 illustrates a portion of this iterative procedure.

Example 6.9 Pressure Drop Through Vacuum System

Consider the mold vent hole and vacuum line assembly outlined in Examples 6.7 and 6.8, with the vent hole length of 0.250 in, the vacuum line being 2-in smooth bored pipe 100 ft in length and having eight elbows, two tees, one solenoid valve and one check valve and one globe valve. Assume that air flow through the vacuum box represents 10 equivalent ft of smooth bored pipe, and that there are two flow expansions and two flow contractions. Use a mean air density between the surge tank and the vent hole outlet. Assume the flow to be isothermal, for the most part.

Density of air at the exit of the vent hole is directly proportional to the pressure at that point.

$$\rho_{\text{vent exit}} = \rho_{\text{atmospheric}} (P_{\text{exit}}/P_{\text{atm}})$$

$$\rho_{\text{vent exit}} = 0.082 \cdot (1/1.519) = 0.054 \text{ lb}_m/\text{ft}^3$$

The pressure in the surge tank is assumed to be 0.05 atmospheres (absolute). The density at 70°F is therefore:

$$\rho_{\text{surge}} = 0.082 \cdot (0.05/1) = 0.004 \text{ lb}_m/\text{ft}^3$$

The mean density is:

$$\rho_{\text{mean}} = \sqrt{\rho_{\text{surge}} \cdot \rho_{\text{vent exit}}} = 0.015 \text{ lb}_m/\text{ft}^3$$

Assume the Reynolds number in the 2-in pipe = 18,900.

From Fig. 6.13 for smooth-bored pipe, $f = 0.0251$. So:

$$fL/D = 0.0251 \cdot (100 + 10) \cdot 12/2 = 15.67$$

The head losses from the rest of the system, with the exception of the vent hole and solenoid losses, include:

| | |
|-------------------------------|-------------|
| 2 expansions $\times 1.0 =$ | 2.0 |
| 2 contractions $\times 0.5 =$ | 1.0 |
| 8 elbows $\times 0.9 =$ | 5.4 |
| 2 tees $\times 1.8 =$ | 3.6 |
| 1 check valve = | 2.5 |
| 1 globe valve = | 10.0 |
| | <u>24.5</u> |

Thus the total head loss value is given as:

$$K_{\text{total}} = 15.67 + 24.5 = 40.2$$

The velocity through the 2-in pipe is given as 24.5 ft/s:

The total head loss, h_{total} is then given as:

$$h_{\text{total}} = 40.2 \cdot (v^2/2g_c) = 374.7 \text{ ft}$$

The pressure drop is then:

$$\Delta P = h_{\text{total}} \cdot \rho_{\text{mean}} = 374.7 \cdot 0.015/144 = 0.04 \text{ lb}_f/\text{in}^2$$

The pressure drop through the solenoid is given in Example 6.5 as $\Delta P = 0.57 \text{ lb}_f/\text{in}^2$ and that through the vent holes in Example 6.7 as $\Delta P = 5.01 \text{ lb}_f/\text{in}^2$.

Thus the total pressure drop is:

| | |
|------------------------------------|--------------------------------|
| Pressure drop through vent holes = | 5.01 |
| Pressure drop through solenoid = | 0.57 |
| Pressure drop through piping = | 0.04 |
| Total pressure drop = | 5.62 lb_f/in^2 |

Since the calculated pressure drop is less than the maximum available pressure drop $(1 - 0.05) \cdot 14.7 \text{ lb}_f/\text{in}^2 = 14.0 \text{ lb}_f/\text{in}^2$, the rate of evacuation is restricted by sonic velocity at the vent holes. Increased evacuation is possible by increasing the number of vent holes or increasing the vent hole diameter.

Vent Hole Diameter

Mold vent hole diameter depends on several factors, including the modulus of the hot plastic sheet, the sheet thickness over the hole and the allowable draw depth into the vent hole. The maximum deflection δ , of a sheet of thickness h and modulus E into a hole diameter d is given as [24]:

$$\delta = \alpha h = \frac{3qd^4 \cdot (5 + \nu)}{16 \cdot Eh^3 \cdot (1 - \nu)} \quad (6.26)$$

where the maximum deflection is proportional to h , with α as the proportionality or acceptable nib or nipple height. q is the applied pressure, and ν is Poisson's ratio (Table 5.15). For many plastics, $0.35 < \nu < 0.5$. If $\nu = 0.5$:

$$\alpha = 0.516 \cdot \frac{q}{E} \cdot \left(\frac{d}{h}\right)^4 \quad (6.27)$$

The maximum nib or nipple height is usually specified by the user or the designer. This establishes an upper limit for $\alpha = \delta/h$. Rearranging Equation 6.27:

$$\frac{d}{h} = 1.18 \left(\frac{\alpha E}{q}\right)^{1/4} \quad (6.28)$$

This is shown in Fig. 6.14. As discussed in Chapter 4, the secant modulus or $\phi(T)$ is about $100 \text{ lb}_f/\text{in}^2$ or 0.7 MPa for vacuum forming where the pressure is about $15 \text{ lb}_f/\text{in}^2$ or 0.1 MPa . Thus the E/q is 7. A typical range for E/q is $2 < E/q < 10$. A good range for d/h in Equation 6.28 is:

$$1.4 \alpha^{1/4} < \frac{d}{h} < 2.1 \alpha^{1/4} \quad (6.29)$$

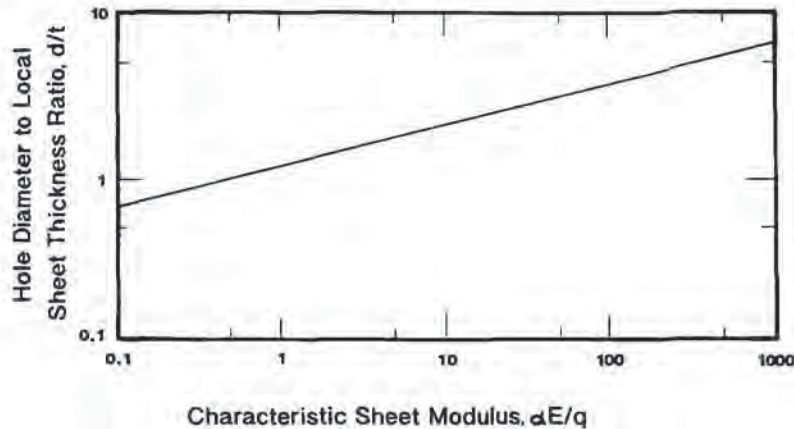


Figure 6.14 Specific vent hole design parameter, d/t , as function of modulus-to-pressure ratio, E/q , and relative nib height, α . This is for initial draw-down into vent hold

Example 6.10 further explores this relationship. If the nib or nipple height is restricted to no more than the sheet thickness, the vent hole diameter must be less than 2.1 times the sheet thickness. This value is compared with Gruenwald's rule [25]:

“... vacuum hole sizes smaller than the (local) material thickness will not become visible...”

That is, holes where $d/h \leq 1$ yield acceptable nib heights. Example 6.11 tests the sensitivity of Equation 6.28 as regards local sheet thickness and sheet temperature. As illustrated, locally thin sheet produces a much greater effect on nib or nipple size than does locally hot sheet. It is recommended that the vent hole diameter be based on the first common drill size *below* the calculated value. The vent holes should be drilled perpendicular to the plane of the mold. The backs of the vent holes must be enlarged by machining vacuum channels or drilling large holes on the reverse side or back of the mold (Fig. 6.15). Since the objective is to reduce flow resistance through the long vent hole, the counterboring, “back-drilling” or “back-drafting” should be taken within 0.5 in or 13 mm of the mold surface or closer if possible. This counterboring must be done carefully to minimize locally weakening the mold in the

Example 6.10 Relative Nipple Height

Determine the maximum vent hole diameter for 0.040 in PS sheet drawn 4:1 against the vent hole area. Assume $E/q < 10$. Consider the maximum nipple height to be equal to the local sheet thickness.

From Equation 6.29, $d/h < 2.1 \alpha^{1/4}$ for $E/q < 10$. At 4:1 draw ratio, the local sheet thickness is 0.010 in. The maximum nipple height is 0.010, with $\alpha = 1$. The hole diameter must be less than $2.1 \cdot h$ or $d_{\max} = 0.0210$ in.

vent hole region. Drilling too closely or milling a channel that is too wide invites long-term metal fatigue and possible local collapse [26]. Experienced mold-makers avoid drilling too few vent holes of diameters that are too large. If the vent hole diameters are too large, objectionable nibs or nipples result, even though the volume of entrapped air is exhausted in a reasonable time. Large diameter vent holes force the fabricator to lower sheet temperature. If stretching forces are limited or the sheet is particularly stiff, poor part replication results.

Example 6.11 The Relative Sensitivity of Nipple Height to Process Parameters

Consider polymers having the following temperature-dependent elastic moduli:

$$E(T) = A e^{-\beta T}$$

Determine the relative effects on nipple height on:

- $\pm 10\%$ change in pressure,
- $\pm 10\%$ change in sheet thickness, and
- $\pm 20^\circ\text{C}$ change in sheet temperature

for PMMA where $1/\beta = 20^\circ\text{C}^{-1}$ and PE where $1/\beta = 85^\circ\text{C}^{-1}$.

Equation 6.28 is differentiated as follows:

$$\frac{dd}{d} = \frac{dh}{h} + \frac{1}{4} \frac{d\alpha}{\alpha} + \frac{1}{4} \frac{dE}{E} + \frac{1}{4} \frac{dq}{q}$$

Now $dd/d \equiv 0$. The expression for dE is:

$$dE = -\beta A e^{-\beta T} dT = -\beta E dT$$

Therefore:

$$\frac{d\alpha}{\alpha} = \pm 4 \frac{dh}{h} \pm \beta dT \pm \frac{dq}{q}$$

For PMMA:

$$\frac{d\alpha}{\alpha} = \pm 0.400 \pm 1.00 \pm 0.100$$

The sheet temperature affects the PMMA nipple height the most.

For PE:

$$\frac{d\alpha}{\alpha} = \pm 0.400 \pm 0.235 \pm 0.100$$

The sheet thickness variation affects the PE nipple height the most.

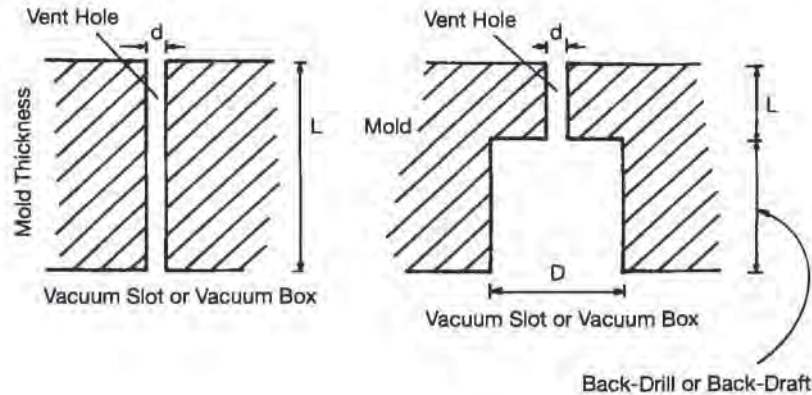


Figure 6.15 Characteristic geometric factors for vacuum or vent hole without back-drilling (left) and with back-drilling (right)

Occasionally a mold that is functional for one polymer yields unacceptable nipple or nib heights with another. Peening the vent hole area will reduce the vent hole size, albeit at the risk of deglossing the mold in that area¹. Note that Equation 6.28 is also acceptable for determining vent hole size for pressure forming. As discussed in Chapter 9, pressure forming pressures are typically four to six times greater than vacuum forming pressure. As a result, the lower inequality in Equation 6.29 is operative. A properly dimensioned vent hole for vacuum forming would yield a relative nib or nipple height that is four times greater with pressure forming. One saving aspect is that pressure forming sheet temperatures are usually somewhat lower than equivalent vacuum forming temperatures. Cooler sheet implies higher elastic modulus and shorter nibs or nipples.

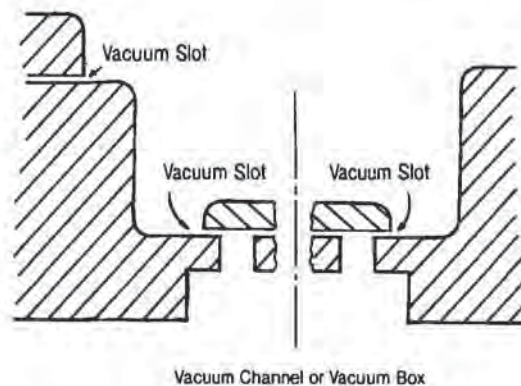


Figure 6.16 Vacuum or vent slots for two-piece female mold (left) and one-piece female mold (right)

¹ Plugging and re-drilling the hole is always an option.

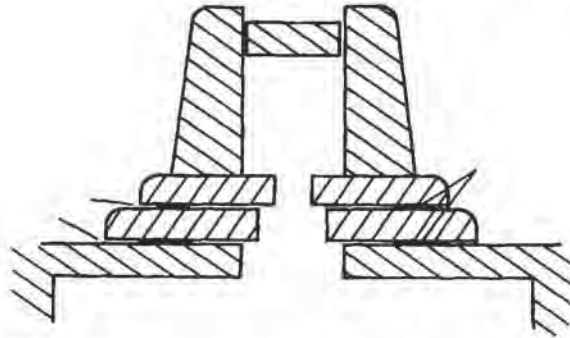


Figure 6.17 Vacuum or vent slots for male mold

Other Types of Vents

Slot vents are used when linear protruding elements occur inside a female mold (Fig. 6.16) or along the bottom rim of a male mold (Fig. 6.17). Slots are end-milled or cut with a wire EDM along the two-dimensional corner. Exit vents are then drilled from the reverse side. The width of the slot vent is determined in a manner similar to that for round holes. From Fig. 6.18, let d be the slot width. The maximum deflection, δ , is given as [27]:

$$\delta = \alpha h = \frac{qd^3}{4Eh^3} \quad (6.30)$$

Rearranging:

$$\frac{d_{\text{slot}}}{h} = 1.414 \left(\frac{\alpha E}{q} \right)^{1/4} \quad (6.31)$$

Since this equation is of the same form as Equation 6.28 for a circular hole, Fig. 6.14 is used for slot vents if:

$$d_{\text{slot}} = 1.2d_{\text{hole}} \quad (6.32)$$

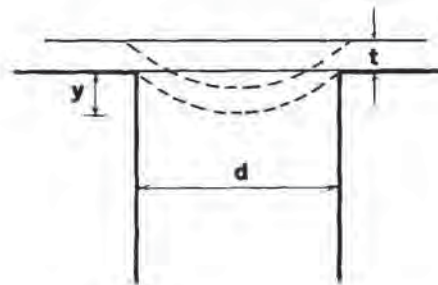


Figure 6.18 Vacuum or vent hole geometric factors

Table 6.15 Porous Metal Product Manufacturers
(Specialties in parentheses)

| | |
|--|--|
| Allied Sinterings, Inc. (small parts) 29 Briar Ridge Rd. Danbury CT 06810 203-743-7502 | National Sintered Alloys, Inc. (parts, powder metallurgy) 10 Heritage Park P.O. Box 332 Clinton CT 06413 203-669-8653 |
| Arrow Pneumatics, Inc. (bronze) 500 Oakwood Rd. Lake Zurich IL 60047 708-438-9100 | Newmet Krebsoge, Inc. (stainless steel, bronze, titanium) P.O. Box 68 Terryville CT 06786 800-426-0977 |
| Astro Met, Inc. (stainless steel, powder metallurgy) 9974 Springfield Pike Cincinnati OH 45215 | Pacific Sintered Metals, Inc. (bronze, stainless steel) [Also Permaflow, Inc. at the same address] 14002 S. Avalon Blvd. Los Angeles CA 90061 310-715-9800 |
| Atlantic Sintered Metals (powder metallurgy) 12 Cushing Dr. Wrentham MA 02993 508-384-3100 | PTI Technologies, Inc. 950 Rancho Conejo Blvd. Newbury Park CA 91320 800-491-0781 |
| Helsel, Inc. (stainless steel) State Rd. 60 W. P.O. Box 68 Campbellsburg IN 47108 813-755-4501 | SSI Technologies, Inc. (stainless steel, bronze) 3332 Palmer Dr. Janesville WI 53566 608-755-1900 |
| Mott Metallurgical Corp. (stainless steel) Farmington Industrial Park 84 Spring Lane Farmington CT 06032-3159 203-677-7311 | The Wakefield Corp. (stainless steel, bronze) 35 Foundry St. Wakefield MA 01880 800-548-9253 |

For the same allowable depth of draw into the vent, slot vent widths need to be only 83% of circular vent diameter. For a given dimension, slot vents have two to four times greater venting area. Reverse side exit holes must be large enough to allow unrestricted air flow from the cavity. And slot vent width must be small enough to minimize part undercutting into the vent or the formation of an unsightly line.

Porous metal plugs are used in flat areas in place of multiple vent holes. Sintered powders of bronze, brass or stainless steel of about 50% open area are commercially available (Table 6.15). These plugs are machined to fit an existing vent hole region or can be custom ordered to meet a specific design. A hole large enough to vent the area, usually 6.4 mm or 0.250 in or more, and deep enough to accommodate the plug, usually 6.4 mm or 0.250 in or more, is drilled in the primary mold surface (Fig. 6.19).

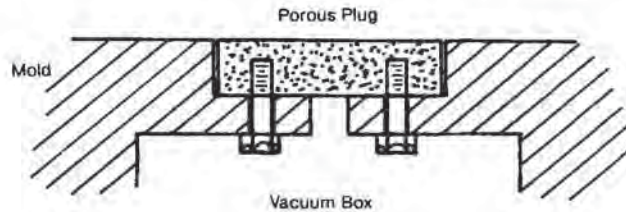


Figure 6.19 One method of fastening porous plug in mold cavity for evacuation

Exit holes are then drilled from the reverse side to facilitate venting. Another approach is to use a tapered hole and a tapered plug that is inserted from the reverse side and held in place with a simple spring ring or screw (Fig. 6.20). The effective porous metal venting area width is as much as ten times greater than the venting area from clustered vent holes. Nipples cannot form when porous vent plugs are used. However, the open areas or pores in the plugs tend to fill with detritus, particularly if in-mold trimming is used. Other sources of detritus include sander and router dust, atmospheric dust and contamination on the incoming sheet. Venting efficiency gradually decreases with time, necessitating periodic plug replacement.

Fine stainless steel, nickel and brass welded wire screen is also commercially available. Open area for ≈ 100 mesh screen is usually 35% to 65%. Screen must be supported to minimize bending under sheet draw-down forces. Screen may also leave an undesirable pattern on the part.

The poppet valve is usually mechanically operated and is used in injection molding to break the suction between a part and the mold surface on flat, large-area parts. The poppet valve can be used in this fashion for parts thermoformed onto male molds. In venting, poppet valve is used to rapidly exhaust cavity air in large-volume deep-draw female molds (Fig. 6.21). The evacuating poppet valve is spring loaded and is normally open. It is closed either on a clock timer or by the sheet draw-down force. Example 6.12 illustrates the high evacuating efficiency of a poppet valve.

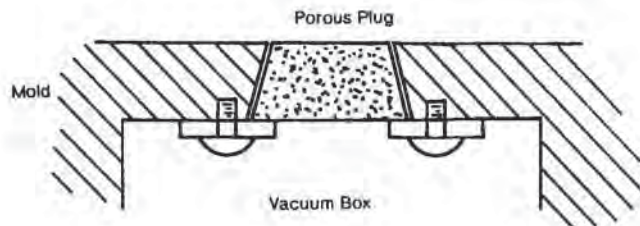


Figure 6.20 One method of fastening porous plug in mold cavity for evacuation

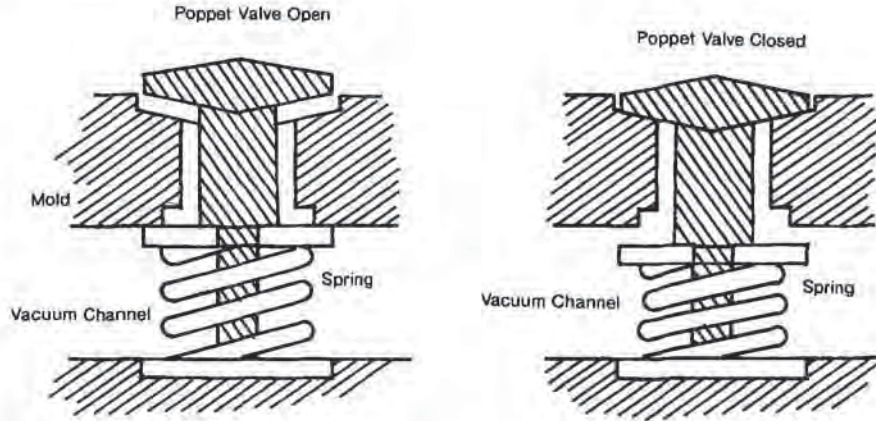


Figure 6.21 Spring-loaded poppet valve for evacuating large-volume or deep female mold cavities

Example 6.12 Poppet Valve in Mold Evacuation

A 6-in diameter \times 8-in deep female mold cavity is currently being evacuated in 1.0 s through 18 vent holes, each 1/16-in in diameter. Determine the maximum evacuation rate if the number of vent holes is doubled. Then compare this with the evacuation rate if a 3-in diameter poppet valve with an open gap of 0.020 in is installed in the cavity bottom.

The cavity volume is $\pi D^2 L / 4 = 226.2 \text{ in}^3$.

The current volumetric evacuation rate is $226.2 \text{ in}^3 / 1.0 \text{ s} = 226.2 \text{ in}^3/\text{s}$.

The area of current vacuum holes is:

$$\frac{N \cdot \pi d^2}{4} = 18 \cdot 0.7854 \cdot (0.0625)^2 = 0.0552 \text{ in}^2$$

The current air flow is $226.2 / 0.0552 = 4096 \text{ in}^3/\text{s} = 341 \text{ ft}^3/\text{s}$ or subsonic flow.

If the number of holes doubles and the air flow remains the same, the cavity is evacuated in $1.0 / 2 = 0.5 \text{ s}$.

The vent area of the open gap of 0.020 in on the poppet valve is $\pi d_p \cdot 0.020 = 0.1885 \text{ in}^2$. The total vent area is then $0.0552 + 0.1885 = 0.2437 \text{ in}^2$.

If the air flow remains the same, the cavity is evacuated in $1.0(0.0552 / 0.2437) = 0.23 \text{ s}$.

Vent Hole Placement

It is apparent that there must be venting in areas where the plastic last contacts the mold surface. These areas are usually two- and three-dimensional corners. There is substantial verification that adequate parts can be made by vacuum forming into a five-sided female mold having venting only in the four three-dimensional corners.

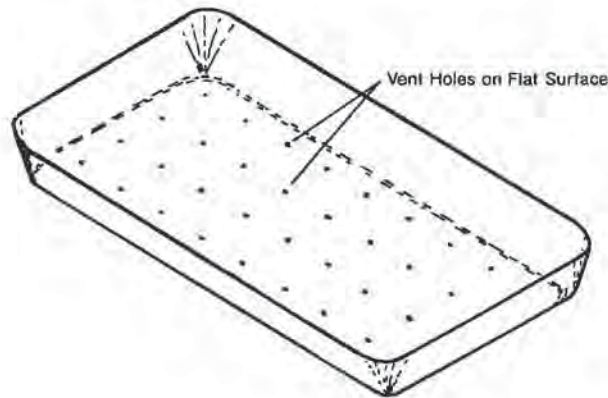


Figure 6.22 Vent hole location on flat or planar mold surface for both male and female molds

The wall thickness prediction programs of Chapter 7 are most useful in defining where other potential late evacuation regions are. Other areas where vent holes are desirable include:

- Flat, large-area horizontal surfaces on both male and female molds (Fig. 6.22). The sheet usually touches the mold surface here first. Subsequent shrinkage can tightly lock the sheet to the surface. The vent holes are used primarily to blow the cool sheet from the mold surface.
- Vertical walls and vertical two-dimensional corners, in particular (Fig. 6.23). These vents serve primarily to lock the sheet against the mold surface during stretching. These vents are particularly important for low coefficient of friction polymers such as polypropylene, polyamide and PTFE.
- In and around lettering, bosses, ribs, and corrugations. Since it is not always apparent how the plastic will form around and into these details, venting must be adequate and vent holes regularly spaced (Fig. 6.24).
- In the rim regions for female molds, particularly when dams or moats are used (Fig. 6.25). These help lock the sheet against the mold and minimize the amount of web area sheet drawn over the rim and into the mold cavity.

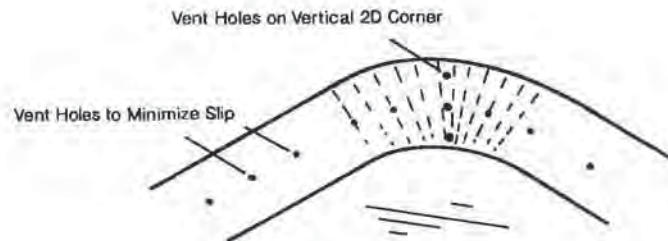


Figure 6.23 Vent hole location on vertical two-dimensional female mold surfaces

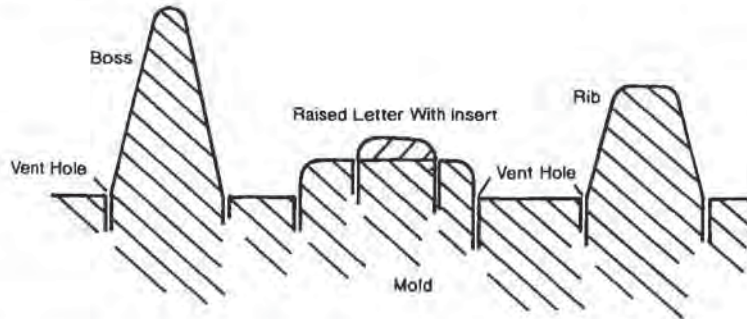


Figure 6.24 Vent hole location around bosses, raised sections and ribs

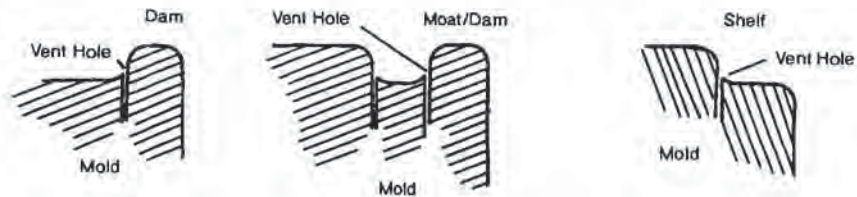


Figure 6.25 Venting around moat (left), moat/dam (center), and shelf rims (right) for female molds

- Along the double step for male molds (Fig. 6.26). These help lock the sheet against the mold before most of the forming occurs. This locking effect minimizes air bleed under the sheet during the final stages of draw-down.
- Along two- and three-dimensional corners on male molds (Fig. 6.27).

Although usually not necessary, vent holes are regularly spaced along horizontal two-dimensional corners on female molds (Fig. 6.28). These regularly spaced holes

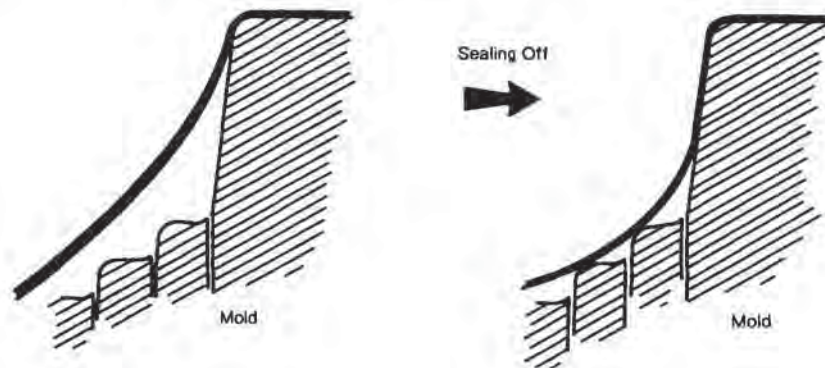


Figure 6.26 Two-step hold-down for male mold, showing seal-off effect on right

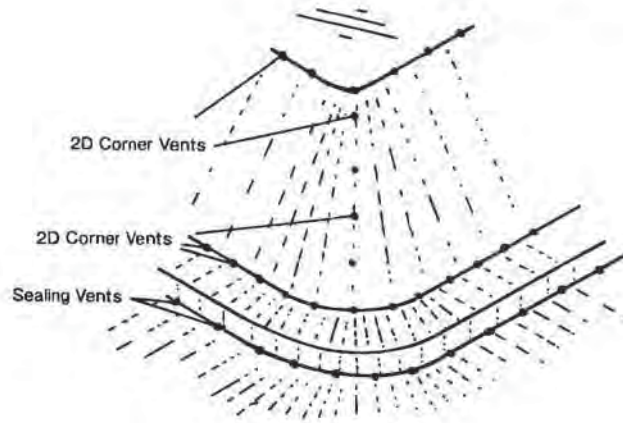


Figure 6.27 Vent hole locations on two-dimensional vertical and horizontal male mold surfaces and sealing locations

are used in place of vent holes clustered in three-dimensional corners. Functionally, they do not perform as well as clustered vent holes but are more esthetically pleasing.

6.6 Surface Treatments

Unlike injection molds, thermoform molds rarely require intermittent topical applications of mold release in areas where the formed shape is particularly difficult to release from the mold surface. There are several reasons for this:

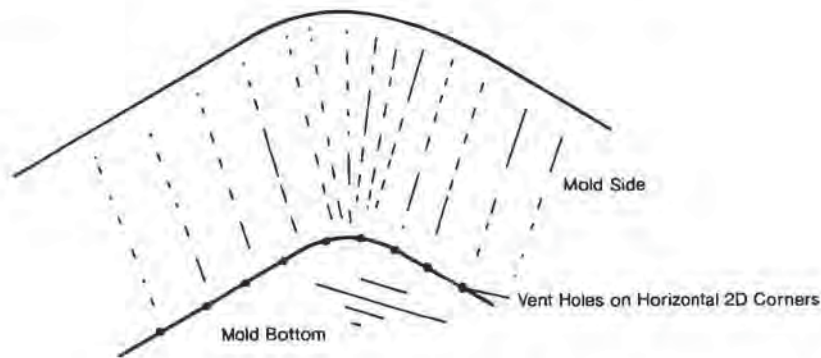


Figure 6.28 Uniformly spaced vent hole locations on horizontal two-dimensional corners in female mold

- The pressures used in thermoforming are modest,
- The plastic is a rubbery solid rather than a sticky fluid and so polymer adhesion is minimal¹,
- The plastic shape is usually quite flexible when stripped from the mold and so vacuum pockets usually do not form, and
- The mold surfaces are usually vented in precisely those areas where sticking might occur.

Surface treatments on thermoform molds are used for other reasons. When biaxially stretched, hot sheet contacts a cold high energy surface such as metal mold and stretching ceases. Walls of simple vacuum-formed female parts thin with draw depth as described in Chapters 4 and 7. In order to avoid excessive draw-down, or to effect preferential draw-down into a specific region, permanent surface treatments are used. Baked-on surface treatments of low-friction materials such as PTFE and FEP are common. These treatments produce surfaces that are essentially integral parts of the mold surface. In certain mold designs, the sheet must not slide against the surface. Olefins tend to alternately slip and stick when vacuum formed. This causes visible ridges in the part surface. These are sometimes wrongly attributed to plug mark-off. Roughening the mold surface does little to prevent sliding and may aggravate the problem. Roughening may actually reduce contact area as shown in schematic in Fig. 6.29. A better alternative is to treat the surface with a high frictional coefficient substance such as a curable polyurethane, polybutadiene or silicone rubber. Also additional forming pressure is used to minimize sliding.

The relationship between frictional force F_s and normal force F_n is:

$$F_s = c \cdot F_n^2 \quad (6.33)$$

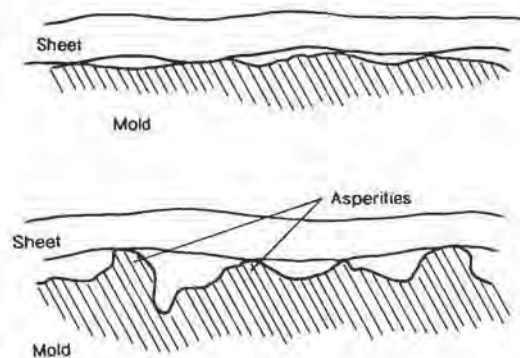


Figure 6.29 Aspects of mold surface texture replication by thermoformed sheet. Matte surface at top, rough textured surface at bottom

¹ There are exceptions to this, of course. Parts can stick if the polymer contains an adduct that blooms to the surface and/or becomes tacky, if there are sufficient undercuts or if the mold is very hot.

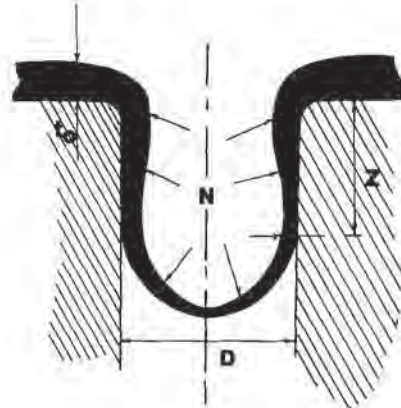


Figure 6.30 Geometric factors for extensional draw-down v. sliding of sheet into female mold

where c is the kinetic frictional coefficient and takes the experimental range of 0.67 to 1.0. Larger values of α indicate that the deformation of contact area of the plastic is determined by its viscoelastic properties. Values of c are in the range of 0.1 to 0.25 for typical smooth-surface metal molds and most solid plastics [49]. To better understand the surface effect on forming, consider a simple example of draw-down of a sheet of initial thickness t_0 and tensile strength τ into a cylindrical female mold of diameter D with a differential pressure P . As shown in Fig. 6.30, the sheet has already contacted the cylinder to a depth Z and has thinned to a thickness h . The normal force holding the sheet against the surface is:

$$F_n = P \cdot \pi D Z \quad (6.34)$$

The second part of the term on the right is the contact area of the sheet on the mold. If the sheet is to slide on the mold rather than stick to the mold, it must be pulled with a force greater than this. This is written as:

$$F_s > c \cdot F_n \equiv c \cdot P^n \cdot (\pi D Z)^\alpha \quad (6.35)$$

The force required to draw the sheet is the polymer tensile strength times the cross-sectional area, A :

$$F_s = \tau \cdot A = \tau \cdot \pi D h \quad (6.36)$$

Note that the cross-sectional area is at the point where the sheet last contacts the mold surface. If the force needed to slide the sheet exceeds that needed to draw it, the sheet will tend to draw. This is written as:

$$F_s > F_d \rightarrow c \cdot (P \pi D Z)^\alpha > \tau \cdot \pi D h \quad (6.37)$$

Consider the example where $\alpha \equiv 1$:

$$c P Z > h \tau \quad (6.38)$$

or:

$$Z > \frac{h \tau}{c P} \quad (6.39)$$

If the force needed to draw the sheet exceeds that needed to slide it, the sheet will slide. Thus:

$$Z < \frac{ht}{cP} \quad (6.40)$$

Example 6.13 illustrates how much sliding occurs before the sheet actually sticks to the mold surface. It is apparent from Equation 6.39 that if the sheet is to stick to the mold rather than slide, c must be as large as possible. Increasing the applied pressure and reducing sheet temperature, an action that increases the tensile strength, reduces the depth at which the sheet stops sliding.

Example 6.13 Sliding Sheet into Mold Cavity

Hot PP sheet is easily marked when it slides against cool metal. The amount of marking on a drink cup must be restricted to no more than 0.25 in below the rim. Determine the extent of mark-off for local 0.020 in sheet if the sheet tensile strength is 150 lb_f/in² or 1 MPa and the applied pressure is 40 lb_f/in² or 0.276 MPa. The coefficient of friction, $c = 0.25$.

The appropriate equation is Equation 6.39:

$$Z = \frac{ht}{cP}$$

For the data given:

$$Z = \frac{0.020 \cdot 150}{0.25 \cdot 40} = 0.3 \text{ in}$$

The mark-off will be seen below the $\frac{1}{4}$ -in line. To reduce the extent of mark-off, the coefficient of friction needs to be increased to at least 0.30. A slight roughening of the region just below the rim will minimize the extent of mark-off. Note that for straight vacuum forming, $P_{\text{max}} = 15 \text{ lb}_f/\text{in}^2$ and the coefficient of friction must be at least 0.80 to minimize the extent of mark-off.

Surface Texture

The primary factors influencing replication of mold surface texture by hot rubbery plastic sheet are applied pressure and sheet temperature. Very high surface replication is intrinsic to compression and injection molding processes where applied pressures are normally on the order of 10 MPa or 1,450 lb_f/in². In low pressure structural foam molding [28,29], pressures are on the order of 2 MPa or 290 lb_f/in² and so finer mold surface details, measured in microns or μm , are not accurately replicated. Typically, these absences are seen as loss in sharpness of detail in product code lettering and boss and rib edges. Parts are therefore designed with larger edge radii and lettering. For low pressure molding, the relationship between applied

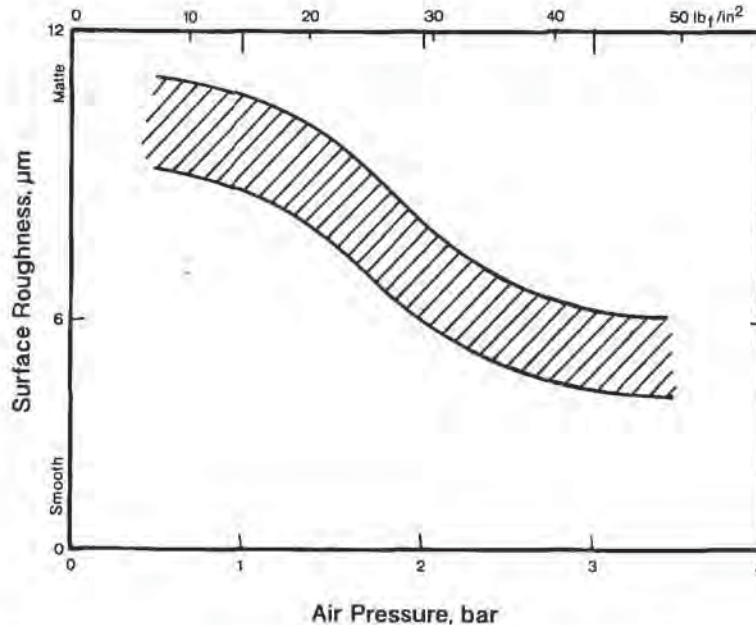


Figure 6.31 Experimental relationship between applied air pressure and extent of texture on formed sheet. Redrawn from [51] and used with permission of Society of Plastics Engineers, Inc.

pressure and molded part surface texture is shown in Fig. 6.31 [51]. This relationship is applicable to pressure forming, as well. In traditional vacuum thermoforming, the ability to replicate the mold is further reduced by the normally lower applied pressure and the less pliable nature of the polymer¹. The inability to faithfully reproduce fine mold detail must be recognized during early design. Furthermore, part appearance depends primarily on the sheet surface quality *prior to contact* with the mold. Excessive mold surface preparation cannot differentially improve low pressure thermoformed part surface appearance [30].

The analysis used to determine the height of nibs or nipples in vent holes is applicable to determination of the maximum depth of texture. Consider Fig. 6.32, a slight reworking of Fig. 6.18. Let d be the relative width of the lettering, grain or texture in the mold. The maximum depth of sheet penetration into this texture, δ , is given as Equation 6.26, as cited before [27]:

$$\delta = \frac{qd^3}{4Eh^3} \quad (6.41)$$

¹ Recall that the amorphous polymer in thermoforming is in a rubbery elastic state. Crystalline polymer is usually liquid but is formed only a few degrees above its melting temperature range and so is an elastic liquid. Mobility of thermoformable polymers at their forming temperatures is limited to mild chain extension and chain segment rotation. As a result, the thermoforming polymeric sheet cannot orient into fine mold details in the manner characteristic of injection molding or compression molding polymeric fluids.

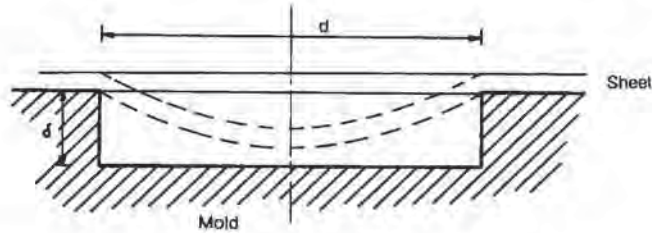


Figure 6.32 Geometric factors for draw-down onto textured mold surface

where q is the applied pressure, h is the local sheet thickness, and E is the modulus of the sheet at the time of forming into the texture. The depth of penetration is considered to be a measure of sheet replication of the mold surface. Note that for a given texture, d is constant and the replication is proportional to the applied pressure. Doubling the pressure doubles the ability of the sheet to replicate the mold. Further, replication is strongly dependent on the local sheet modulus. Since the modulus is highly temperature-dependent, decreasing local sheet temperature a few degrees results in dramatic loss in replication. Probably the most important aspect of Equation 6.41, however, is the strong relationship between replication and local sheet thickness. Note that small changes in local sheet thickness yield dramatic changes in replication. For example, a 10% change in sheet thickness results in a 30% change in the value for δ .

Equation 6.41 is rearranged to relate minimum applied pressure to the geometric parameters, as:

$$q_{\min} = 4\delta E(T) \frac{h^3}{d^3} \quad (6.42)$$

For a given texture, δ and d are fixed. For a given sheet thickness, h , the local sheet thickness is predictable within reason, according to Chapter 7 arithmetic. For given process parameters, $E(T)$ is known. As a result, Equation 6.42 yields the *minimum* pressure needed to achieve mold replication. Pressures in excess of this minimum value ensure replication despite variation in local sheet thickness or temperature. Example 6.14 illustrates this.

Example 6.14 Mold Texture Replication

The texture in a Eurograin-textured mold is 0.001 in deep and the minimum span is 0.005 in. Determine the pressure needed to force 0.030 in thick FPVC into this texture of the polymer modulus is 100 lb_f/in² or 0.69 MPa.

The operative equation is Equation 6.42:

$$q_{\min} = 4\delta E(T) \frac{h^3}{d^3}$$

$$q_{\min} = 4 \cdot 0.001 \cdot 100 \cdot \frac{(0.030)^3}{(0.005)^3} = 86.4 \text{ lb}_f/\text{in}^2 = 0.60 \text{ MPa}$$

6.7 Plug Design Considerations

Mechanical pushers or plugs were first developed for heavy-gage, cut-sheet forming. They are now used extensively in thin-gage, roll-fed forming as well. As detailed in Chapter 7, the role of the plug is to aid in polymer redistribution. Plugs are made of many materials. On large, simple forming presses, plugs are usually wood. In many cases, they are manually advanced along greased channels or hand-cranked along rack-and-pinion channels. On most automated heavy-gage operations and for all thin-gage operations, the plugs are automatically advanced and retracted according to very specific sequences. Mechanical toggle, hydromechanical action and pneumatic action are the common mechanisms used to activate automatic plug travel. The choice of plug mechanism depends on the linear travel distance of the plug, the surface area of the plug and the gage and toughness of the polymer being pushed. Very large plugs require auxiliary guide rods to maintain planar travel. Air pressure actuated cylinders are easy to maintain and are relatively inexpensive. As a result, they are commonly used for relatively simple pushing operations. There are five general characteristics to plugs:

- Plug material,
- Plug temperature,
- Plug shape,
- Plug rate of travel, and
- Relative time of plug contact with sheet surface.

The first two are considered in this section. The last three are discussed in Chapter 7.

Plug Materials

The choice of plug materials is somewhat dictated by:

- Whether the operation is prototype or production,
- Whether the plug design is fixed or is still being modified,
- Whether the polymeric sheet is marked by certain plug materials,
- Whether the plug needs to be active, and
- The gage of the sheet and the sheet temperature.

There are two general categories of plugs. Plug materials such as plastics (syntactic foams, nylon or PA, epoxy, PTFE) and wood are thermally passive. That is, the final plug temperature is determined by the relative contact time the plug has with the hot sheet. Plug materials such as aluminum are active. That is, positive temperature control of the plug surface is achieved with coolant fluid flow. Table 6.16 gives typical property values for several plug materials.

Table 6.16 Comparative Properties of Non-Metallic Plug Materials

| Plug material | Density | Compressive strength | Service temperature | | Thermal conductivity | | |
|-------------------|----------------------|----------------------|-------------------------------------|------|----------------------|-------------------|-------------------|
| | (g/cm ³) | | (lb _f /in ²) | (°C) | (°F) | (cal/cm · s · °C) | (Btu/ft · h · °F) |
| Wood—sugar maple | 0.55 | 10 | 1,500 | 150 | 300 | 0.00037 | 0.09 |
| Wood—oak | 0.60 | 7 | 1,000 | 135 | 275 | 0.00041 | 0.10 |
| Wood—black walnut | 0.55 | 7 | 1,000 | 150 | 300 | 0.00079 | 0.19 |
| Syntactic foam | 0.50 | 45 | 6,500 | 175 | 350 | 0.00025 | 0.06 |
| PA 66 | 1.15 | 80 | 12,000 | 200 | 400 | 0.00024 | 0.058 |
| PTFE | 2.20 | 12 | 1,700 | 120 | 250 | 0.0006 | 0.145 |
| Epoxy—unfoamed | 1.90 | 45 | 6,500 | 150 | 300 | 0.0010 | 0.242 |

Wood Plugs

The easiest and in many aspects the best plug material is hardwood. Typically, end-grain maple, ash and walnut make excellent, easily fabricated plugs. Oak and mahogany are also used. As with wood for molds, wood for plugs needs to be kiln-dried to minimize checking and cracking. Wood plugs are usually sanded to 320 grit or more to minimize plug mark-off¹. Polyurethane and epoxy coatings are also used. If the mark-off is attributed to the sheet being chilled by the colder plug, blanket or pool table felt is used to cover and insulate the plug end. Wood plugs are commonly used with HDPE and styrenics such as ABS and HIPS.

Plastic Plugs

There are several types of plastic plugs. Nylon 66 or PA 66, mineral-filled epoxies and PTFE such as Teflon[™] have been used for many years. Solid plastic plugs have exceptional compressive strength and excellent high temperature capability. These polymers have higher thermal conductivities than wood or syntactic foams, discussed below. As a result, plug mark-off can be more serious. And these polymers are heavier than wood or syntactic foams. As a result, the plug supports need to be more robust. Solid polymeric plugs are used for PVC and polyolefins. PTFE is usually recommended for PP.

Syntactic foam is quite popular. These foams are made by incorporating sintered or foamed microspheres of fly-ash or phenolic into a polyurethane or phenolic resin matrix. The matrix, too, may be foamed. These foams are normally available from the foam supplier as plank, slab-stock or block in density ranges of 0.2 g/cm³ to 0.8 g/cm³ or 12 lb/ft³ to 50 lb/ft³. Casting grade foams have recently become available as well. Table 6.17 lists typical properties for one of these syntactic foams. Syntactics are used for styrenics such as HIPS and ABS, amorphous PET and PVC. In certain cases, syntactic surfaces are coated. Polyurethane coating is used for amorphous PET. Epoxy enamel or PTFE-impregnated epoxy enamel is used for amorphous PET and POM or polyacetal.

Metal Plugs

Machined aluminum is used whenever the plug surface temperature must be carefully controlled, as with oriented polystyrene or OPS and crystallizing PET or CPET. If the plug temperature is to be heated, electric cartridge heaters are inserted

¹ Plug mark-off or chill mark is a line or region on a part that exhibits slightly different texture than the region next to it. In some cases, there is a distinct change in the part wall thickness at this point. There are two known reasons for mark-off. One is that the plug actively removes heat from the sheet in contact with it. Once the sheet is free of the plug, the colder sheet region does not stretch as much as the hotter region and so a demarcation is evident. A second reason is that hot sheet in contact with a solid surface tends to replicate the solid surface texture, whereas hot sheet that is free does not. This difference in texture can be quite apparent.

Table 6.17 Typical Properties for Thermoforming Syntactic Plug Material [Syntac 350-W. R. Grace Co.]

| | | |
|----------------------------------|--|--|
| Coefficient of thermal expansion | $17 \times 10^{-6} \text{ } ^\circ\text{C}^{-1}$ | $10 \times 10^{-6} \text{ } ^\circ\text{F}^{-1}$ |
| Thermal conductivity | 0.06 Btu/ft · h · °F | 0.0010 W/cm · °C |
| Specific heat | 0.30 Btu/lb · °F | 0.30 cal/g · °C |
| Shear strength | 3000 lb _f /in ² | 21 MPa |
| Service temperature | 350°F | 175°C |
| Compressive strength | 6500 lb _f /in ² | 45 MPa |

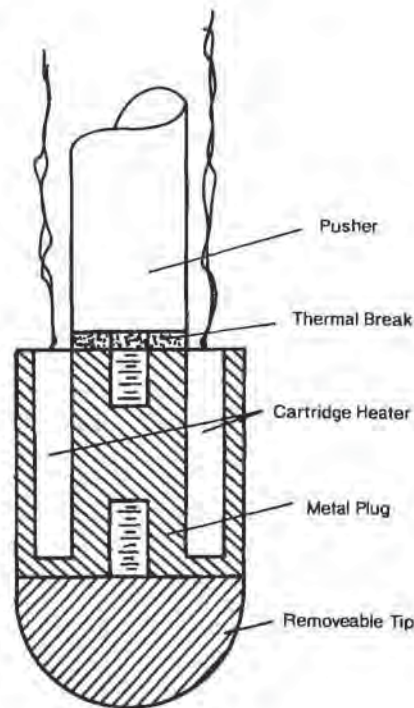


Figure 6.33 Schematic of electrically heated metal plug

into predrilled holes in the plug tip (Fig. 6.33). The leads are passed up the shaft of the plug to the region where the plug is attached to the cylinder rod. Usually a thermal break such as PA 66 or nylon is placed between the heated plug tip and the main body of the plug to minimize heat conduction to the body and the pushing mechanism (Fig. 6.33). Liquid coolant is used if the plug temperature is expected or predicted to rise above the acceptable maximum value during sustained production. It is difficult to adequately control plug temperature with liquid coolant. Large diameter coolant lines remove cross-sectional area from the plug and could weaken it. The plug tip may be designed with circular milled grooves so that the coolant floods

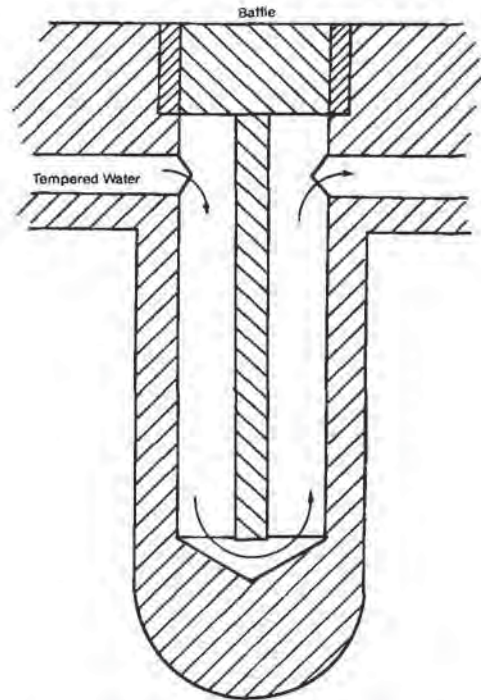


Figure 6.34 Schematic of hot water heated metal plug similar to injection mold bubbler

the back of the tip (Fig. 6.34) [31], in much the same fashion as for actively cooled injection mold cores [32]. The coolant lines exiting the plug top must be flexible enough to allow for adequate plug travel. For a large aluminum plug, copper rods are embedded in the plug tip. The free ends of the copper rods are cooled with liquid coolant or are finned and cooled with directed air jets. Heat pipes are effective for small diameter plugs [33]. The heat pipe is a hollow metal tube, usually stainless steel. The tube contains a fine metallic mesh. It is evacuated and partially filled with an ultrapure fluid such as methanol or ethanol. One end of the tube is placed in a heated zone and the other in a suitable coolant. The fluid in the heated end of the tube evaporates. The vapor diffuses to the cooled end where it condenses. The fine mesh draws the condensed fluid to the heated end by capillary action (Fig. 6.35). At steady temperature input, these devices are many times more efficient than solid copper rods.

The decision to actively heat or cool a plug must be made early in the mold design. If the plug is very cold, the sheet will surely freeze to it. As detailed in Chapter 7, drawing always occurs between the point where the plug and the sheet separate and the sheet and the mold rim meet. Usually, no drawing occurs on the plug surface during pushing. If the plug is very cold, very little drawing occurs after the sheet has been stripped from the plug by the stretching forces. In extreme cases, the sheet will shrink onto the plug during stretching. If the plug is very hot, the sheet may tear at

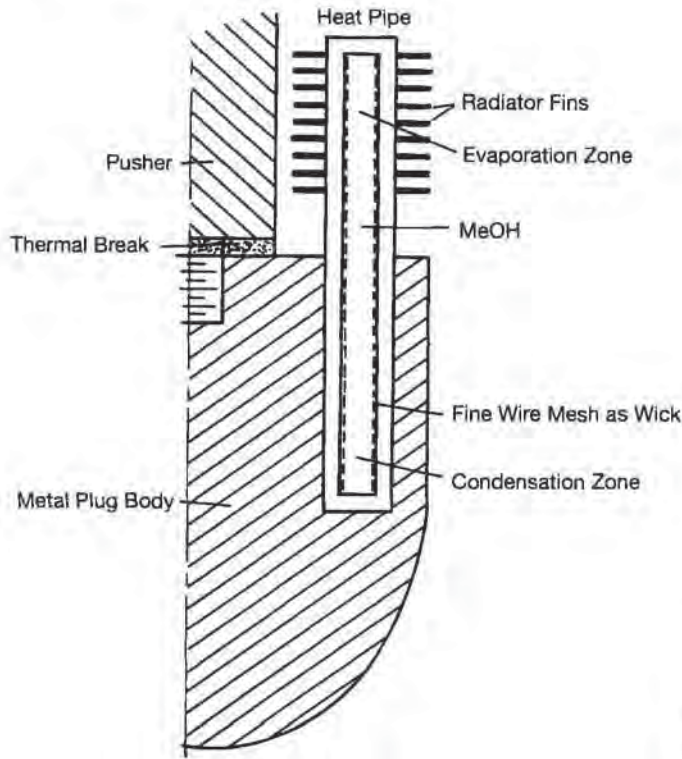


Figure 6.35 Section of thermal pin heated metal plug

the point where the plug enters the sheet. Actively controlled plug temperatures are usually between the sheet forming temperature and the mold surface temperature. For most amorphous plastics, the most effective plug temperatures are 20 to 30°F or 10 to 15°C below the surface temperature of the sheet as it exits the oven. Example 6.15 illustrates the relative effect plug temperature has on formability of sheet [52].

Example 6.15 Effect of Plug Temperature on Sheet Properties

A 0.120-in thick PS sheet at 375°F is stretched with an aluminum plug at 300°F. The plug is in contact with the sheet for 36 s. Determine the average sheet temperature and the relative sheet modulus when it releases from the plug. The thermal diffusivity of PS is $2.2 \times 10^{-3} \text{ ft}^2/\text{h}$. The exponential coefficient for PS modulus is 50°C^{-1} .

Fig. 6.36 gives the time-dependent average temperature of the sheet. The unaccomplished temperature change is given as:

$$Y = \frac{375 - T}{375 - 300}$$

The dimensionless time, Fo , is:

$$Fo = \alpha\theta/L^2 = 2.2 \times 10^{-3} \cdot \frac{36}{3600} \left(\frac{12}{0.120} \right)^2$$

$Fo = 0.22$. From Fig. 6.36, $Y = 0.15$. Therefore the average sheet temperature is:

$$T = 375 - 0.15 \cdot (375 - 300) = 363.8^\circ\text{F}$$

The effect on modulus is given as:

$$\frac{E_{363.8}}{E_{375}} = e^{(375 - 363.8)/50} = 1.25$$

The modulus of the sheet just released from the plug is 25% greater than the sheet that has not touched the plug.

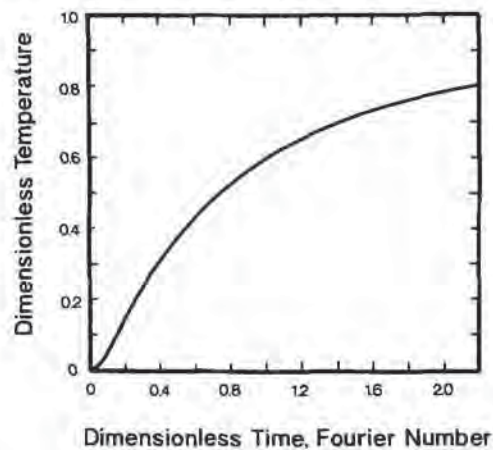


Figure 6.36 Dimensionless temperature loss from sheet when contacting solid plug. Dimensionless temperature, $Y = (T_o - T)/(T_o - T_p)$ where T_o is the initial sheet temperature and T_p is the plug temperature. Fourier number, $Fo = \alpha\theta/L^2$, where α is sheet thermal diffusivity, θ is time, and L is sheet thickness

Plug Design Concepts

As detailed earlier, the purpose of a plug is to influence final part wall thickness. Plug shape has the greatest influence on final part wall thickness. A flat or blunt-nose plug (Fig. 6.37), allows maximum sheet drawing in the annulus between the plug and the rim, while fixing the sheet thickness in contact with the plug bottom. A part made with this type of plug will have a heavy bottom and thin sidewalls. And there will be a ridge or sharp wall thickness demarcation between the freely stretched portion and the plugged portion of the sheet. Blunt-nose plugs are also used where sheet must be brought in from the rim region or where the sheet is billow-stretched prior to plugging.

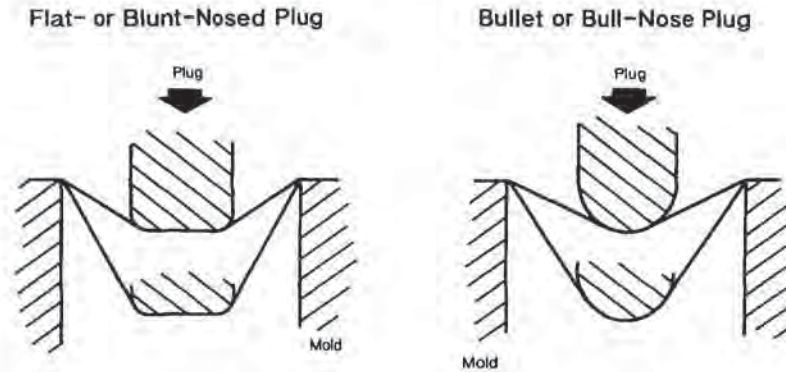


Figure 6.37 Two plug tip shapes

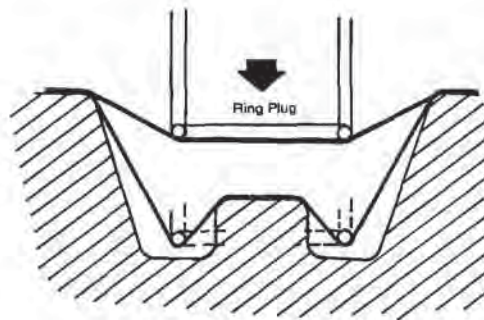


Figure 6.38 Ring plug for forming over male projections in female mold

Initially, only a small amount of the sheet contacts the tip of a bullet- or bull-nosed plug (Fig. 6.37). More and more sheet contacts the plug surface as the plug penetrates the sheet. Differential sheet stretching continues as the plug advances and so there is no sharp demarcation between the plugged sheet and stretched sheet. Ring-type or wire-frame plugs are used when a large portion of the bottom of the sheet must remain pliable and formable. Wire-frame plugs are used when the sheet must replicate a mold texture or lettering or a logo or when the sheet must stretch over a male portion of the female mold (Fig. 6.38). Wire-frame assisted stretching is similar to that for the blunt-nose plug. Once the plug has fully advanced, the sheet is stripped away from the plug by applied pressure. The disk in the middle is then stretched into the mold cavity. The wall thickness in the vicinity of the polymer that contacted the wire frame is usually quite irregular.

Plugs are used in pressure forming as well. The shaft holding the plug is pressure-sealed with O-rings. If the internal pressure is quite high, on the order of 1 MPa or 145 lb_f/in² or so, special labyrinth seals or hard, nonextrudable O-rings are used.

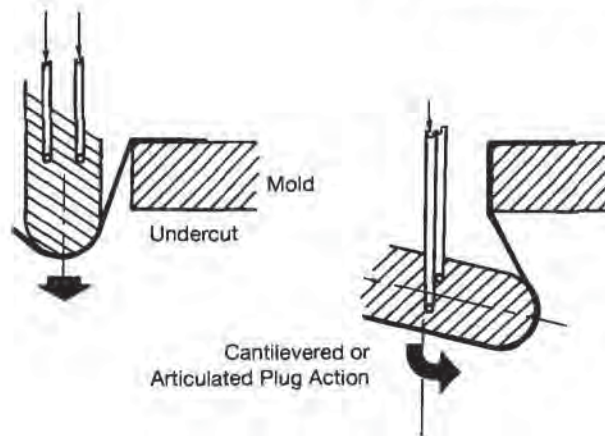


Figure 6.39 Example of articulated plug motion

Table 6.18 Application Areas for Various Plug Types

| Plug type | Application |
|--------------------------------|--|
| Blunt-nosed, flat bottom | Maximum drawing from rim, where rim material must be drawn into cavity, shallow draw parts. |
| Tapered, bullet- or bull-nosed | Very deep draws, where thinning of sidewall is critical, where wall thickness uniformity is important, where polymer chills rapidly. |
| Wire-frame, can | Where bottom detail is required, where sheet must stretch over male portion in female mold. |
| Articulated | Where sheet must be tucked under in deep undercut, where local wall thickness is increased from local thicker sheet. |

On certain occasions, articulated plugs are required. The simplest of these plugs operates on a cam (Fig. 6.39). As the plug shaft advances, the plug head moves down, then out. These articulated plugs are used with deep undercuts, Table 6.18. More complex articulation is needed if polymer must be stretched from the bottom of the sheet to the corners. As an example, a tulip-like device enters the sheet in its closed form (Fig. 6.40a). As plug advances, the vanes or sections of the device expand outward from the axis (Fig. 6.40b). When the plug and its sections are fully extended, the sheet is stripped from the mold (Fig. 6.40c). The plug sections collapse as the plug withdraws. Owing to the complexity of this plug design, plug cooling is usually not possible. A variation to this, called "cuspatation", was patented and saw limited commercialization in deep-drawn, parallel-walled cans in the 1980s [34,35].

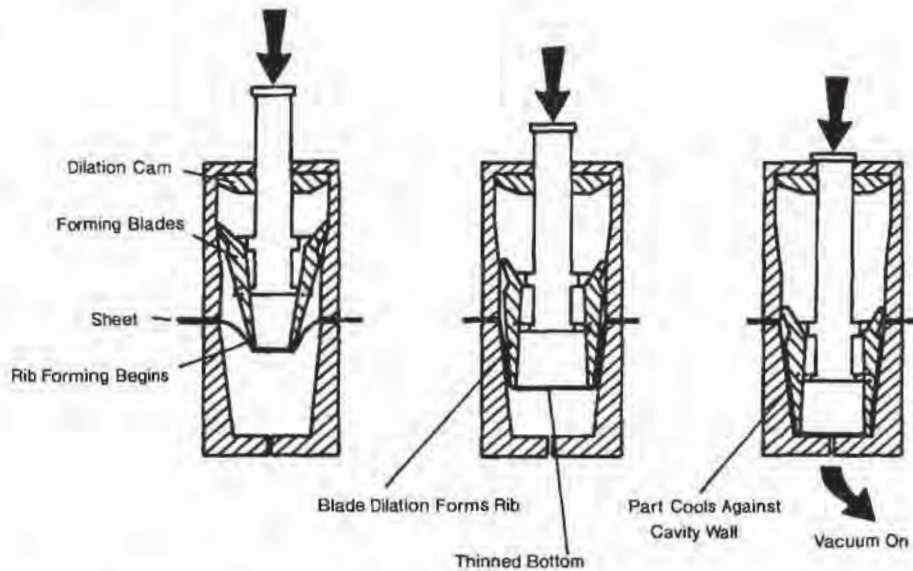


Figure 6.40 Schematic of Hitek cusputation-dilation forming, showing stretching sequence [34]

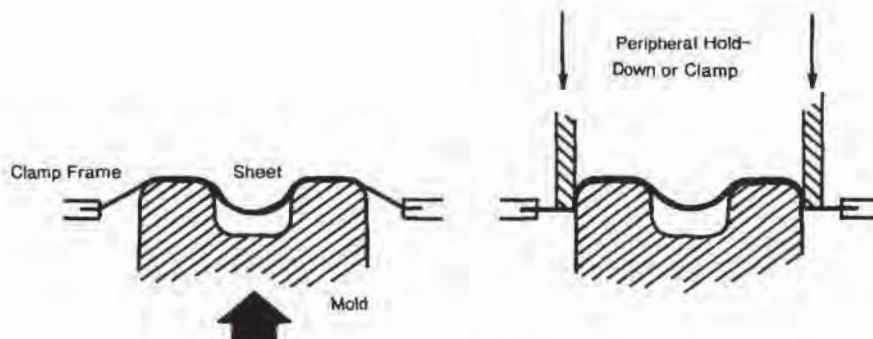


Figure 6.41 Schematic showing mold sealing cavity, followed by peripheral clamping

6.8 Sheet Clamping

As discussed in Chapter 1, the sheet clamp has several functions. Holding the sheet rigidly during draw-down is one of its most important functions. For cut-sheet forming, the sheet is clamped everywhere along its perimeter. During forming, the mold pushes into the hot sheet past the plane of the clamp prior to initiation of mechanical plugging or forming pressure (Fig. 6.41) [36]. This effectively seals the hot sheet against the mold surface. A secondary sheet clamp is used for some tough

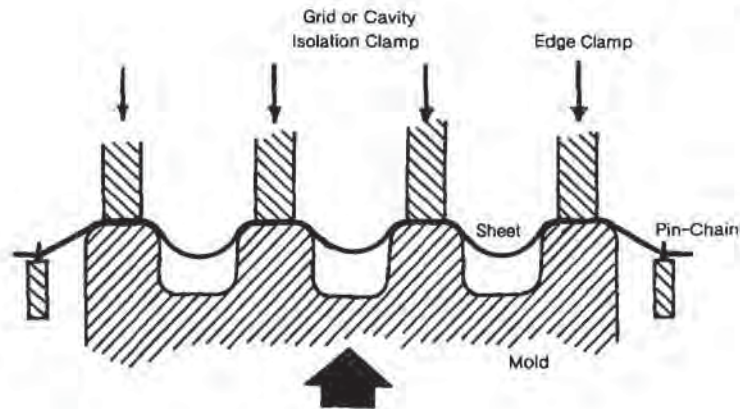


Figure 6.42 Schematic of individual cavity isolation or grid in combination with peripheral clamping

polymers such as ABS and PC. The secondary or perimeter clamp presses the sheet against the mold surface after the mold has passed the clamp plane (Fig. 6.41). This ensures a positive sheet seal against the mold surface. For prestretching with a vacuum or draw box, the edge of the vacuum box acts as the secondary sheet clamp as the mold enters the billow. In pressure forming, the edge of the pressure bell serves as the secondary sheet clamp.

For roll-fed forming, the sheet is only held along two edges. If secondary sheet clamping is not used during multicavity mold travel and forming, the sheet is pulled into the leading and trailing edges of the mold. The result is nonuniform part weight, warping and distortion. The full perimeter clamp is the most common secondary sheet clamp (Fig. 6.42). This clamp engages the sheet just prior to the time the mold touches the sheet and before the mold has reached its final position. The clamp resides above the sheet for forming presses where the mold is situated below the sheet. Individual cavity clamps, cages or grids are used for products that have stringent wall thickness requirements. Individual cavity clamping ensures that polymer from one cavity region will not be preferentially pulled into another. The cavity clamp framework is also positioned above the sheet for forming presses where the mold is situated below the sheet. The cavity clamp framework may also contain the perimeter clamp or it may be on a separate framework and may be sequenced to engage the sheet after the mold has reached its final position but before the plugs and vacuum sequences have begun. In certain cases, the cavity clamp may provide other functions, for example:

- The clamp may contain steel rule dies for trimming. The dies may partially cut through the polymer during the initial phase of the clamp. The die then acts as the clamp. When the part is formed and cool, the die resumes its travel, cutting through the sheet as a trim-in-place die (Fig. 6.43) [36].
- The clamp may contain a forming ring that compresses the rim region. This is called "coining" and is used whenever the formed part must have a molded-to-tolerance rim thickness. Deli container rims are sometimes coined. Coining may also

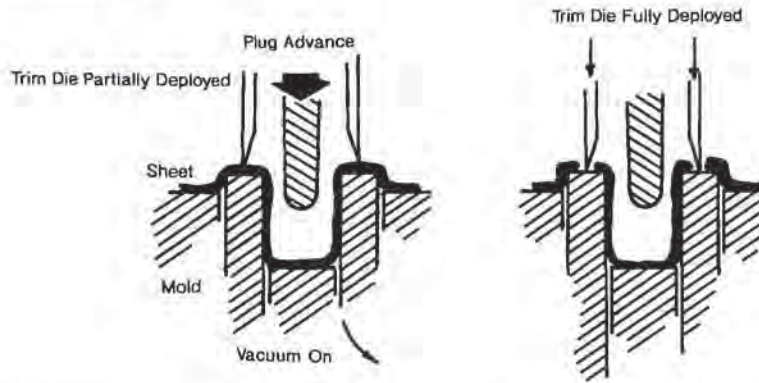


Figure 6.43 (Left) Example of in-mold trim die acting as cavity isolator followed by (right) trimming after forming

be used if the container rim must be rolled to provide rim stiffness, as discussed below. The force required to coin a lip is a function of the compressive strength of the polymer at its instant temperature. Consider a polymer with the following temperature-dependent compressive stress-strain relationship:

$$\sigma_c = C(T) \cdot \epsilon^n \quad (6.43)$$

where σ_c is the applied compressive stress, being the compressive force per unit area of the lip, $C(T)$ is the temperature-dependent compressive modulus of the polymer, ϵ is the compressive strain, with $0 < \epsilon < 1$, and n is an empirical shape factor for the stress-strain relationship. The amount of force required to compress the polymer in the lip a specific amount is given as:

$$F = \sigma_c \cdot 2\pi R w = C(T) \cdot 2\pi R w \cdot \epsilon^n \quad (6.44)$$

where R is the radius of the lip and w is its width. Example 6.16 illustrates the application of this expression to the forming of a cup lip.

Example 6.16 Coining Force for PP Lid

Consider a 4-in diameter PP deli cup having a lip width of 0.100 in. Determine the force required to coin the lip from a thickness of 0.055 in to 0.050 in. The value for $C(T)$ is $800 \text{ lb}_f/\text{in}^2$ and the compressive stress-strain relationship for PP is Hookean, or $n = 1$. If 24 cups are coined simultaneously, what is the force the mold must resist.

The force is given by Equation 6.44 as:

$$F = 800 \frac{\text{lb}_f}{\text{in}^2} \cdot 2\pi \cdot 2 \cdot 0.1 \text{ in}^2 \cdot \frac{(0.055 - 0.050)}{0.050} = 100.5 \text{ lb}_f$$

For 24 cups, the mold resistance is:

$$24F = 2412 \text{ lb}_f = 1.2T$$

- The clamp may combine with an ejection ring on the cavity to allow separation of the part from the trim. The formed part is held momentarily stationary between the ring and the clamp while the mold moves away and the trim is pulled downward. Then the clamp retracts, leaving the part on the ejection ring. The trim moves once the part and ring assembly have cleared the trim plane.

6.9 Sag Bands and Sheet Supports

Sheet sag is one of the most vexing problems in thermoforming. All polymers sag to some degree when heated. Certain polymers are quite weak when heated to forming temperatures¹. As a class, crystalline polymers are more problematic than amorphous ones. HDPE, PP and PA or nylon sag greatly when heated. Certain amorphous polymers such as cellulose acetate and toughened FPVC sag when heated to their upper forming temperatures. Sheet supports or sag bands are used in roll-fed forming to minimize catastrophic drooping during the final stages of heating. There are two common types of sheet supports. Stationary PTFE-coated hollow rods are placed parallel to the rails in the last section of the oven. PTFE-coated steel wires are also used. These wires may be stationary but are sometimes driven at the speed of the chain rail. Sag bands sometimes extend into the mold area and beyond. Provision for them must be included in the overall mold design layout. The presence of sag band slots in the mold structure can seriously restrict the arrangement of parts of unequal size in family mold designs. Early consideration must be given to their presence if forming of sagging polymers is ever to be considered.

Sheet supports are not used in heavy-gage forming with single cavity molds. Pneumatic lifting methods are preferred.

6.10 Other Aspects of Mold Design

Often, seemingly impossible designs are achieved through thoughtful, mature mold design. Mold designs that are impossible with high pressure applied against sticky fluids such as injection molding are quite feasible with thermoforming. This is because thermoforming is a process that uses only modest pressure applied against a rubbery solid sheet. So long as a portion of the sheet remains rubbery, in theory it can be stretched. As a result, secondary in-mold forming steps are frequently used. One technique moves male plugs against the sheet that is already formed in a female mold. This technique allows bosses and ribs to be formed of polymer having a thickness different from that of the main surface [37].

¹ Sag is also discussed in some detail in Chapter 5.

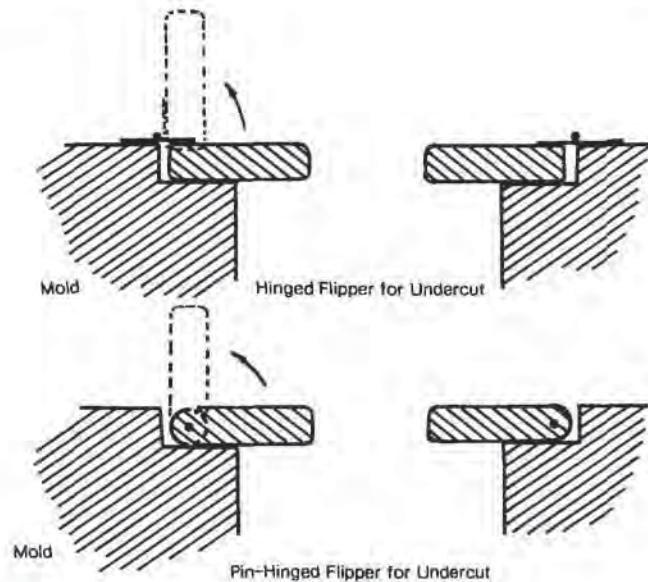


Figure 6.44 Two examples of flipper design for shallow or thin undercuts

Undercuts

Molds, particularly large prototype molds, can be made in sections that move in different directions. In this way, parts with severe undercuts are fabricated. For some severe undercuts, the trapped mold section is built like an interlocking wooden puzzle. A key section is removed first to allow the remaining segments to unlock and fall free. These sections are then reassembled and the key section reinserted to lock the segments in place for the next forming operation. This is not an uncommon technique on prototype tooling, but it requires great ingenuity by the mold designer. Flippers and hinged sections are used in automated molds. Figure 6.44 shows an example of a flipper or pin-held rotating section. Figure 6.45 shows examples of single- and double-hinged sections. The double-hinged section is used when the section to be swung away is very thick and would interfere with sheet extraction if only attached with a single hinge.

For some prototype parts, the undercut is so severe that even these approaches are infeasible. If alternate methods such as post-forming assembly are also infeasible, forming around a disposable mold section is possible. A very soft grade of plaster is used. It is shaped and hardened in the traditional way described above. It is held in the mold with alignment pins as the sheet is formed around it. The disposable section is then adequately softened with very hot water and removed in chunks. In order to minimize gas trapping and part distortion around the disposable insert, its surface is covered with a single thin layer of cheesecloth, held in place with tape or daubs of

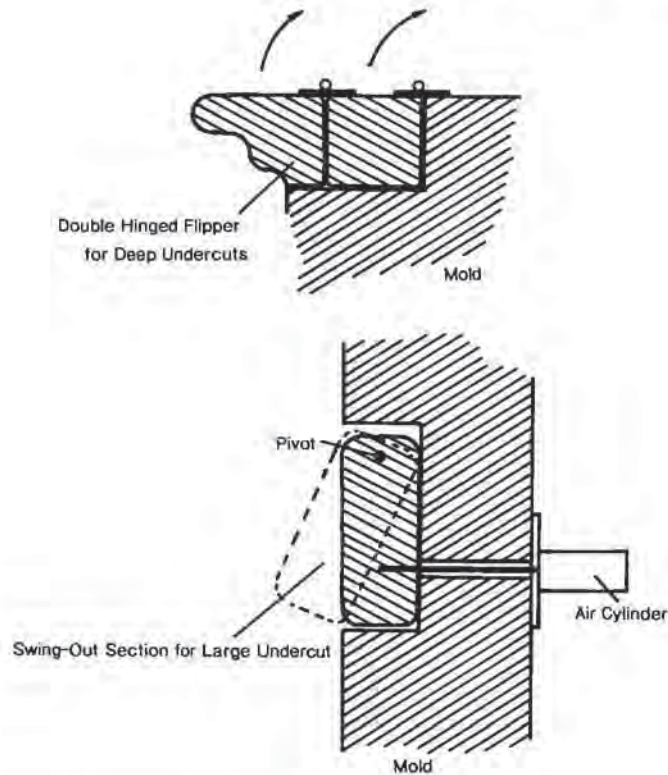


Figure 6.45 (Top) For deep undercuts, double-hinged flipper is used; (bottom) for large undercuts, pneumatic swing-out mold wall segment is used

water-thinned plaster. Sculptor's wax has also been used as a disposable insert when forming lower temperature polymers such as LDPE and FPVC [3].

Encapsulation

In certain special cases, the insert becomes part of the product. Usually inserts are restricted to captured stiffening agents such as rods and angles. One thermoformed industrial single-deck shipping pallet has the rim reinforced and stiffened with hollow aluminum conduit. In sequential twin-sheet thermoforming, reinforcing elements of wood or metal pipe or channel are often used. Forming around this superstructure is surprisingly straight-forward. Care must be taken to allow for the nearly ten-fold difference in coefficients of thermal expansion between the plastic and the aluminum. If the sheet is pulled too tightly around the tubing or if the tubing is too rigid, the plastic will crack on cooling or during low temperature usage. A car-top sign formed on a male mold uses encapsulated gussets on the two-dimensional vertical corners.

These gussets eliminate the traditional webbing problem with male molds and also help reinforce the corners of the part.

Moving Elements

Many injection molding devices are successfully used in thermoforming [38]. These include:

- Collapsing cores. As noted above, expanding cores can be used as plugs for special stretching cases. Tulip collapsing cores are used in injection molding with undercuts such as large diameter molded-in internal threads.
- Unscrewing devices are used in injection molding when complete molded-in internal threads are needed. The best application for these devices is in pressure forming.
- Cammed sections. As with injection molding, cammed sections move away from the molded part with the mold action. One application is full perimeter undercut on a female mold (Fig. 6.46) [39].
- Slides. There are many slide designs [40]. Most are used to remove parts with undercuts. One example is the formation of a hinge in a five-sided box (Fig. 6.47). Another is the formation of an isolated undercut for a recessed door handle. In

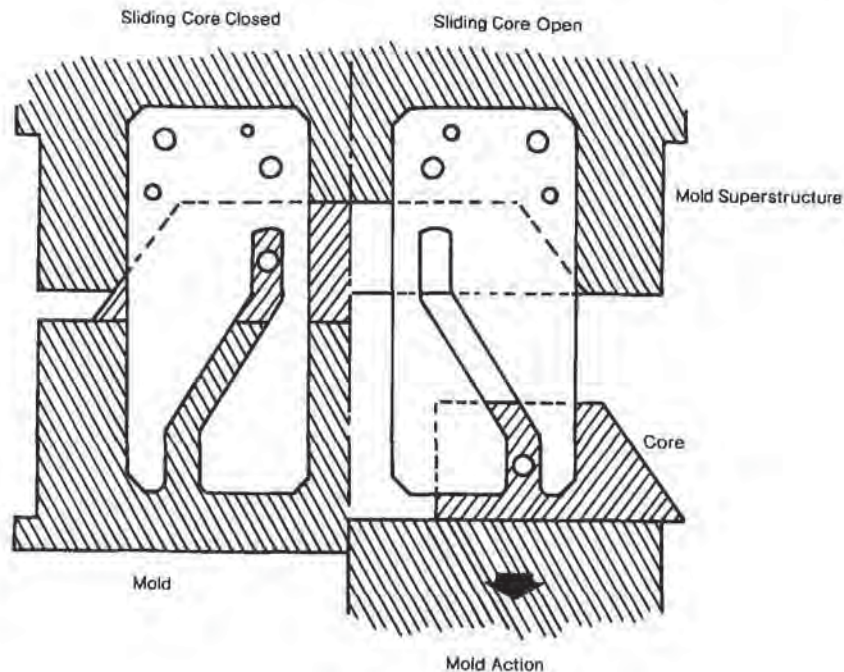


Figure 6.46 For complex undercuts, (left) sliding cores are actuated by (right) mold motion

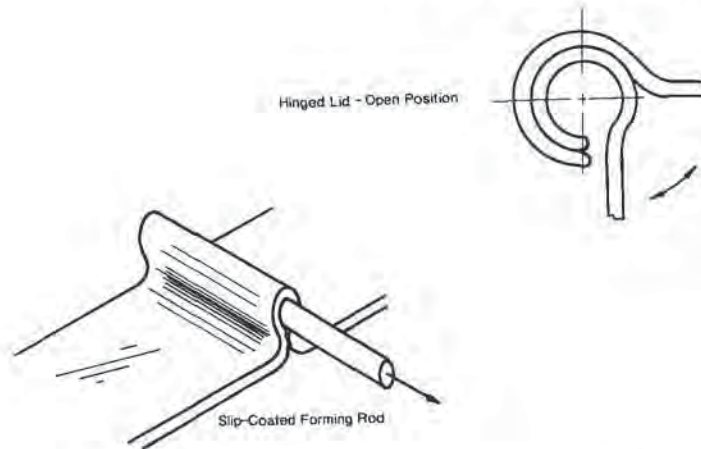


Figure 6.47 (Left) For pin hinges, mold around forming rod; (right) for nested hinge lid, mold both pieces around forming rods

certain cases, slides are used to stretch plastic into an undercut during forming, much like a plug.

Many of these techniques work best when the mold pressure is greater than one atmosphere. The standard material for these devices is machined aluminum. The temperature of long, thin cams, slides and unscrewing devices is difficult to control. Poor temperature control leads to mold mark-off and sheet adhesion to the devices.

Stripper Plates/Bars

In most cases, part design is simple enough and draft angles large enough to allow the part to simply fall or be easily plucked from the mold. For cut-sheet parts, the trim serves as the region against which force is applied to free the formed sheet from the mold. Mechanical part removal is necessary if:

- The mold surface is deeply textured,
- The mold is a male mold,
- The mold temperature is low and the mold is male,
- The mold is a shallow five-sided box,
- The mold bottom is quite flat and the mold is smooth,
- There are male portions to the female mold,
- The mold is very hot and the polymer is crystalline,
- The polymer shrinks greatly during cooling,
- The polymer is crystalline and is processed in its melt phase,
- The polymer has very low shrink, the mold is female and the draft angle is very small,
- There are substantial incidental undercuts.

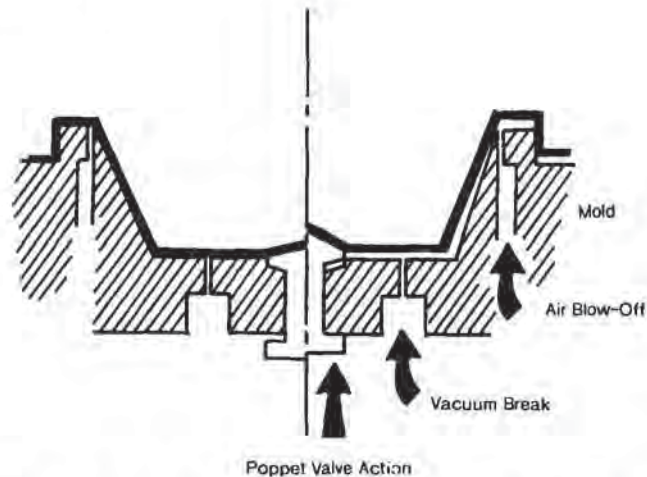


Figure 6.48 Vacuum break, air blow-off and poppet valve opening for part release from mold

- The polymer is very rigid, is heavy gage and there are deliberate or incidental undercuts,
- The mold is used to form polymers that out-gas corrosives that attack or pit the mold surface, and
- The mold is old and/or its surface has not been well-protected.

Very rigid parts are difficult to remove from molds with slight incidental undercuts or tool damage. Very soft polymers such as LDPE, TPEs, PP and FPVC are difficult to remove from very smooth molds. It is apparent that adequate draft, proper surface texture, and diligent mold surface maintenance are vital to ensuring a stick-free surface. Nevertheless, there are occasions when positive methods for ejecting a part or parts from mold cavities are necessary. For heavy-gage sheet, a poppet or ejector valve located at the bottom of the mold aids in breaking the vacuum between the sheet and the mold surface (Fig. 6.48). The poppet is used in combination with air blow-back through the vent holes. For multicavity thin-gage thermoforming, ejector rings are used. For a female molded part, a perimeter ejector ring is used directly under the part lip (Fig. 6.49). The ejector ring is driven by ejector pins that pass through the mold to an ejector plate. The ring is actuated by mold action. Ring recovery is either through springs or stops during mold motion [41]. If there are many cavities and substantial trim area, large diameter ejector pins are placed between the cavities on the trim. These advance and touch the trim shortly after the ejector rings deploy.

Mold Releases

Ejection is sometimes aided by mold releases. There are two common types of mold releases:

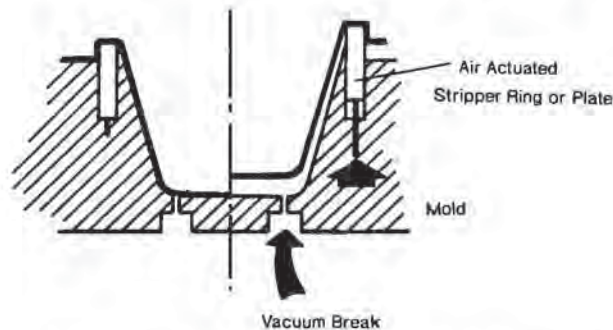


Figure 6.49 Air-actuated stripper ring or plate in combination with air blow-off for part release from mold

- Temporary mold releases. Usually available in 12 oz or 400 g aerosol containers, these mold releases are used when only a few parts are needed, when evaluating a new polymer or during production start-up. Although silicones are ideal mold releases, they must be used with caution. Silicones interfere with decorating, sealing, painting and labeling. Even though silicones might be acceptable for one product, they are typically atomized and the spray may contaminate other areas of the plant where other surface-sensitive products are being manufactured. Most aerosols are CFC- and HCFC-free today. If the formed part is to contain food, FDA approved mold releases are needed. Vegetable oil spray is an effective, FDA-approved temporary mold release.
- Permanent mold releases. PTFE and FEP-derived coatings are used with aluminum molds and plug assists. These coatings are applied by powder spraying onto a suitably prepared metal surface. Usually, fluoropolymer coatings last 100,000 or more cycles. The primary mode of failure is uneven wear. Delamination or peeling is a sign of improper metal surface preparation. Cuts and slices are signs of improper mold protection during storage and set-up. Florian [42] notes that:

“The extra cost of Teflon (sic) coating becomes a luxury only when it is completely unnecessary.”

Web Breakers, Catchers and Chasers

Webs are formed when the hot stretched plastic surface area in a local region is greater than the surface area of the mold in that region. Even though the plastic is considered to be an elastic rubbery solid, as the sheet is drawn toward the mold surface, certain sections of the sheet touch other sections before they touch the mold surface. When hot plastic touches hot plastic, the forces required to pull them apart are far greater than the force needed to stretch surrounding plastic against the mold surface. As a result, a web is formed (Fig. 6.50). In many cases, the mold design is such that the web cannot be completely eliminated. This is most common in female parts that have

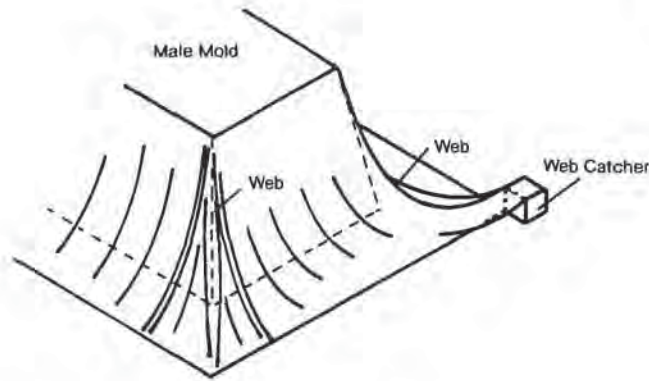


Figure 6.50 Web formation and web catcher for male forming

male projections. Multiple plug assists, pre-blown bubbles, prestretching restraints and articulated plug assists are sometimes used to minimize web formation. If the web forms near the rim of the part, web catchers are used. These are simple outriggers, posts or stanchions positioned beyond the rim of the part (Fig. 6.50). The stretching sheet catches on these posts. The web is formed at the bases of these posts and away from the part rim. Web breakers are usually incorporated in mold designs by experience. For simple prototype molds, wood is used. For production molds, aluminum is used. There is no technology available to design web catcher dimensions.

Moats, Dams and Double Steps

A moat or dam is used to seal the sheet against the lip region of a female mold. A double step serves the same function for a male mold. A moat is a groove or indentation outside the lip region (Fig. 6.51). These devices provide an early seal of the sheet to the mold surface, thus minimizing air leak. They also are used to minimize the amount of sheet drawn into the mold cavity from the rim region. The minimum moat width should be five times the local sheet thickness. A moat width of ten times the local sheet thickness is recommended. The moat depth should be at least equal to the local sheet thickness and a depth of twice the local sheet thickness is recommended. For polymers that have low coefficients of friction such as polyolefins

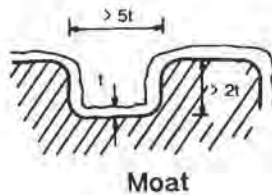


Figure 6.51 Design parameters for moat

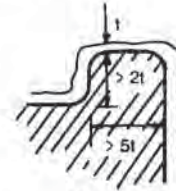


Figure 6.52 Design parameters for dam

Dam

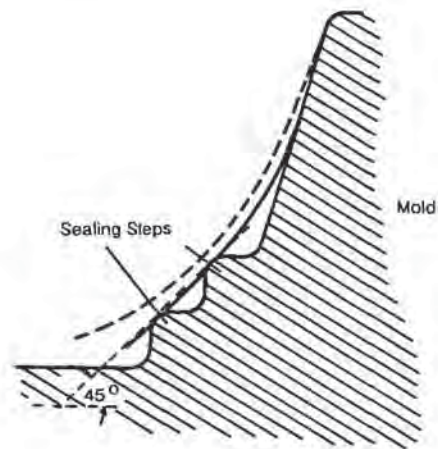


Figure 6.53 Double-step design for male mold to minimize air leak

or fluoropolymers, and for heavy-gage sheet, a dam is more effective (Fig. 6.52). The minimum height of the dam should be twice the local sheet thickness. The width is less important than the height. Sharp-edged dams are quite effective with heavy-gage sheet. Male molds are difficult to seal against air leakage. The double step (Fig. 6.53) is frequently used. The draping sheet bridges the edges of the two steps before vacuum is applied. The ideal design has the sheet touching the edges at 45 degrees or $\pi/4$ radians at this time. The plastic between the two edges forms the seal once vacuum is applied. The exact spacing and height of these steps depends on the depth of draw of the mold and the amount of plastic between the edge of the mold and the clamp. For tall molds, the steps need to be high and narrow. For shallow molds or where there is substantial web, the steps need to be low and wide. Molds are sometimes built with a single step. Once the press and sheet dimensions are confirmed, the second step is added as a separate plate attached to the vacuum box.

Chamfers and Radii

Designers have always used two-dimensional and three-dimensional radii for corner configurations in thermoformed parts. As shown in Chapter 7, the relative draw-down into a two-dimensional corner radius is given as:

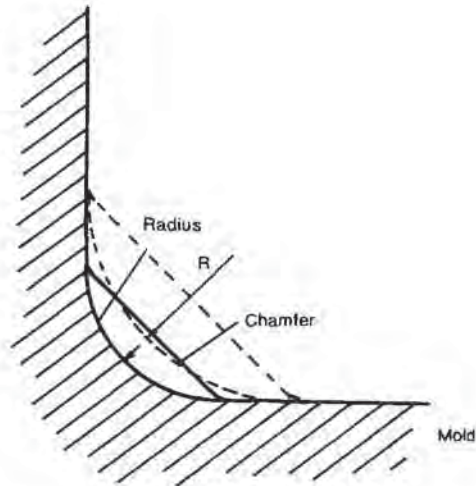


Figure 6.54 Geometric factors for chamfers and radiuses

$$\frac{t}{t_0} = \left(\frac{r}{r_0}\right)^{4/\pi - 1} \quad (6.45)$$

where t is the local thickness at radius r and t_0 is the thickness at radius r_0 . The relative draw-down into a three-dimensional corner radius is given as:

$$\frac{t}{t_0} = \left(\frac{r}{r_0}\right) \quad (6.46)$$

To get crisp corners, small radii are needed. For two-dimensional corners, the local sheet thickness is reduced about 21% when the corner radius is reduced by 50%. For three-dimensional corners, the local sheet thickness is reduced by 50% for the same radius reduction. Since the thinnest section of the part is the weakest under load, sharp radii dramatically weaken the part. This is true whether the part is a thin-walled deli container or a heavy-gage spa.

Recently, designers have rediscovered the chamfer as a way of maintaining corner thickness and stiffness (Fig. 6.54). The chamfer is typically 45 degrees or $\pi/4$ radians to the bottom or top rim or lip. It is easy to show that the plastic in the two-dimensional chamfer is $\pi/2 = 1.57$ times that in the equivalent radius. As a result, the stiffness of the chamfer corner is about three times that of the radius corner¹.

¹ The stiffness of the chamfer also depends on the folding strength of the line where the chamfer intersects the side wall and the bottom. The polymer thickness along this line is less than that in the rest of the chamfer, as shown in Chapter 7. Furthermore, the mechanism of bending of the chamfer as a plate differs from the mechanism of bending of a radius [43] and so the relative stiffnesses really cannot be compared.

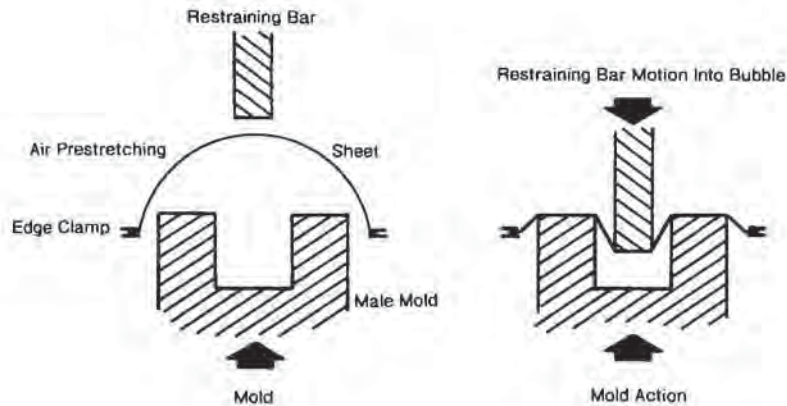


Figure 6.55 Restraining bar to provide two bubbles for double compartment male part

Prestretching Restraints

On occasion, air inflation is used to form a bubble into which a compartmented mold is plunged (Fig. 6.55). A severe web will be formed if the mold is plunged directly into the bubble. To overcome this, a restraint is lowered into one side of the bubble as the mold enters the other. The restraint acts to push the web to the edges of the forming sheet, beyond the perimeter of the part. This technique is used to form heavy-gage refrigerator liners, two-basin lavatories, and outdoor signs.

6.11 Efficient Use of Sheet

The economics of thermoforming turn on the efficient use of extruded sheet. As discussed in detail in Chapter 8, excessive incorporation of regrind can lead to:

- Multiplying extrusion costs,
- Polymer deterioration owing to multiple extrusion and forming,
- Processing problems with lowered polymer hot strength, and
- Customer concerns about loss in mechanical properties or appearance,

among other problems. The efficient use of sheet depends on using the smallest sheet dimension to produce the part.

Heavy-Gage Sheet

Usually in heavy-gage forming, only one part is made at a time. The part geometry dictates the absolute minimum sheet dimension (Fig. 6.56). The following dimensions must be added to these dimensions:

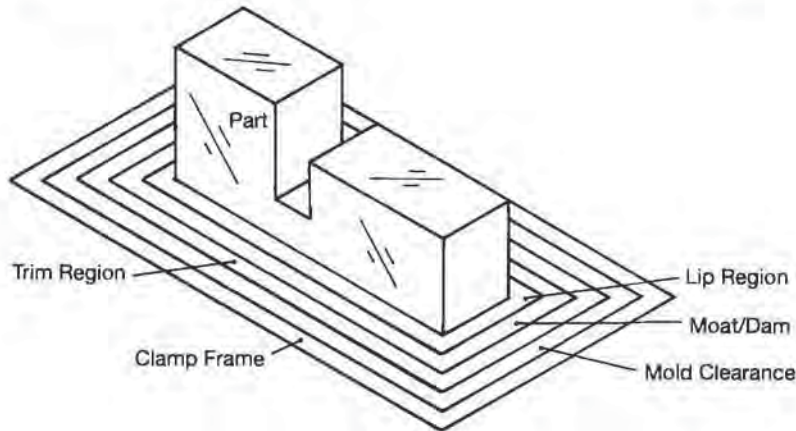


Figure 6.56 Various elements that make up sheet usage in forming molded part

- Any lip or rim area needed for the functioning of the part,
- Any trim area including trim tolerance,
- Any moats, dams or steps needed to seal the sheet against the mold surface prior to forming,
- Any additional sheet dimensions needed to ensure adequate pre-blowing¹,
- Additional sheet dimensions needed to allow the mold to clear the edge of the clamp frame without substantial tensile or shearing effects on the sheet in the clamp, and
- Sufficient dimension to allow the sheet to be adequately clamped in the clamp frame².

These are shown in Fig. 6.56. Example 6.17 gives an illustration. Typically, heavy-gage trim is 20% to 40% of the total sheet surface area.

Example 6.17 Efficient Sheet Use for Heavy-Gage Sheet

A rectangular part, 48 in × 40 in, with 2 in corner lip radiuses is to be formed from 0.250 in sheet. The lip must have 0.5 in width for trimming. A dam requires another 0.5 in width. The mold mounting frame extends an additional 3 in in all directions beyond the dam dimension. A 1 in clearance between the mold mounting frame and the clamp frame is required to minimize sheet pullout during mold travel. The clamp frame is 1.5 in wide. Determine the minimum sheet dimension and the amount of trim.

- ¹ These dimensions are important since the sheet at the clamp frame is uniaxially oriented whereas that in the center of the sheet is biaxially oriented. Sufficient distance between the clamp frame and the lip of the part must be provided if the polymer has known splitting tendencies.
- ² Although some clamp frames are designed to hold sheet with as little as 0.5 in or 12 mm of sheet in the clamp frame (Fig. 6.57), this requires that the sheet must be absolutely square to the clamp frame. Since sheet dimensions are usually not that accurate, a good rule of thumb is to allow a minimum of 1 in or 25 mm beyond the outer mold dimensions on all edges.

The amount of plastic that extends from the part surface in each direction by the amount:

$$0.5 + 0.5 + 3 + 1 + 1.5 = 6.5 \text{ in}$$

Thus the sheet dimensions are:

$$40 + 6.5 \times 2 = 53 \text{ in by } 48 + 6.5 \times 2 = 61 \text{ in}$$

The sheet dimensions are $53 \times 61 \times 0.25$ in. The sheet area is $53 \times 61 = 3233 \text{ in}^2$.

The plastic that is trimmed off the corner radii is given as:

$$(4 - \pi) \cdot R^2 = 3.4 \text{ in}^2$$

The plastic part surface area is then $40 \times 48 - 3.4 = 1916.6 \text{ in}^2$. The amount of trim is therefore:

$$\% \text{ Trim} = 100 \times \frac{(3233 - 1916.6)}{3233} = 40.7\%$$

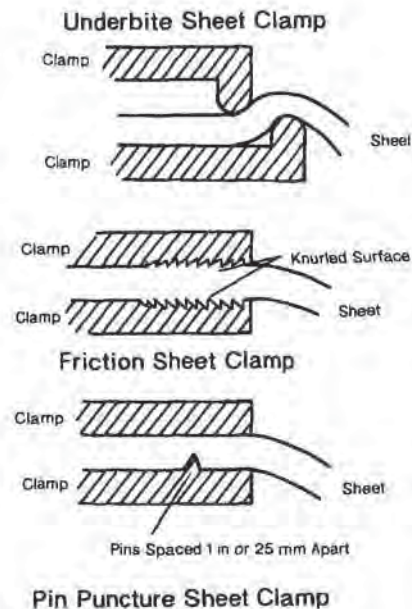
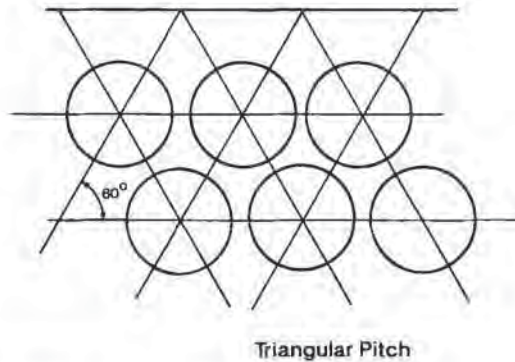


Figure 6.57 Three ways to clamp sheet in heavy-gage forming

Thin-Gage Sheet

Usually roll-fed forming has a higher trim fraction than heavy-gage forming. There are several reasons for this:

- Part dimensions are smaller relative to lip area,
- Many parts are round or oval,



Triangular Pitch

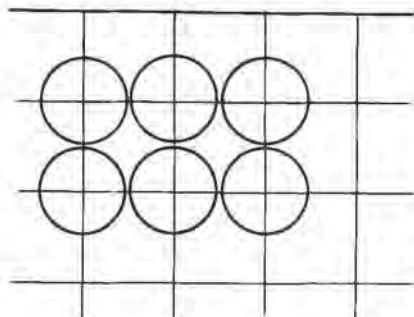
Figure 6.58 Triangular pitch part and mold layout

- The head and tail of the sheet on the mold surface are unclamped, requiring perimeter in-mold clamping area,
- Individual cavity clamps are used for plug assisted parts, and
- The relative amount of plastic outside the mold frame is large.

In an effort to efficiently use sheet surface, part layout on mold surfaces can be creative, particularly with circular or oval parts. Equilateral and other triangular pitches yield the greatest number of parts per unit area (Fig. 6.58). However, most mold builders prefer rectangular pitch (Fig. 6.59). Rectangular pitch mold designs are preferred because:

- The molds fit well on rectangular mold bases,
- Coolant channels are easier to lay out, and
- Rectangular pattern provides more satisfactory modular designs.

Example 6.18 illustrates trim fraction for three pitch designs. For circular parts formed in rectangular sheet, the trim percentage ranges from 40% to 75% or more. More on this important subject is found in Chapter 7.



Rectangular Pitch

Figure 6.59 Rectangular pitch part and mold layout

Example 6.18 Efficient Use of Sheet—Thin-Gage

Consider the forming of 2-in diameter drink cups. The required lip and moat region is 0.5 in, half of which remains with the cup. The space between cavities must be at least an additional 0.5 in to accommodate individual cavity clamps. The mold must clear the former rails by at least 1 in. And 0.5 in sheet space is needed in the pin rail to ensure adequate clamping. Determine the minimum sheet width if the maximum mold base is 34 in wide by 46 in long. Determine the number of cavities if the molds are placed on rectangular pitch. Rework the arithmetic for molds on triangular pitch and triangular pitch when cavity perimeters abut.

Consider the rectangular pitch first. The outer effective diameter of each cavity is given as:

$$2 \text{ in} + 2 \times 0.5 \text{ in (lip and moat)} + 2 \times (0.5/2) \text{ in (clamp)} = 3.5 \text{ in}$$

For the 34 in wide mold, $34/3.5 = 9.7$ cavities are possible on a rectangular pitch. For 9 cavities:

$$9 \times 3.5 + 0.5 \text{ (cavity clamp)} = 32 \text{ in}$$

For the 46 in wide mold, $46/3.5 = 13.1$ cavities are possible. For 13 cavities:

$$13 \times 3.5 + 0.5 \text{ (cavity clamp)} = 46 \text{ in}$$

The minimum sheet width is then:

$$32 + 2 \times 1 \text{ (clearance)} + 2 \times 0.5 \text{ (pin-chain)} = 35 \text{ in.}$$

The total number of parts produced on the 32 × 46 mold are:

$$9 \times 13 = 117 \text{ per shot.}$$

The amount of plastic in each cup is given as:

$$\frac{\pi D^2}{4} = \frac{\pi}{4} (2 + 2 \cdot 0.5/2)^2 = 4.91 \text{ in}^2$$

The amount of plastic as product:

$$4.91 \times 117 = 574 \text{ in}^2$$

The total surface area used to form these parts:

$$35 \times 46 = 1610 \text{ in}^2$$

Thus the trim total percentage is given as:

$$\text{Trim} = 100 \cdot \frac{(1610 - 574)}{1610} = 64\%$$

For equilateral triangular pitch, the triangle must inscribe a circle of $2r = 3.5$ in diameter (Fig. 6.60). The base of the triangle, b , is given as:

$$b = \frac{r}{\tan \alpha} = \frac{r}{\tan 30^\circ} = \frac{3 \cdot r}{\sqrt{3}}$$

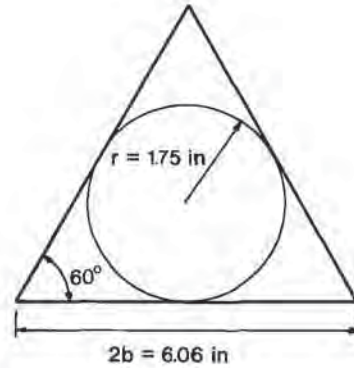


Figure 6.60 Geometric factors on triangular pitch

The distance from the apex to the center of the circle, c , is given as:

$$c = \frac{r}{\sin \alpha} = \frac{r}{\sin 30^\circ} = 2r$$

The total height of the triangle, $h = r + c = 3r$. The area of the triangle is:

$$A = \frac{1}{2}(2b)h = \frac{3 \cdot 3 \cdot r^2}{\sqrt{3}} = 5.2r^2$$

The base of the triangle, $2b = 6r/\sqrt{3} = 3.464r$. For $2r = 3.5$ in, $2b = 6.06$ in. For the maximum mold length of 46 in, there are places for 7.6 triangle bases or 7 complete triangles. Between each triangle is another triangle on apex. With proper adjustment, one triangle on apex can be fit at one end or the other of the triangle bases. Therefore 13 complete triangles fit within the 46 in mold length. The height of the row of triangles is 5.25 in. For the 34 in wide mold, 6.5 parallel rows are possible, or 6 integer rows. As a result, for triangular pitch molds, $6 \times 13 = 78$ molds are possible. Again, the area for a single cup is 4.91 in². For 78 cavities:

$$4.91 \times 78 = 383 \text{ in}^2$$

The total surface area used to form these parts:

$$35 \times 46 = 1610 \text{ in}^2$$

Thus the trim total percentage is given as:

$$\text{Trim} = 100 \cdot \frac{(1610 - 383)}{1610} = 76\%$$

This triangular pitch is less efficient than the previous rectangular pitch. A more efficient equilateral triangular pitch mold layout follows.

If the outer perimeters of the molds touch (Fig. 6.61), there are 13 cavities in odd rows and 12 cavities in even rows. The relationship between the width of the mold, W , and the number of rows, N , is given as:

$$W = (N - 1) \cdot h + 2r$$

where $h = \sqrt{3} \cdot r/3$. For $W = 34$ in and $r = 3.5/2$ in, N is 11.1 rows, or 11 integer rows. With six odd rows and five even rows, there are $6 \times 13 + 5 \times 12 = 138$ cavities.

Since the surface area of a single cavity is 4.91 in^2 , the total surface area for molded parts is:

$$4.91 \times 138 = 677.6 \text{ in}^2$$

The total surface area used to form these parts:

$$35 \times 46 = 1610 \text{ in}^2$$

Thus the trim total percentage is given as:

$$\text{Trim} = 100 \cdot \frac{(1610 - 677.6)}{1610} = 58\%$$

6.12 References

1. L. Sors, *Plastic Mould Engineering*, Pergamon, London (1967), p. 108.
2. Anon., *Wood Handbook: Wood as an Engineering Material*, Forest Products Lab., Madison WI, USDA Agriculture Handbook #72 (Aug 1974).
3. R.M. Miller, *Figure Sculpture in Wax and Plaster*, Watson-Guptill, New York (1971), p. 11.
4. C. Chaney and S. Skee, *Plaster Mold and Mold Making*, Van Nostrand Reinhold, New York (1974), pp. 114-120.
5. W.P. Benjamin, *Plastic Tooling*, McGraw-Hill Book Co., New York (1972), p. 20.
6. Ren[™] epoxies available from Ciba-Geigy Corp., Polymers Division, Seven Skyline Dr., Hawthorne NY 10532-2189, 914-785-2000.
7. Anon., "Toolrite Composite Tooling Materials System", Fiberite Corp., 501 W. Third St., Winona MN 55987, undated.
8. M.E. Thorp, "Progress Report: Sprayed Metal Faced Plastic Tooling", 35th Annual conference, RP/C, New Orleans LA (4 Feb 1980).
9. Nickel Tooling Technology, Highway 12, P.O. Box 399, Midland Ontario Canada L4R 4L1 (June 1994).
10. J. Worbye, "Steels for Molds", SPE ANTEC Tech. Papers, 30 (1984), pp. 948-951.
11. J.L. Throne, *Plastics Process Engineering*, Marcel Dekker, New York (1979), p. 530.
12. D.A. Schrage, "Prototype Molds: Getting Out of Them What You Need", *Plast. Mach. Equip.*, 13: 6 (Jun 1984), p. 35.
13. R.G.W. Pye, *Injection Mould Design: A Design Manual for the Thermoplastics Industry*, 2nd Ed., George Godwin, London (1978), pp. 155-185.
14. H.R. Osmer, "Mold Cooling Concepts", Handout in W.K. McConnell, Jr., SPE Industrial Thermoforming Symposium and Workshop, Arlington TX (12-14 March 1985).
15. V.L. Streeter, *Fluid Mechanics*. 5th Ed., McGraw-Hill Book Co., New York (1971), p. 277.
16. V.L. Streeter, *Fluid Mechanics*. 5th Ed., McGraw-Hill Book Co., New York (1971), Figure 5.32, pp. 288-289.
17. O.W. Eshbach (late) and M. Souders, Eds., *Handbook of Engineering Fundamentals*, 3rd Ed., John Wiley & Sons, New York (1975), p. 618.
18. D.T. Wood, "An Explicit Friction Factor Relationship", *Civil Eng.*, 36: 12 (Dec 1966), pp. 60-61.
19. V.L. Streeter, *Fluid Mechanics*. 5th Ed., McGraw-Hill Book Co., New York (1971), p. 292.
20. V.L. Streeter, *Fluid Mechanics*. 5th Ed., McGraw-Hill Book Co., New York (1971), p. 297.

21. O.W. Eshbach (late) and M. Souders, Eds., *Handbook of Engineering Fundamentals*, 3rd Ed., John Wiley & Sons, New York (1975), p. 622.
22. A.H. Shapiro, *The Dynamics and Thermodynamics of Compressible Fluid Flow*, 2 Vols, The Ronald Press Co., New York (1953).
23. V.L. Streeter, *Fluid Mechanics*, 5th Ed., McGraw-Hill Book Co., New York (1971), Chapter 6, "Compressible Flow".
24. R.J. Roark and W.C. Young, *Formulas for Stress and Strain*, 5th Ed., McGraw-Hill Book Co., New York (1975), p. 363.
25. G. Gruenwald, *Thermoforming: A Plastics Processing Guide*, Technomic Publishing Co., Lancaster PA (1987), p. 38.
26. G. Gruenwald, *Thermoforming: A Plastics Processing Guide*, Technomic Publishing Co., Lancaster PA (1987), pp. 39-40.
27. R.J. Roark and W.C. Young, *Formulas for Stress and Strain*, 5th Ed., McGraw-Hill Book Co., New York (1975), p. 97.
28. J.L. Throne, "Principles of Thermoplastic Structural Foam Molding", in N.P. Suh and N.H. Sung, Eds., *Science and Technology of Polymer Processing*, MIT Press, Cambridge MA (1979), p. 77.
29. J.L. Throne, *Thermoplastic Foams*, Chapman & Hall, New York (1995), Chapter 7, "Skins and Surfaces on Foams".
30. Anon., "Thermoforming Lustran ABS, Lustrex Polystyrene, and Cadon Engineering Thermoplastics", Monsanto Bulletin #6547, undated.
31. R.G.W. Pye, *Injection Mould Design*, 2nd Ed., G. Godwin, London (1978), p. 180.
32. R.G.W. Pye, *Injection Mould Design*, 2nd Ed., G. Godwin, London (1978), p. 174.
33. Heat pipes designed for the plastics industry are available from Noren Products, Inc., 1010 O'Brien Dr., Menlo Park CA 94025, 415-322-9500.
34. A Brockschmidt, "Thermoforming Barrier Containers: How It's Different", *Plastics World*, 42:9 (Sep 1984), pp. 67-71.
35. J.L. Throne, "Thermoforming—A Look Forward", *SPE ANTEC Tech. Papers*, 29 (1983), pp. 464-465.
36. This technology is once again being promoted as an effective way of clamping and trimming very thin-gage sheet by Paul Kiefel Thermoformmaschinen GmbH, Industriestraße 17-19, Postfach 16 60, 83395 Freilassing Germany.
37. W.K. McConnell, Jr., *SPE Industrial Thermoforming Symposium and Workshop*, Arlington TX (12-14 March 1985).
38. R.G.W. Pye, *Injection Mould Design*, 2nd Ed., G. Godwin, London (1978).
39. R.G.W. Pye, *Injection Mould Design*, 2nd Ed., G. Godwin, London (1978), p. 210.
40. R.G.W. Pye, *Injection Mould Design*, 2nd Ed., G. Godwin, London (1978), Chapter 9, "Side Cores and Side Cavities".
41. R.G.W. Pye, *Injection Mould Design*, 2nd Ed., G. Godwin, London (1978), Chapter 3, "Ejection".
42. J. Florian, *Practical Thermoforming: Principles and Applications*, Marcel Dekker, Inc., New York (1987), p. 308.
43. A.C. Peterson, *Applied Engineering Mechanics: Strength of Materials*, 2nd Ed., Allyn and Bacon, Boston (1982).
44. Fiberboard is available from Al Grosskopf, Alpine Plywood, Inc., 12210 W. Silver Spring Rd., Milwaukee WI, 414-462-5450.
45. PVI Mold Board™ is available from Plasti-Vac Inc., 214 Dalton Ave., Box 5543, Charlotte NC 28225, 704-334-4728.
46. Repro™ PUR systems available from Freeman Mfg. & Supply Co., 1246 W. 70th St., Cleveland OH 44102-2097.
47. M. Burns, *Automated Fabrication: Improving Productivity in Manufacturing*, PTR Prentice Hall, Englewood Cliffs NJ (1993), particularly Chapter 3.
48. D.S. Cummings, "Utilizing Stereolithography to Produce a Rapid Prototype Thermoforming Mold", *SPE ANTEC Tech. Papers*, 40 (1994), pp. 3550-3554.

49. H. Chang and R.A. Daane, "Coefficient of Friction for Solid Polymers in Various Forms", SPE ANTEC Tech. Papers, 20 (1974), pp. 335-.
50. One sprayed metal system is offered by TAFE Metallisation, Inc., Dow Rd., P.O. Box 1157, Bow (Concord) NH 03301.
51. S. Semerdjiev, *Introduction to Structural Foams*, Society of Plastics Engineers, Brookfield Center CT 06804 (1982), p. 52.
52. P.J. Schneider, "Conduction", Chapter 3 in W.R. Rohsenow and J.P. Hartnett, *Handbook of Heat Transfer*, McGraw-Hill Book Co., New York (1973), Figure 33, pp. 3-60.

7 Parts Design

- 7.1 Introduction
- 7.2 Elements of Parts Design
 - Material Testing and Its Relevance to Part Performance
 - Philosophy of Parts Design
 - Minimizing the Amount of Sheet to be Reground
 - Rules for Part Layout on Heavy-Gage
 - Rules for Multiple Part Layout on Thin-Gage
 - Economics of Buying Sheet of Specific Size
- 7.3 Prototyping as a Justification for Thermoforming
- 7.4 Draw Ratio
 - Areal Draw Ratio
 - Linear Draw Ratio
 - H:D
 - Rim and Lip Sheet for Female Cavities
 - Draw Ratio Usage—A Rationale
 - Mechanical Assists—Some Design Features
 - Preblowing or Inflation—Comments
 - Plug Assist—Comments
- 7.5 Computer-Aided Design in Thermoforming
- 7.6 Wall Thickness Prediction—A Justification
 - Geometric Element Analysis or GEA
 - Finite Element Analysis
 - General Comments on Plug Design
 - Plug Assist Analysis
 - Plug Design—Geometric Element Analysis
 - Plug Design—Finite Element Analysis
- 7.7 Regrind
 - Material Property Deterioration on Regrind
 - Property Value Loss—Experiment and Protocol
 - Cascading 100% Regrind
- 7.8 General Guidelines for Part Design
 - General Tips
 - Process Tips
 - Mold Tips
 - Prestretch Tips
 - Part Design Tips
 - Rim and Edge Designs
 - Design—A Comment
- 7.9 References
- Appendix 7.I Draw Ratios for Truncated Cone
- Appendix 7.II Mechanical Property Loss in Regrind

7.1 Introduction

It is apparent that there are many variations on the basic sheet stretching process and that there are many potential polymers from which to choose. As a result, design of thermoformed parts must of necessity follow careful protocol. In this chapter, the philosophy of parts design forms the basis for the specific details on parts design. Prototyping is usually the first step in any molding program. It rarely succeeds without problems and these problems frequently reveal potential problems in production processing. Many typical processing problems and courses of action are highlighted in the trouble-shooting section and some general do's and don't's are presented.

There are several ways of defining *draw ratio*. Areal and linear draw ratios and depths of draw are defined for several simple geometries. Rim draw down is also arithmetically accounted for. Draw ratios are gross and imperfect measures of the amount of stretching a sheet must endure in order to replicate the mold and produce a perfect part. As will be seen, polymer is stretched least just below the mold rim and most as the sheet is drawn into three-dimensional corners. Polymer sheet must have sufficient elongation at the drawing temperature and applied pressure or it will either split or fail to replicate the mold. Overall draw ratios fail to accurately predict potential stretching of the sheet to ultimate elongation. Differential draw ratios yield more relevant information. Accurate prediction of local wall thickness yields the most useful information.

Part wall thickness is a function of the depth of draw and the geometry of the part. The arithmetic is presented for conical and other simple shapes. Frequently the sheet is prestretched by inflation or with plug assist. The obvious reason is polymer sheet material redistribution or *material reallocation*. Advanced finite element methods are being developed for wall thickness prediction of more complex shapes. Designers are beginning to use computer-assisted software programs for their toughest thermoforming designs.

As with other chapters, this chapter's material progresses from descriptive to technically advanced concepts. Regardless of the degree of technology needed to achieve adequate designs on today's parts, the designer should take comfort in knowing that the technical support for the tough designs of the future is at hand.

7.2 Elements of Parts Design

The ultimate objective of polymer processing is the fabrication of a product that must meet certain nominal performance requirements. There are many concerns that must be met in the manufacture of any product. Three important ones are:

- Will the finished part meet all required and specified design criteria?
- Can the part be produced at the minimum cost for the projected market size?
- What are the consequences if the part fails to meet minimum requirements?

The last concern is important today. Plastics parts fail in use for several fundamental reasons. The most common is customer “misuse”, in that the device is used in a way that is beyond the designer’s original intent. It is impossible to design against all levels of stupidity. However, safety factors and sources of inherent product weakness must always be considered in critical parts design. Whenever possible, parts should always be designed to fail safely when used beyond design conditions.

The polymers selected for the product must have certain inherent characteristics such as:

- Stiffness,
- Toughness,
- Environmental resistance, and/or
- Optical/electrical properties.

When the polymer is transformed from pellets to product, certain other characteristics are imposed, such as:

- Dimensional changes,
- Color, or
- Internal stresses.

Assembly or initial use may impose other characteristics, such as:

- Differential expansion,
- Color shift or mismatch,
- Loss in gloss, or
- Abrasion or scuffing.

The ultimate use of the product imposes other parameters, such as:

- Environment,
- Periodic or aperiodic loading,
- Time under load, and/or
- Temperature.

All polymers have a myriad of inherent properties, only a few of which are important in the performance of a specific product. For products assembled of sub-products, subsets or basic elements, each of the subsets places specific mechanical and/or chemical demands on the polymer used. The property set required by the assembled product must be a “mean” of the properties of the subsets. The polymer material properties needed to delineate the performance criteria are ascertained *only* when the subset demands are clearly identified. A proper design approach establishes a formal *design check list*. Typical items for such a check list include:

- Environmental conditions, both nominal and extreme,
- Materials specifications,
- Part mechanical behavior and tolerance under environmental conditions, and
- Dimensional tolerances.

Table 7.1 lists some additional items that require identification and definition. From this master list, secondary check lists are written, Tables 7.2 through 7.7.

Table 7.1 First-Level Design Elements for Thermoformed Parts, See [80,81] For Additional Information, Additional Detail Given in Noted Tables

| | |
|--|--|
| <ul style="list-style-type: none"> ▪ Field of application—Table 7.2 <ul style="list-style-type: none"> Food packaging Materials handling Disposable Permanent ▪ Part function—Table 7.3 <ul style="list-style-type: none"> Decorative Protective Container (liquid, solid) Structural ▪ Environment—Table 7.4 <ul style="list-style-type: none"> Temperature Nature (corrosive, liquid solid) Nature of load (static, cyclical) ▪ Appearance—Table 7.5 <ul style="list-style-type: none"> Surface quality (Class A) Nonappearance Trim line appearance | <ul style="list-style-type: none"> • Cost—Table 7.6 <ul style="list-style-type: none"> Balanced against material requirements Number of parts required ▪ Competitive processes—Table 7.6, Chapter 10 <ul style="list-style-type: none"> Injection molding Blow molding Rotational molding ▪ Part design limitations—Table 7.7 <ul style="list-style-type: none"> Strength Load characteristics Potential abuse ▪ Government regulations <ul style="list-style-type: none"> Standards (FDA, FM, EPA) Biodegradability Fire retardancy ▪ Interaction with other elements—Table 7.3 <ul style="list-style-type: none"> Assembly requirements Metal-to-plastic concerns |
|--|--|

Table 7.2 Check List for Thermoform Parts Design: Application

| | |
|---|--|
| <ul style="list-style-type: none"> • General field <ul style="list-style-type: none"> Packaging Leisure Transportation Military Medical • Sub-category, such as packaging <ul style="list-style-type: none"> Food <ul style="list-style-type: none"> Disposable Storage Cook-in Barrier Animal feed | <ul style="list-style-type: none"> Cosmetics Pharmaceuticals Chemicals Electronics Display items And so on • Part life <ul style="list-style-type: none"> Permanent, such as swimming pool Part of a permanent assembly, such as computer housing Limited life, such as celery boxes Disposable, such as blister packs and unit servings |
|---|--|

Material Testing and Its Relevance to Part Performance

Once the designer has selected appropriate polymer candidates for the proposed product, he/she must verify that the product will perform in accordance with the desired and necessary design criteria. In other words, the designer must *test* his/her selection. The most obvious test specimen is the part itself. However, if the part is still conceptual or is too large or too small, alternate testing data are needed. Usually polymers are selected on the basis of resin producers' design and material data sheets. The designer must select properties from these sources with great caution:

Table 7.3 Check List for Thermoform Parts Design: Part Function

| | |
|--|---|
| <ul style="list-style-type: none"> • Container <ul style="list-style-type: none"> Single-use Continuous Solids Liquids (corrosive nature) Convenience • Protective <ul style="list-style-type: none"> Shipping Food packaging Blister pack • Decorative <ul style="list-style-type: none"> Architectural Interior decoration Cosmetic | <ul style="list-style-type: none"> • Structural <ul style="list-style-type: none"> Total load bearing Temporary support Compression load function (foams) • Interaction with other elements <ul style="list-style-type: none"> Stand-alone Covering, edge contact/interlocking only Elements assembled into formed shapes Formed shape incorporated into others Plastic/plastic assembly Plastic/nonplastic assembly |
|--|---|

Table 7.4 Check List for Thermoform Parts Design: Environmental Conditions

- Use temperature range
- Design temperature range (maximum and minimum)
- Extreme temperature range (maximum and minimum)
- Limitation on part shape deformation (under expected load, at use temperature)
- Extreme chemical environment (under load, at temperature)
- UV environment (outdoor, fluorescent)
- Nature of load
 - Static (expected and maximum)
 - Vibrational or periodic (expected and maximum)
- Interface with user (casual, continuous, leisurely, in crisis situation)

Table 7.5 Check List for Thermoform Parts Design: Appearance

| | |
|---|---|
| <ul style="list-style-type: none"> • Quality <ul style="list-style-type: none"> Class-A (automotive) Plating substrate • Optical <ul style="list-style-type: none"> Aircraft Automotive/RV Furniture Cosmetics Blister pack Food containers Medical containers | <ul style="list-style-type: none"> • Decorative <ul style="list-style-type: none"> Deckled Textured Painting substrate Replication of letters, logos, symbols • Nonappearance • Trim line appearance <ul style="list-style-type: none"> Secondary finishing Buffing Location of trim line |
|---|---|

- First, the test data should accurately represent polymer properties.
- Then, there should be a unique set of relationships between material properties and measured parameters.

**Table 7.6 Check List for Thermoform Parts Design:
Cost and Competitive Processes**

-
- Target part cost
 - Materials cost
 - Quality of extrusion
 - Level of regrind
 - Property requirements (price, property, performance)
 - Quantity of material needed (price break)
 - Prototype cost
 - Tooling
 - Parts fabrication
 - Performance evaluation
 - Allowable cost of fabrication, tooling
 - Tooling quality
 - Run length
 - Tolerance
 - Cycle times
 - Maintenance
 - Alternate/competitive process cost
 - Injection molding
 - Rotational molding
 - Stamping from hot sheet
 - Blow molding
 - Metals/ceramics (non-polymer) processing
-

- And finally, there needs to be a causal relationship between measured properties and polymer performance.

Two criteria of test acceptability are proposed [1-3]:

Criterion I: The mechanical state must be definable in physical terms.

The physical state can be dimension, applied load, applied stress, strain, rate-of-strain, dimensional change, color change and/or temperature.

Criterion II: The mechanical state must be definable in causal mathematical terms.

The stress-strain data should be capable of being fitted with an Ogden or Rivlin model, for example. Or the sheet dimensions should be predicted from coefficient of expansion data. With acceptance of standard testing routines by such organizing bodies as ISO, DIN, and ASTM, proper protocol for performing a specific procedure is clarified. These tests are referred to as *performance tests*. Care must be taken in assuming that the results from these tests can be directly applied to the performance of a given product. It has been noted that [4]:

“The ASTM tests for plastics were designed as quick, easy, reproducible tests to provide a rough comparison among similar materials—but principally for material quality control, not for material performance. Thus, these test data should be regarded only as material specifications for purchasing and quality control, not as indications of performance under long-time real-life conditions...”

Table 7.7 Check List for Thermoform Parts Design: Part Design Limitations

-
- Intrinsic polymer material properties
 - At nominal use conditions
 - At extreme conditions
 - Process/polymer interactions
 - Draw ratio
 - Strength of thinned material
 - Strain-induced brittleness
 - Recycle property loss
 - Allowable corner/lip design
 - Allowable part tolerance, dimensional variation, draft angle
 - Part appearance
 - Warp, racking
 - Optical distortion
 - Draw lines, stretch marks
 - Trim edge appearance
 - Mold detail replication (texture, letters)
 - Interaction with non-plastics
 - Nature of interference
 - Slip-fit
 - Adhesive
 - Mechanical assembly
 - Interference
 - Snap-over
 - Undercut
 - Detent
 - Strain under temperature extremes
 - Strain during, after assembly
-

Most ASTM tests yield *non-design* properties for polymers. They do not meet the criteria of test acceptability and as a result they are not useful in determining the in-use performance of most polymer parts. In addition, the designer must realize that the effects of the process must also be included in any performance analysis of the product under its environmental influence. This is in addition to testing the polymer. If the test data are to bear any relationship to product performance in actual use, the test specimen must include the appropriate effects of the process¹.

Philosophy of Parts Design

Regardless of the nature and depth of prior experiences of the designer, the mold maker, the thermoformer or the customer, no plastics fabrication should be at-

¹ Furthermore, the designer must guard against using statistics to verify that the data are significant. The collection of more and more data usually does not contribute to bridging the gulf between test specimen properties and the final performance of the product made of the polymer [5].

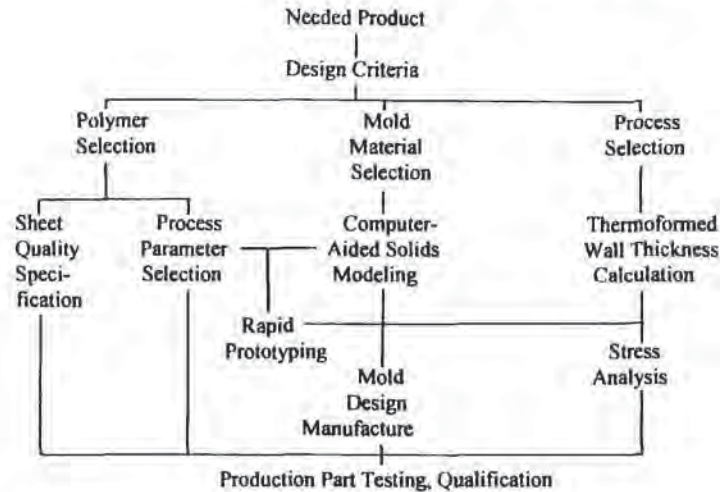


Figure 7.1 Computer-aided engineering flow chart for thermoforming

tempted without strict, formal *written* protocol on parts design. All parties must clearly understand the project objective and ancillary part performance standards. Guidelines must be carefully written and agreed on, *in writing*, by all principals. This should be done with all principals present, *just prior to* issuance of purchase orders for materials, molds and forming time. Processes, applications and materials continue to grow in sophistication. As a result, the parts designer is destined to play an increasingly important role as project coordinator. It is incumbent on him/her to ensure correct protocol, particularly in this increasingly litigious era. Figure 7.1 [6] shows a particularly useful scheme when computer-aided mold design, part design and structural analysis are available.

Once the overall design concepts are well understood by all parties, initial part designs, material specifications, process elements as identified in Chapter 1, and cycle parameters can be estimated. These should be kept quite preliminary and should focus on general fitting of proper materials and process elements to the application. The objective of this portion of the effort is to make an early test of *concept feasibility*. At this point, no prototype should have been authorized. Designers should be working from quality sketches or computer renderings. Not every potential application results in a thermoformed part. Some reasons for *not* selecting thermoforming include:

- The application may require polymers that are not successfully extruded into sheet,
- The candidate polymer is not successfully drawn to the requisite depth,
- The forces required to stretch the candidate polymer may exceed the available process equipment capability,
- The part may be too large for available equipment,
- The part may be too small for available equipment,

- The customer may need too few parts to make thermoforming economical,
- The customer may need too many parts,
- The design may waste too much material,
- The web material may be unprocessable as regrind, resulting in prohibitive material and processing costs,
- The design may require structural polymers that are not normally thermoformed,
- The design may require highly reinforced polymers or highly filled polymers that are difficult to thermoform or beyond the thermoformer's ability,
- The tolerances and draft angles may require exotic mold designs for thermoforming,
- The design may require parts with uniform wall thicknesses, or
- Competitive processes may be more economic¹.

Once it is apparent *to all* that thermoforming offers a technically feasible, economically viable process to make a part of a polymer needed to meet the application constraints, the sketched out process may be ready for prototyping. Prototyping is discussed in the section that follows. Certain emerging technologies, such as stereolithography and LOM, have altered the way in which prototypes are developed. Not all these new techniques are directly applicable to thermoforming, however. In certain instances, prototyping is not necessary and the design is ready for fine tuning. Techniques for determining part wall thickness are described in detail below. In general, fine tuning should focus on optimizing material distribution across the part to achieve the greatest local part strength at the lowest material usage. And every fine tuning should concentrate on minimizing web.

Minimizing the Amount of Sheet to be Reground

The amount of plastic to be trimmed as non-product begins by minimizing trim and web area through intelligent mold design and careful sheet size selection². Proper part design minimizes unnecessary trim, particularly in rim area for thin-gage multiple part forming. Usually the fraction of regrind generated is a function of several components of the thermoforming process:

- Conservative part designs usually generate less out-of-specification parts than exotic designs.
- Exotic, multi-step, and/or relatively new processes usually produce more trim for regrind than that from some one-step processes such as vacuum or drape forming.

¹ Competitive process design and economics are discussed in Chapter 10.

² In an earlier book by this author [92], and in other books and encyclopedic chapters on thermoforming, the term "scrap" was used to categorize that portion of the sheet of plastic that is not the desired product. In fact, the economics of thermoforming dictate that the non-product portion of the sheet *must* be recovered, reground, and reextruded into sheet for subsequent thermoforming. For thermoformers, the term "scrap" is in fact this non-product portion of the sheet. However, in general, the term connotes a wasteful process. Therefore, the industry has agreed to the terms "trim" or "web" to denote the non-product portion of the sheet.

- Polymers that are drawn close to their extensional limit will usually cause higher regrind levels.
- Process equipment that is not in good operating condition or that has inadequate or inferior automatic cycle control generates more off-specification parts than equipment that is automated and maintained well.
- Workers who are not fully trained in the nuances of:
 - the requisite forming process,
 - the trimming process,
 - the polymers of choice, and/or
 - the specific design details,
 typically generate higher-than-anticipated quantities of regrind.

Rules for Part Layout on Heavy-Gage

Usually only one part is made from a section of cut sheet for heavy-gage. If the contribution of plastic from the rim is negligible, as shown in Fig. 7.2, the plastic that makes up the part comes from the sheet clamped against the rim. Consider a simple five-sided box of dimensions $A \times B \times C$ deep to be formed from a sheet having dimensions $A \times B \times h_0$ thick. The average sheet wall thickness, h , is given as:

$$\frac{h}{h_0} = \frac{A \times B}{A \times B + 2 \cdot A \times C + 2 \cdot B \times C} \quad (7.1)$$

As shown shortly, the average wall thickness has little value. The reciprocal of the wall thickness ratio is the overall areal draw ratio, R_a :

$$\left(\frac{h}{h_0}\right)^{-1} = R_a = \frac{A_{\text{part}}}{A_{\text{sheet}}} \quad (7.2)$$

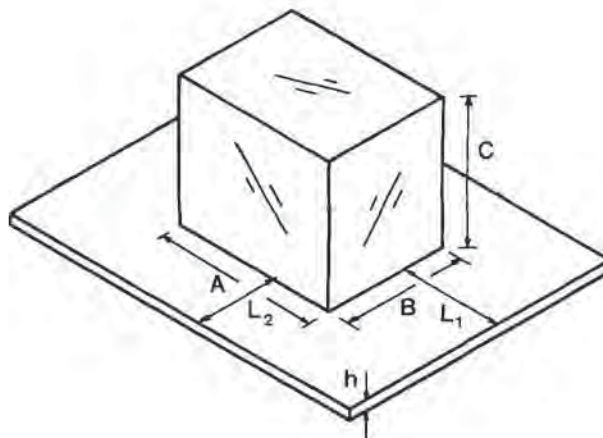


Figure 7.2 Part, rim and edge material layout for heavy-gage thermoforming

If the initial sheet dimension is $A + 2L_1 \times B + 2L_2$ where L_1 and L_2 are the respective distances from the rims of the part to the cut edges of the sheet, the amount of trim, T , is given as:

$$T = (A + 2L_1) \times (B + L_2) - A \times B \quad (7.3)$$

Example 7.1 illustrates how the fraction of trim is determined for heavy-gage sheet. For many parts, plastic in the rim region is deliberately drawn into the mold cavity. The effect is to increase the average sheet thickness and reduce the fraction of trim. Even though the purpose of sheet prestretching is to increase the sheet wall thickness uniformity, it also increases the average sheet thickness and reduces the fraction of trim. It is apparent that trim is minimized by minimizing the distance from the mold rim to the edge of the sheet. However, as discussed in detail in Chapter 6, the sheet must be clamped sufficiently well to prevent extrusion and pull-out during stretching. Certainly, trim is minimized by forming rectangular parts from rectangular sheets. Examples 7.2 and 7.3 illustrate how the shape of a part affects the amount of trim.

Example 7.1 Trim Fraction for a Heavy-Gage Part

If the distance from the mold rim to the edge of the sheet must be at least 2 in, determine the amount of trim generated for a five-sided box, $17.3 \times 38.7 \times 12.4$ in deep. Then determine the amount of trim if the sheet is most economically purchased as 24×48 in blanks.

The sheet dimensions are:

$$(17.3 + 2 \cdot 2) \times (38.7 + 2 \cdot 2) = 909.51 \text{ in}^2$$

The surface area of the box is given as $17.3 \cdot 38.7 = 669.51 \text{ in}^2$.

The amount of trim is:

$$\frac{909.51 - 669.51}{909.51} = 0.26 \text{ or } 26\% \text{ of the initial sheet.}$$

For the 24×48 sheet, its area is 1152 in^2 . The amount of trim is:

$$\frac{1152 - 669.51}{1152} = 0.42 \text{ or } 42\% \text{ of the initial sheet.}$$

Example 7.2 Trim Fraction for an Oval Heavy-Gage Part

If the distance from the mold rim to the edge of the sheet must be at least 2 in, determine the amount of trim generated for an oval box, $17.3 \times 38.7 \times 12.4$ in deep. Then determine the amount of trim if the sheet is most economically purchased as 24×48 in blanks.

The sheet dimensions are:

$$(17.3 + 2 \cdot 2) \times (38.7 + 2 \cdot 2) = 909.51 \text{ in}^2$$

The surface area of an oval or elliptical box is given as:

$$A = \pi ab/4$$

where a and b are the major and minor axes of the ellipse. For the example:

$$A = \pi(17.3 \cdot 38.7)/4 = 525.83 \text{ in}^2$$

The amount of trim is:

$$\frac{909.51 - 525.83}{909.51} = 0.42 \text{ or } 42\% \text{ of the initial sheet.}$$

For the 24×48 sheet, its area is 1152 in^2 . The amount of trim is:

$$\frac{1152 - 525.83}{1152} = 0.54 \text{ or } 54\% \text{ of the initial sheet.}$$

Example 7.3 Trim Fraction for a Circular Heavy-Gage Part

If the distance from the mold rim to the edge of the sheet must be at least 2 in, determine the amount of trim generated for two cylinders, 17.3 in diameter \times 12.4 in deep. Then determine the amount of trim if the sheet is most economically purchased as 24×48 in blanks.

The sheet dimensions are:

$$(17.3 + 2 \cdot 2) \times (38.7 + 2 \cdot 2) = 909.51 \text{ in}^2$$

The surface area of the cylinder is:

$$A = \pi d^2/4$$

where d is the diameter of the cylinder. For the example:

$$A = \pi(17.3)^2/4 = 235.06 \text{ in}^2$$

Since there are two cylinders, the total area is 470.12 in^2 . The amount of trim is:

$$\frac{909.51 - 470.12}{909.51} = 0.48 \text{ or } 48\% \text{ of the initial sheet.}$$

For the 24×48 sheet, its area is 1152 in^2 . The amount of trim is:

$$\frac{1152 - 470.12}{1152} = 0.59 \text{ or } 59\% \text{ of the initial sheet.}$$

Rules for Multiple Part Layout on Thin-Gage

In thin-gage forming, the web between the multiple cavities contributes a great amount of recyclable trim. For rectangular parts, the layout is simply a multiple of that used for heavy-gage. Cavity spacing depends on a number of factors:

- The rim design and width of the individual cavity,
- The required width of the sheet clamp or cavity isolator,

- The required wall thickness of the mold,
- The mechanics of connecting individual mold elements, such as:
 - Coolant lines,
 - Air blow-off lines,
 - Vacuum lines, and/or
 - Sliding and moving core interactions, and
- Stripper or ejector plate width requirements.

The area of sheet used for an individual rectangular cavity, for example, is written as:

$$\text{Area}_n = (A_n + L_{1,n}) \times (B_n + L_{2,n}) \quad (7.4)$$

where $L_{1,n}$ and $L_{2,n}$ represent the half-distances between the cavities. The total sheet area is the sum of the individual areas plus that portion of the sheet between the outermost row of cavities plus the allowable half-distances and the edge of the sheet:

$$\text{Area}_{\text{sheet}} = \sum \text{Area}_n + \left[\sum (A_n + L_{1,n}) + L_A \right] + \left[\sum (B_n + L_{2,n}) + L_B \right] \quad (7.5)$$

For cylindrical parts, such as cups or plates, there are two layout methods (Fig. 7.3). The square pitch is more common than the equilateral triangular pitch, since the molds are all square and mold assembly is easy. The square pitch layout generates more trim than the triangular pitch, however, as illustrated in Example 7.4. The added bother and expense of triangular pitch molds might be tolerated if the amount of trim is important to the economic success of the product, as might be the case with medical products.

Example 7.4 Triangular and Rectangular Pitches for Molding Drink Cups

3-in diameter drink cups are to be molded 6-wide and 48-up. The polymer selected is known to sag extensively even at moderate sheet widths. Determine the minimum sheet width for rectangular pitch if a 1-in spacing is needed between each cavity and if the mold edge-to-sheet edge is 2 in. Determine the extent of trim for each.

Using the square pitch of Fig. 7.3, the rectangular mold dimensions are 24×32 in. The sheet width is $24 + 22 = 28$ in.

For the triangular pitch of Fig. 7.3, the diagonal is the sum of the mold cavity diameters and the intercavity spacing, $6 \cdot 3 + 5 \cdot 1 = 23$ in. The vertical is given as:

$$y = r \sin \theta = 23 \cdot 0.866 = 19.9 \text{ in} \approx 20 \text{ in}$$

The mold width is an addition $\frac{1}{2} + \frac{1}{2}$ in, for a total of 21 in and the sheet width is $21 + 2 \cdot 2 = 25$ in. Molds on the rectangular pitch require a sheet

that is 3 in or 12% wider than molds on a triangular pitch. The triangular pitch mold shape is a parallelogram, with the overall mold length being $32 + 23 \cdot \cos \theta = 43.5$ in. Even though the square pitch mold base is wider than the triangular pitch mold base, it is square and the individual cavities are also square. Right angles are much easier to fabricate than equilateral angles.

If the mold-to-edge distance on the free sheet edge is also 2 in, the total sheet area for each shot is $28 \times (32 + 2 \cdot 2) = 1008$ in². The area used to produce the required 48 drink cups is $48 \cdot \pi 3^2/4 = 339.3$ in². The trim amount is:

$$\text{Trim} = \frac{1008 - 339.3}{1008} = 0.66 \text{ or } 66\% \text{ of the total sheet.}$$

For the triangular pitch sheet, the parallelogram area is $25 \times (32 + 2 \cdot 2) = 900$ in². The trim amount is:

$$\text{Trim} = \frac{900 - 339.3}{900} = 0.62 \text{ or } 62\% \text{ of the total sheet.}$$

The difference in trim amount between the two pitch layouts is small in this case and would be significant only if the trim could not be recycled.

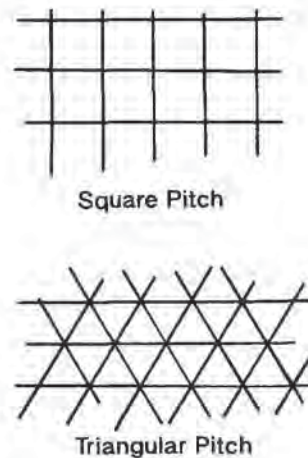


Figure 7.3 Square and triangular parts and mold cavity layouts

Economics of Buying Sheet of Specific Size

Usually sheet extruders produce sheet product to custom dimensions. As a result, the designer, processor and mold builder agree to the minimum acceptable sheet dimensions and the extruder then supplies sheet to that specification. There are some instances where a less expensive sheet of a ready-made size is available. For example:

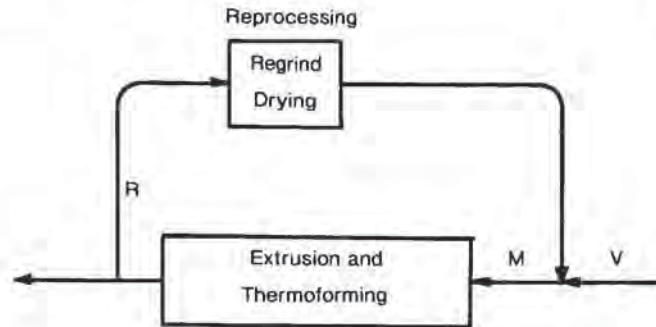


Figure 7.4 Simple steady-state reprocessing loop

- The extruder may have an inventory of sheet in standard widths, lengths and gages,
- A resin supplier may be sampling the thermoforming industry with a new polymer product,
- The extruder may have sheet left from an earlier production run, or
- The thermoformer may have sheet left from an earlier production run.

As discussed later in this chapter, on regrind, there are material property penalties attached to regrinding and re-extruding trim. There are also economic penalties. The economic penalty decreases with increasing extruder throughput but nevertheless is never a negligible cost to the product. The economics of recycle are obtained in the following fashion. Consider a recycle stream as shown in Fig. 7.4 [7]. Assume that the polymer material costs M units, is used at 100%, and that the process is 100% efficient. The cost of the salable fabricated part, F , is:

$$F = M + C \quad (7.6)$$

where C is the unit conversion cost. For thermoforming, the conversion cost is the sum of extrusion and thermoforming unit costs. Now assume that a fraction, Y , of the fabricated product is trim. If the trim value is zero, the unit cost of the salable fabricated product must be increased to account for the loss in efficiency:

$$F = \frac{M + C}{1 - Y} \quad (7.7)$$

Note that the processing cost is included since it logically costs the same to produce unsalable parts and non-product trim as it does to produce quality parts. Now assume that the trim has a value S on the open market. When the trim is sold, the processing cost is reduced by an amount YS . With no recycle and virgin polymer, the final unit cost is:

$$F = \frac{M + C - (YS)}{1 - Y} \quad (7.8)$$

If the polymer material is 100% virgin, its cost $M = V$, the cost of the virgin polymer. If a mixture of two materials is used as the feed, the material cost, M , is linearly proportional to the cost of the individual materials:

$$M = (1 - Y)V + YR \quad (7.9)$$

where Y is the amount of second source used and R is the value of the second source. Now let the trim, with a value, S , be reprocessed at a cost X . This reprocessing cost may include grinding, drying, and/or re-extrusion into pellets, but does not include extrusion and thermoforming costs, C . The cost of the repurchased trim is $S + X$. Let this be the second source:

$$R = S + X \quad (7.10)$$

The polymer material cost is now:

$$M = (1 - Y)V + Y(S + X) \quad (7.11)$$

And the unit fabrication cost, F , is:

$$F = \frac{M + C - YS}{1 - Y} = V + \frac{C + YX}{1 - Y} \quad (7.12)$$

The first term on the right is just the cost of virgin polymer. The second term includes the cost of conversion and the cost of reprocessing the trim. It is apparent that if there is no trim, $Y = 0$ and the production cost is just $V + C$. As the extent of trim increases, the unit cost increases. As expected, as the trim content approaches unity, $Y \rightarrow 1$ and the production costs approach infinity, $F \rightarrow \infty$. Example 7.5 illustrates this. To determine the effect of using a standard size sheet and tolerating greater trim, consider Equation 7.12 for two cases:

$$F_{\text{custom}} = V + \frac{C + Y_c X}{1 - Y} \quad (7.13)$$

$$F_{\text{std}} = V + \frac{C + Y_s X}{1 - Y_s} \quad (7.14)$$

Y_c is the fraction of regrind generated from the custom sheet, and V_c is the cost of the sheet. Similarly, Y_s is the regrind from the standard sheet and V_s is the cost of that sheet. Accordingly, $Y_c < Y_s$ and all other things are equal, F_{custom} is greater than F_{standard} . Example 7.6 illustrates this.

Example 7.5 Economics of Reusing Trim—I

It costs \$0.20/lb to extrude ABS and \$0.10/lb to thermoform and trim it. It costs \$0.05/lb to regrind it. Virgin ABS costs \$1.00/lb and the market value of clean reground ABS trim is \$0.40/lb. If the thermoforming process generates 40% trim, determine the unit product cost with and without recycling the trim.

The unit cost for salable formed parts is given from:

For the first case, the trim is sold after grinding. As a result, $M \equiv V$, $C = 0.1 + 0.2$, $V = 1.00$, $Y = 0.4$, $S = 0.4 - 0.05^1$. From Equation 7.8:

$$F = \frac{M + C - YS}{1 - Y}$$

the value for F is \$1.93/lb. For the second case, the unit cost with recycling is given from the same equation, written as,

$$F = V + \frac{C + YX}{1 - Y}$$

It is assumed that $R = S + X$. Therefore $F = \$1.53/\text{lb}$. The savings on using regrind is \$0.40/lb of salable parts.

¹ Note that the market value of ABS requires regrinding at $X = \$0.05/\text{lb}$.

Example 7.6 Economics of Reusing Trim—II

Consider the economic information of Example 7.5. Compare these results with advantages of purchasing ABS sheet at \$0.18/lb even though 45% of it must be recycled. Reconsider if the sheet extrusion cost is \$0.10/lb, but 55% must be recycled.

From the information in Example 7.5, $F_{\text{custom}} = \$1.53/\text{lb}$ for recycled trim. For standard sheet, $C = 0.1 + 0.18$, $V = 1.00$, $Y = 0.45$, $X = 0.05$. F_{std} is given from Equation 7.14 as \$1.55/lb. Products made of custom sheet are a couple of pennies per pound cheaper than those made from standard sheet. For the second case, $C = 0.1 + 0.1$ and $Y = 0.55$ and F_{std} is \$1.51/lb. In this case, standard sheet leads to a cheaper product.

7.3 Prototyping as a Justification for Thermoforming

In the plastics industry, prototype parts are produced primarily to check part design and appearance. Frequently, thermoforming is used to produce prototype parts for other processes such as injection molding, rotational molding and blow molding. Prototype thermoformed parts are used when:

- Materials are relatively unproven,
- One aspect of the design is particularly critical, or
- The part is to fit with other components.

Prototyping can serve as an important *early warning* to future processing problems, such as:

- Narrow processing windows,
- Badly sagging sheet, or
- Sheet orientation problems.

It is frequently used to identify possible post-forming problems, such as:

- Warping and distortion,
- Trimming problems,
- Long-term dimensional change, particularly with ABS, CPET and certain olefins, and
- Assembly problems.

Mold designs can be evaluated and trimming fixtures developed and refined during prototyping. And of course, prototype thermoformed parts are excellent visual aids when promoting a new concept or application.

The field of rapid prototyping or "RP" has grown dramatically in the last few years. The objective of RP is to produce a part for customer approval in a very short time. All concepts begin with computer modeling of the designer's idea. The three-dimensional model is then sliced into electronically thin wafers, each of which is stored as a separate file. These files are then exported to an appropriate device that "reassembles" them into a solid three-dimensional object. Some of the assembly techniques include:

- Stereolithography or SLA, where a ultraviolet beam is directed against a polymer syrup that reacts when exposed to UV. The beam is controlled by the computer that simply reads the outline of the electronic wafer file. After each computer file "slice" is completed, the reacted polymer is lowered by the thickness of the wafer, and the process repeats. The final shape takes about 24 h to complete. The reacted syrup structure is jelly-like as it emerges from the unreacted syrup bath. The structure is then drained of unreacted resin and thoroughly cured in a convection oven. Large parts are formed by electronically slicing the original designer's concept into quadrants, individually reaction-forming the quadrants, then gluing the quadrants together after curing. The wall thickness is typically greater than about 0.010 in.
- Polymer powder fusion, where a thermal laser beam is directed against fusible polymer powder such as nylon or polyethylene. Again the beam is controlled by the computer. After each pass, the fused powder in the bed is lowered by the thickness of the wafer, fresh powder is layered on the surface, and the process repeats. The final shape has a sand casting-like surface and can be friable or fragile. Wall thickness is greater than about 0.015 in.
- Layered sheet molding, where a thermal laser beam is directed against a film of polymer such as polyethylene, nylon or PET. The polymer film has a heat-sensitive coating on the reverse side. Before laser cutting, it is stretched over the last shape cut. Again the beam is controlled by the computer. After the laser has completed cutting the sheet, the cut film is pressed with a heated platen or iron against the stack of previously cut film, thus fusing it to the stack. The laminate is indexed downward by the thickness of the film, which should be the exact thickness of the electronic wafer. The final plastic shape has minutely stepped edges but otherwise appears identical to the designer's concept. Wall thickness is greater than about 0.015 in but thinner walls are contemplated.
- Layered paper molding, where a thermal laser beam is directed against a sheet of SBS paperboard. The paperboard is usually about 0.010 in thick and usually has

a heat-sensitive adhesive on the reverse side. Some work is underway to use paperboard with pressure-sensitive adhesive. The final paper shape has faint stepped edges and is heavier than the plastic models. This technique is reported to be very fast, with models being produced in half to one-third the time of plastic models. Wall thickness is greater than about 0.020 in.

- Water-cut paper molding, where a water jet instead of a laser beam is used to cut the paperboard. It is said that this technique generates no odor, smoke or dust and a very smooth surface is obtained on the final shape. It is slower than the laser cutter and has about the same wall thickness restrictions.
- A very recent development uses a desktop technique similar to ink-jet printing, where 0.0025 in diameter polymer droplets are dispensed according to the scanned image. The technique uses a second plotter head to dispense wax in areas where undercuts and removable support structures occur. The wax and plastic are finished with a horizontal milling cutter. All elements are microcomputer or PC driven [8]. No lay-down speeds or minimum wall thicknesses are available.

Four of these techniques are shown in Fig. 7.5 [9]. When early versions of these techniques were introduced a decade ago, the units cost in excess of US\$200,000, the operation was dusty or messy, and the parts were restricted to no more than 20 in on a side by the sizes of the chemical tanks. The equipment for some of the newer techniques now costs less than US\$100,000 and parts of 40 in on a side have been fabricated. When "cut-and-paste" techniques are fully developed, part sizes appear to be unlimited [10]. In addition to making prototypes, RP technology is beginning to be used to make prototype thermoforming molds [11]. RP allows the molder or mold maker to make changes in mold details such as texture, polymer shrinkage and boss and rib locations quite rapidly. This is an important addition to getting a functional product to the marketplace quickly.

7.4 Draw Ratio

Draw ratio¹ is a common measure of thermoformability. There are at least three accepted ways of representing draw ratio:

- Areal draw ratio, R_a ,
- Linear draw ratio, R_L , and
- H:d or H:D.

In addition, reduced thickness or thickness ratio, (t/t_0) , is also used. Some of this was introduced in an earlier section. The draw ratio concept is usually given more importance than it deserves. For example, areal draw ratio is usually considered to be a measure of the biaxial orientation of the sheet. However, it is an *artificial concept*, since it yields an *average* sheet thickness. No thermoforming process yields

¹ Draw ratio is also called "depth of draw" or "extent of draw".

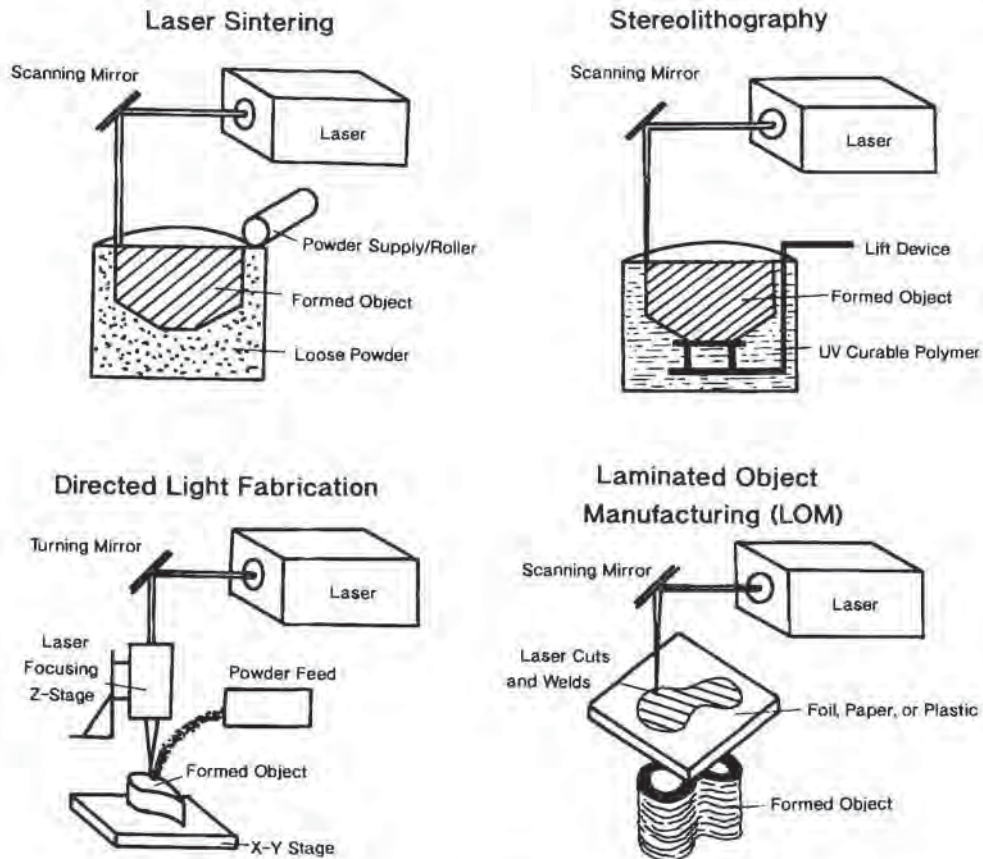


Figure 7.5 Four examples of automated fabrication of rapid prototyping, used in thermoforming for the production of prototype molds and for plugs

a uniform wall thickness part, however. No form for the draw ratio uniquely defines the events of biaxial and/or uniaxial stretching [12]. And no draw ratio describes the *local* extent of elongation at every point across the part surface. Nevertheless, since the draw ratio concept is so pervasive, certain definitions and rules are in order.

Areal Draw Ratio

Regardless of the stretching process used to produce the formed shape, initial sheet of plastic with an area A_0 and thickness t_0 is stretched to provide a part having a surface area A and an average thickness t_a . Since the plastic volume is constant:

$$V = t_0 A_0 = \int t \, dA = t_a A \quad (7.15)$$

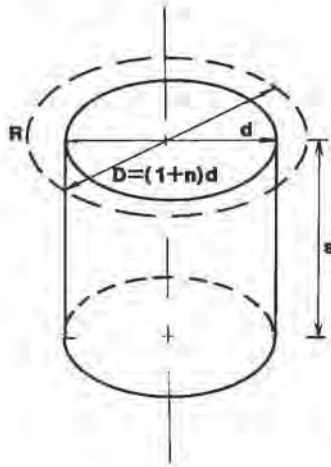


Figure 7.6 Geometric factors for draw-down into parallel-walled cylinder with rim material contribution

The simplest measure of stretch is the areal draw ratio, $R_a = A/A_o$. R_a is also the reciprocal thickness ratio, $R_a = (t/t_o)^{-1}$. The areal draw ratio is a measure of the biaxial orientation of the sheet. The areal draw ratio of a parallel-sided cylindrical female part, Fig. 7.6, for example is:

$$R_a = \frac{A_{\text{sidewall}} + A_{\text{bottom}}}{A_o} = \frac{\pi ds + \pi d^2/4}{\pi d^2/4} = \frac{4s}{d} + 1 \quad (7.16)$$

where s is the part and d is its diameter. Sometimes, a reduced areal draw ratio, $R_a^* = R_a - 1$, is used [12]. The areal draw ratio is known by other names:

- Stretch ratio [64],
- Stretching ratio [13],
- Stretch factor [65], or
- Areal elongation [66].

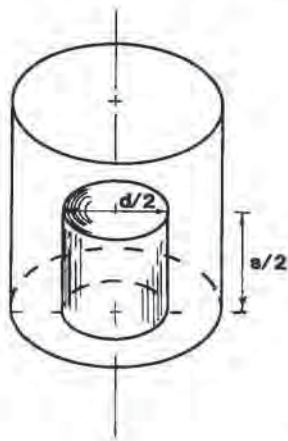





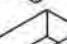





Figure 7.7 Geometric factors for draw-down into parallel-walled cylinder with male segment

Table 7.8 Areal Draw Ratios for Regular Shapes

| Shape | Figure | Area | Areal draw ratio, Ra |
|--|---|--|---|
| Hemisphere |  | $2\pi R^2$ | 2 |
| Right cylinder |  | $\pi R^2 + 2\pi R h$ | $1 + (2h/R)$ |
| Right cone |  | $\pi R(R^2 + h^2)^{1/2}$ | $[1 + (h/R)^2]^{1/2}$ |
| Truncated cone |  | $\pi r^2 +$ $\pi(R + r) \cdot [(R - r)^2 + h^2]^{1/2}$ | $(r/R)^2 +$ $(1 + r/R) \cdot [(1 - r/R)^2 + (h/R)^2]^{1/2}$ |
| Square, a = side |  | 5a | 5 |
| Right rectangle a × b × h ¹ |  | 2ah + 2bh + 2ab | $2(1 + h/b + h/a)^2]^{1/2}$ |
| Wedge a × b × h |  | $2h + 2b[h^2 + (a/2)^2]^{1/2}$ | $(h/b) + [1 + (2h/a)^2]^{1/2}$ |
| Right pyramid a × b × h |  | $(ab/2)[1 + (2h/b)^2]^{1/2} +$ $(ab/2)[1 + (2h/a)^2]^{1/2}$ | $(1/2)[1 + (2h/b)^2]^{1/2} +$ $(1/2)[1 + (2h/a)^2]^{1/2}$ |
| Truncated right pyramid a × b × h and a × b |  | $1/2(ab - ab)[1 + (2h/b)^2]^{1/2} +$ $1/2(ab - ab)[1 + (2h/a)^2]^{1/2} +$ ab | $1/2[1 - (ab/ab)][1 + (2h/b)^2]^{1/2} +$ $1/2[1 - (ab/ab)][1 + (2h/a)^2]^{1/2} +$ (ab/ab) |

¹ h is the perpendicular height for the right rectangle, wedge, right pyramid and the truncated right pyramid

Areal draw ratios for other simple geometries are given in Table 7.8. Areal draw ratios for complex shapes are obtained by combination, as seen in Examples 7.7 and 7.8. The average areal draw ratio is also insensitive to local drawing. Figure 7.8 compares the average areal draw ratio of a rounded bottom cylinder with a corner radius, $r = a \cdot d$ with a square bottom cylinder, $r = 0$. The area of the rounded bottom cylinder is:

$$\begin{aligned}
 A_{\text{round}} &= \text{Area}_{\text{bottom}} + \text{Area}_{\text{side}} + \text{Area}_{\text{torus}}/4 \\
 &= \frac{\pi(d^2 - r^2)}{4} + \pi d(s - r) + \frac{4\pi^2 dr}{4 \cdot 2}
 \end{aligned} \tag{7.17}$$

Example 7.7 Areal Draw Ratios for Cylindrical Parts—I

Consider a female straight-walled cylinder of diameter d and height s , with a solid center rod of diameter $d/2$ and height $s/2$ in its center, Fig. 7.7. Determine the overall areal draw ratio. Then replace the solid center rod with a hollow cylinder of the same dimensions but zero wall thickness.

The wall area of the outer cylinder is:

$$A_{\text{wall}} = \pi ds$$

The area of the bottom outer cylinder is:

$$A_{\text{bottom}} = \pi d^2/4 - \pi(d/2)^2/4 = 3\pi d^2/16$$

The wall area of the inner cylinder is:

$$A_{\text{wall}} = \pi(d/2)s$$

The area of the top of the inner cylinder is:

$$A_{\text{top}} = \pi(d/2)^2/4 = d^2/16$$

The total area of the two cylinders is:

$$A_{\text{total}} = \frac{3\pi ds}{2} + \frac{\pi d^2}{4}$$

The area of the initial disk is:

$$A_o = \pi d^2/4$$

Therefore the areal draw ratio is:

$$R_a = 6 \frac{s}{d} + 1$$

For the hollow cylinder, the area of the sides is [inside and outside of the short cylinder]:

$$A_{\text{side}} = 2 \times \pi ds/2 = \pi ds$$

The area of the bottom is:

$$A_{\text{bottom}} = \pi(d/2)^2/4$$

The total area of the double cylinder is:

$$A_{\text{total}} = 2\pi ds + \pi d^2/4$$

And the areal draw ratio is:

$$R_a = 8 \frac{s}{d} + 1$$

Example 7.8 Draw Ratios for Cylindrical Parts—II

Using the information from Example 7.7, determine the draw ratio for the hollow inner cylinder only. Compare the overall draw ratio value with this local draw ratio value for $s = d$.

If the inner surface of the inner cylinder of Fig. 7.7 is drawn only from the disk of material formerly on the top of the cylinder, the areal draw ratio for this is:

$$R_u = \frac{4s}{d} + 1$$

But this material has already been drawn. The material touching the inner cylinder rim has been drawn into a hemisphere of area, $A_{\text{hemi}} = \pi d^2/2$. The draw ratio of a hemisphere is:

$$R_{u,\text{hemi}} = \frac{\pi d^2/2}{\pi d^2/4} = 2$$

Therefore the average draw ratio of the polymer forming the inside of the inner cylinder is the product of draw ratios:

$$R_{\text{inner}} = R_u \cdot R_{u,\text{hemi}} = 2 \cdot (4s/d + 1)$$

If $s = d$, then $R_{\text{inner}} = 10$. From Example 7.7, the overall draw ratio for the hollow inner cylinder is:

$$R_u = \frac{8s}{d} + 1 = 9$$

The areal draw ratio is:

$$R_u = 1 - \left(\frac{r}{d}\right)^2 + 4\left(\frac{s-r}{d}\right) + \frac{2\pi r}{d} = R_{u,\text{square}} - \frac{r}{d} \left(\frac{r}{d} + 4 - 2\pi\right) \quad (7.18)$$

As seen in Example 7.9, average areal draw ratios for bottom-radiused cylinders are not much less than that for a cylinder with a zero corner radius. Yet for the square bottom cylinder, the last polymer sheet drawn into the sharp corner must be infinitely elongated. This is even more apparent when the linear draw ratio is used.

Example 7.9 Areal Draw Ratio of Round-Cornered Cylinder

If the round-cornered can of Fig. 7.8 has a radius $r = d/8$, determine the areal draw ratio relative to a square bottomed can. What is it for $r = d/2$, a hemispherical bottom? If $s = d$, determine the absolute values.

From Equation 7.18:

$$R_{u,\text{round}} = 1 - \left(\frac{r}{d}\right)^2 + 4\left(\frac{s-r}{d}\right) + \frac{2\pi r}{d} = R_{u,\text{square}} - \frac{r}{d} \left(\frac{r}{d} + 4 - 2\pi\right)$$

For $r = d/8$:

$$R_{a,round} = R_{a,square} - 0.125(0.125 + 4 - 6.28) = R_{a,square} - 0.27$$

For a hemispherical bottom, $r = d/2$:

$$R_{a,round} = R_{a,square} - 0.5(0.5 + 4 - 2\pi) = R_{a,square} - 0.89$$

If $s = d$:

$$R_{a,square} = 4s + 1 = 5$$

$$R_{a,round} = 5 - 0.27 = 4.73$$

$$R_{a,round} = 95\% \text{ of } R_{a,square}$$

Linear Draw Ratio

The linear draw ratio, R_L , is the ratio of the length of a line projected onto a part surface to its length on the unformed sheet (Fig. 7.9). Note that it is possible to define several linear draw ratios for unsymmetric parts. Traditionally the largest



Figure 7.8 Draw-down into (top) sharp-cornered cylinder and (bottom) radiused cylinder. Corner radius, $r' = d/8$, where d is cylinder diameter

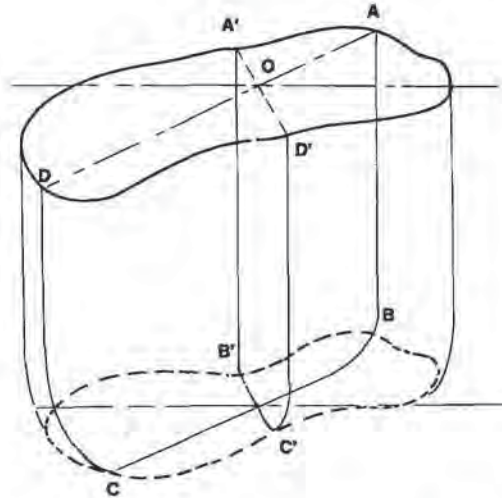


Figure 7.9 Geometric factors for linear draw-down into irregular shape. $R_{L,1} = ABCD/AOD$.
 $R_{L,2} = A'B'C'D'/AOD$

value of R_L is used. R_L reflects uniaxial stress-strain behavior of a polymer. For example, the linear draw ratio for the parallel-sided cylinder of Fig. 7.6 is:

$$R_L = \frac{2s + d}{d} = \frac{2s + 1}{d} \quad (7.19)$$

R_L is also called the depth of draw ratio [12]. A reduced linear draw ratio is sometimes used. It is written as $R_L^* = R_L - 1$. Except in simple geometric cases, there is no relationship between the areal draw ratio and any of the linear draw ratios. As with areal draw ratio, R_L is an artificial concept, since the local draw down usually differs substantially from the average value. Example 7.10 illustrates linear draw ratios for the straight-walled cylinder of Fig. 7.6.

Example 7.10 Linear Draw Ratios for the Cylindrical Shapes of Examples 7.7 and 7.8

Consider the straight walled cylinder of Fig. 7.7 with solid and hollow inner cylinders. Determine the linear draw ratios for these.

The linear draw ratio for the solid cylinder is the ratio of the line scribed on the surface of the cylinder to that scribed on the disk.

$$\text{Line}_{\text{solid cylinder}} = 2s + \frac{d}{2} + 2\left(\frac{s}{2}\right) + \frac{d}{2} = d + 3s$$

$$\text{Line}_{\text{disk}} = d$$

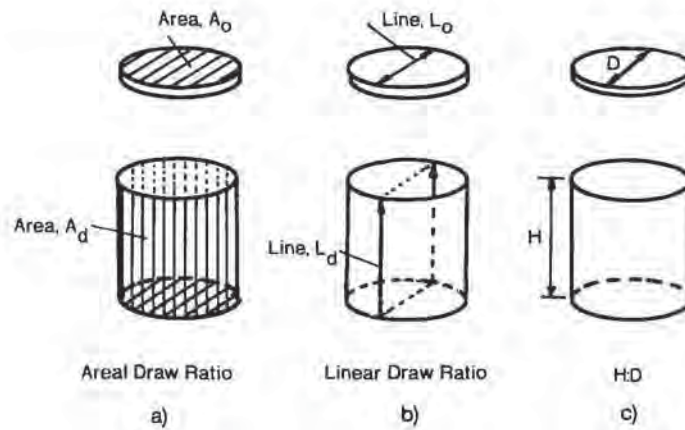


Figure 7.10 Geometric factor comparison for (a) areal draw ratio, R_A , (b) linear draw ratio, R_L , and (c) H:D or H:d

$$R_{L,\text{solid}} = 1 + 3 \frac{s}{d}$$

$$\text{Line}_{\text{hollow cylinder}} = 2s + \frac{d}{2} + 4\left(\frac{s}{2}\right) + \frac{d}{2} = d + 4s$$

$$R_{L,\text{hollow}} = 1 + 4 \frac{s}{d}$$

H:D

Another form of linear draw ratio is the ratio of depth of draw to mold opening at the rim. It is written H:D or H:d [13]. Except for simple shapes, it too is difficult to define unambiguously. For a simple parallel-side cylindrical part of Fig. 7.6, the relationship between H:D and R_L is:

$$R_L = 1 + 2(H:D) \quad (7.20)$$

Figure 7.10 shows all three draw ratios for a straight-sided cylinder. The draw ratio relationships are given in Fig. 7.11. The three draw ratios for draw-down into a two-dimensional corner are compared in the following way¹. Figure 7.12 shows a three-dimensional view and an end-on view of the two-dimensional corner. The initial area of the sheet at radius R is $\pi RL/2$. Its volume is $V = \pi RLt/2$ where t

¹ The approach used here is Geometric Element Analysis, or GEA. That is, the sheet is assumed to be an infinitely extensible membrane having a thickness much less than its surface area. The arithmetic assumes no causal relationship between the amount of force required to stretch the membrane and the extent of stretching. Furthermore, there are no physical limits such as elongation at break to prevent the sheet from stretching any desired amount. GEA is discussed in more detail in Section 7.6.

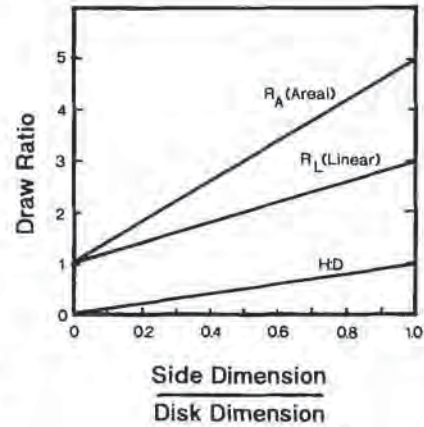


Figure 7.11 Comparison of areal draw ratio, linear draw ratio and H:D for parallel-sided female cylinder as a function of extent of draw

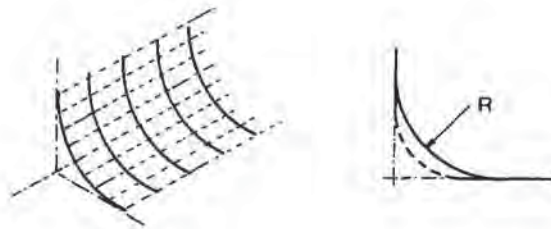


Figure 7.12 Draw into two-dimensional corner, two views

is the sheet thickness. The volume of polymer sheet on the wall after a differential draw is $2L(\delta R)(t - \delta t/2)$. That remaining in the stretched sheet not in contact with the wall is $(\pi L/2)(R - \delta R)(t - \delta t)$. The material balance yields:

$$\pi R L t / 2 = (\pi L / 2)(R - \delta R)(t - \delta t) + 2L(\delta R)(t - \delta t / 2) \quad (7.21)$$

This is rearranged and $\delta R \delta t$ is assumed to be less than either δR or δt :

$$\frac{\delta t}{t} = (4/\pi - 1) \frac{\delta R}{R} \quad (7.22)$$

This is integrated to yield:

$$\frac{t}{t_0} = \left(\frac{R}{R_0} \right)^{4/\pi - 1} \quad (7.23)$$

where t_0 is the sheet thickness when $R = R_0$. This is the instant thickness of the sheet at the instant radius, R . The average thickness does not depend on the radius at all. The areal draw ratio is:

$$R_a = \frac{\text{final area}}{\text{initial area}} = \frac{2RL}{(\pi RL/2)} = \frac{4}{\pi} = \left(\frac{t}{t_0} \right)^{-1} \quad (7.24)$$

The linear draw ratio is:

$$R_L = \frac{\text{final line length}}{\text{initial line length}} = \frac{2R}{(\pi R/2)} = \frac{4}{\pi} \quad (7.25)$$

And H:D is:

$$H:D = \frac{\text{initial line length}}{\text{inscribed circle gap}} = \frac{\pi R/2}{(\sqrt{2}R/2)} = \frac{\pi}{\sqrt{2}} \quad (7.26)$$

Note that the reciprocal average thickness ratio, the areal draw ratio and the linear draw ratio all agree. From Equation 7.23, it is apparent that the sheet thickness approaches zero as the radius approaches zero. This demonstrates the general problem with the global draw ratio concept. Example 7.11 considers progressive drawing into this corner to illustrate this point.

Example 7.11 Differential Drawing into a Two-Dimensional Corner

Consider progressive draw-down into a two-dimensional corner, Fig. 7.13. The initial sheet length is $\pi R/2$. At $r = nR$, the sheet length is $\pi r/2 + 2(R - r)$. The linear draw ratio is:

$$R_L = n + \frac{4}{\pi} (1 - n)$$

Determine the average linear draw ratio when $n = 1$ and $n = 0$. Then consider a progressive draw where the distance to the corner is halved in each draw. Compare the draw ratios.

The average linear draw ratio for $n = 1$ is $R_L = 1$. When $n = 0$, $R_L = 4/\pi$, as expected.

Consider drawing the sheet from $r = R/2$ ($n = \frac{1}{2}$) to $r = R/4$ ($n = \frac{1}{4}$). Now:

$$R_{L,1} = \frac{1}{2} + \frac{2}{\pi} = 1.137$$

$$R_{L,2} = \frac{1}{4} + \frac{3}{\pi} = 1.205$$

Consider drawing the free surface from $r = R/4$ to $r = R/8$. Now:

$$R_{L,3} = \frac{1}{8} + \frac{7}{2\pi} = 1.239$$

The free portion of the sheet in this step has been drawn:

$$R_{L,1} \cdot R_{L,2} \cdot R_{L,3} = 1.698$$

In fact for the M th draw step, the local draw ratio is:

$$R_{L,M} = \sum_{m=1}^M 2^{-m} + \frac{4}{\pi} \sum_{m=1}^M 1 - \left(\frac{1}{2}\right)^m$$

The first term approaches 2 as M approaches ∞ . The second term approaches M as M approaches ∞ . In other words, $R_{L,\infty} = \infty$. Thus the last infinitesimal amount of sheet is drawn to an infinitely small thickness, even though the average linear draw ratio, $R_L = 4/\pi$.



Figure 7.13 Progressive draw-down into two-dimensional corner

Rim and Lip Sheet for Female Cavities

The volume of polymer found in formed parts is usually greater than that in the material free of the mold surface prior to forming [14-16,74]. In some cases, sheet is deliberately pulled over the edge and into the female mold cavity in order to aid in wall thickness distribution. In other cases, the design of the part restricts the use of a moat or moat and dam combination. The plastic on the flat lip therefore tends to be drawn into the female mold cavity. The amount of plastic drawn into the mold varies from 15% to 35% or so, depending on the lip geometry. Additional sheet can be supplied by billow pre-stretching or it can be drawn from the lip or rim region into the mold cavity during draw-down (Fig. 7.14). To account for the excess material, it is recommended that the calculated areal draw ratio values include 50% of the sheet surface area between the lip and the clamping ring [17]. Consider forming a parallel-sided cylinder

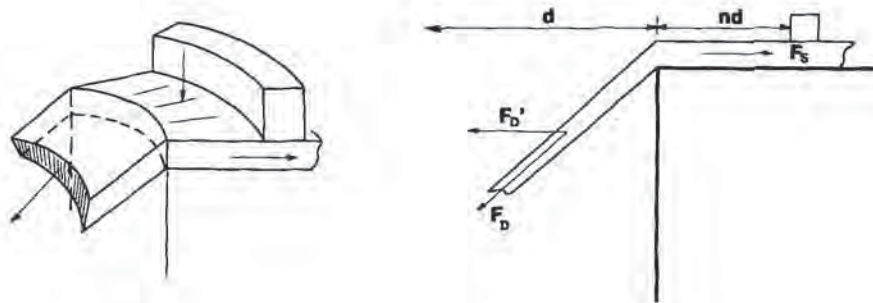


Figure 7.14 Schematic of rim area coordinates, comparing stretching force, F_d , and sliding force, F_s . F_d' is the component of the stretching force in the sliding force direction

of depth s and diameter d , clamped at diameter $D = (1 + n)d$, as shown in Fig. 7.14. The areal draw ratio with no rim material is given as Equation 7.16:

$$R_{a,i} = \frac{4s}{d} + 1 \quad (7.16)$$

If all the rim material is included in the draw ratio:

$$R_{a,rim} = \frac{A_{sidewall} + A_{bottom} + A_{rim}}{A_o + A_{rim}} = 1 + \frac{4ds}{D^2} \quad (7.27)$$

If only a fraction, g , of the rim material is included:

$$R_{a,rim} = \frac{A_{sidewall} + A_{bottom} + g \cdot A_{rim}}{A_o + A_{rim}} \quad (7.28)$$

or:

$$R_{a,rim} = g + (1 - g) \left(\frac{d}{D} \right)^2 + \frac{4ds}{D^2} = 1 + \frac{4ds}{D^2} + (1 - g) \left[\left(\frac{d}{D} \right)^2 - 1 \right] \quad (7.29)$$

If $D = (1 + n)d$, this expression is written as:

$$R_{a,rim} = 1 + \frac{4s}{(1 + n)d} + (1 - g) \left[\left(\frac{1}{1 + n} \right)^2 - 1 \right] \quad (7.30)$$

Example 7.12 illustrates how the draw ratio is affected by the rim material. Figure 7.15 illustrates this where n is the rim fraction of polymer drawn into the female cavity. For the experimental observations of 15% to 35% greater volume, $n = 0.07$ to 0.16 on a circular cavity.

Example 7.12 Effect of Rim Material on Draw Ratio

Consider a parallel-sided cylindrical part where $s = d$ and $D = 1.2d$. Determine the effect of rim material if 100% is involved in draw-down and if 50% is involved in draw down.

Equation 7.30 is the proper equation:

$$R_{a,rim} = 1 + \frac{4s}{(1 + n)d} + (1 - g) \left[\left(\frac{1}{1 + n} \right)^2 - 1 \right]$$

$$R_{a,rim} = 1 + \frac{4}{1.2} + (1 - g) \left[\left(\frac{1}{1.2} \right)^2 - 1 \right] = 1 + 3.33 - 0.3055(1 - g)$$

When $g = 1$, $R_{a,rim} = 3.78$. When $g = 0$, $R_{a,rim} = 5$. When $g = 0.5$, $R_{a,rim} = 4.28$.

A more formal analysis examines the relationship between the forces required to stretch the sheet and those needed to slide it along the mold surface. A simple force balance illustrates this. The stretching force, F_d , is written as:

$$F_d = \tau \cdot A' \quad (7.31)$$

where τ is the tensile strength of the sheet at the forming temperature and A' is the sheet cross-sectional area at the edge of the cavity (Fig. 7.14). The sliding force, F_s , is written as:

$$F_s = CN^a = C(P \cdot A)^a \quad (7.32)$$

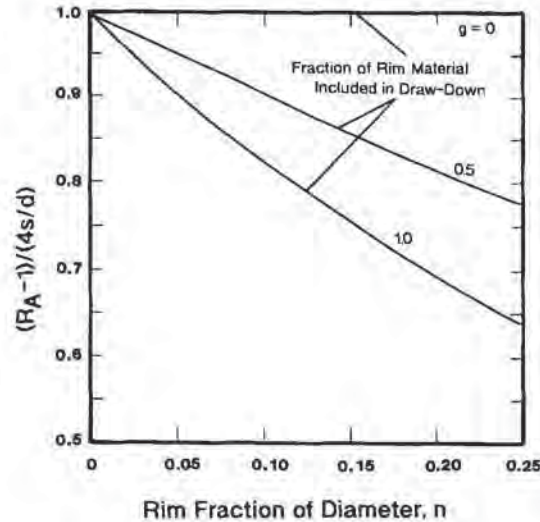


Figure 7.15 Effect of rim material contribution on areal draw ratio. g = fraction of rim material included in draw-down

where N is the normal force, P is the pressure applied to the free-to-deform rim material and A is the contact area between the clamp and the rim. C is the kinetic coefficient of friction between the polymer and the mold surface [67,68]. The experimental value of a is 0.67 to 1 [69]. The force required to slide the sheet along the rim is vectored perpendicularly to the draw axis. The deformation force, F_d , is initially vectored in the sliding force direction, but as the sheet draws, F_d^* , the component of F_d in the horizontal or F_s direction, diminishes rapidly. $F_d^* = 0$ when the sheet touches the wall of the parallel-sided female cylinder mold, as an example. F_d^* is given as:

$$F_d^* = F_d \cos \beta = \tau \cdot \pi d h_0 \cos \beta \quad (7.33)$$

where β is the sheet angle to the horizontal and h_0 is the initial sheet thickness. If the rim is clamped at $D = (1 + n)d$, the force needed to slide this area of the sheet, F_s , is:

$$F_s = CP^a \cdot \left\{ \frac{\pi d^2}{4} [(1 + n)^2 - 1] \right\}^a \quad (7.34)$$

The sheet stops sliding when $F_d^* < F_s$. Since P is the amount of pressure that is holding the sheet against the rim, this equation is solved for P :

$$P > \frac{2 \cdot \left\{ \frac{\tau \cdot \pi d h_0 \cos \beta}{C} \right\}^{1/a}}{\pi d^2} \cdot [(1 + n)^2 - 1]^{-1} \quad (7.35)$$

For the special case where $a = 1$:

$$P > \left\{ \frac{\tau \cdot 4 h_0 \cos \beta}{dC} \right\} \cdot [(1 + n)^2 - 1]^{-1} \quad (7.36)$$

The amount of pressure required to keep the sheet from sliding is proportional to the tensile strength of the polymer, its initial thickness and the diameter of the cavity. It is inversely proportional to the coefficient of friction and to the amount of plastic on the rim, n . Example 7.13 illustrates this relationship. If the mold is a parallel-sided cylinder, the sheet stops sliding and begins stretching before the sheet contacts the wall. If the mold is a cone with an angle less than 74.4° , contact occurs first.

Example 7.13 Sliding and Stretching Forces

Given a 0.030 in thick sheet of plastic having a hot tensile strength of $\tau = 0.7 \text{ MPa} = 100 \text{ lb}_f/\text{in}^2$, determine the angle β where the stretching forces exceed the sliding forces for a 2-in drink cup. The coefficient of friction is 0.25, $a = 1$ and $n = 0.2$.

The operative expression is Equation 7.36:

$$P > \left\{ \frac{\tau \cdot 4h_0 \cos \beta}{d \cdot c} \right\} \cdot [(1+n)^2 - 1]^{-1}$$

$$P > 24.0 \cos \beta [2.273] = 54.55 \cos \beta \text{ [lb}_f/\text{in}^2]$$

If the maximum applied pressure is $14.7 \text{ lb}_f/\text{in}^2$, then the angle is:

$$\beta = \cos^{-1} (14.7/54.55) = \cos^{-1} 0.269 = 74.4^\circ$$

In other words, the sheet slides on the surface until that portion that is in the mold cavity reaches an angle of 74.4° with the horizontal.

For billow prestretching, the dimensions of the expanding sheet differ from the mold dimensions. An appropriate factor must be included in the rim-included draw ratio definitions to account for this type of prestretching. Example 7.14 illustrates this. Prestretching is also considered in the text below.

Example 7.14 Areal Draw Ratio With and Without Prestretching

Determine the areal draw ratio of a straight-sided cylinder with and without prestretching. For prestretching, the bubble diameter $D = (1+n)d$, where d is the diameter of the cylinder. Determine the proper equation for a bubble height from $y = 0$ to $y = D/2$.

The areal draw ratio of a straight-sided cylinder without prestretching is given by Equation 7.16:

$$R_a = \frac{4s}{d} + 1$$

The area of a spherical zone or cap is given as:

$$A_{\text{cup}} = \frac{\pi}{4} [4y^2 + D^2]$$

When $y = 0$, the area is a disk:

$$A_{\text{disk}} = \frac{\pi D^2}{4}$$

When $y = D/2$, the area is a hemisphere:

$$A_{\text{hemi}} = \frac{\pi D^2}{2}$$

The areal draw ratio is given as:

$$R_{a,\text{preblow}} = \frac{\text{final surface area}}{\text{initial surface area}} = \frac{\pi ds + \pi d^2/4}{\pi[4y^2 + (1+n)^2 d^2]/4}$$

where the initial surface area is the area of the cap. This equation is rewritten as:

$$R_{a,\text{preblow}} = \left[\frac{4s}{d} + 1 \right] \cdot [4(y/d)^2 + (1+n)^2]^{-1} = R_a \cdot [4(y/d)^2 + (1+n)^2]^{-1}$$

The last bracketed term represents the effect of pre-blowing on the draw ratio. If $n = 0$ and $y = d/2$, or the bubble is a hemisphere, $R_{a,\text{preblow}} = R_a/2$.

Draw Ratio Usage—A Rationale

Average draw ratios are used primarily to screen candidate polymers. For example, CAB, PS, PETG and HDPE can be pre-blown into bubbles that are greater than hemispherical [17]. Usually, PVC, PMMA and PC cannot. Low-density PS foam cannot be drawn greater than about H:D = 1:1 [18] unless coated with an unfoamed capsheet. Crosslinked polyethylene foam cannot be drawn greater than about H:D = 0.6:1 to 0.8:1 [19]. Practical temperature-dependent H:D draw ratios for several polymers and several initial sheet thickness for simple vacuum forming into a parallel-sided female mold are shown in Fig. 7.16.

Mechanical Assists—Some Design Features

The wall thickness analyses that follow concentration on the geometric prediction of part wall thickness during simple female forming. Many forming processes described in Chapter 1 depend on prestretching to improve material distribution. Inflation and plug assist are two common prestretching methods.

Preblowing or Inflation—Comments

Figure 7.17 shows experimental draw down for sheet into the bottom corner of a truncated cone [20]. The sheet thickness ratio, h/h_0 , is experimentally shown to be

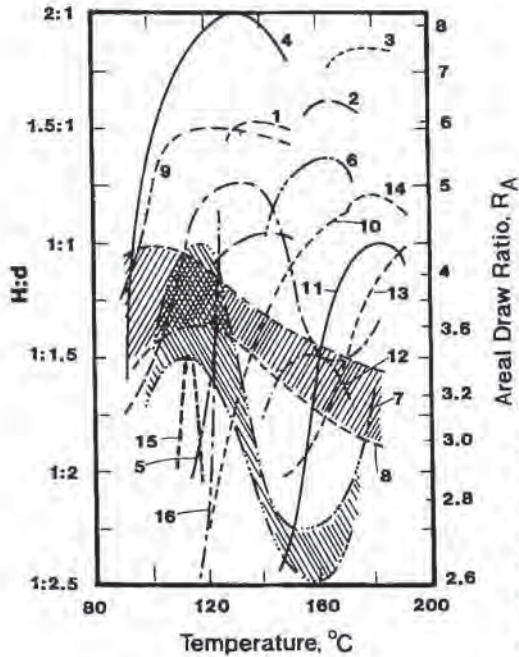


Figure 7.16 Temperature-dependent areal draw ratio and H:D for tapered cylindrical female mold for several polymers: 1. 0.4 mm LDPE; 2. 0.5 mm HDPE; 3. 0.4 mm PP; 4. 0.3 mm HIPS; 5. 0.25 mm OPS; 6. 0.5 mm ABS; 7. 0.3 mm RPVC; 8. 0.3 mm FPVC; 9. 0.5 mm PVC copolymer; 10. 0.3 mm cellulose acetate; 11. 0.2 mm PC; 12. 0.3 mm PMMA; 13. 0.5 mm CAB; 14. 0.5 mm CAP; 15. 0.5 mm Hostalit Z; 16. 0.5 mm PS foam. Figure used with permission of Carl Hanser Verlag

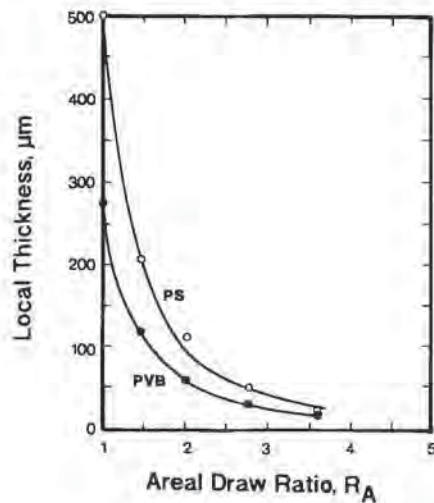


Figure 7.17 Experimental sheet thickness as function of areal draw ratio for draw-down into truncated cone bottom cylinder. PS = polystyrene, PVB = polyvinyl butyral. Figure redrawn from [20] and used with permission of copyright owner

inversely proportional to the square of the areal draw ratio. Inflation is a method of prestretching sheet (Fig. 7.18). For inflation of an unformed sheet, experiments show that the sheet thickness away from the rim region is a function only of the inflation height, y (Fig. 7.19) [15]. For very large inflation ratios, exceeding hemispherical, the sheet thickness is constant only in the polar region [17]. An analytical solution to the

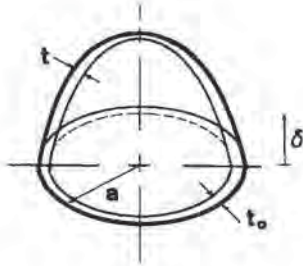


Figure 7.18 Geometric factors for bubble inflation

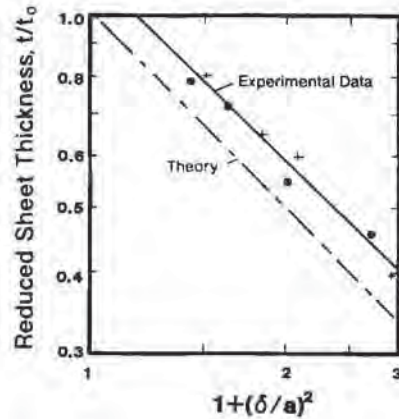


Figure 7.19 Experimental and theoretical inflated bubble thickness [15]. Solid circles are polymethyl methacrylate, PMMA. Pluses are polystyrene, PS. Solid line is best fit of data. Dashed line is theory. Figure redrawn and used with permission of Ellis Harwood, Ltd., copyright owner

nonlinear clamped-edge plate deformation problem is also available [21]. If the polymer in the cap is assumed to have a uniform overall thickness [22]:

$$\frac{h}{h_0} = \frac{1}{1 + (y/a)^2} = \frac{1}{R_u} \quad (7.37)$$

For purely elastic sheet [15,17], the relationship between inflation height, y , and inflation pressure, P , is:

$$\frac{P_u}{2h_0E} = \ln [1 + (y/a)^2] \cdot \frac{[2(y/a)]}{[1 + (y/a)^2]^2} \quad (7.38)$$

where E is the modulus obtained from the polymer elastic stress-strain equation, $\sigma = E$. As seen in Fig. 7.19 for HIPS and PMMA, there is a distinct offset in the thickness ratio relationship to y/a . An approximate relationship is:

$$\frac{h}{h_0} \approx \frac{(5/6)}{1 + (y/a)^2} \quad (7.39)$$

The offset is the result of the sheet in the rim area being substantially thicker than the average.

The extent of inflation is determined by the amount of prestretching desired to achieve the desired wall thickness uniformity and on the ability of the polymer to inflate without bursting, as discussed in Chapter 4. Typical prestretching air pressure values for several polymers are given in Table 7.9. If the inflated cap is to be snapped into a female mold, the cap surface should not touch the mold bottom on

Table 7.9 Typical Prestretching Air Pressure

| Polymer | Temperature range | | Pressure range above atmospheric | |
|------------------|-------------------|---------|----------------------------------|-------------------------------------|
| | (°C) | (°F) | (kPa) | (lb _r /in ²) |
| PS | 135–150 | 275–300 | 14–28 | 2–4 |
| PS—foam | | | NR | NR |
| ABS | 140–150 | 280–300 | 10–28 | 1.5–4 |
| HIPS | 135–150 | 275–300 | 14–28 | 2–4 |
| CA | 140–155 | 280–310 | 7–21 | 1–3 |
| PMMA | 160–180 | 325–360 | 48–70 | 7–10 |
| PMMA/PVC | 155–170 | 310–340 | 35–48 | 5–7 |
| PC | 175–190 | 350–375 | 41–70 | 6–10 |
| FEP | | | NR | NR |
| PET | 135–160 | 275–300 | 14–28 | 2–4 |
| HDPE | 130–150 | 270–300 | 7–21 | 1–3 |
| LDPE | 125–145 | 260–290 | 7–21 | 1–3 |
| PP | 150–165 | 300–330 | 7–14 | 1–2 |
| 10% talc—PP | 150–165 | 300–330 | 55–70 | 8–10 |
| 20% talc—PP | 150–190 | 300–380 | 55–70 | 8–10 |
| PSO ₂ | 215–250 | 420–480 | 41–55 | 6–8 |
| RPVC | 115–140 | 240–280 | 10–21 | 1.5–3 |
| FPVC | 115–140 | 240–280 | 7–21 | 1–3 |
| PVC—foam | | | NR | NR |

NR = Not recommended

eversion (Fig. 7.20). As a starting point for predicting draw-down, the sheet thickness can be considered as uniform everywhere. In a more advanced program, the thicker material near the rim can be considered, through application of the approximate relationship above, Equation 7.38.

Preinflation is used with a male mold to minimize the amount of plastic on the surface that first contacts the sheet. A balance on the extent of preblowing bubble height must be struck. If the bubble is blown too large, webs are formed on the outside three-dimensional corners. If the bubble is too small, the corners of the mold can tear the sheet as the mold is inserted. Bubbles do not always tend toward hemispherical. Flat-topped and rectangular bubbles are formed with proper temperature programming. Although the amount of trial-and-error effort needed to achieve

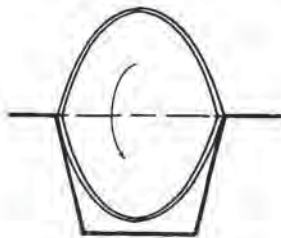


Figure 7.20 Bubble eversion schematic

non-symmetrical bubbles is great, the reward is the ability to form splitty or weak polymers into parts with excellent wall thickness distribution.

Plug Assist—Comments

Plugs are used to mechanically prestretch sheet in applications where a product would otherwise be only marginally acceptable. The plug redistributes polymer along the part wall. Wall thickness distribution with simple vacuum forming into a near-parallel sided cylindrical mold with $H:D = 1:3$ or $R_a = 2.33$ and $R_L = 1.67$ is shown in Fig. 7.21 for several polymers. In Fig. 7.22, the effect of plug assist for 0.016 in. or 0.4 cm MIPS into a cylindrical cup at $H:D = 1:3$ and $H:D = 1:1$, or $R_a = 5$ and $R_L = 3$, acts to distribute polymer from the side and bottom of the part to the traditionally thinner corner.

The plug usually moves along the center axis of a female mold (Fig. 7.23). The plug design parameters include:

- The shape of the plug tip,
- The plug penetration depth relative to the cavity depth,
- The plug diameter relative to the cavity diameter,
- The plug surface temperature, and
- The coefficient of friction between the plug surface and the stretching sheet.

7.5 Computer-Aided Design in Thermoforming

There are many reasons for computerizing the entire forming process. Some of these are:

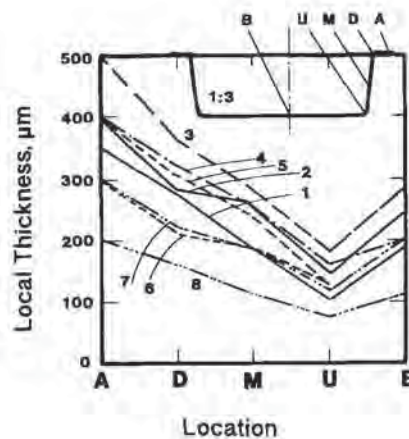


Figure 7.21 Wall thickness distribution for several polymers under typical vacuum forming conditions. $H:D = 1:3$, polymers are: 1. PP; 2. PVC formed at low temperature; 3. LDPE; 4. HIPS; 5. PVC formed at high temperature; 6. PVC copolymer; 7. Cellulose acetate; 8. PC. Figure redrawn from [91] and used with permission of Carl Hanser Verlag

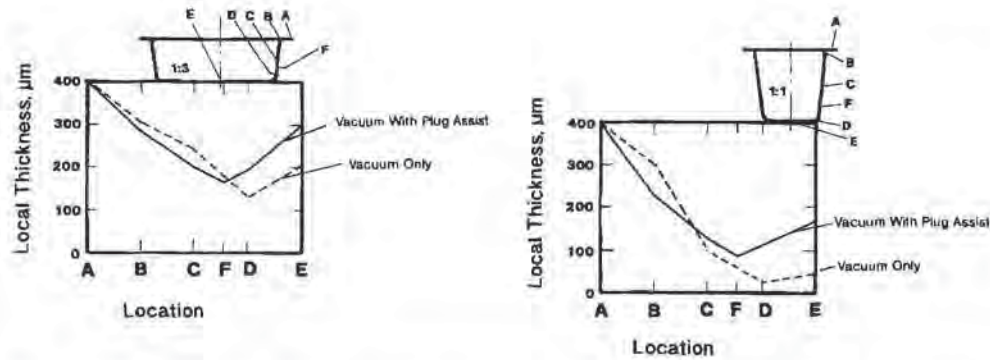


Figure 7.22 Effect of plug assist on wall thickness distribution for 0.4 mm or 0.016 in MIPS for H:D = 1:3 and H:D = 1:1. Dashed line, vacuum only. Solid line, vacuum with plug assist. Figure redrawn from [73] and used with permission of Paul Kiefel GmbH

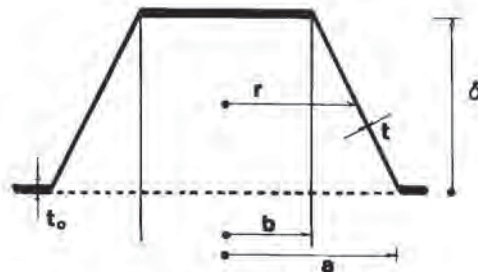


Figure 7.23 Geometric factors for blunt-nose plug assist penetration

- Production of sheet from pellets or powders is a process expense that most other technologies do not incur. The added extrusion costs range upward from \$0.15/lb or US\$0.33/kg.
- Most thermoforming operations convert only 50% to 75% of the ready-to-be-formed sheet into formed products. The rest—web, edge, cutouts, trim, selvage—must be reprocessed at additional costs with some loss in properties. In some cases such as medical products, web material cannot be used.
- Despite technical advances in processing equipment, thermoforming is an energy intensive process. As a result, processing costs are usually higher than those in other converting industries.
- The nature of the thermoforming process is biaxial deformation and thinning of a rubbery elastic sheet. Thus, the average part thickness is substantially less than the initial sheet thickness.
- As a first approximation, plastic sheet draws only when free of the solid surface. This leads to parts of nonuniform wall thickness. In one-step natural drawing—

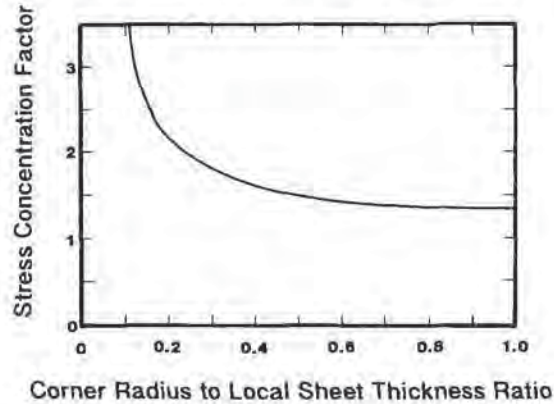


Figure 7.24 Stress concentration factor as function of radius per unit local sheet thickness

vacuum forming, pressure forming or drape forming—parts are thinner in two-dimensional corners and thinnest in three-dimensional corners.

- The nature of the forming process dictates that the plastic in the thinnest areas is stretched the most. This material is therefore closest to its ultimate strength. Part performance under load therefore depends on the method of stretching the sheet and on the thinnest section under load. The stress in a formed corner is strongly dependent on the radius to local wall thickness ratio. As seen in Fig. 7.24, the stress concentration factor exceeds 2 when $R/t < 1/4$. A strong corner design has $R/t \geq 3/4$.
- Conversely, many regions of the formed part are relatively unoriented, are weaker or thicker than desired, and thus are wasteful of expensive polymer.
- Computer-aided engineering or CAE of the thermoforming process encompasses many of the following:
 - Control of sheet temperature prior to forming,
 - The application of the applied forming forces to include necessary sequencing of pressure to allow inflation and/or plug assist prestretching, and
 - Proper sheet cooling techniques to ensure optimum overall cycle time or optimum energy efficiency.
- Computer-aided part design or CAD, is only one facet of CAE. It depends on material allocation or distribution. For a given processing history and a given mold configuration, a specific element of the unformed sheet will always transform into a specific element on the formed part (Fig. 7.25). The controllable CAE parameters such as:
 - Local sheet temperature,
 - Applied pressure
 - Relative pre-inflation parameters,
 - Relative plug parameters, and
 - Stretching sequence,

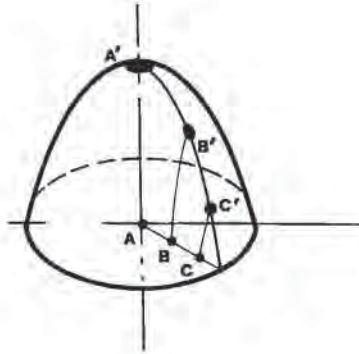


Figure 7.25 Concept of polymer sheet allocation. Translation of [A,B,C] points on flat sheet to [A',B',C'] points on inflated bubble

only differentially alter the relative location, differential area and thickness of that element.

- The easiest approach to material allocation is to assume large-scale isothermal biaxial stretching of an isotropic rubbery elastic sheet.
- This assumption allows two-dimensional finite-element analysis to be used to determine wall thickness for one-step formed shapes. With proper selection of the initial deformation mesh, prestretching can be added as a preliminary step.
- As a further simplifying assumption, the material allocation algorithm includes a non-slip condition. Only the sheet free of a solid surface will stretch under applied force.
- Two further aspects of free surface stretching can be included in model-building. A material balance shows that the volume of free sheet that continues to stretch is simply the difference between the initial volume of material in the unformed sheet and that already deposited on the mold wall. And the free material thickness tends to be uniform across its surface at any time during the stretching process.
- Computer-assisted thermoforming may be of greatest value when multi-layer rigid barrier containers become economically viable. Thermoforming will then meet a specific product need as the packaging industry, in particular, moves toward products requiring precise wall thickness control.

7.6 Wall Thickness Prediction—A Justification

By its very nature of the stretching and forming process called thermoforming, the product so produced has wall thicknesses that are not uniform. Stretching nearly always occurs only in the plastic sheet that is free of the wall. The last area of the mold to be covered by sheet is usually the thinnest. Traditionally, the thinnest walls of female parts are in the bottom three-dimensional corners. The thinnest walls on male parts can be in the outside three-dimensional corners or in the inside three-

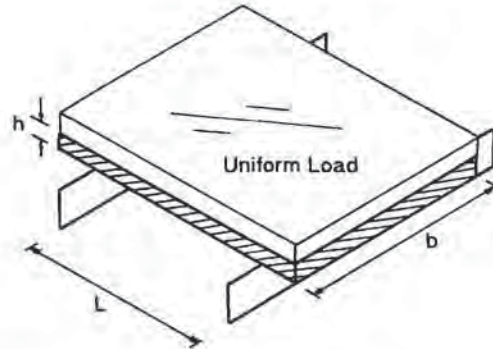


Figure 7.26 Uniform flexural loading of simply-supported beam

dimensional corners. Prestretching devices aid in polymer material redistribution but in general, thermoformed parts have nonuniform wall thicknesses. For some thermoformed products, structural integrity is a secondary function. For many applications, however, the formed part must withstand mechanical loads. Consider two examples of mechanical loading:

- One-dimensional flexural loading of a simple beam (Fig. 7.26). The product might be a thin-gage fast-food container or a heavy-gage spa. The appropriate causal relationship between uniform load, w , and maximum deflection, y_{\max} , is:

$$y_{\max} = \frac{5(wL)L^3}{384 \cdot EI} \quad (7.40)$$

where L is the span, E is the modulus of the polymer and I is the moment of inertia. I is given as:

$$I = bh^3/12 \quad (7.41)$$

where b is the beam width and h is its thickness. Combining these equations:

$$y_{\max} = \frac{60(wL)L^3}{384 \cdot Ebh^3} \quad (7.42)$$

Note that the extent of deflection of the beam is inversely proportional to the cube of its thickness. If the beam thickness or if the thermoformed sheet thickness varies by 10%, the extent of deflection varies by 33%.

- One-dimensional buckling of a plate (Fig. 7.27). The product might be a thin-gage disposable drink cup or the side of a heavy-gage formed equipment cabinet. The appropriate causal relationship is the Euler buckling equation:

$$F = \frac{\pi^2 EI}{L^2} \quad (7.43)$$

where F is the buckling load, E is the polymer modulus, L is the effective length of the column and I is the moment of inertia, as before. Again, substituting the moment of inertia yields:

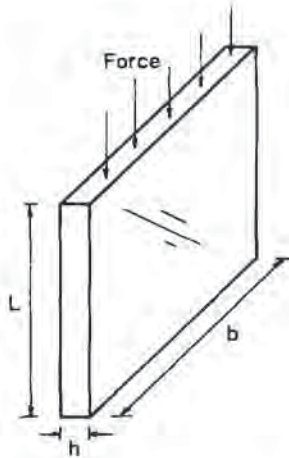


Figure 7.27 Uniform compressive loading and buckling of uniform-walled plate

$$F = \frac{\pi^2 E b h^3}{12 \cdot L^2} \quad (7.44)$$

- Again a 10% variation in the column thickness or the thickness of the thermoformed sheet results in a 33% variation in the ability of the product to support a buckling load.

As noted above, prestretching enables material redistribution, with the objective being an increase in part wall thickness in load bearing regions. Consider the benefits for material redistribution. If the design wall thickness is currently adequate to support the design loads, material redistribution will allow sheet thickness downgaging. Consider the following:

- Reduction in sheet thickness results in reduction in purchased cost of sheet.
- Reduction in sheet thickness results in more rapid and more uniform heating, resulting in lower cycle times and higher productivity.
- More uniformity in sheet heating can result in fewer surface problems such as scorching, off-gassing, or blistering.
- Reduction in sheet thickness may result in less sag since the weight of the sheet is reduced.
- Reduction in sheet thickness results in lowered forces required to stretch the sheet.
- Lowered forming forces may allow for deeper draws, faster forming, more surface texture.
- With lowered forming forces, the sheet does not need to be heated as much, meaning that further cycle time reduction is possible.
- Reduction in sheet thickness results in shorter cooling time on the mold.
- Reduction in sheet thickness may result in reduced trimming costs and efforts, in that dies may not need to be resharpened as frequently and trimming defects such as splits may not be as prevalent.
- Product shipping costs may be reduced since the parts weigh less.

There are two approaches to part wall thickness prediction. The first, a geometric method, has been used extensively in blow molding as well as thermoforming in Germany, Poland, Russia and Japan for more than a quarter century [26,55-57,75-83,85,87-90]. The method follows a protocol for the stretching of an infinitely extensible membrane over a surface of known geometry. No polymer properties are needed and since the method is manual, no computer is needed. The technique is called *Geometric Element Analysis* or GEA. The second method is based on *Finite Element Analysis* or FEA. It stretches a mesh-like membrane over a surface of known geometry. A causal stress-strain relationship is needed to predict the relative forces generated by the stretching. The method depends on forming a nodal network of elements and the simultaneous solution of the stress-strain equations at each of these elements. A relatively large-capacity computer is needed.

Geometric Element Analysis or GEA

The simplest illustration of GEA is draw-down of a sheet into a conical mold, as shown in Fig. 7.28. At time θ , a sheet of initial thickness, t_0 , has been drawn into the cone of angle β to a depth, h_1 . The sheet is in contact with the mold surface for

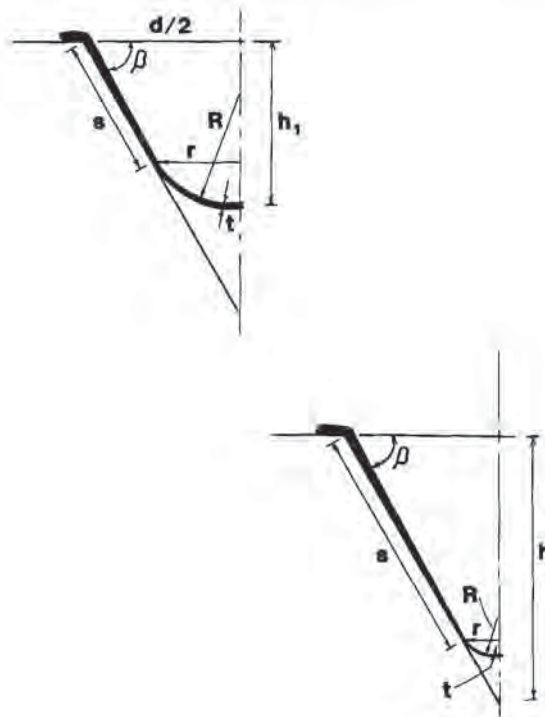


Figure 7.28 Geometry and coordinates for progressive draw-down into female conical mold

a diagonal distance or slant height, s . That portion of the sheet not in contact with the mold forms a spherical cap of radius, R . The plastic sheet in the cap has a uniform thickness, t . The cap area is:

$$A_{\text{cap}} = 2\pi R^2(1 - \cos \beta) \quad (7.45)$$

At time $\theta + d\theta$, a differential amount of material from the edge of the cap has been deposited on the cone surface. The cap material has been differentially stretched so that it is differentially thinner. A material balance [20] gives:

$$At|_{\theta} = At|_{\theta + d\theta} + A_{\text{cone}} \cdot t \quad (7.46)$$

$$2\pi R^2(1 - \cos \beta) = 2\pi(R + dR)^2(1 - \cos \beta)(t + dt) + (2\pi R t) \sin \beta ds$$

R is written in terms of h , s and β as:

$$R = h - \frac{s \sin \beta}{\sin \beta \tan \beta} \quad (7.47)$$

and $dR = -ds/\tan \beta$. The differential material balance is written as:

$$\frac{dt}{t} = \left[2 - \frac{\tan \beta \sin \beta}{(1 - \cos \beta)} \right] \cdot \left[\frac{\sin \beta}{h - s \sin \beta} \right] ds \quad (7.48)$$

This is integrated to yield:

$$\frac{t}{t^*} = \left[1 - \frac{s \sin \beta}{h} \right]^{\sec \beta - 1} \quad (7.49)$$

where t^* is the sheet thickness when $s = 0$. The sheet does not initially touch the cone side as it sags into the cavity. It touches when $A_o t_o = A_{\text{cap}} t^*$ at $s = 0$:

$$t^* = \frac{t_o}{2} (1 + \cos \beta) \quad (7.50)$$

Since $h = (d/2) \tan \beta$, the sheet thickness ratio is given in terms of the initial sheet thickness as:

$$\frac{t}{t^*} = \frac{(1 + \cos \beta)}{2} \left[1 - \frac{2s \cos \beta}{d} \right]^{\sec \beta - 1} \quad (7.51)$$

Example 7.15 shows that for $\beta = 60^\circ$, the sheet thickness decreases linearly with distance down the cone side. At the 60° cone tip, $s = d$, and $t/t_o = 0$. Appendix 7.I gives expressions for areal draw ratio as a function of draw-down. This thickness equation for a cone has been experimentally verified for many amorphous polymers [14,20,23,86].

Example 7.15 Slant Height Wall Thickness for 60° Cone

Determine the expression for wall thickness for thermoforming into a 60° cone.

From Equation 7.49, for $\cos 60^\circ = \frac{1}{2}$, $\sec 60^\circ = 2$, $t^* = 3/4$, and:

$$\frac{t}{t_o} = \left(\frac{3}{4} \right) \left[1 - \frac{s}{d} \right]$$

The wall thickness for a 60° cone is linear with slant angle.

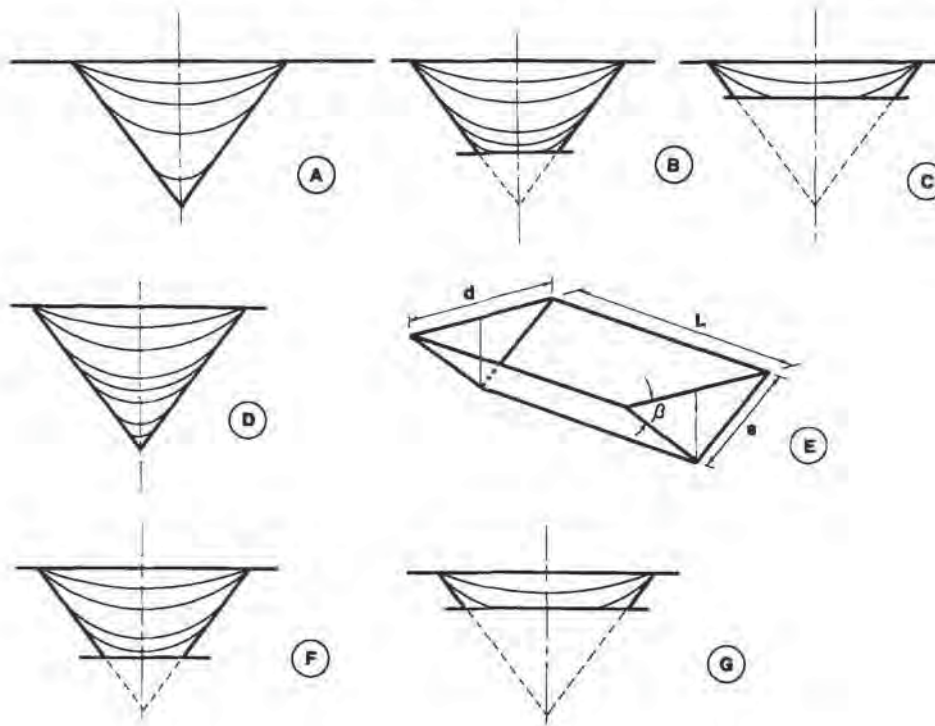


Figure 7.29 Various geometric shapes that have been analyzed using geometric analysis: (A) Full cone; (B) deep truncated cone; (C) shallow truncated cone; (D) triangle or wedge-shaped channel; (E) prism; (F) deep truncated wedge; (G) shallow truncated wedge

Note that this derivation depends solely on part geometry. No material properties are required. Initial sheet thickness and material temperature can only affect the depth of draw and not material distribution. Thickness equations for other shapes such as those shown in Fig. 7.29 are also available and are tabulated elsewhere [20,24,25]. For even the simplest three-dimensional shapes such as truncated wedges, these equations are very complex and a computer is needed to rapidly obtain meaningful functional relationships. A more functional approach, GEA, segments the mold geometry into very simple geometric elements, calculates the relative thickness reduction in those elements, then combines the results for an overall view of the local thickness.

GEA assumes that any thermoform mold can be described by combinations of simple shapes. Differential material balances on these simple shapes result in simple equations. The first step is *sectioning*. The mold is envisioned to be divided into sections. Each section is idealized as one of five forming shapes, discussed below. The sheet thickness at each of these sections is calculated and the calculated local sheet thickness is the product of the thicknesses of each shape used to arrive at that point [26]. The application of each of these shapes is the *design protocol*.

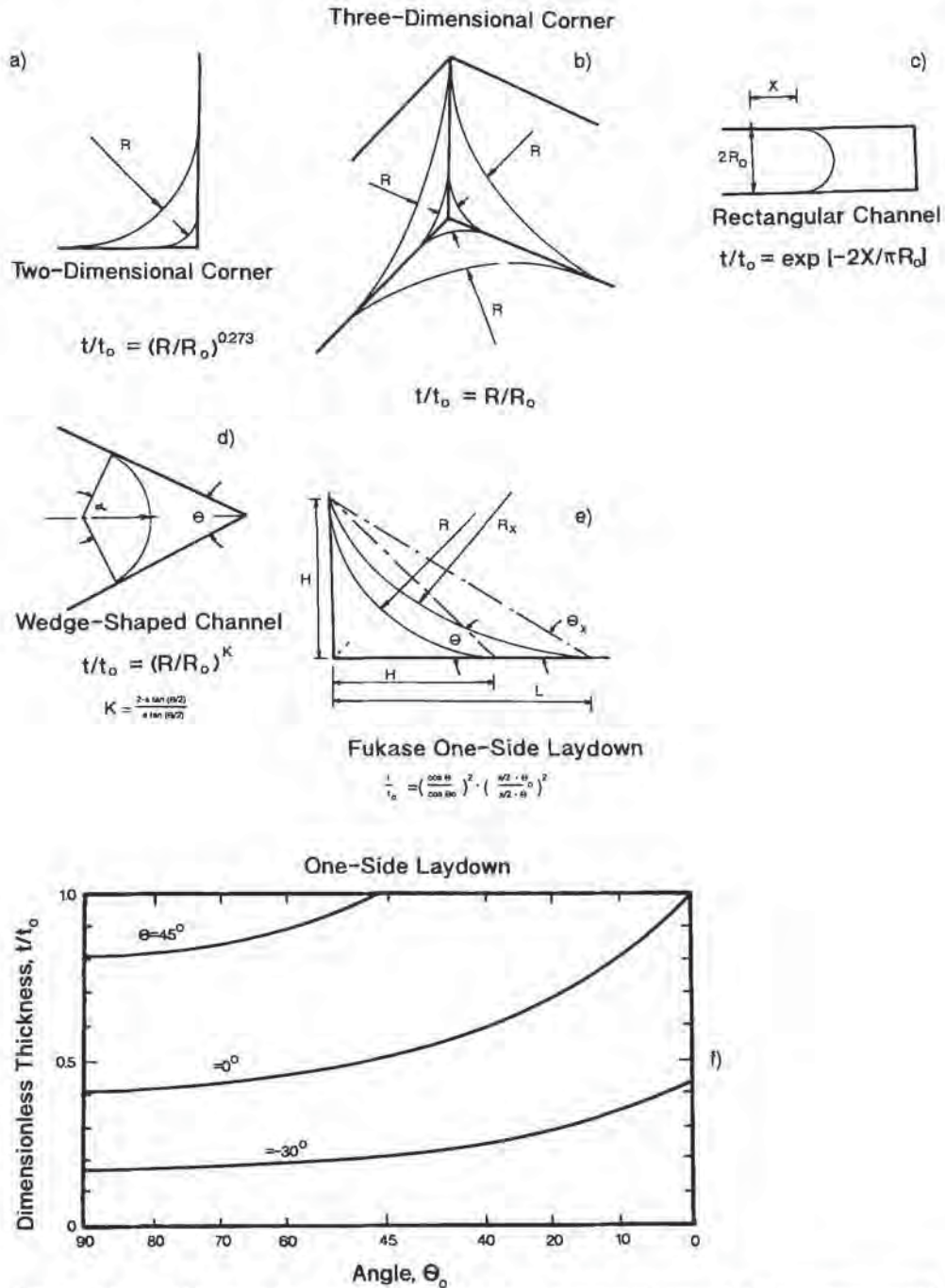


Figure 7.30 Five elements of geometric analysis: (a) Two-dimensional corner; (b) three-dimensional corner; (c) rectangular channel; (d) wedge-shaped channel; (e) one-side laydown; (f) relative thickness for one-side laydown

1. The *two-dimensional corner* (Fig. 7.30A). The thickness ratio is given as:

$$\frac{t}{t_o} = \left(\frac{R}{R_o}\right)^{4/\pi-1} = \left(\frac{R}{R_o}\right)^{0.273} \quad (7.52)$$

where t_o is the thickness of the quarter-circle of radius R_o .

2. The *three-dimensional corner* (Fig. 7.30B). The thickness ratio is given as:

$$\frac{t}{t_o} = \frac{R}{R_o} \quad (7.53)$$

Again t_o is the thickness of the sphere octant of radius R_o . Note that the 3D corners thin at a much greater rate than 2D corners¹.

3. *Parallel walls* (Fig. 7.30C). The rubbery sheet touches both walls at the same initial point. It freely expands as a two-dimensional semi-circle between the walls, with X being the distance down the walls and R_o is the half-distance between the walls. The thickness ratio is given as:

$$\frac{t}{t_o} = \exp\left[\frac{-2X}{\pi R_o}\right] \quad (7.54)$$

4. *Converging walls* or the *wedge* (Fig. 7.30D). The rubbery sheet expands freely as a two-dimensional arc of a circle. The thickness ratio is given as:

$$\frac{t}{t_o} = \left(\frac{R}{R_o}\right)^{\kappa} \quad (7.55)$$

Example 7.16 Chamfers and Radiused Corners

Compare the material thicknesses of a 2D corner of radius R and an equivalent corner with 45° chamfers.

The length of an arc forming a corner of radius R is given as:

$$L_{\text{radius}} = \left(\frac{\pi}{2}\right) \cdot R$$

The length of a chamfered corner, Fig. 7.31, is:

$$L_{\text{chamfer}} = \left(\frac{\sqrt{2}}{2}\right) \cdot R$$

The relative thickness ratio is given as:

$$\frac{t_{\text{chamfer}}}{t_{\text{radius}}} = \frac{\pi}{\sqrt{2}} = 1.11$$

Since stiffness is proportional to the cube of thickness, the chamfered corner is $1.11^3 = 1.37$ or 37% stiffer than the radiused corner.

¹ Note that other corner shapes are stiffer than sections of circles or spheres. Example 7.16 shows that a 45° chamfer yields a corner that is considerably stiffer than the equivalent 2D corner.

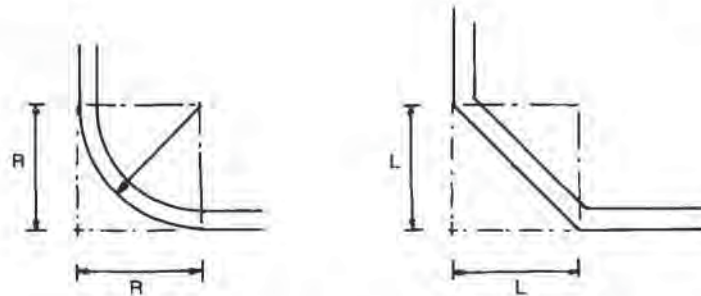


Figure 7.31 Geometric factors for (left) two-dimensional radius and (right) chamfer

where K is given as:

$$K = \frac{2 - \alpha \tan(\theta/2)}{\alpha \tan(\theta/2)} \quad (7.56)$$

When $\theta = \pi/2$, the walls intersect at right angles, and $K = 0.273$. The equation agrees with that for 2D corners, Equation 7.52. When $\theta > \pi/2$, the results are useful for prediction of draw-down into a two-dimensional corner with substantial draft. Example 7.17 illustrates this.

Example 7.17 Prediction of the Effect of Draft Angle on Wall Thickness

Consider a right angle corner where $R/R_n = 0.1$. Determine the thickness ratio. Then consider the case where the corner has a 10° draft.

From Equation 7.52, the thickness ratio for a right angle 2D corner is:

$$t/t_o = (0.1)^{0.273} = 0.533$$

From Equation 7.55, for $\theta = 100^\circ$, $K = 0.202$. Therefore the thickness ratio for a 2D corner with 10° draft is:

$$t/t_o = (0.1)^{0.202} = 0.628$$

If stiffness is a design criterion, the corner with draft is $(0.628/0.533)^3 = 1.636$ or more than 64% stiffer than that without draft.

5. *One-side lay-down* (Fig. 7.30E). This was first used in blow molding [26]. The concept is somewhat difficult to comprehend. Basically, one edge of the sheet pivots against a mold point while the other edge lays onto the mold surface. It is considered here only in two dimensions. It always represents an intermediate step. As soon as the sheet touches all intersecting walls at the same relative angle, the design criterion shifts to one of the other four cases. In the case of right-angle two-dimensional intersecting walls, this occurs when the angle $\theta = 45^\circ$ or $\pi/4$. The

initial angle, θ , that the sheet forms with the pivot point is usually greater than 45° ¹. The thickness ratio is given as:

$$\frac{t}{t_0} = \left[\frac{\cos \theta}{\cos \theta_0} \right]^2 \cdot \left[\frac{\pi/2 - \theta_0}{\pi/2 - \theta} \right]^2 \quad (7.57)$$

Figure 7.30F gives a plot of thickness ratio as a function of θ with θ_0 as a parameter.

In addition to the five basic elements given above, some ancillary expressions are valuable. In order to apply the sectioning method, it is necessary to determine *a priori* whether the freely expanding sheet touches the sides of the mold before or after it touches the bottom of the mold. A shallow mold is defined as one in which [27]:

$$H < \frac{L \sin \beta}{2(1 + \cos \beta)} \quad (7.58)$$

where L is the shortest side of the mold and β is the angle of the mold at the rim (Fig. 7.32) [28]. For a mold with right angle sides, $\beta = 90$ and the mold is shallow if $H < L/2$. For a long shallow mold, where the length, L , is much greater than the width, W , the uniform thickness of the sheet at the point of its contact with the bottom is given as:

$$\frac{t}{t_0} = \frac{L'^2}{L'^2 + 4H^2} \quad (7.59)$$

where t_0 is the initial sheet thickness and L' is the length of the longer side. For a shorter mold, it is recommended that the thickness ratio be calculated from Equation 7.59 first for $L = L'$, then $L = W$ and that the product be considered the thickness ratio:

$$\frac{t}{t_0} \approx \left[1 + \frac{4H^2}{(1/L^2 + 1/W^2)} \left(\frac{4H^2}{LW} \right)^2 \right]^{-1} \quad (7.60)$$

For a deep mold, the sheet contacts the mold walls before it contacts the bottom. As a result, the sheet deformation and thinning is calculated from parallel walls or the wedge arithmetic.

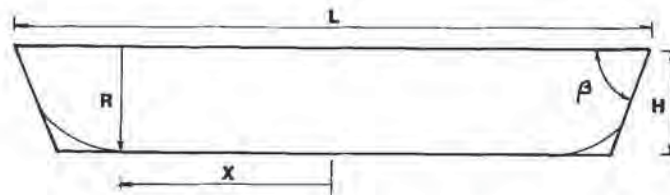


Figure 7.32 Geometric factors for shallow rectangular mold [28]

¹ For forming into a recess or undercut, θ_0 can be less than 45° . Care must be taken in laying out the segment to ensure that the proper pivot point is chosen.

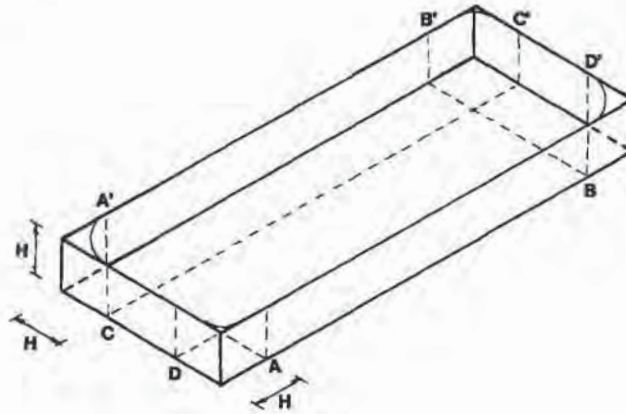


Figure 7.33 Sequential factors for geometric analysis of shallow rectangular mold [29]

The protocol for a shallow mold (Fig. 7.33) [29] is as follows:

- Calculate the thickness ratio for the sheet as it just touches the bottom of the mold.
- Identify lines A-A', B-B', C-C', and D-D' as being H units from the projected zero radius two-dimensional corners of the mold.
- Identify lines E-E' and F-F' as being lines that bisect lines C-C', D-D' and A-A', B-B', respectively, as shown in Fig. 7.34.
- The bottom wall thicknesses at E-E' and F-F' are determined by applying one-side lay-down arithmetic.

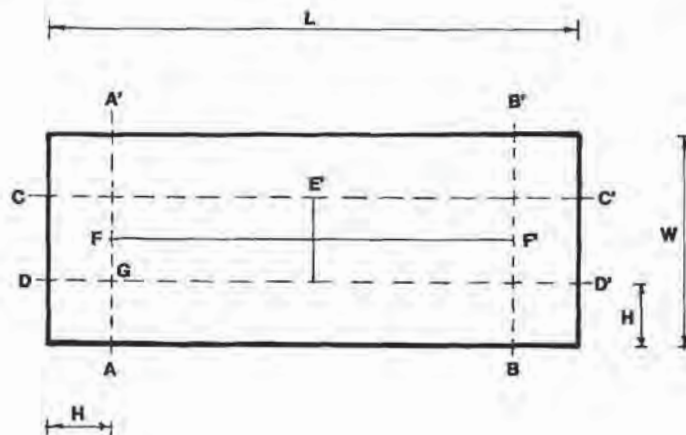


Figure 7.34 Top view of geometric analysis factors of shallow rectangular mold of Figs. 7.32 and 7.33

- The bottom thicknesses at points G are now determined by multiplying the thicknesses at E by those at F.
- The wall thicknesses in the 2D corners at E, E', F, F' and G are determined from the 2D corner Equation 7.50.
- The thickness in the 3D corners H is obtained from Equation 7.53. Make certain that the value used for t in this equation is the value obtained for G, above.
- Finally, calculate the 2D vertical wall thickness from the 2D corner, Equation 7.52.

Since the GEA method does not involve forces, the model is applicable to thin-gage and heavy-gage, alike [30,31]. Accuracies within 20% of measured thickness are expected. Typically, accuracy in horizontal 2D and 3D corners is within 10%. Vertical 2D corner measured values usually show the most variation with the arithmetic with errors of 30% common [32]. Figure 7.35 shows a comparison of measured and GEA-calculated wall thicknesses for a shallow mold.

The GEA method is also applicable to plug assist, as detailed below.

Finite Element Analysis

As noted, even though there are arithmetic equations for some relatively simple geometries, it is necessary to solve them with some form of electronic computer. Approximate thickness values for complex mold geometries are obtained by assuming that the actual shape of the mold surface is approximated by a simple geometry or series of geometries. Finite element analysis or FEA is a practical scheme for determining the wall thickness of well-behaved stretched elastic membranes. The general scheme is to overlay the surface to be stressed with a grid or network (Fig. 7.36). The grid pattern is triangular or quadrangular. Depending on the sophistication of the computer model, the elements are two-dimensional (2D) with X and Y coordinates but no thickness, or they are three-dimensional (3D), with X and Y coordinates and a finite thickness. The three-dimensional elements are sometimes layered through the thickness. It is thought that 3D elements are necessary when there may be heavy-gage sheet bending resistance over sharp edges or when shear is expected [33]. For most applications, 2D or thin membrane elements are acceptable. The elements are connected via nodes. The connected elements form a discrete surface or mesh that replicates the actual continuous surface (Fig. 7.36). Since a finite number of elements are used to describe an infinite number of points on the sheet surface, the analysis is usually called *finite element analysis*, or FEA. When forces are applied to the simulated surface, the elements distort, with the extent of distortion determined by balancing the forces and moments at each intersection or node. The relationship between applied force and resulting strain is called the *constitutive equation of state* of the material. Many hundreds or thousands of elements are needed to faithfully simulate structure response to applied load. Since many equations are needed for each node and three or four nodes are on each element, thousands of equations must be solved simultaneously to affect a solution. As a result the artificial computer time step must be very small to minimize error

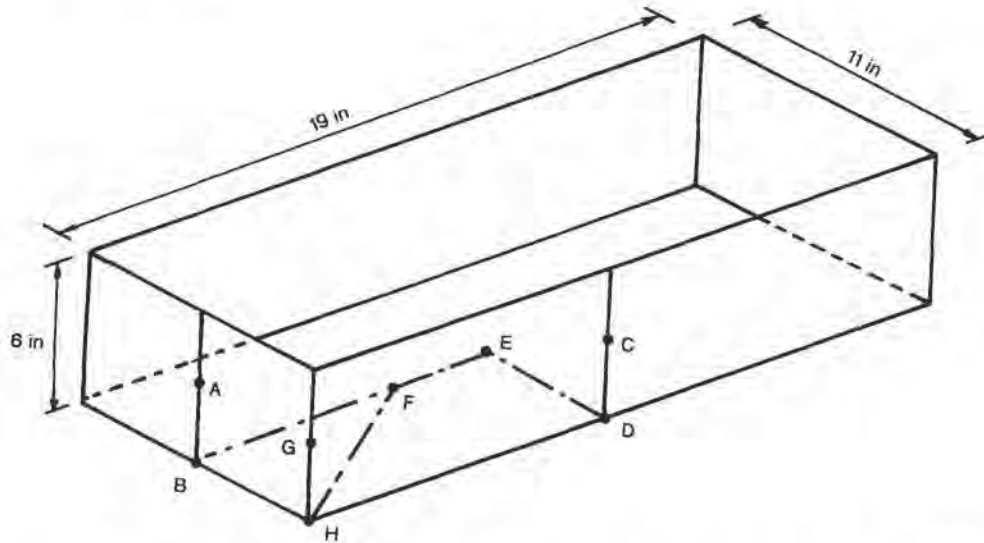


Figure 7.35 Geometric factors for draw-down into 19 × 11 × 6 in deep deli pan mold. Initial sheet thickness was 0.145 in. Three wall thickness values obtained at various locations:

| Location | Measured thickness (in) | Measured circles (in) | GEA calculated (in) | FEA calculated (in) | Comments |
|----------|-------------------------|-----------------------|---------------------|---------------------|-----------------|
| A | 0.080 | 0.085 | 0.074 | 0.070 | Short—midwall |
| B | 0.043 | 0.045 | 0.053 | 0.050 | Short—2D corner |
| C | 0.050 | 0.089 | 0.067 | 0.070 | Long—midwall |
| D | 0.045 | 0.054 | 0.051 | 0.050 | Long—2D corner |
| E | 0.069 | 0.066 | 0.062 | 0.060 | Bottom center |
| F | 0.048 | 0.047 | 0.049 | 0.050 | Bottom 45° |
| G | 0.070 | 0.071 | 0.042 | 0.040 | Vert 2D midwall |
| H | 0.021 | 0.038 | 0.015 | 0.020 | 3D corner |

generation during iteration. The simulation of a structure response to applied load requires extensive computer capacity, thousands of equations and many time steps. Despite these caveats, FEA is a given, accepted way of determining how a conceptual part will respond to applied load.

FEA has been used for many years for structural analysis. As a result, the methodology is well-established [31]. When FEA is extended to thermoforming, difficulties arise. The very large deformation experienced by the sheet, or equivalently, by the replicating elements, leads to rapid error generation and eventual instability in the surface contour. For the large scale deformations encountered in thermoforming, the area of a given element may increase ten-fold or more. If that element is deforming into a sharp corner in the mold, for example, its final size must

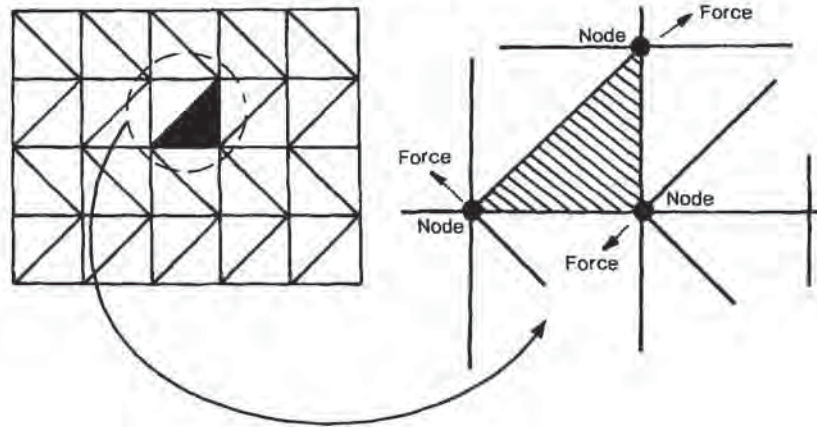


Figure 7.36 Geometric factors and methodology for finite element analysis, FEA

be as small as possible to replicate the actual forming process. This means its initial size must obviously be even smaller, and simple constitutive equations must be replaced with more complex hyperelastic equations as discussed in Chapter 4.

Consider the deformation of a triangular element. The location of the element at computer time is given by the $[X_1, Y_1, Z_1]$ coordinates of each of three nodes. The nodes can rotate, translate and separate under force. At computer time $\theta + d\theta$, there are new coordinates $[X_2, Y_2, Z_2]$, and there are nine coefficients describing the linear deformation of the element. For each iteration, the forces acting to deform the element are in equilibrium. Internal forces represent the sheet response to the applied forces. If W is the internal energy function and u is the displacement coordinate, the internal force for the i th element is:

$$F_{i,int} = \frac{-\partial W}{\partial u_i} \quad (7.61)$$

The external force for the i th element is the pressure, p , acting perpendicularly to the surface in the normal direction, n :

$$F_{i,ext} = p \cdot n_i \quad (7.62)$$

For the entire surface of the sheet, an equilibrium force balance is:

$$\sum_N (F_{i,int} + F_{i,ext}) = \sum_N \left(-\frac{\partial W}{\partial u_i} + p \cdot n_i \right) = 0 \quad (7.63)$$

where the summation is over all N elements. This set of equations are nonlinear in both geometrical and physical structure. The stress-strain constitutive equations of state discussed in Chapter 4 are used to determine the appropriate values for the internal force terms. In one computer model [34], the equations are solved using a standard Newton-Raphson iterative method [35]. In another, the Galerkin weighted residuals method is found to be the most efficient in finding appropriate values [36]. Iteration is performed in a given computer time step until the change in geometric

position for each node is less than some very small fraction of the sheet dimension. The nodal positions for each element are scanned to determine if any element has a node on or outside the mold $[X,Y,Z]$ plane. If so, that node is fixed against the mold surface, thus restricting the movement of the remaining nodes on that element. When all three nodes are against the mold surface, the element is immobilized. Computation ends when all the nodes are immobile or when the maximum allowable pressure is reached and the elements can no longer deform. Computational time is strongly dependent on the number of elements. Typically, up to ten iterations are needed for each $d\theta$ computer time step. Doubling the number of elements usually more than doubles the real time required to achieve a given $d\theta$ computer time step.

The key to successful FEA application to thermoformed parts having complex shapes is the proper initial selection of the sizes of elements across the mesh. Three approaches are used in current FEA programs:

- Initial specification of element sizes, without recourse to altering their sizes throughout the computation. This approach is quite successful if a standard protocol is followed. A coarse mesh is assumed for the first pass. Examination of the computer results reveals the regions showing great element areal increase. The mesh for a second pass is then constructed, with those specific regions having finer mesh. Additional passes may be required, each having finer meshes in critical areas.
- An adaptive mesh generator where, during computation, elements are split when their area increases beyond some proscribed limit.
- An adaptive mesh generator where, during the later stages of computation, elements inside critical regions such as corners or edges are remeshed automatically.

Regardless of the technique used, instability is still the major problem of commercial programs. Instability manifests itself as:

- Localized elements that increase very rapidly in area in very few computer time steps,
- Elements that interfere with other elements that are affixed to solid surfaces,
- Neighboring elements that try to occupy the same spatial areas, and
- Elements that are fixed to solid surfaces at computer time θ but are freed from the surfaces at computer time $\theta + d\theta$, such as with elements against plug assists.

Unfortunately, instability problems manifest themselves near the end of a computation time that may have lasted several hours. Figure 7.37 shows the initial chosen mesh for simple vacuum forming up into a five-sided box with an insert. Figure 7.38 shows the extended mesh at the time the computation was terminated by an instability caused by elements trying to occupy the same space. However, the scheme clearly demonstrates the formation of a web at each insert corner. Figure 7.39 shows the local sheet thickness at the mid-plane in the YZ-direction. Figure 7.40 shows the forming sequence for forming over a five-sided male mold and Fig. 7.41 shows the thickness contours for the sheet having attained its final shape¹. The actual practice

¹ These FEA programs use hyperelastic models such as the Ogden or Mooney-Rivlin model discussed in Chapter 4. As a result, mathematically, forming is instantaneous. The intervals shown are therefore computed forming intervals, not real time intervals.

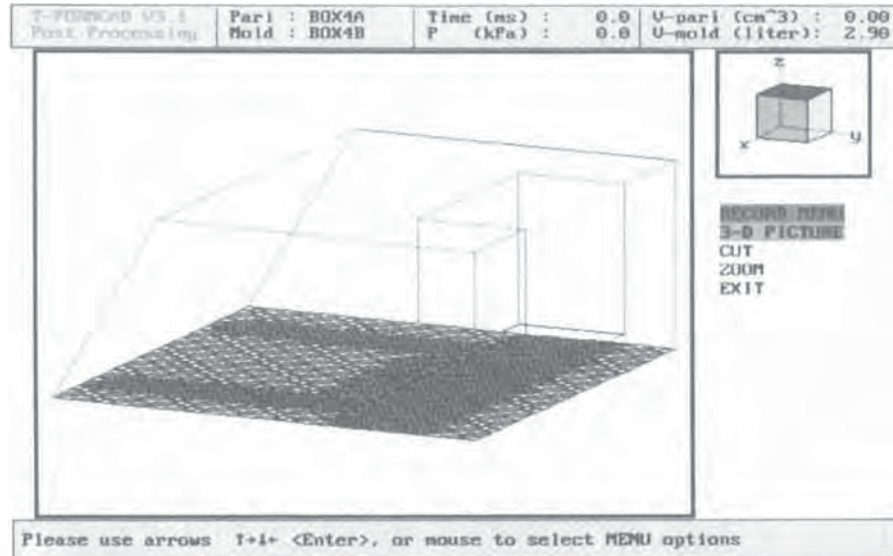


Figure 7.37 FEA-gridded sheet positioned over female mold, shown as dotted line. T-FormCad Program, Hamilton ON Canada

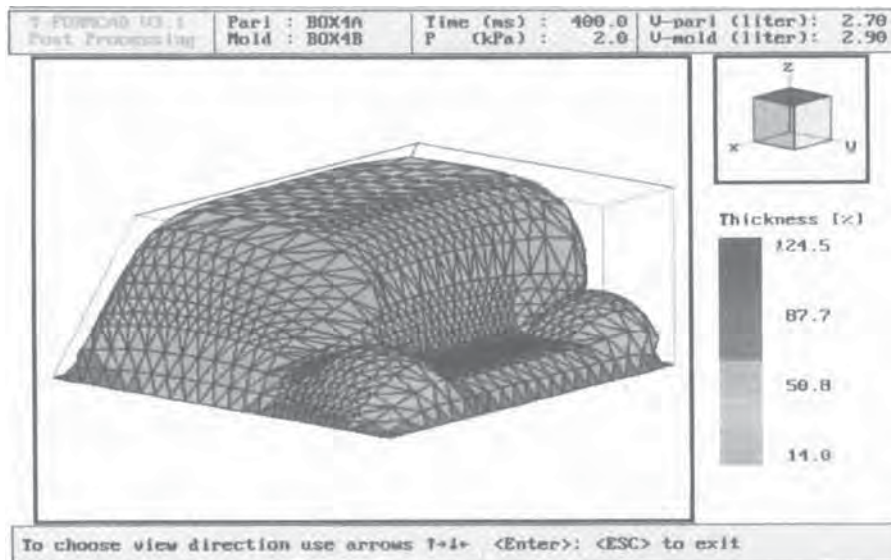


Figure 7.38 FEA sheet stretched into mold, showing corner element “buckling” and element “webbing”

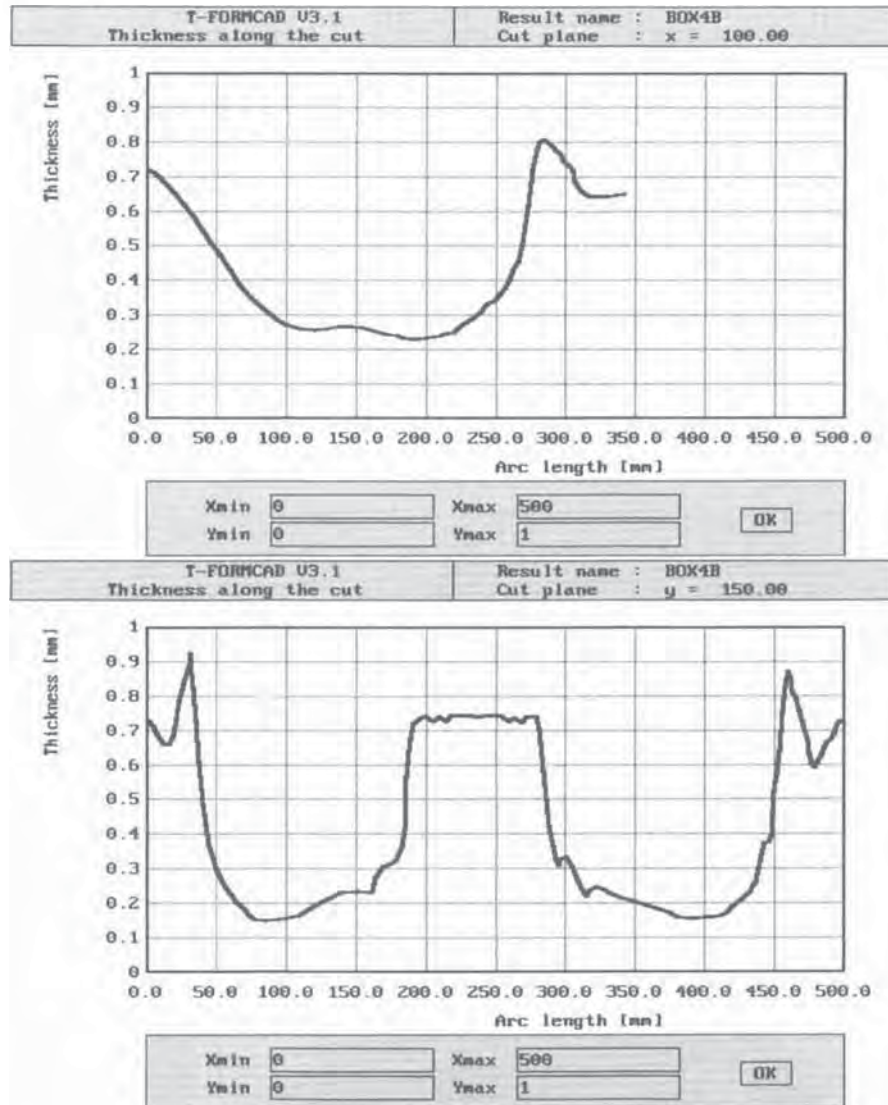


Figure 7.39 FEA-calculated local sheet thickness through the lengthwise and widthwise center of Fig. 7.38

of folding of plastic against outside three-dimensional corners is tricky, with webs frequently formed. Figure 7.42 demonstrates a wrinkle that is in many respects the FEA equivalent of a web.

An extensive effort is underway to verify FEA models. For example, the Treloar experiment in which the inflation pressure passes through a maximum as a rubber

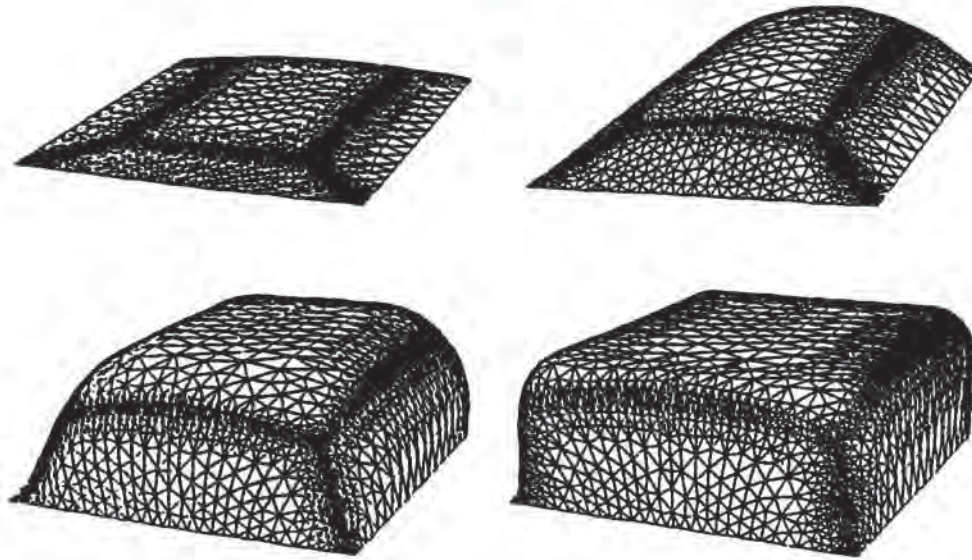


Figure 7.40 FEA computer-time plot of sheet formation over male five-sided box. PITA program by A.C. Technology, Ithaca NY. [32]. Used with permission of Society of Plastics Engineers, Inc.

sheet is inflated [37], is considered a true test of the stability of the simulation arithmetic. Figure 7.43 compares the Treloar data with an FEA program using neo-Hookean stress-strain elasticity and a special limit point algorithm [38]. Figure 7.35 shows a comparison of GEA and FEA results with experimental data. Although FEA should yield more accurate wall thickness results than GEA, it is apparent that the two analytical models agree more with each other than with the experimental data. Figure 7.44 shows a comparison of experimental wall thickness measurements for several polymers with an FEA model. Even though the polymers have forming temperatures more than 100°C apart, the experimental data agree better with each other than with the computer values [70]. Since these polymers have widely diverse stress-strain curves at their forming temperatures, the implication is that geometry dominates local wall thickness distribution, not polymer properties.

General Comments on Plug Design

A substantial effort is needed to properly shape plugs. Generally, plug shape for symmetrical products such as cups begins as either a blunt-nosed tapered cylinder or as a truncated cone with generous edge radii (Fig. 7.45). Usually, the design is material-safe. Plug material is then removed on a trial-and-error basis, depending on the location and intensity of the plug mark. For unsymmetric parts, plug design is trial-and-error from the beginning. Regardless of the initial shape of the plug, the final plug will have generous corner radii and domed rather than flat surfaces. Plug

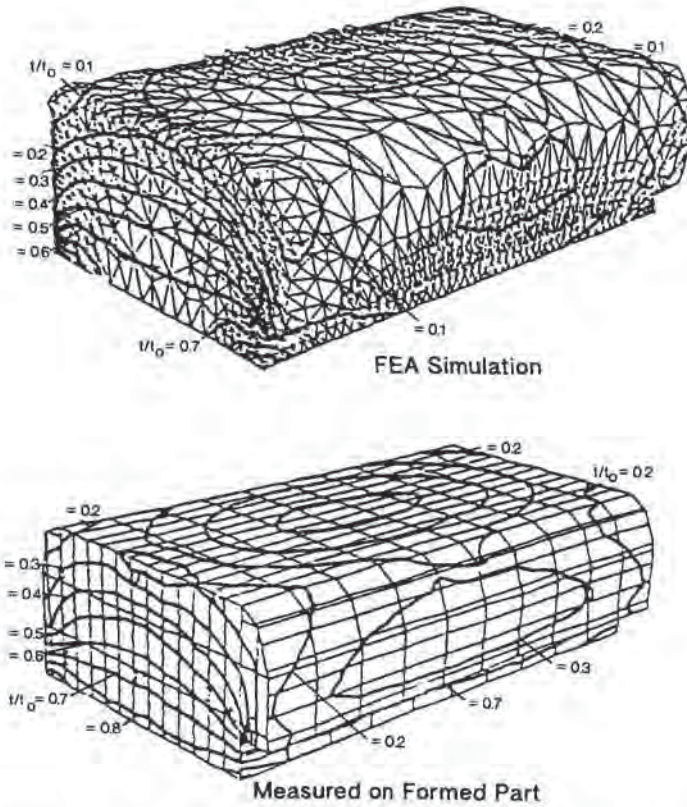


Figure 7.41 Comparison of calculated and experimental wall thickness distribution for male five-sided box. See Fig. 7.40

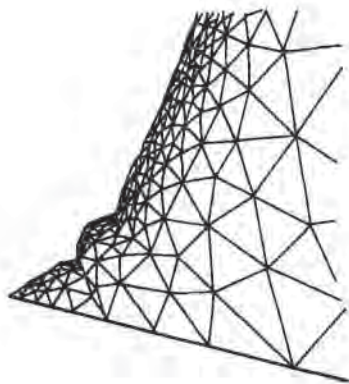


Figure 7.42 Finite element analysis, FEA of corner of sheet draped over male mold. Figure redrawn from [32]

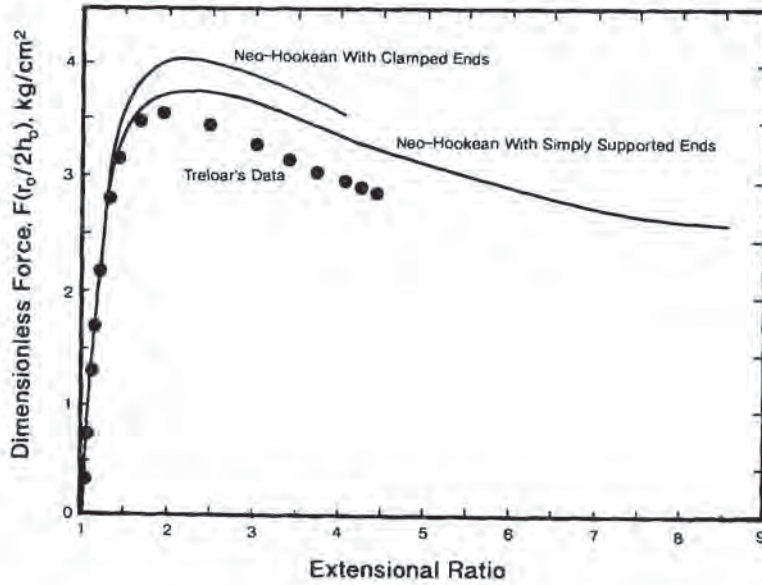


Figure 7.43 Internal check on computer results—comparison with inflation of rubber sheet, solid circles [37]

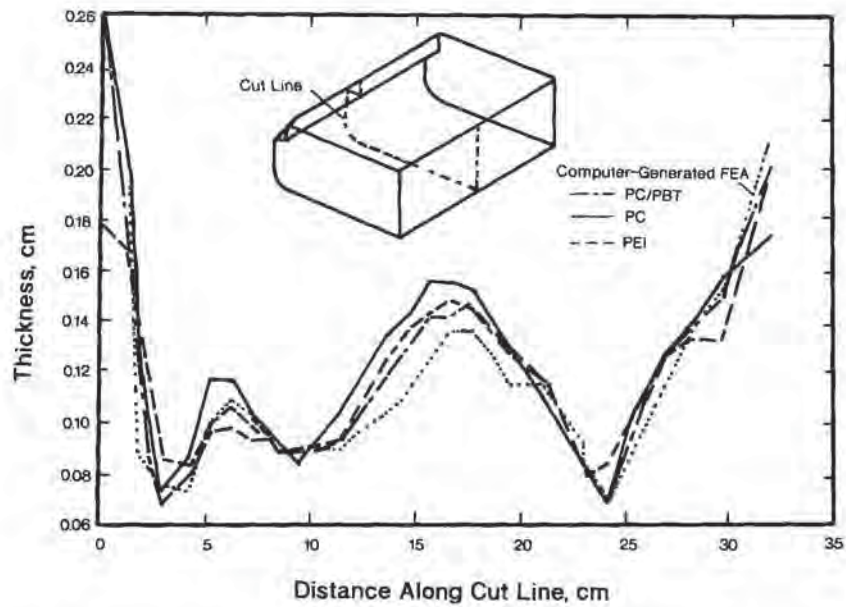


Figure 7.44 Comparison of local thermoformed wall thicknesses of several polymers with general electric PITA finite element analysis, FEA [70]

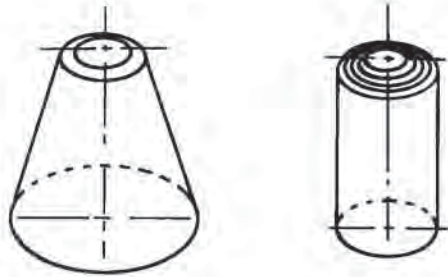


Figure 7.45 Plug geometries for symmetrical products. (Left) Truncated cone with generous radius and (right) blunt-nosed cylinder

functions are discussed in detail in Chapter 4. For a female mold, the plug usually moves along the center axis of the mold. For a male mold, the plug moves along a line that bisects a corner (Fig. 7.46). For a male portion of a female mold, the plug may be hollow. For a boss, the plug may be a ring (Fig. 7.47). Plugs can be articulated to allow plastic sheet to be tucked under a lip or moved out of vertical plane to minimize a web on the female portion of a male mold.

Consider a prototypical flat symmetrical plug of Fig. 7.23, with radius b and penetration depth δ , stretching a sheet of radius a . The sheet thickness ratio is:

$$\frac{t}{t_0} = \left[1 + \left(\frac{\delta}{r \ln a/b} \right)^2 \right]^{-1/2} \quad (7.64)$$

where r is the sheet radius, $b < r < a$ [22]. The sheet thickness on the plug surface is t_0 . At values of δ/a greater than about 0.4, the thickness ratio from b to a is about equal to the radius ratio, b/a , as shown in Example 7.18. The initial volume of plastic is $V = \pi a^2 t_0$. The sheet is distributed unstretched over the top of the plug and is

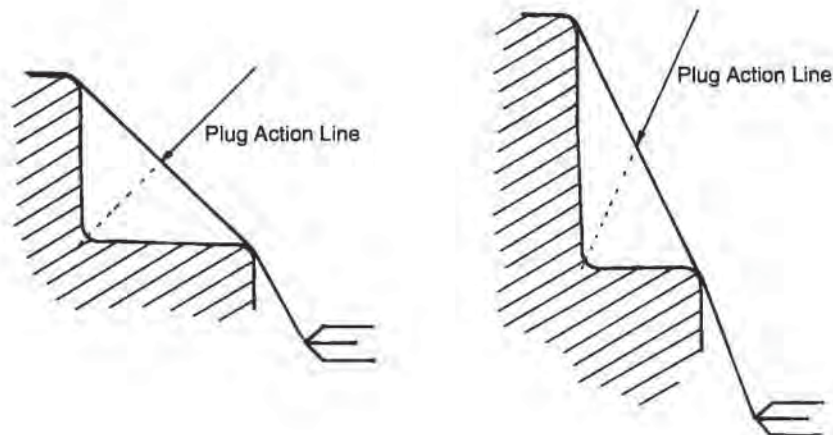


Figure 7.46 Examples of off-axis plug motion for male molds

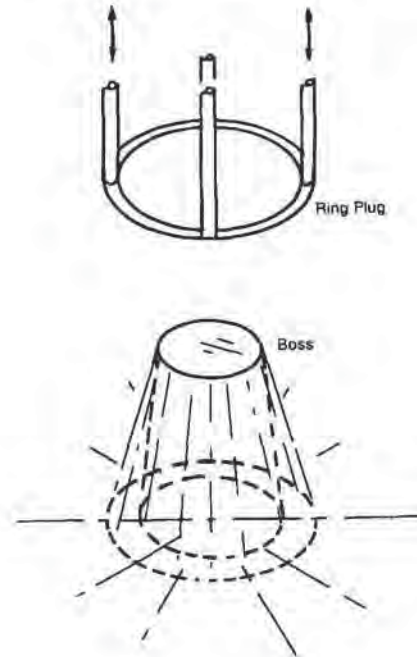


Figure 7.47 Ring plug for stretching sheet over bosses

stretched in a truncated cone between the plug edge and the mold rim. The volume of plastic on the plug surface is $V_p = \pi b^2 t_0$. The polymer volume in the stretched sheet is:

$$V_s = \int_b^a \delta \cdot t(r) \cdot 2\pi \, dr \quad (7.65)$$

This is approximated as:

$$V_s \approx \delta \cdot t_{\text{avg}} \cdot 2\pi(a + b)/2 \quad (7.66)$$

Since $V = V_p + V_s$, the average thickness ratio is given as:

$$\frac{t_{\text{avg}}}{t_0} = \frac{1 - b/a}{\delta/a} \quad (7.67)$$

As seen in Example 7.18, the average value is very close to the calculated value for $\delta/a > 0.5$ or so. The approximation fails as b/a decreases in value. Nevertheless, this simple computation can save extensive computer time if only approximate wall thicknesses are needed.

Example 7.18 Wall Thickness of Polymer Stretched with a Flat Plug

The thickness ratio of the plastic stretched between the edge of a flat plug and the rim of the mold is given by Equation 7.64. Determine the thickness ratio for $\delta/a = 1.0$ and $\delta/a = 0.2$ for $b/a = 0.8$. Compare with the appropriate r/a value. Then calculate the average sheet thickness ratio from Equation 7.66. Finally, compare the results for $\delta/a = 1$ and $b/a = 0.4$.

Equation 7.64 for this example for $\delta/a = 1$ is:

$$\frac{t}{t_0} = \left[1 + \left(\frac{a}{r \ln 1/0.8} \right)^2 \right]^{-1/2} = [1 + 20.08(a/r)^2]^{-1/2}$$

For $r/a = 1$, $t/t_0 = 0.218$.

For $r/a = 0.9$, $t/t_0 = 0.197$.

For $r/a = 0.8$, $t/t_0 = 0.176$.

The average sheet thickness ratio is given from Equation 7.67 as:

$$\frac{t_{\text{avg}}}{t_0} = \frac{1 - 0.8}{1} = 0.200$$

The average value is quite close to the calculated one.

Equation 7.64 for this example for $\delta/a = 0.2$ is:

$$\frac{t}{t_0} = \left[1 + \left(\frac{0.2a}{r \ln 1/0.8} \right)^2 \right]^{-1/2} = [1 + 0.803(a/r)^2]^{-1/2}$$

For $r/a = 1$, $t/t_0 = 0.745$.

For $r/a = 0.9$, $t/t_0 = 0.709$.

For $r/a = 0.8$, $t/t_0 = 0.666$.

The average sheet thickness ratio is given from Equation 7.67 as:

$$\frac{t_{\text{avg}}}{t_0} = \frac{1 - 0.8}{0.2} = 1.00$$

The average value is not accurate for this case.

Equation 7.64 for this example for $\delta/a = 1$ and $b/a = 0.4$ is:

$$\frac{t}{t_0} = \left[1 + \left(\frac{a}{r \ln 1/0.4} \right)^2 \right]^{-1/2} = [1 + 1.191(a/r)^2]^{-1/2}$$

For $r/a = 1$, $t/t_0 = 0.676$.

For $r/a = 0.7$, $t/t_0 = 0.540$.

For $r/a = 0.4$, $t/t_0 = 0.344$.

The average sheet thickness ratio is given from Equation 7.67 as:

$$\frac{t_{\text{avg}}}{t_0} = \frac{1 - 0.4}{1} = 0.600$$

The average value is not accurate in this case.

The plug tip shape aids in stretching the sheet, as discussed in Chapter 4. The effect of plug surface curvature is approximated by using an effective value of b , the plug radius. Consider a spherical plug tip (Fig. 7.48), of radius b , penetrating a sheet

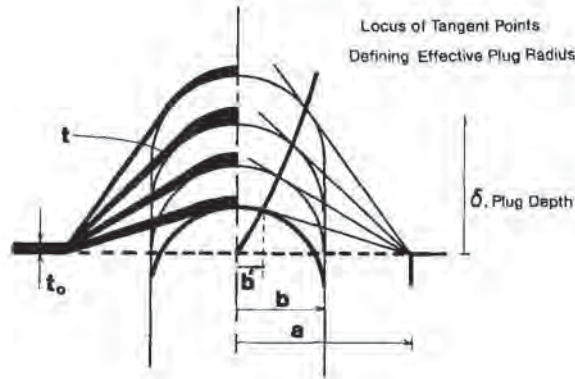


Figure 7.48 Spherical nose plug assist, showing locus of sheet tangent to plug during penetration

of radius a . Let b' be the effective plug radius. When the plug tip just touches the sheet, $b' = 0$. When the plug has penetrated to a depth $\delta = b$, the sheet touches it at $b'/a = (b/a)^2$. And when it has penetrated to a depth $\delta = 2a$, the effective reduced radius is $b'/a = 1 - \cos 2\alpha$, where $\alpha = \tan^{-1}(b/a)$. If the sheet does not slide on the plug, a conservative estimate of the sheet thickness at any plug depth, δ/a , is obtained by using the effective radius, b'/a , in Equation 7.64. As expected, draw-down at the same value of δ/a is less with a spherical plug than with a blunt one.

Plug Assist Analysis

The force required to stretch the sheet to a given penetration depth δ with the flat plug is given for large values of δ as [22]:

$$F = \frac{2\pi\delta E(T)t_0}{\ln(a/b)} \quad (7.68)$$

where $E(T)$ is the temperature-dependent neo-Hookean modulus discussed in Chapter 4. For the large strain model, the force is directly proportional to the penetration depth and the initial sheet thickness. Example 7.19 illustrates this. A similar relationship is used for the bull-nosed plug, except that b is replaced with b' , the effective plug radius.

Example 7.19 Linear Force for Shallow Plugging

A 1 in diameter dosage cup of 0.050-in sheet is to be stretched to a depth of 0.2 in using a flat plug of 0.8-in diameter. Determine the force if the neo-Hookean modulus of the plastic is 80 lb_f/in².

From equation 7.68:

$$F = \frac{2\pi\delta E(T)t_0}{\ln(a/b)} = \frac{2\pi \cdot 0.2 \cdot 80 \cdot 0.05}{\ln(1/0.8)} = 22.5 \text{ lb}_f$$

Since the area of the plug is $\pi(0.8)^2/4 = 0.5 \text{ in}^2$, the pressure needed to push the plug is:

$$P = \frac{F}{A} = \frac{22.5}{0.5} = 45.1 \text{ lb}_f/\text{in}^2$$

The extent of sheet stretching over a plug tip is estimated from the force balance used for rim material draw-down. To obtain an appropriate thickness ratio relationship for stretching over a curved plug tip, a differential force balance is integrated over the length of plug travel. The force holding the sheet against the plug increases with increasing penetration. The component of tensile force stretching or sliding the sheet on the plug tip decreases with increasing plug penetration. Thus, any biaxial extension of the sheet in contact with the plug probably occurs just as the plug penetrates the sheet. In practice, stretching of the free sheet dominates throughout the plug motion.

As stretching continues, the stretching becomes nonlinear. The sheet is extended in a "plane strain" fashion. That is, the view of the sheet from the vertical shows no relative effect of the plug (Fig. 7.49), even though stretching is extreme [39,40,72]. The plane strain relationship between force and extension for the Mooney-Rivlin constitutive equation is given as:

$$(\lambda_1^2 - 1)^{1/2}(1 - \lambda_1^{-2}) = (F/2\pi)(2C_{01} + 2C_{10})h_0 \quad (7.69)$$

where F is the force applied to the plug to stretch the sheet and r is the radius position, $a < r < b$ (Fig. 7.50) [41]. The predicted force-deflection profile for a conventional rubbery sheet is compared with the experimental profile and with the linear version of Equation 7.69 in Fig. 7.51 [42]. As is apparent, the linear force-deflection profile representing the large strain solution overestimates the initial extent of deflection and underestimates the later extent of deflection. Figure 7.52 compares the analytical model, the FEA model and the experimental data [43].

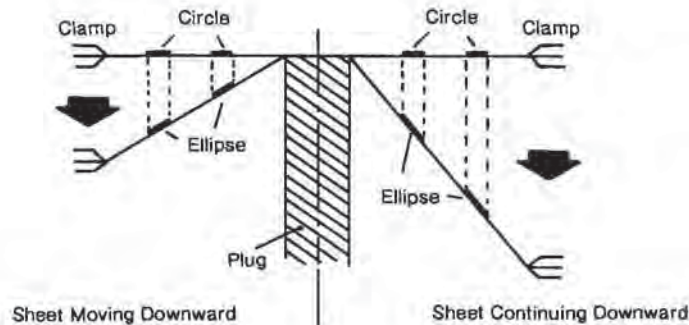


Figure 7.49 Schematic showing how distorted element appears undistorted when viewed from above

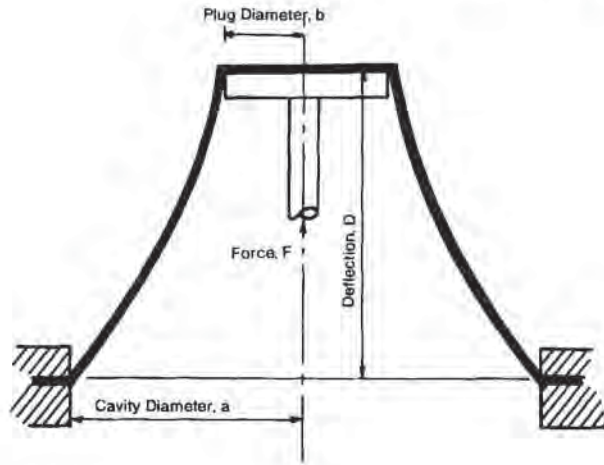


Figure 7.50 Plane strain stretching geometric factors

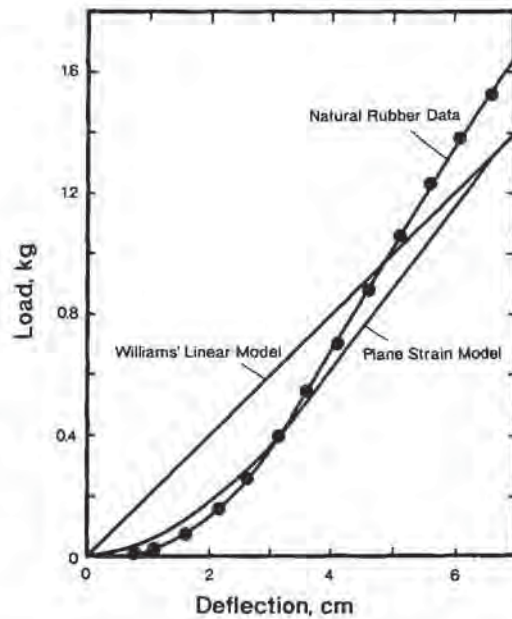


Figure 7.51 Experimental and theoretical load-deflection values for plug assisted plane strain stretching of natural rubber sheet. Solid circles are natural rubber data

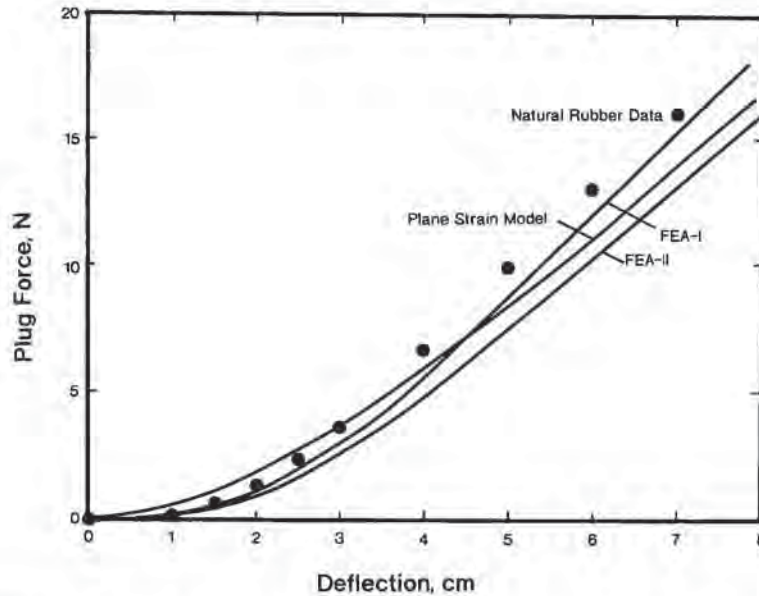


Figure 7.52 Comparison of experimental and theoretical load-deflection curves for plug assisted plane strain stretching of natural rubber sheet. Solid circles are natural rubber data. FEA models are described in [49]

Plug Design—Geometric Element Analysis

The GEA protocol discussed earlier holds for plug assist as well [44]. The stretching protocol is shown in a series of steps in Fig. 7.53. Plug assist is useful for the stretching of elastic membranes so long as the angle the sheet makes with the horizontal exceeds $\pi/4$ or 45° (Fig. 7.53A). When the plug reaches its maximum, the sheet is stripped from the plug, as shown in Fig. 7.53B. The GEA element in Fig. 7.53A and 7.53B is one-side lay-down. Once the sheet is horizontally tangent with the plug face, it is stripped from it (Fig. 7.53C, 7.53E₁ or 7.53E₂). If the plug is near the bottom of the mold, the sheet simply lays onto the mold surface without stretching. This is the most probable case. If the sheet is not near the bottom of the mold, the sheet continues to stretch in a semicircular or hemispherical fashion until it touches the mold bottom. Once the sheet is on the mold bottom, stretching takes place by one-side lay-down until the angle between the vertical and horizontal sections of the sheet reaches $\pi/4$ or 45° . After that, the sheet is stretched according to the 2D protocol discussed above. Figures 7.54, 7.55, and 7.56 show the relative effects of cavity depth on reduced thickness as a function of the relative depth of the plug. In all cases, $b/a = 0.7$ but the relative plug depth, δ/a varies. As is apparent, as the plug depth increases, the 2D corner thickness increases to a maximum value and the bottom thickness also increases. The reason for the latter effect is that the sheet in contact with the plug simply is laid down onto the bottom without substantial

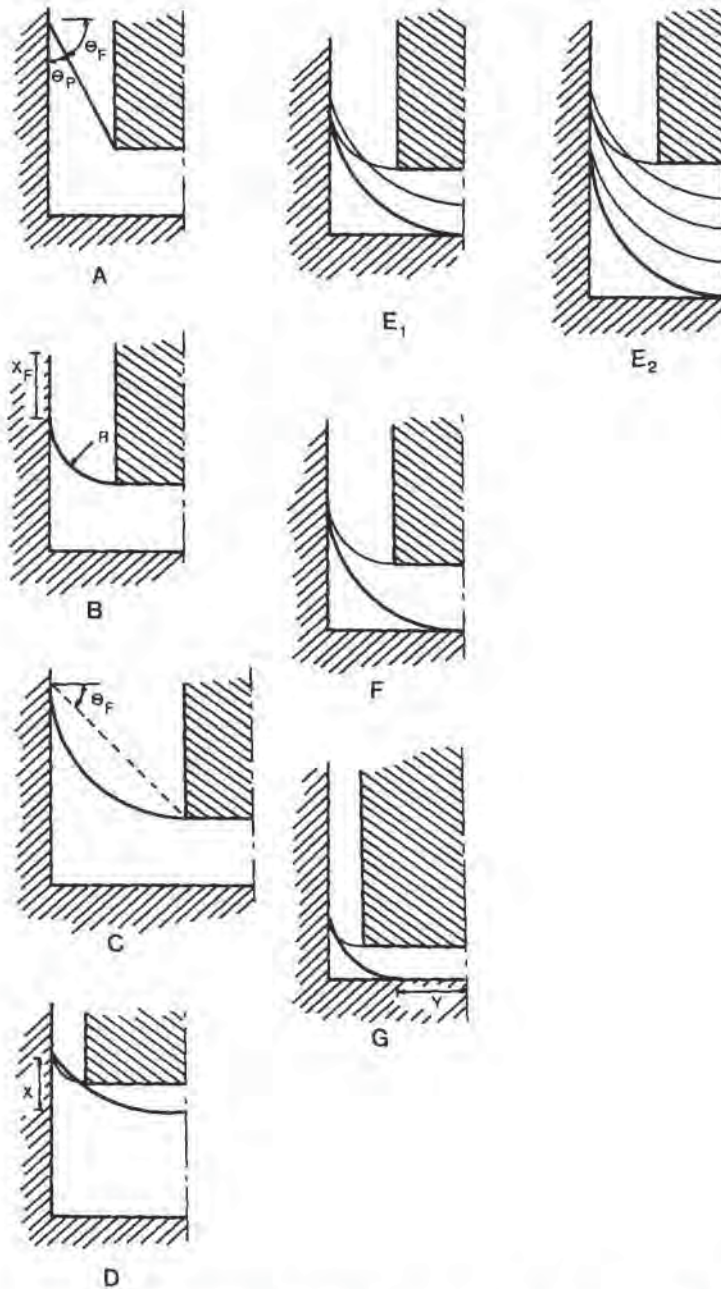


Figure 7.53 Sequence of stripping sheet from plug and laying sheet onto mold surface: A = End of plug travel; B = sheet laying onto vertical mold surface; C = sheet releases from plug when $F = 45^\circ$; D = sheet shape at instant of release from plug; E_1 = sheet laydown for deep plug, shallow cavity; E_2 = sheet laydown for shallow plug, deep cavity; F = sheet contacts mold bottom; G = sheet draws into mold corner

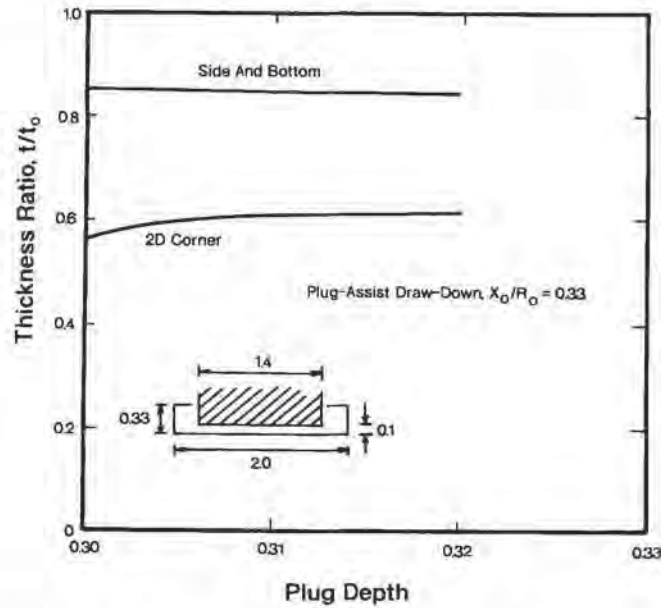


Figure 7.54 Computed plug depth-dependent sheet thickness at side, bottom and two-dimensional corner for $X_0/R_0 = 0.33$

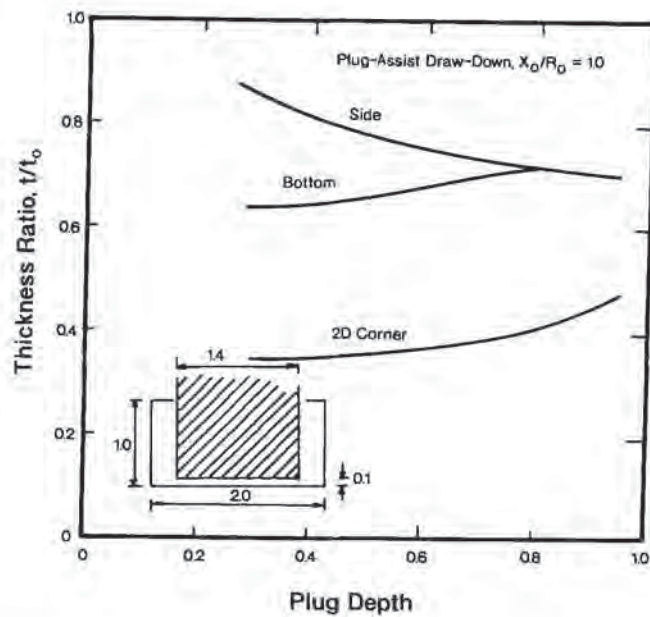


Figure 7.55 Computed plug depth-dependent sheet thickness at side, bottom and two-dimensional corner for $X_0/R_0 = 1.0$

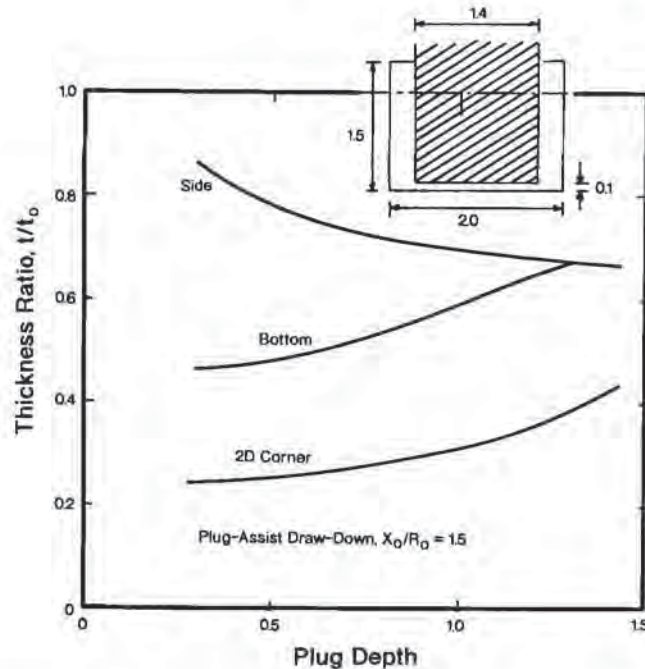


Figure 7.56 Computed plug depth-dependent sheet thickness at side, bottom and two-dimensional corner for $X_0/R_0 = 1.5$

stretching. The closer the plug comes to the cavity bottom, the less stretching occurs before the sheet contacts the cavity bottom.

Plug Design—Finite Element Analysis

One of the earliest tests for FEA models was the prestretching of the sheet with a plug. As noted, mechanical stretching of a membrane is plane strain deformation. All elements on the sheet surface appear undistorted when viewed in the stretching direction, regardless of the extent of deformation. This is seen for circular plug stretching a thin rubber membrane in Fig. 7.57. FEA yields accurate plane strain simulation of a barrel-shaped plug penetrating a rectangular sheet in top and side views (Fig. 7.58). The sheet grid shows distortion only along the vertical edges of the plug. Viscoelasticity is most significant in plug stretching in the region where the plug edge touches the sheet [46,85]. As noted in Chapter 4, the classic K-BKZ viscoelastic model is used [47]. As with the Ogden stress-strain model, the K-BKZ model theoretically has an infinite number of coefficients. As seen in Fig. 7.59 [46], three coefficients do not fit the strain-rate dependent curves very well. However, more constants result in extended computational times and potential instabilities [46].

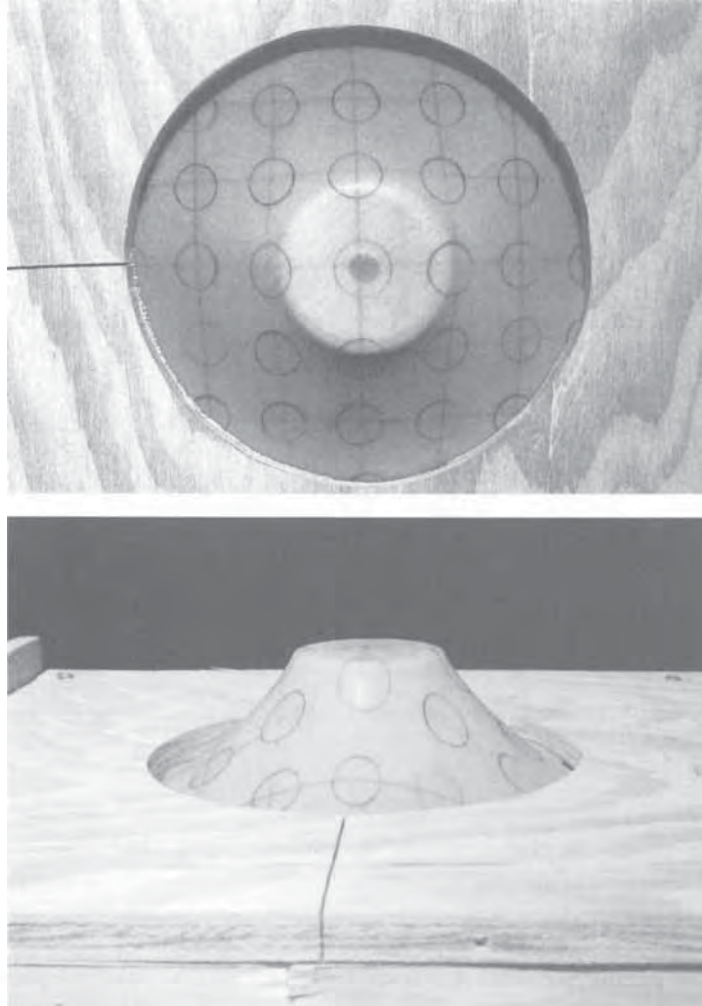


Figure 7.57 Photo showing plug-assist plane strain stretching. Top view (top) shows limited distortion of circles. Side view (bottom) shows substantial distortion of circles

If the sheet is to be freely stretched between the plug tip and the mold rim, the pressure on each side of the sheet must be the same (Fig. 7.60a). If the cavity pressure is allowed to build (Fig. 7.60b), the sheet is forced against the plug sides. The formed part will be thin in the rim area. If the cavity pressure is low, the sheet is forced against the mold sides (Fig. 7.60c). This reduces the effectiveness of the plug and results in parts that are thin in corners. Control of sheet position becomes much more difficult as b/a approaches unity. A tapered plug stretching sheet into a mold having the same sidewall taper helps overcome this lack of control (Fig. 7.60d).

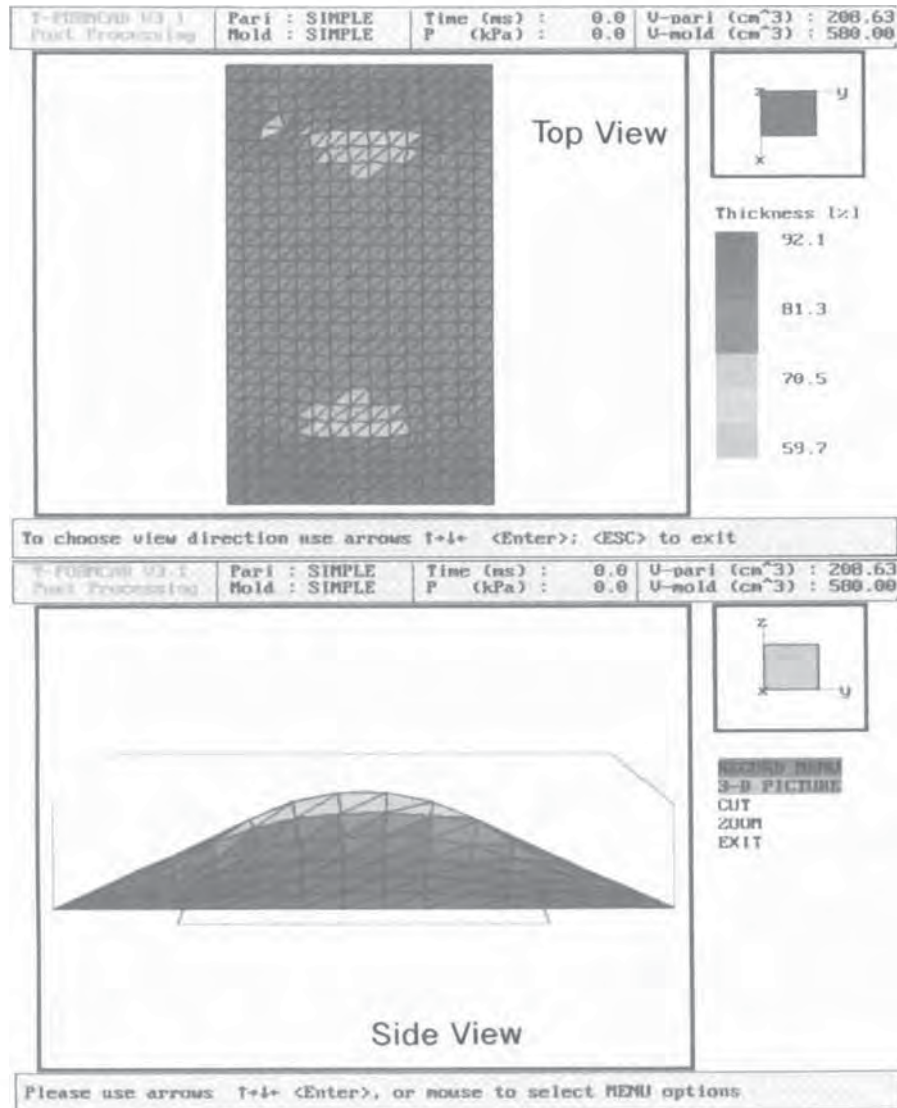


Figure 7.58 Top and side views of finite element analysis, FEA solution of sheet stretched over shaped plug. FEA program is T-FormCad from McMaster University

From practical considerations [44,68,84], polymers are elastic liquids. For GEA and FEA running without the K-BKZ option, the sheet is treated as a rubbery elastic membrane. As a result, when the sheet is stripped from the plug, the instantaneous response of the sheet, prior to any additional stretching, is to elastically recover to a uniform sheet thickness in the free portion of the sheet. The sheet that adheres to the mold surface during the plugging phase is assumed to keep its local thickness

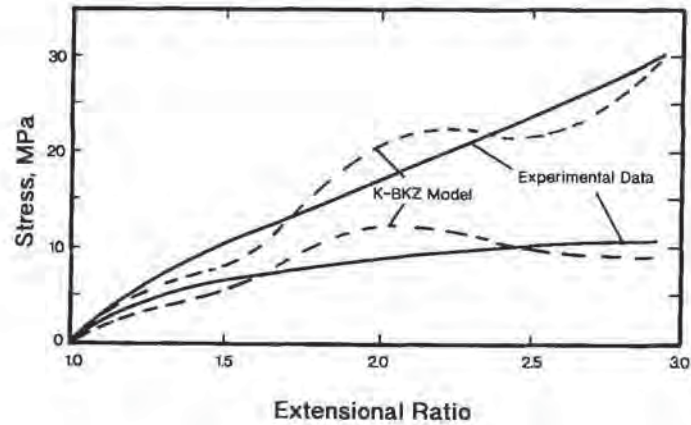


Figure 7.59 Stress-strain comparison of K-BKZ viscoelastic model with experimental data at two temperatures. Redrawn from [46]

throughout the rest of the stretching sequence. As a result, the ideal elastic sheet response produces a part wall thickness discontinuity at the point of elastic recovery (Fig. 7.61a) [48]. This discontinuity usually occurs on the side wall of the part and

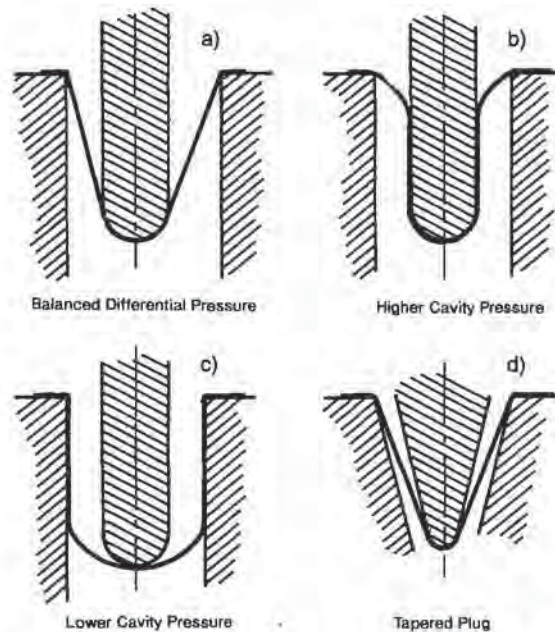


Figure 7.60 Schematic effect of differential pressure on draw-down during plug penetration

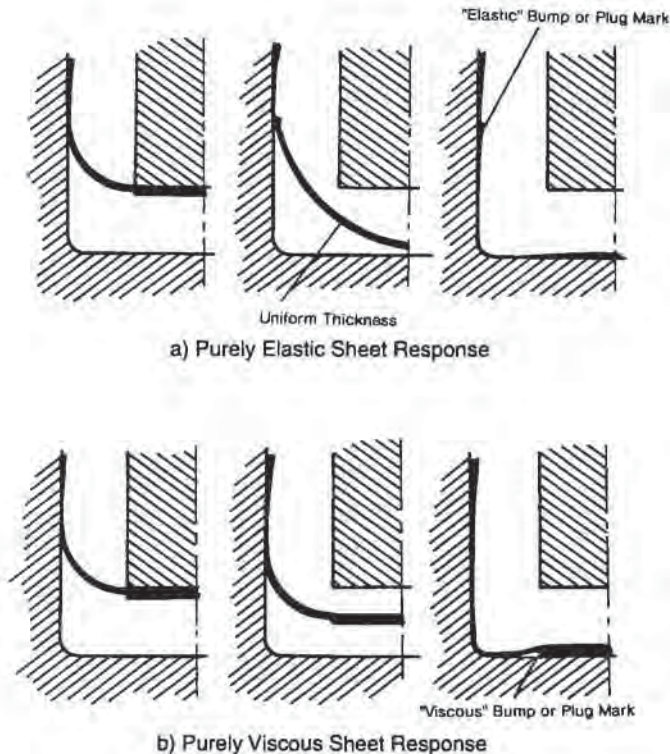


Figure 7.61 Schematic local wall thickness as sheet leaves plug. (a) Purely elastic response and (b) purely viscous response

is usually called a plug mark or chill mark. On the other hand, if the sheet is considered to respond in an ideally viscous way, no free sheet thickness recovery can occur. As a result, the ideally viscous sheet yields a part wall thickness discontinuity at the point where the sheet was attached to the plug surface (Fig. 7.61b). This discontinuity should occur on the bottom of the part. FEA computer simulation using the K-BKZ viscoelastic model shows how the sheet thickness changes as the sheet is stripped from the plug (Fig. 7.62) [49]. From examination of many plug-assisted thermoformed parts, ridges are occasionally seen on the side walls of parts. Bottom ridges are rarely seen. This is a strong indication that the sheet recovers more elastically than viscously as it is stripped from the plug.

In general, a blunt plug with generously rounded edges, essentially a compromise between a flat plug and a hemispherical one, is the best basic design (Fig. 7.63). The plug is usually kept warm, to within 20°C or 40°F, of the set temperature of the plastic or is insulated to minimize conduction heat loss, as discussed in Chapter 6 on plug materials. Heated plugs are needed whenever the polymer in contact with the plug must be drawn further in subsequent forming steps.

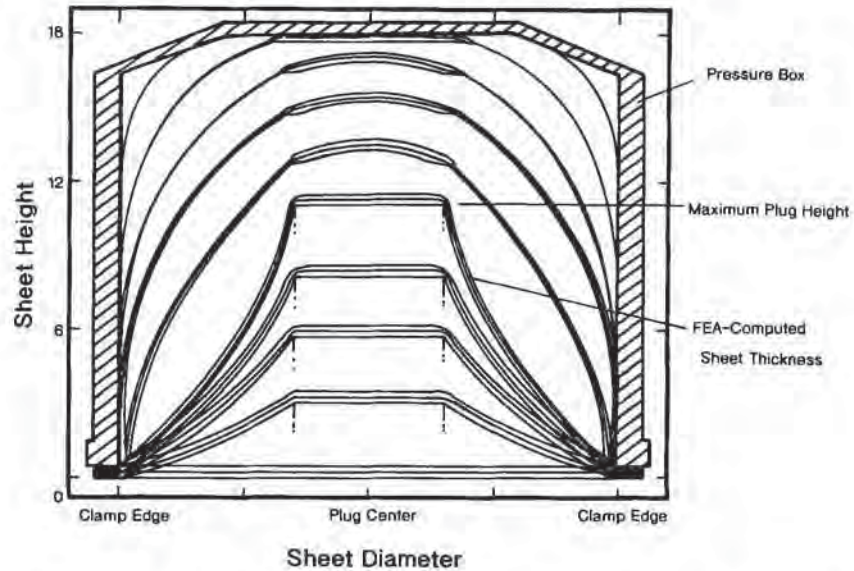


Figure 7.62 FEA computer simulation of sheet wall thickness during and after plugging, using K-BKZ viscoelastic model. Redrawn from [49]

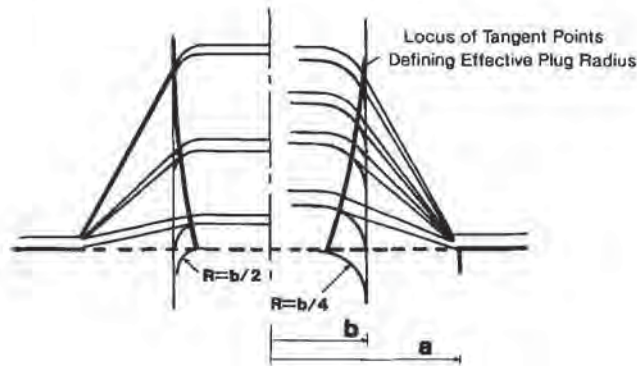


Figure 7.63 Schematic of blunt plug with generous corner radii

7.7 Regrind

Regrind is an economic necessity in all but the most mission-oriented thermoformed product. The polymer is exposed to shearing and heating throughout the extrusion, thermoforming and regrinding process. The way in which the trim from the forming

process is recovered, reground, stored, dried, and re-extruded is quite important to the success of a forming program.

Material Property Deterioration on Regrind

A large portion of the thermoformed sheet is web or trim. The efficient recovery and reuse of trim is essential to the economic viability of the process. For roll-fed sheet, rectangular shapes yield up to 25% trim. For small, round shapes, about 50% trim is expected. In cut sheet thermoforming, sheet-stock of standard dimension may be more economical than sheet cut to special size. But the use of standard dimension sheet-stock may lead to high percentages of trim. Even if trim can be totally recycled with minimum loss in material properties, the cost of regrinding, drying, and reextruding must be carefully considered in the process economics. This is discussed earlier in this chapter.

The action of heat and shear in grinding, extrusion and to some extent, thermoforming, can thermomechanically degrade most polymers. The typical mechanical effect is chain breaking. This results in loss of ultimate tensile strength, elongation at break, toughness or the area under the stress-strain curve, and impact strength. With some polymers such as RPVC or PP and other polyolefins, oxidative degradation occurs. This results in yellowing and odor generation. Polymers with extensive plasticizer packages become brittle owing to deterioration or loss of effectiveness of the packages. Flexible polyvinyl chloride or FPVC is a classic example. Polymers with fire retardants and UV stabilizers are particularly sensitive to the high time-temperature environments common in multiple recyclings. Regrinds of moisture-sensitive polymers must be carefully dried to minimize dehydrolysis. Condensation polymers such as PET, PA and PC are classic candidates. In glass-fiber reinforced polymers, fiber length is quickly reduced by mechanical grinding and shear in extrusion.

Usually, thermomechanical deterioration is not catastrophic. Small changes in observed physical properties usually do not cause dramatic changes in processing conditions. And final part performance is not substantially lowered. Nevertheless, the mechanical properties of a polymer that has been reground and recycled many times should be lower than those of the virgin polymer. As an example, CPET was dried, extruded, reground, dried, and mixed 50:50 with dried virgin PET and reextruded. The effect of reprocessing on mechanical properties is shown in Table 7.10. Note the loss in intrinsic viscosity or deterioration in molecular weight, and an indication of loss in elongation at break, ultimate tensile strength and Spencer impact. These property values losses are small and are usually not considered detrimental to the final part performance.

For thermoforming to be a viable technology, web, edge trim, beginning and ends of roll-stock and unacceptable formed parts must be recycled into new sheet. Regrinding, drying, re-extruding and re-thermoforming are mechanical and thermal environments that may cause loss in important polymer characteristics such as:

- Molecular weight,
- Impact strength,

Table 7.10 Effect of Regrind Material on Room Temperature Polyethylene Terephthalate Mechanical Properties (\pm Standard Deviation)

| Property | Run 1 virgin | Run 2 50% virgin | Run 3 50% virgin |
|---|-----------------------|----------------------|----------------------|
| Intrinsic viscosity | 0.83 | 0.68 | 0.68 |
| Secant modulus | | | |
| MD $\times 10^3$ lb _r /in ² | 2.59 (± 0.075) | 2.44 (± 0.06) | 2.45 (± 0.06) |
| TD $\times 10^3$ lb _r /in ² | 2.375 (± 0.135) | 2.07 (± 0.098) | 2.36 (± 0.167) |
| Percent elongation at yield | | | |
| MD | 10.0 (± 2.9) | 10.0 (± 0.7) | 9.8 (± 0.8) |
| TD | 10.2 (± 1.1) | 10.0 (± 0.7) | 9.7 (± 1.2) |
| Tensile strength, yield | | | |
| MD $\times 10^3$ lb _r /in ² | 5.0 (± 0.39) | 4.9 (± 0.20) | 5.1 (± 0.16) |
| TD $\times 10^3$ lb _r /in ² | 4.6 (± 0.15) | 4.6 (± 0.23) | 4.6 (± 0.54) |
| Tensile strength, break | | | |
| MD $\times 10^3$ lb _r /in ² | 8.3 (± 0.61) | 7.9 (± 1.90) | 7.0 (± 2.30) |
| TD $\times 10^3$ lb _r /in ² | 7.8 (± 0.39) | 7.1 (± 0.58) | 4.7 (± 1.08) |
| Spencer impact, 1000 g | 2.8 (± 0.65)* | 2.3 (± 1.03) | 2.4 (± 0.91) |

* Two of 5 specimens did not break at 6400 g

- Elongation at break,
- Tensile and flexural strengths,
- Tensile and flexural moduli,
- Fire retardancy,
- Ultraviolet resistance,
- Fibrous or particulate coupling agent effectiveness,
- Pigment color, and
- Fiber length.

Theoretically, in a closed loop process, a small amount of polymer is regrind and reprocessed many times. The arithmetic needed to predict the effect of regrind property loss on final part performance depends on:

- The way in which the specific property deteriorates with time at processing temperature, and
- The way in which the specific property of the regrind and that of the virgin polymer are melded.

The simplest form of closed-system reprocessing is shown in Fig. 7.64a [50]. The black box represents the effect of extrusion and forming processes. The effect of the regrinding process is ignored. Figure 7.64b includes the effect of the regrinding process on property deterioration. Figure 7.64c considers reprocessing of extruded but unthermoformed sheet and again ignores the regrinding process. As is apparent, more complex schemes can be considered.

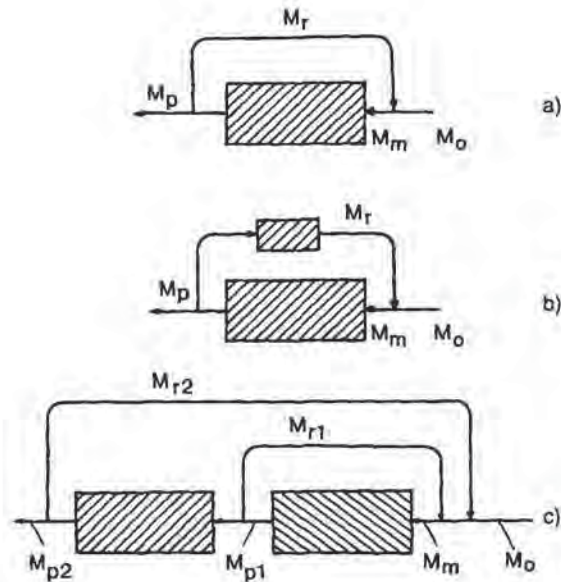


Figure 7.64 Closed-loop steady-state reprocessing or recycling of trim. (a) Represents effect of extrusion and thermoforming and ignores effect of regrinding. (b) Represents extrusion and thermoforming and includes effect of regrinding. (c) Represents separate effects of extrusion and thermoforming, with separate recycle streams being added to virgin

Single-pass property value loss data are relatively easy to generate [51-53,73]. Algorithms are used to relate single-pass property value loss data to steady-state property value loss. There are two general types of laws of mixtures:

- The *linear law of mixtures* for which the important property of a combined polymer stream is additive:

$$A = yB + (1 - y)C \quad (7.70)$$

where A is the property of the mixed stream, B is the property of polymer B , C is that of polymer C , and y is the weight fraction of B in the mixed stream.

- The *logarithmic law of mixtures* for which the logarithm of the important property of a combined polymer stream is additive:

$$\ln A = y \ln B + (1 - y) \ln C \quad (7.71)$$

This is also written as:

$$A = B^y \cdot C^{1-y} \quad (7.72)$$

In addition, there are several models to describe the way in which the polymer loses its important property. Three such models are:

- The *proportional property loss* is given as:

$$D = X \cdot M \quad (7.73)$$

Table 7.11 Typical Polymer Properties and Their Proposed Recycle Algorithmic Interactions [7]*

| Material property | Linear law of mixtures | | | | Logarithmic law of mixtures | | |
|-------------------------|------------------------|----------------|----------------|-------------|-----------------------------|----------------|-------------|
| | Linear loss | Declining loss | Power-law loss | Offset loss | Linear loss | Power-law loss | Offset loss |
| Tensile strength | × | | | | | | |
| Flexural strength | × | | | | | | |
| Tensile modulus | × | | | | | | |
| Flexural modulus | × | | | | | | |
| Elongation at break | | | × | | | | |
| Impact strength | | | × | × | | | |
| Impact strength (foams) | | × | | | | | |
| Ductility (toughness) | | | × | | | | |
| Fire retardancy | | × | | × | | | × |
| UV stability | | × | | × | | | |
| Oxidative resistance | | | | × | | | |
| Molecular weight | | | | | × | × | |
| Intrinsic viscosity | | | | | × | × | × |
| Melt viscosity | | | | | | × | |

* In many cases, experimental data are too few and so the proper method is frequently inconclusive. Furthermore, property loss may be so small that more than one algorithm may seem to fit. If so, the simplest algorithm should always be used

where M is the property before processing, D is the property after processing and X is a proportionality.

- The *power-law property loss* is given as:

$$D = X \cdot M^a \quad (7.74)$$

where a is an exponent, usually less than 1.

- The *offset property loss* is given as:

$$D = M - Z \quad (7.75)$$

where Z is a fixed amount of property.

Table 7.11 compares typical polymer properties and corresponding proposed algorithmic recycle types. The derivation for the linear property value loss-linear mixture case is given in Appendix 7.II. The resulting equation is:

$$\frac{M_x}{M_o} = \frac{X(1-Y)}{1-XY} \quad (7.76)$$

where M_x is the steady-state mixed property value, M_o is the property value of the virgin polymer, X is the fraction of property value retained by the polymer after a single pass through the processing equipment, and Y is the weight fraction of the recycled polymer in the mixed stream. The value of X is determined by standard

100% regrind/recycle studies. As noted in Appendix 7.II, if $X = 0.9$ and $Y = 0.5$, the specific property of the mixed polymer after three cycles is 83.5% of that of the virgin polymer and after an infinite number of cycles or steady state, the mixed polymer property is 81.8%.

Property Value Loss—Experiment and Protocol

There are several studies on material property deterioration with regrind [51-54]. Nearly all studies use conventional injection molding machines and focus on determining mechanical properties of 100% regrind after several passes. Standard processing conditions such as temperature and shear rate profiles and residence times are usually not given. As a result, extrapolation of these data to the thermoforming process is tenuous at best. Tables 7.12 and 7.13 give experimental and calculated values for multiple passes of 100% regrind high-impact polystyrene (HIPS) and ABS. Tables 7.14 and 7.15 give experimental and calculated values for the effect of regrind level on the second pass properties of HIPS and ABS. The agreement is relatively good, considering the scatter in the data and the assumption of simple laws of mixture and property loss.

Mechanical shear at melt condition seems to be the primary way in which polymer properties deteriorate *mechanically*. Mechanical grinding is a secondary way. Long residence time at melt condition in the extruder is the primary way in which polymers *thermally* deteriorate. Heating in the thermoforming oven is a secondary effect. As a result, an appropriate protocol for regrind studies of thermoformed web or trim should focus on extrusion rather than injection molding. One protocol follows:

Table 7.12 Comparison of Experimental and Calculated Impact Strengths and Elongations at Break for High-Impact Polystyrene [54]

| Property | Unit | Number of passes | | | | | | | |
|-------------------------|-------------------|------------------|------|------|------|------|------|------|--|
| | | 0 | 1 | 2 | 3 | 4 | 5 | 6 | |
| Impact resistance | | | | | | | | | |
| Measured | kJ/m ² | — | 17.0 | 15.0 | 14.0 | 15.0 | 13.0 | 12.0 | |
| Calculated ¹ | kJ/m ² | 18.7 | 17.0 | 15.4 | 14.0 | 12.7 | 11.5 | 10.4 | |
| Notched impact strength | | | | | | | | | |
| Measured | kJ/m ² | — | 5.4 | 4.1 | 3.3 | 4.0 | 2.5 | 2.1 | |
| Calculated ² | kJ/m ² | 6.3 | 5.2 | 4.3 | 3.6 | 3.0 | 2.5 | 2.1 | |
| Elongation at break | | | | | | | | | |
| Measured | % | — | 10.3 | 7.9 | 8.0 | 7.6 | 7.1 | 7.2 | |
| Calculated ³ | % | 12.7 | 10.3 | 8.9 | 8.1 | 7.6 | 7.4 | 7.2 | |

¹ Model used is: $M_{pN} = X^N \cdot M_o$ where $X = 0.833$

² Model used is: $M_{pN} = X^N \cdot M_o$ where $X = 0.907$

³ Model used is: $M_{pN} = X^N \cdot M_o + B \cdot (1 - X^N)/(1 - X)$ where $B = (1 - X) \cdot M_{asympt}$ and $X = 0.576$, $M_{asympt} = 7.0$ and $B = 2.97$

- Select a production extruder commonly used to produce thermoformable sheet.
- Establish the appropriate extrusion conditions to produce sheet at commercial rate.
- After steady state, obtain sufficient sheet for both the regrind study and the thermoforming study. Label this as "First Pass". This should be several hundred pounds or kg.

Table 7.13 Comparison of Experimental and Calculated Impact Strengths and Elongations at Break for ABS [54]

| Property | Unit | Number of passes | | | | | | |
|-------------------------|-------------------|------------------|------|------|------|------|------|-----|
| | | 0 | 1 | 2 | 3 | 4 | 5 | 6 |
| Impact resistance | | | | | | | | |
| Measured | kJ/m ² | — | 49.0 | 33.0 | 18.0 | 15.0 | 10.0 | 6.1 |
| Calculated ¹ | kJ/m ² | 72.9 | 49.0 | 32.9 | 22.0 | 14.9 | 10.0 | 6.7 |
| Notched impact strength | | | | | | | | |
| Measured | kJ/m ² | — | 25.0 | 13.0 | 10.5 | 7.6 | 4.1 | 2.3 |
| Calculated ² | kJ/m ² | 39.3 | 25.0 | 15.9 | 10.1 | 6.4 | 4.1 | 2.6 |
| Elongation at break | | | | | | | | |
| Measured | % | — | 24.0 | 10.4 | 8.6 | 8.9 | 8.0 | 7.7 |
| Calculated ³ | % | 96.4 | 24.0 | 10.9 | 8.5 | 8.1 | 8.0 | 8.0 |

¹ Model used is: $M_{pN} = X^N \cdot M_o$ where $X = 0.672$

² Model used is: $M_{pN} = X^N \cdot M_o$ where $X = 0.636$

³ Model used is: $M_{pN} = X^N \cdot M_o + B \cdot (1 - X^N)/(1 - X)$ where $B = (1 - X) \cdot M_{asymp}$ and $X = 0.181$, $M_{asymp} = 8.0$ and $B = 6.55$

Table 7.14 Effect of Regrind Level on Second Pass Impact Strength and Elongation at Break for High-Impact Polystyrene [54]

| Property | Unit | Regrind level (fraction) | | | | | |
|-------------------------|-------------------|--------------------------|------|------|------|------|------|
| | | 0 | 0.05 | 0.10 | 0.15 | 0.25 | 0.50 |
| Impact resistance | | | | | | | |
| Measured | kJ/m ² | 17.5 | 17.0 | 16.0 | 16.0 | 15.5 | — |
| Calculated ¹ | kJ/m ² | 17.5 | 16.9 | 16.8 | 16.7 | 16.5 | 16.1 |
| Notched impact strength | | | | | | | |
| Measured | kJ/m ² | 5.4 | 5.2 | 5.3 | 4.7 | 4.7 | — |
| Calculated ² | kJ/m ² | 5.2 | 5.1 | 5.1 | 5.0 | 4.9 | 4.7 |
| Elongation at break | | | | | | | |
| Measured | % | 10.3 | 10.4 | 9.3 | 9.2 | 8.0 | — |
| Calculated ³ | % | 10.3 | 10.1 | 10.0 | 9.8 | 9.5 | 8.7 |

¹ The model is: $M_{p2} = [X(1 - Y)(1 + XY) + (XY)^2]M_o$ where $X = 0.907$ and $M_o = 18.7$

² The model is: $M_{p2} = [X(1 - Y)(1 + XY) + (XY)^2]M_o$ where $X = 0.833$ and $M_o = 6.2$

³ The model is: $M_{p2} = [X(1 - Y)(1 + XY) + (XY)^2]M_o + B$ where $X = 0.576$, $B = 2.97$ and $M_o = 12.7$

Table 7.15 Effect of Regrind Level on Second Pass Impact Strength and Elongation at Break for ABS [54]

| Property | Unit | Regrind level (fraction) | | | | | |
|-------------------------|-------------------|--------------------------|------|------|------|------|------|
| | | 0 | 0.05 | 0.10 | 0.15 | 0.25 | 0.50 |
| Impact resistance | | | | | | | |
| Measured | kJ/m ² | 49.0 | 48.5 | 48.5 | 39.5 | 45.5 | — |
| Calculated ¹ | kJ/m ² | 49.0 | 48.2 | 47.4 | 46.6 | 45.0 | 41.0 |
| Notched impact strength | | | | | | | |
| Measured | kJ/m ² | 26.5 | 21.0 | 14.4 | 12.2 | 12.2 | — |
| Calculated ² | kJ/m ² | 25.0 | 24.5 | 24.1 | 23.6 | 22.7 | 20.4 |
| Elongation at break | | | | | | | |
| Measured | % | 24.0 | 26.4 | 20.9 | 19.9 | 15.6 | — |
| Calculated ³ | % | 24.0 | 23.3 | 22.6 | 21.9 | 20.4 | 16.9 |

¹ The model is: $M_{p2} = [X(1 - Y)(1 + XY) + (XY)^2]M_o$ where $X = 0.672$ and $M_o = 72.9$

² The model is: $M_{p2} = [X(1 - Y)(1 + XY) + (XY)^2]M_o$ where $X = 0.636$ and $M_o = 39.3$

³ The model is: $M_{p2} = [X(1 - Y)(1 + XY) + (XY)^2]M_o + B$ where $X = 0.181$, $B = 6.55$ and $M_o = 96.4$

- Regrind a sizable quantity of “First Pass” and extrude it at 100% to produce “Second Pass”. Again save a quantity of this sheet for thermoforming study and regrind the rest.
- Continue regrinding and reextruding for N passes where N is at least 3 and preferably 5.
- Injection mold the various regrind passes to obtain samples for mechanical property evaluation. At the same time, injection mold virgin polymer to obtain samples for mechanical properties.
- Test all samples according to the proper ASTM, DIN or ISO protocol.
- From the injection molding data, determine the relative influence of the injection molding process on the material properties. This effect is important since each regrind step is subjected to injection molding *after* the extrusion process history and so this effect must be extracted from the experimental data.
- Curve-fit the data to determine the appropriate mathematical models for the 100% regrind study. In particular, appropriate values are sought for M_o , the virgin mechanical property, and X, the fraction of property retained after each pass through the extruder. Offset and asymptotic values and other ancillary values are determined at this point also.
- Next, reestablish the extrusion processing conditions on 100% virgin.
- If there is substantial property loss between the virgin polymer and “First Pass” regrind, dry-blend this regrind with virgin at 50:50 ratio. If the property loss is not significant until the Nth 100% regrind pass, dry-blend this regrind with virgin at 50:50 ratio. The objective here is to determine what law of mixtures is appropriate—linear or logarithmic.
- Again injection mold the necessary test samples, and again back out the effect of injection molding on the property loss to establish the relative experimental effect

of regrind on appropriate mechanical properties. Then determine what law of mixtures is appropriate for each mechanical property.

- Return to the extruder and reestablish the processing conditions on 100% virgin.
- Dry-blend virgin and “First Pass” at 50:50 and run to steady-state. Collect it as “50:50 First Pass” and regrind this and dry-blend it with virgin at 50:50 to produce “50:50 Second Pass”.
- Continue the above for N passes. Again injection mold each of these “50:50” passes, again test according to ASTM or DIN protocol, and again extract the effect of injection molding from the data. The purpose of this is to verify that the combined property loss model and the law of mixtures model predict the *steady-state* or *infinite recycle* physical properties.
- Note that this protocol includes a grinding step for each pass. The effect of grinding on the mechanical properties is usually much smaller than the effect of extrusion. However, if there is concern about mechanical damage induced by grinding, test samples can be pressed from extruded sheet.
- If there is concern about the thermal effects of thermoforming, the sheet saved from each pass can be thermoformed conventionally, then reground in the manner outlined for the extrusion/regrind protocol. In many cases, thermoforming may affect only one or two properties, such as color or fire retardancy. As a result, the testing level is substantially reduced.

Note that the protocol has several pivotal keys:

- It must be carried out on commercial equipment, to ensure that the thermal and shear histories are comparable to that expected in commercial thermoforming operations,
- Care must be taken to extract the effect of injection molding test samples from the data, and
- Regrind level must be at a level typical of thermoforming operations. The 50:50 ratio is chosen for this reason.

Many thermoformed products must meet performance criteria based on polymer material properties. The obvious purpose for this apparently elaborate protocol is to ensure that the polymer in the products being thermoformed has not deteriorated unduly during the regrinding and re-extrusion process. Example 7.20 illustrates how to obtain the necessary values for the arithmetical models.

Example 7.20 Determination of Long-Term Physical Properties From Regrind Data

The table below gives measured properties of 100% regrind and 50% regrind (in regular face type). Determine the method of predicting the effect of regrind level on physical properties.

| | 100% Regrind (Extrusion) | | | | | | | |
|------------------|--------------------------|------|------|------|-------------|-------------|-------------|----------|
| Number of passes | 0 | 1 | 2 | 3 | 4 | 5 | 6 | ∞ |
| Property value | 1.00 | 0.90 | 0.81 | 0.73 | 0.66 | 0.59 | 0.53 | 0 |

| Mixed Regrind/Virgin (First Pass) | | | |
|---|-----|-------------|-------------|
| Regrind level | 0 | 25% | 50% |
| Property value | 0.9 | 0.88 | 0.86 |
| Mixed Regrind/Virgin (Second Pass) | | | |
| Regrind level | 0 | 25% | 50% |
| Property value | 0.9 | 0.87 | 0.86 |
| Mixed Regrind/Virgin (∞ Pass or Steady State) | | | |
| Regrind level | 0 | 25% | 50% |
| Property value | 0.9 | 0.87 | 0.82 |

From the 100% regrind data,

$$M_{pN} = X^N \cdot M_o$$

or $X = 0.900$. The values for the 4th and higher regrinds are calculated and given in bold face in the table. Note that this predicts that the physical property goes to zero after an infinite number of 100% regrind cycles.

The equation for Y fraction of recycle in virgin polymer is:

$$M_{pN} = \left[\frac{X(1-Y)(1-(XY)^N)}{(1-XY)} + (XY)^N \right] \cdot M_o$$

The calculated values are given in bold face in the tables for first pass, second pass and infinite pass or steady-state virgin/regrind ratio.

Cascading 100% Regrind

The concept of cascading 100% regrind is growing in acceptance. As shown in Fig. 7.65, the process begins with 100% virgin sheet. $(1 - Y)$ fraction of this sheet is converted into quality parts. The Y fraction of web, trim and other recyclable non-product sheet is reground and re-extruded as 100% regrind into new sheet. $(1 - Y)$ of the reground sheet produces acceptable parts and the Y fraction of that is reground and recycled. After N passes, only Y^N fraction of the original virgin polymer remains. This is considered sufficiently small to be discarded. The philosophy behind cascading 100% regrind focuses on the following points:

- With closed-loop recycling, contamination simply goes around and around. As a result, it can accumulate to a level where the entire sheet is contaminated. This does not happen with the cascading process, where unacceptably contaminated regrind is simply discarded.
- Even for relatively large recycle fractions, only a few cascades are needed before the economics favor discarding rather than re-extrusion.

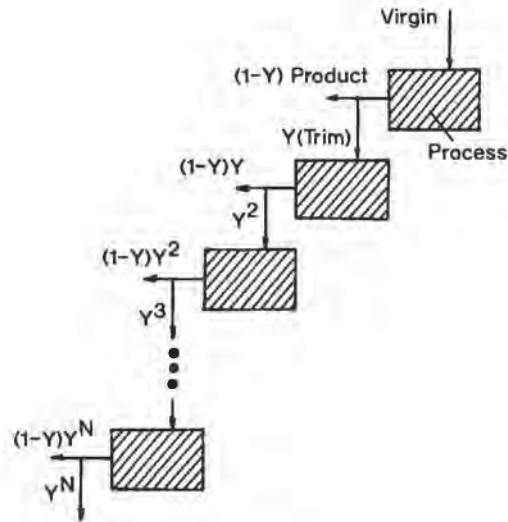


Figure 7.65 Cascade reprocessing or recycling of trim

- Usually physical properties do not deteriorate dramatically, even with five or six trips through the process equipment. This is particularly true with polyolefins, especially polyethylenes.

The linear property loss algorithm for cascading 100% regrind is quite simple:

$$M_{p,N} = X^N \cdot M_0 \quad (7.77)$$

where N is the cascade number. The fraction of good parts is given as:

$$(1 - Y) \sum_N Y^{N-1} \quad (7.78)$$

The term approaches unity as $N \rightarrow \infty$. Example 7.21 compares cascading 100% regrind property loss with steady-state recycling. Cascading 100% regrind is feasible when the polymer property loss approaches an asymptote, so long as the asymptotic value yields a part with an acceptable property.

Example 7.21 Steady-State and Cascading Regrind

In the current process, the polymer loses 10% of its tensile strength on one pass through the extrusion and thermoforming process. The trim loses no tensile strength on regrind and drying. If trim and off-spec parts comprise 40% of the extruded sheet surface, determine the steady-state tensile strength required in the virgin sheet. Then consider the cascade recycle scheme, where the trim and off-spec parts are discarded after three recycles. Assume the tensile strength properties are linearly additive.

The appropriate steady-state equation is:

$$\frac{M_x}{M_o} = \frac{X(1-Y)}{1-XY}$$

According to the information, $X = 0.9$, $Y = 0.4$. As a result, $M_o = 1.185 \cdot M_x$. In other words, the virgin polymer must have a tensile strength 19% greater than the design specifications. Theoretically 100% of the polymer is converted to good parts in a steady-state scenario.

For the cascade scheme, the tensile strength of the acceptable parts must meet the design criterion after three passes through the processing equipment. The appropriate cascade equation is:

$$M_N = X^N \cdot M_o$$

where N is the cascade number. For $X = 0.9$, $M_o = 1.372 \cdot M_x$. In other words, the virgin polymer must have an initial tensile strength 37% greater than the design specifications. For the cascade process, the fraction of good parts for the three-pass scenario is:

$$(1-Y)\sum Y^{N-1} = (1-Y)[1+Y+Y^2] = 0.936$$

or 93.6% of the initial amount of polymer is converted to good sheets. The remaining 6.4% of the polymer is discarded.

7.8 General Guidelines for Part Design

If the part design has been thoroughly reviewed by all principals, improper mold design or unsuitable polymer choice should not be a cause of unacceptable parts. Unfortunately, in real life, improper mold design, part design, and poor choice of polymer still remain the major causes of product failure in the market place. For novel designs or experimental processes, extensive development and prototyping should be done far in advance of production manufacturing. Again, if everyone has reviewed all details and signed off on their portion of the program, few processing problems should be attributed to improper part design or other aspects of the thermoforming process. In addition to guidelines and steps to correct processing problems, certain do's and don'ts are sufficiently general to be considered as guidelines to thermoforming. In many cases, the items in the list that follows are helpful to the designers. However, designs that violate some of these can also be successful.

General Tips

- Pressure forming is most economical for 5000 to 20,000 parts¹.
 - Pressure forming competes with injection molding at about one-fourth the mold cost and one-fourth to one-half the lead time.
- ¹ Pressure forming details are given in Chapter 9 on advanced thermoforming techniques.

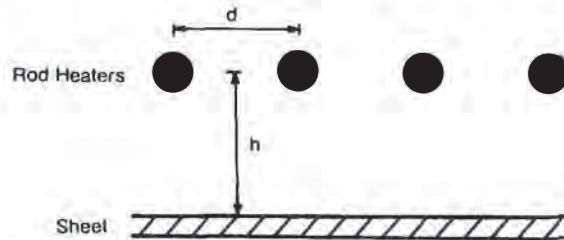


Figure 7.66 Rod heater spacing relative heater-to-sheet spacing

- Silicone is recommended when slip-sliding sheet from the rim to the mold cavity or as a topical lubricant on plugs. However, silicone cannot be used on a given application if it is not allowed in other parts of the plant.
- Sprayed vegetable oil is an effective FDA-approved temporary lubricant for certain parts. However, the oil breaks down after some time and so must be wiped from the molds on a regular basis.

Process Tips

- Most common plastics are formed in a temperature range of 200 to 400°F or 100 to 200°C.
- Sheet thicker than about 0.400 in or 10 mm is best heated in forced convection air ovens.
- Sheet thinner than about 0.010 in or 0.25 mm is best heated by direct contact hot plate.
- For rod heaters, the horizontal distance between heater elements should be less than the vertical distance between the element plane and the sheet (Fig. 7.66).
- The extent of sheet sag during heating is a useful and sometimes the only way of determining material formability.
- Filled or reinforced sheet rarely sags during heating.
- Short fiber-reinforced sheet “lofts” or grows in thickness when heated. As a result, a bladder is sometimes used to recompress the sheet during forming¹. A cap-sheet will also minimize fiber prominence but at an increased cost.
- Low-density foam sheet increases in thickness as it is heated, due to internal gas pressure². This results in a relatively poor free surface finish.
- In vacuum forming, the surge tank volume should be 6 to 20 times the free cavity volume.
- In vacuum forming, the vacuum should always be greater than 500 mm Hg or 20 in Hg and 710 to 725 mm Hg or 28 to 28.5 in Hg is standard.
- The faster the vacuum is applied, the better the draw-down becomes, to a point [84].

¹ Other information is given in Chapter 9 on advanced thermoforming techniques.

² Other information is found in Chapter 9 on advanced thermoforming techniques.

- Excessive draw-down rate leads to excessive webbing.
- Slow vacuum draw-down requires hot molds for mold replication.
- Chatter lines on the formed part are due to variation in draw-down and hot sheet. The vacuum system should be carefully monitored.
- If small amounts of air are used for prestretching, the air does not need to be heated.
- If an excess of blowing air is used, it should be preheated to within 20°F or 10°C of the sheet temperature to minimize premature chilling of the sheet. This is particularly true with sequential twin-sheet forming.
- Woven stainless steel window screen is an effective temporary screen for pattern heating.
- Welded stainless steel wire is the desired permanent screen for pattern heating.
- Aluminum window screen can be used for pattern heating of a few parts but it usually oxidizes and falls apart quite quickly. Since it is easier to cut and is less expensive and more readily available than stainless steel, aluminum window screen is frequently used when developing new pattern heating profiles. Once the final shape is determined, the aluminum screen is used as a pattern for the more permanent stainless steel screen.
- If the formed shape is for an optical application, the hot sheet should not touch a cold surface during forming.
- In pressure forming, the mold and the pressure box should be mechanically or hydraulically locked together during forming.
- Bayonet locking, V-groove locking and overlap joints are typical ways of positively positioning pressure box and mold during pressure forming. A flexible silicone or neoprene gasket is usually required for adequate seal.
- Although air pressures to 500 lb_f/in² or 3.4 MPa have been used to pressure form composites, current practice uses 50 to 100 lb_f/in² or 0.34 to 0.7 MPa air pressure.
- Snap-back forming should actuate when the bubble top intersects a photocell beam.
- Matched die molding is needed when the sheet is normally too stiff at forming temperature to be easily vacuum drawn. Typical polymer states are PS foam, CPET, HDPE, PP, and short-fiber and mineral filled polymers.
- Typical matched die molding clamping pressures are 50 to 100 lb_f/in² or 0.34 to 0.7 MPa.
- Matched die molding is used if details are needed on both sides of the part or if the part design requires abrupt changes in wall thickness or direction.
- Coining or local matched die molding is used if details or dimensional tolerance is only needed in a small section of the part (Fig. 7.67).

Mold Tips

- Owing to their high shrinkage values, crystalline polymers usually require moats in female cavities to prevent air leakage during forming (Fig. 7.68).
- The hotter the mold, the greater the final shape shrinkage becomes.

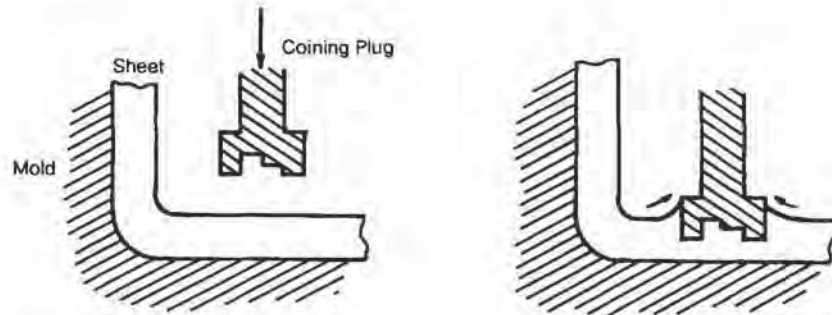


Figure 7.67 Coining or localized compression molding

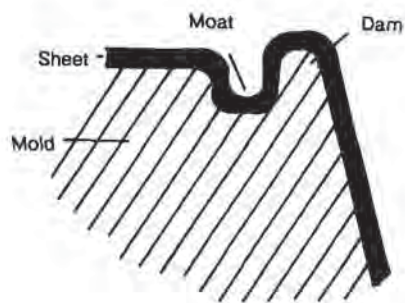


Figure 7.68 Moat and dam female mold configuration for polyolefins and other crystalline polymers

- The colder the mold, the more nonuniform the wall thickness becomes for simple vacuum forming (Figure 7.69) [55].
- The colder the mold, the more apparent chill marks become.
- Male molds are less expensive to make but require greater draft angles than female molds.
- Vacuum hole diameter should be less than the local sheet thickness to prevent nibbing.
- Vacuum holes should be bunched in two-dimensional and three-dimensional corners but are usually spaced along the part corners for appearance reasons. As a result, far more vacuum holes are used than are needed to evacuate the mold cavity. Typical vent hole spacing is about 1 in or 25 mm (Fig. 7.70).
- For twin-sheet forming, edge blow pins can be put in place just as the two sheets meet. Surface or puncture blow pins, on the other hand, need to be pneumatically or mechanically driven through the sheet as it contacts the mold surface¹.

¹ More information about twin-sheet thermoforming is given in Chapter 9 on advanced thermoforming techniques.

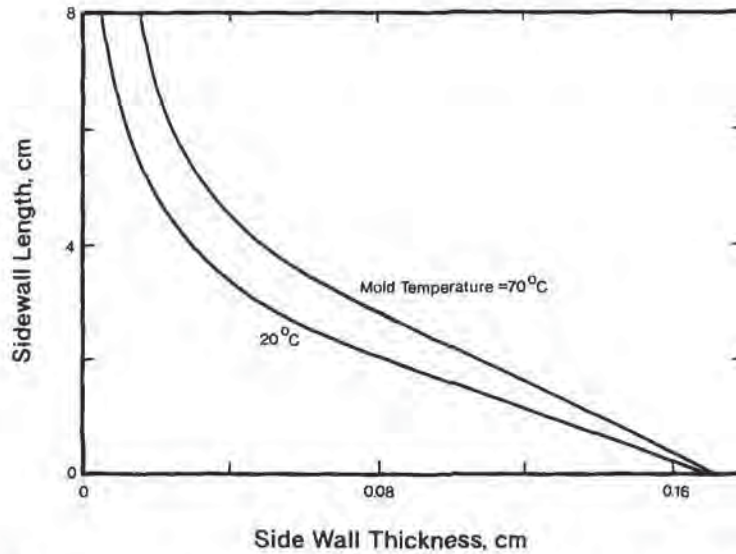


Figure 7.69 Effect of mold temperature on wall and corner thickness uniformity for simple vacuum forming [55]

Prestretch Tips

- Metal plug temperatures should be within 15 to 30°F or 10 to 20°C of the sheet temperatures to minimize plug marks on the sheet.
- Syntactic foam and plastic-surfaced plugs are not heated.
- Plugs with good surface slip reduce but do not eliminate the need for close temperature control.

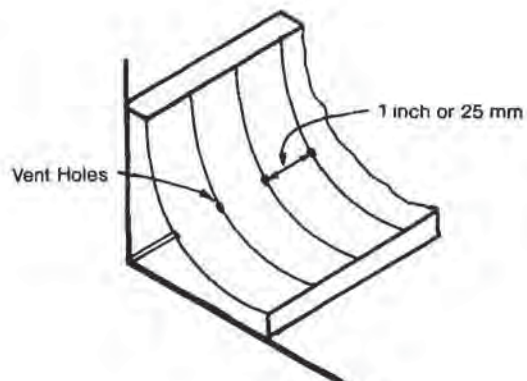


Figure 7.70 Classic vent hole spacing on heavy-gage two-dimensional horizontal corners

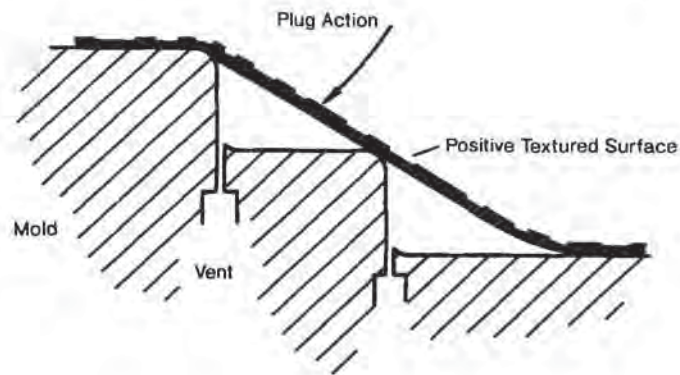


Figure 7.71 Plug forming against the positive, textured surface on male molding

- Plugs can be used on textured appearance surfaces (Fig. 7.71).
- A typical initial prestretch depth equals half the narrowest unformed sheet dimension. Thus for a 100 in \times 200 in rectangle, 50 in is a beginning good prestretch depth (Fig. 7.72).
- If the prestretch bubble is unstable when blown with air pressure, substitute a vacuum prestretch box.
- In snap-back forming, an optimum bubble height is $2/3$ the draw ratio or $H:D = 2:3$ (Fig. 7.73).

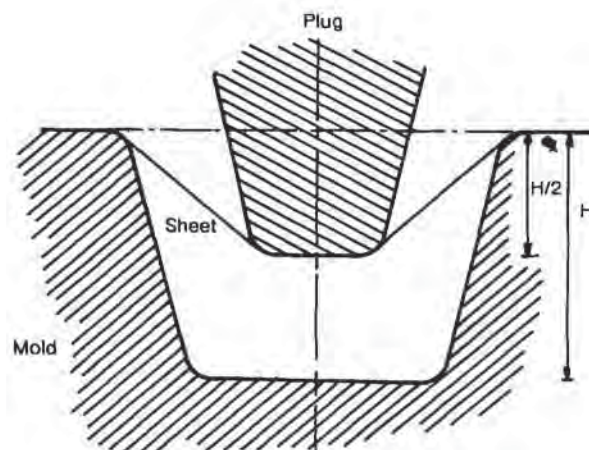


Figure 7.72 Recommended starting plug depth for symmetric parts

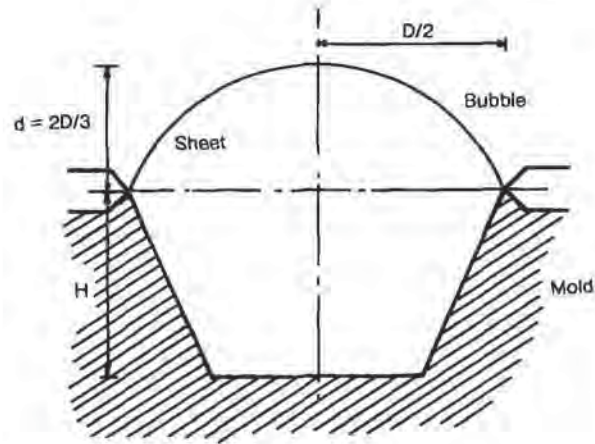


Figure 7.73 Recommended starting bubble height for symmetric parts

Part Design Tips

- Specification on part thickness should be on the thinnest allowable wall thickness needed for mechanical performance.
- If mold features need to be optically or visually read, their dimensions must be at least three times the local sheet thickness (Fig. 7.74).
- Female molds produce parts with thick rims and thin bottoms.
- Male molds produce parts with thick bottoms and thin rims.
- Typical female draft angles are 0° to 2° , with an average of about $\frac{1}{2}^\circ$ to 1° (Fig. 7.75).
- Typical male draft angles are 1° to 5° , with the average of about 4° (Fig. 7.76).
- As with injection molding, draft angles must be increased to compensate for texturing on perpendicular parts. Typically, 1° of draft per 0.2 thousandths depth of texture is acceptable.
- For textured details to be sharp in traditional vacuum forming, their depth should be greater than the local sheet thickness (Fig. 7.77).
- A wide variety of textures and patterns are now possible with pressure forming. However, common aesthetic sense must prevail when placing different textures and patterns on the same part.

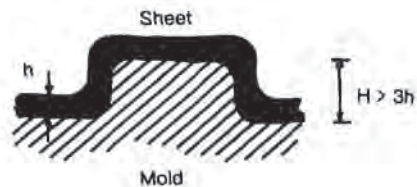


Figure 7.74 Recommended relative mold dimensions for readable features

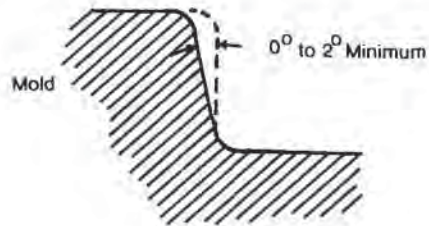


Figure 7.75 Draft angle range for female molds

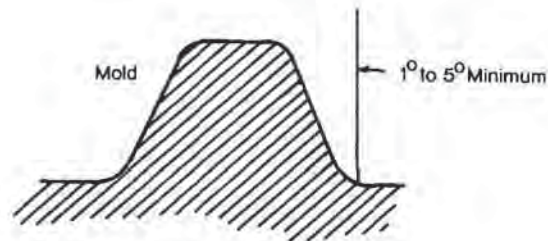


Figure 7.76 Draft angle range for male molds

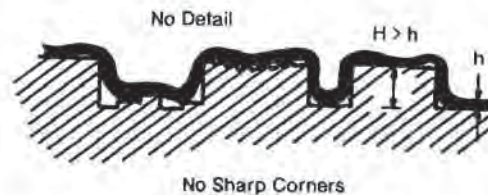


Figure 7.77 Traditional vacuum forming into mold details

- For fine texture detail with vacuum forming, textured sheet is used. Care must be taken in reducing thickness by more than 30%, particularly in corners, as the texture washes easily. Forming is usually done at the minimum possible forming temperature.
- Any draft is better than no draft at all.
- The largest amount of draft that fits within the constraints of the part requirements should be specified.
- Deep undercuts should have generous corner radii. Otherwise the part corner will be very thin (Fig. 7.78).
- Parts with undercuts should be stripped from the mold with strippers pushing uniformly against the part rim (Fig. 7.79).
- Deep undercuts require actuation for part removal even for very ductile or soft polymers. Otherwise extensive scuffing or tearing may occur.
- Both external and internal threads can be molded in with twin-sheet thermoforming (Fig. 7.80).

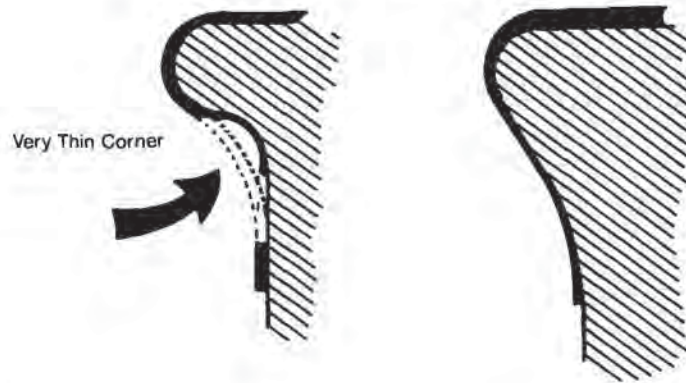


Figure 7.78 Draw into undercuts more successful if radii are generous

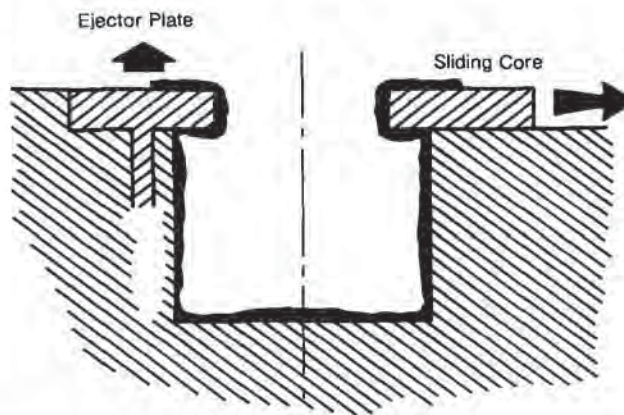


Figure 7.79 Undercuts stripped by (left) ejector plate or (right) sliding core

- Partial internal threads are possible by secondary action with single-sheet thermoforming (Fig. 7.81).
- Typical part shrinkage for amorphous polymers is on the order of 0.5% for male molds and 1% for female molds.
- Typical part shrinkage for crystalline polymers is on the order of 2% for male molds and 2% to 3% for female molds.
- 50% to 75% of part shrinkage occurs before the part temperature has fallen to its heat distortion value.
- For simple vacuum forming, an easy to form radius is 4 times thickness of the starting sheet (Fig. 7.82a).
- For simple vacuum forming, the minimum recommended radius of any two-dimensional or three-dimensional corner is equal to the thickness of the starting sheet (Fig. 7.82b).

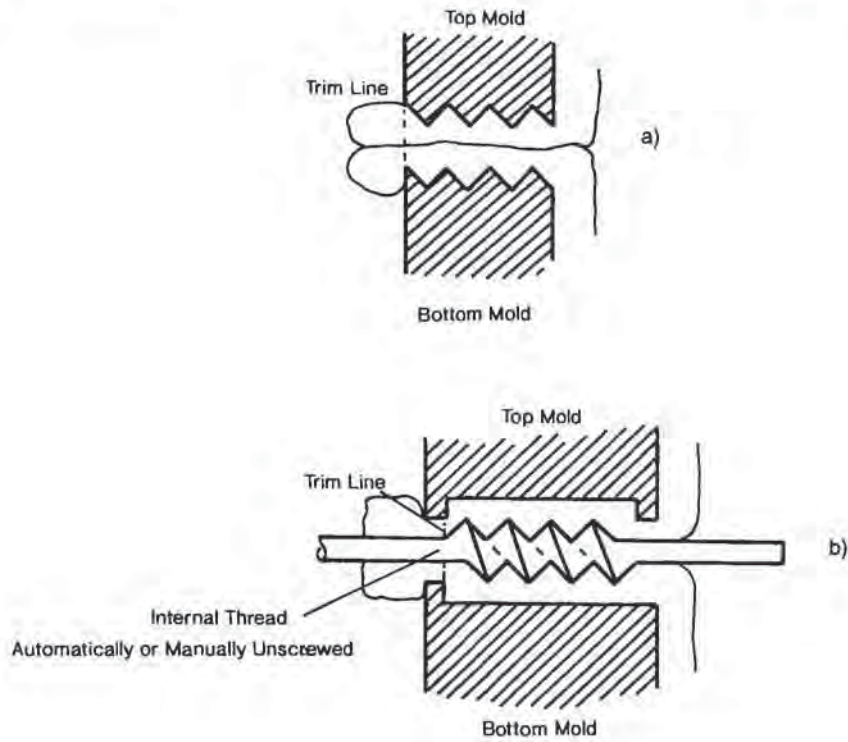


Figure 7.80 Twin-sheet forming of male thread (a) and female thread over unscrewing mandrel (b)

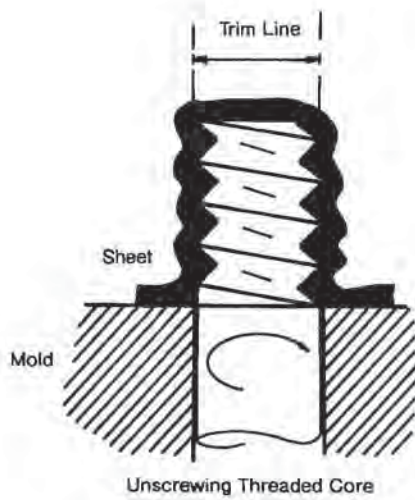


Figure 7.81 Molding over unscrewing core, then trimming for bung

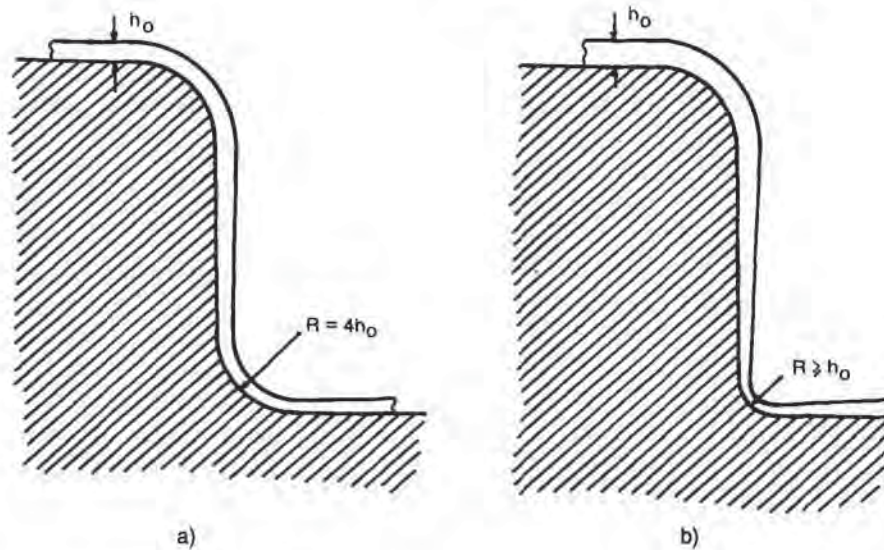


Figure 7.82 Recommended easy-to-form relative radius (a) and minimum relative radius (b)

- Pressure forming allows outside corner radius of 0.015 in for most polymers.
- Higher sheet temperature is required for smaller radii corners (Fig. 7.83) [56].
- Chill marks are usually an indication of rapid thickness change. They are caused by slow vacuum, a cold mold, or an inherent yielding of the polymer at the forming temperature.
- Lakes or shiny spots on parts indicate inadequate vacuum or air trapped between the sheet and a highly polished mold.
- The extent to which a plastic sheet is stretched is a strong function of its hot strength. However, areal draw ratios are usually less than 5, linear draw ratios are less than 3 and H:D ratios are less than 1.
- When notch-sensitive plastics such as PA or nylon, PMMA and PS are drawn into sharp corners, the parts may fail because of the inherent brittleness of the polymer.
- Parts with acute angles or angles of less than 90° can be notch-sensitive regardless of the polymer.
- Polarized filters aid in detecting highly stressed regions in transparent PS, PC, PET and PMMA parts.
- The diameters of solvent-welded bosses should be proportional to the sizes of the metal inserts to minimize torsion cracking during component assembly (Fig. 7.84).
- Dimensional tolerances are rarely specified on free or non-tool surfaces.
- To attain local accuracy in sheet thickness, a heavier gage sheet should be formed and the local area routed to the correct thickness (Fig. 7.85).
- Typical dimensional tolerances are 1% on small parts and 0.2% on large parts.

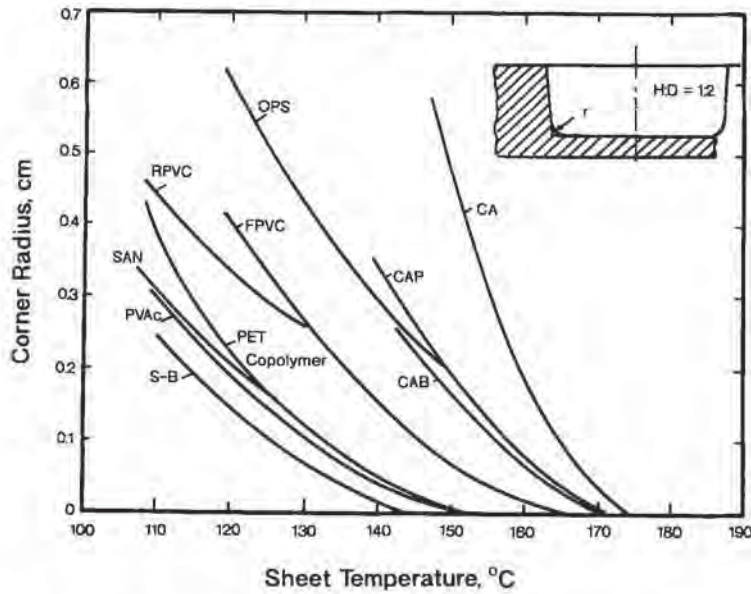


Figure 7.83 Temperature-dependent corner radius for several polymers for H:D = 1:2 draw ratio female part. redrawn from [56]

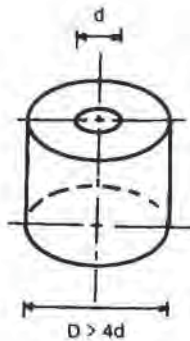


Figure 7.84 Recommended relative solvent- or thermally-welded boss dimensions

- Sheet thickness tolerance is about 5% on medium and heavy gage sheet. This tolerance should be doubled and added to the dimensional tolerance for inside dimensions on parts formed in female molds.
- Stiffening ribs, corrugations, flutes and multiple cones are typical ways of stiffening thermoformed parts.
- Increase stiffness on large surface area parts by
 - adding a slight dome, of 0.15 in/in,
 - adding concentric ribs, or
 - adding radial ribs (Fig. 7.86).

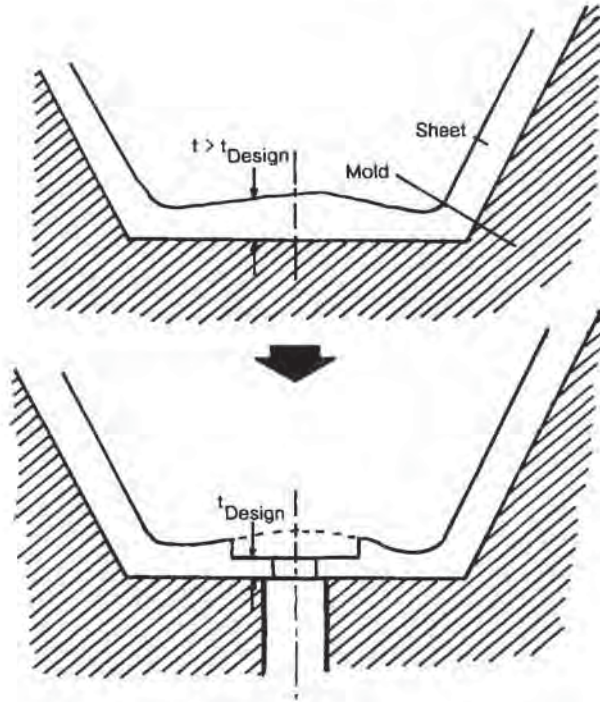


Figure 7.85 Routing high tolerance areas in heavy-gage sheet



Figure 7.86 Using doming, reinforcing rings and/or radial ribs to minimize optical distortion, eversion in thermoformed disks

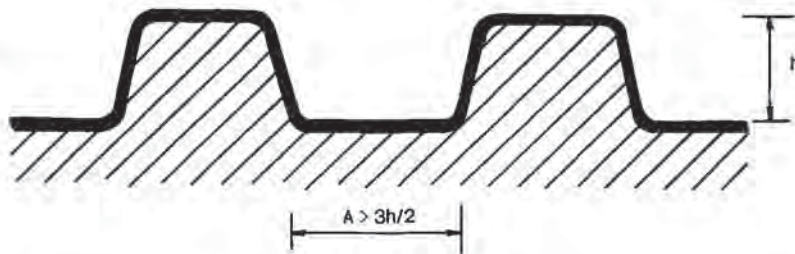


Figure 7.87 Recommended rib height and spacing to minimize distortion in flat parts. Redrawn from [57,58]

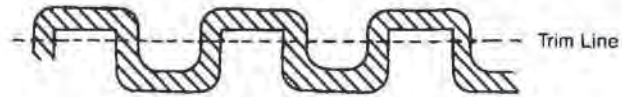


Figure 7.88 Method of forming slots or vents by machining away rib tops

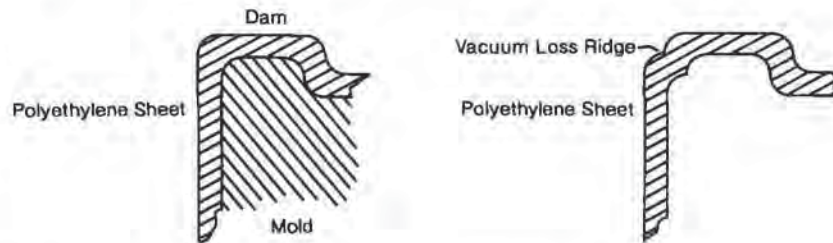


Figure 7.89 Vacuum loss ridge formed on crystalline polymers

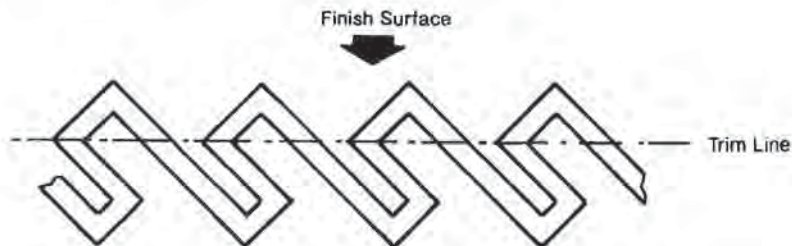


Figure 7.90 Method of forming non-view slots or vents by machining away rib tops

- Distances between multiple male ribs or corrugations should be greater than $D = 1.5 \cdot H$ where H is the height of the rib (Fig. 7.87) [57,58].
- The guideline above holds also for rows of slots, where the top portion of the rib is removed by routing (Fig. 7.88).
- An unexpected ridge at the rim of a polyolefin female part is an indication of air leakage during cooling (Fig. 7.89).
- Shrinkage of fiber-reinforced parts is less important than dimensional changes due to "spring-back" or elastic recovery once the applied forces are removed.
- Non-view slots require side-core action and pressure to achieve detail in the acute angled areas (Fig. 7.90).
- Non-view slots in a female part are best designed with the inside of the slot facing up (Fig. 7.91). This accommodates the natural drape of the sheet.
- Whenever possible, slots on vertical sides of female parts should run parallel to the rim rather than vertical (Fig. 7.91). This minimizes differential distortion between ribs and the splittiness of the uniaxially oriented polymer in vertical walls.

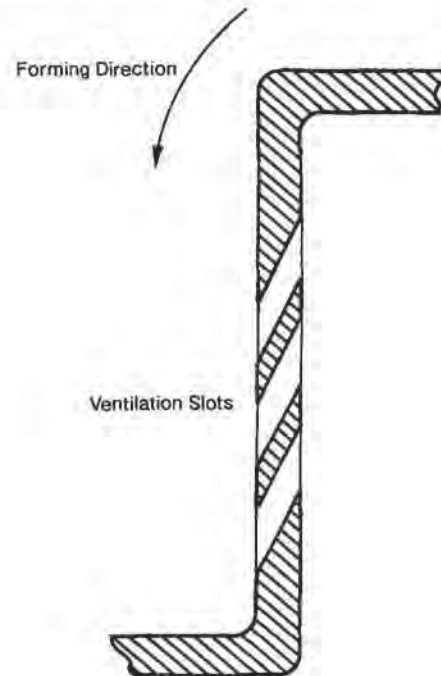


Figure 7.91 Recommended orientation of horizontal non-view slots relative to forming direction

- Although some progress has been made in properly indexing the side core extension during stretching to better stretch sheet in the slot region, fully extended side cores are nearly always used.

Rim and Edge Designs

There are usually fundamental differences in the functions of the edges of heavy-gage and thin-gage parts. For heavy-gage parts, the edge left by trimming of both in-plane and contoured parts is frequently acceptable for the particular application. If the part edge is not assembled or inserted into other parts, further finishing such as sanding or flame polishing may be needed to achieve the desired appearance edge¹. If thermoformed parts are to be adhesively bonded, appropriate traps for the adhesive bead are formed into the part edges (Fig. 7.92) [59]. As with all thermoformed parts, appropriate draft angles and shrinkage factors must be applied to ensure adequate seal with the minimum amount of adhesive used.

The classic example of rim treatment of thin-gage parts is the rolled rim (Fig. 7.93). Although rim rolling is a standard method of reinforcing the rim region of a round thin-gage part such as a cup or a tub, rim rolling is used on occasion for oval,

¹ The design of the edge of a twin-sheet formed part is covered in detail in Chapter 9 on advanced thermoforming techniques.

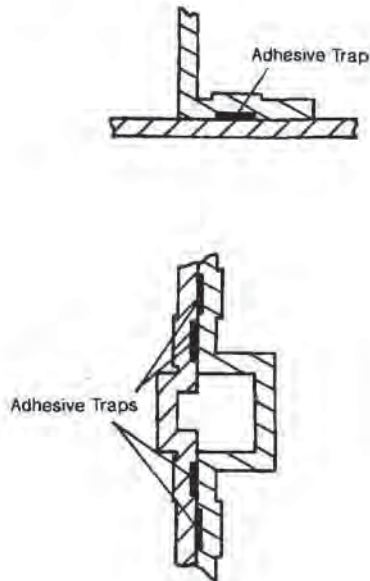


Figure 7.92 Formed-in adhesive traps for assembling, twin-sheet forming

elliptical or oblong parts with generous corner radii. The standard method of rim rolling is shown in schematic in Fig. 7.94. Typically, a heated air jet is directed against the spinning part while the part is held against a simple edge forming fixture. The process is continuous at about 5,000 to 10,000 cups/h. Although there appears to be no science in determining the dimensions of a rim in rim roll design, some guidelines can be established. The bending strength of a round rim is compared with the bending strength of the flat sheet of plastic needed to form the rim in the following way:

The deflection, y_{\max} , of a simply supported beam of width b and length L loaded in the center is given as:

$$y_{\max} = \frac{PL^3}{48EI} \quad (7.79)$$

where I is the moment of inertia, P is the applied load and E is the polymer modulus. This equation is applicable to both the flat sheet and the rolled rim for slight bending loads. Therefore the ratio of deflections is given as:

$$\frac{y_{\max, \text{roll}}}{y_{\max, \text{flat}}} = \frac{I_{\text{flat}}}{I_{\text{roll}}} \quad (7.80)$$

For the flat sheet, the moment of inertia is:

$$I_{\text{flat}} = bt^3/12 \quad (7.81)$$

For the rolled rim, the moment of inertia is:

$$I_{\text{roll}} = \pi r^3 t \quad (7.82)$$

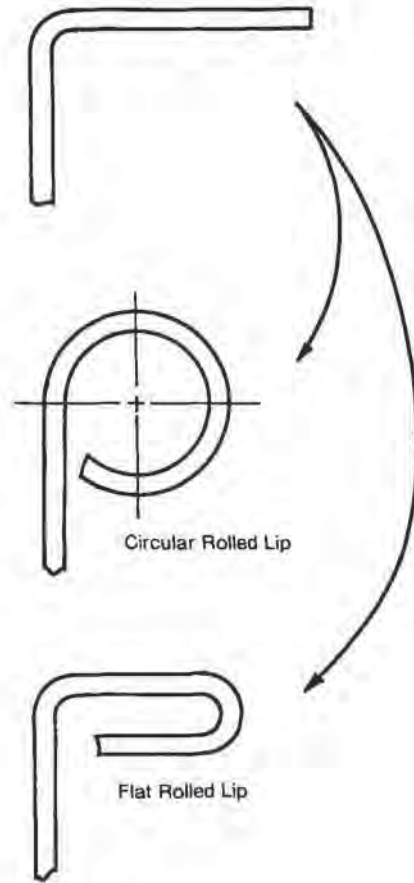


Figure 7.93 Two types of rolled rims beginning with formed flat

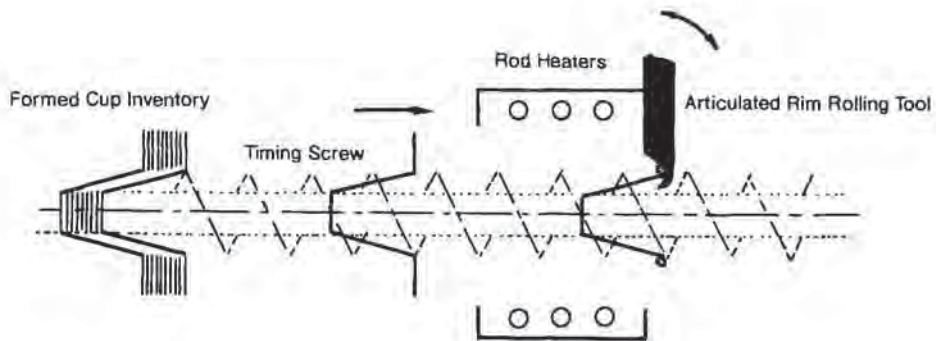


Figure 7.94 Schematic of rim rolling with timing screw feed and articulated rim rolling tool

where r is the radius of the roll. But $2\pi r \equiv b$. Therefore Equation 7.80 is written as:

$$\frac{y_{\max, \text{roll}}}{y_{\max, \text{flat}}} = \frac{2\pi^2 t^2}{3b^2} \quad (7.83)$$

Equation 7.83 shows that so long as $b > 3.85 \cdot t$, the deflection of a rolled rim is always less than the deflection of a flat rim. To put it another way, the rolled rim is stiffer than the equivalent flat rim. Example 7.22 also shows a similar effect for the folded rim of Fig. 7.93. Capillarity in rolled rims is a problem when the product is used as a drink cup. Since the rim is usually not sealed, liquid wicks into the roll tube. Capillary action then forces the liquid up the roll tube, with the result being that the rim “leaks”, or acts as the thermoforming equivalent of a “dribble glass”. Capillary action depends on the surface tension of the liquid, σ , the wettability of the liquid with the wall, the radius of the tube, r , and the density of the liquid, ρ . The appropriate expression is:

$$y = \frac{2\sigma \cos \theta}{\rho \cdot g \cdot r} \quad (7.84)$$

Example 7.22 Rim Stiffness

Determine the relative stiffness of a rolled rim if the sheet thickness is 0.030 in and the flat rim width is 1.5 in. What is the roll radius when the flat rim width is 0.75 in? What effect does this have on stiffness of the rolled rim? Then determine the stiffness if the flat rim is simply folded.

From Equation 7.83:

$$\frac{y_{\max, \text{roll}}}{y_{\max, \text{flat}}} = \frac{2\pi^2 t^2}{3b^2}$$

From the data given, $t = 0.03$, $b = 1.5$, and the roll radius is 0.24 in. The deflection ratio is 0.00263. Or the rolled rim is nearly 400 times stiffer than the flat rim. For the narrower rim, where $b = 0.75$ in, the roll radius is 0.120 in and the deflection ratio is 0.0105 or the rolled rim is about 100 times stiffer than the flat rim.

The deflection ratio for the double thick, half-width rim is:

$$\frac{y_{\max, 2\text{-flat}}}{y_{\max, \text{flat}}} = \frac{I_{\text{flat}}}{I_{2\text{-flat}}}$$

For the flat sheet, the moment of inertia is:

$$I_{\text{flat}} = bt^3/12$$

For the double-flat, the moment of inertia is:

$$I_{2\text{-flat}} = (b/2)(2t)^3/12 = 4bt^3/12$$

Therefore the deflection ratio is:

$$\frac{y_{\max, 2\text{-flat}}}{y_{\max, \text{flat}}} = \frac{1}{4}$$

The double flat has only 25% the deflection as the original flat, but the double flat is still nearly 100 times more flexible than the roll.

where y is the liquid height, θ is the contact angle between the liquid and the tube wall, and g is gravitational constant. For pure water the surface tension is 60 dyn/cm. For other drinkables such as beer or soda, the surface tension is about 30 dyn/cm. The contact angle for water with glass is 0° and for water with paraffin is 107° . For contact angles less than 90° , the interfacial meniscus is positive and liquid rises in the tube. For contact angles greater than 90° , the interfacial meniscus is negative and the capillary liquid level is below the bulk liquid level. For polymers such as PS and PET, the contact angle is on the order of 0° and the $\cos \theta \approx 1$. For polymers such as PP and PE, the contact angle may be as high as 90° . For these, $\cos \theta \approx 0$ and there is no capillarity. This implies that the leaking effect is maximum with PS and PET and is minimized with olefins. Example 7.23 illustrates the relationship between rim roll radius and capillary height.

Example 7.23 The Leaking Rim Roll

Using the information from Example 7.22, determine the height of the capillary, assuming it is closed along the rolled side. Assume the contact angle is 0° and the surface tension is 30 dyn/cm. The liquid is water. If the distance from the lowest point of the rim to the edge of a person's lip is 0.25 in, will either of the two rim dimensions leak? At what radius will the rim begin to leak?

The operative equation is:

$$y = \frac{2\sigma \cos \theta}{\rho \cdot g \cdot r}$$

For the data given:

$$y \text{ (cm)} = \frac{0.06122}{r \text{ (cm)}}$$

For $r = 0.24 \text{ in} = 0.61 \text{ cm}$, $y = 0.1 \text{ cm} = 0.040 \text{ in}$. For $r = 0.12 \text{ in} = 0.305 \text{ cm}$, $y = 0.2 \text{ cm} = 0.080 \text{ in}$. Neither of these values is greater than 0.25 in, so neither will leak. Using $y = 0.25 \text{ in} = 0.635 \text{ cm}$, the minimum radius for a non-leaking rim is $r = 0.096 \text{ cm} = 0.04 \text{ in}$.

Design—A Comment

There are many sources for plastic part design information [60-63]. The emphasis above is on fundamental design tools. Full understanding of these tools is not always required to design thermoformed parts. However, these tools are being used to meet increasingly stringent design standards. Beall [60] notes that overall final piece part inaccuracies today are caused by:

- Tooling-associated inaccuracies,
- Sheet-to-sheet and run-to-run variations,
- Female versus male tooling,
- Piece part geometry,

- Specifics of the vendors' manufacturing processes,
- Operator skill and training, and
- Tooling maintenance procedures.

He further recommends that the customer carefully select "... a vendor with proven capabilities to meet the designer's tolerance requirements." The tools described above should enable all parties to better minimize final part inaccuracies.

7.9 References

1. R.C. Progelhof and J.L. Throne, *Polymer Engineering Principles: Properties, Processes, and Tests for Design*, Hanser Publishers, Munich (1993), p. 504.
2. M. Mooney, *Symposium on Consistency*, American Society for Testing and Materials, Philadelphia (29 Jun 1937), pp. 9–12.
3. S. Turner, *Mechanical Testing of Plastics*, 2nd Ed., George Godwin, London (1983), p. 187.
4. C. Chastain, "In Designing With Plastics, How Much Should You Trust ASTM Test Data?", *Machine Design*, 42: 2 (23 Jan 1975), p. 108.
5. S. Turner, *Mechanical Testing of Plastics*, 2nd Ed., George Godwin, London (1983), p. 181.
6. J.L. Throne, "Computer-Aided Engineering for Thermoforming—The Latest Improvements and What's Coming Next", SPI Conference Proceedings, National Plastics Exposition (7 Jun 1994).
7. J.L. Throne, "Effect of Recycle on Properties and Profits: Algorithms", *Adv. Polym. Tech.*, 7 (1987), pp. 347–360.
8. Additional information available from Sanders Prototype Inc. Wilton NH.
9. J.L. Throne, "Computer Aided Engineering for Thermoforming—The Latest Improvements and What's Coming Next", 7 June 1994, NPE '94 Conference Proceedings, Vol. I.
10. M. Burns, *Automated Fabrication: Improving Productivity in Manufacturing*, Prentice Hall, Englewood Cliffs NJ (1993).
11. D.S. Cummings, "Utilizing Stereolithography to Produce a Rapid Prototype Thermoforming Mold", SPE ANTEC Tech. Papers, 40 (1994), pp. 3550–3554.
12. L.R. Schmidt and J.F. Carley, "Biaxial Stretching of Heat Softened Plastic Sheets Using an Inflation Technique", *Int. J. Eng. Sci.*, 13 (1975), pp. 563–578.
13. H. Voigt, "Lehrgang für Thermoforming", Paul Kiefel Thermoformmaschinen GmbH, Industriestraße 17–19, Postfach 16 60, D-8228 Freilassing Germany, undated, p. 3.4.1.
14. N. Rosenzweig, M. Narkis and Z. Tadmor, "Wall Thickness Distribution in Thermoforming", *Polym. Eng. Sci.*, 19 (1979), pp. 946–951.
15. M.O. Lai and D.L. Holt, "The Extensional Flow of Poly(methyl Methacrylate) and High-Impact Polystyrene at Thermoforming Temperatures", *J. Appl. Polym. Sci.*, 19 (1975), pp. 1209–1220.
16. D. Gruenwald, *Thermoforming: A Plastics Processing Guide*, Technomic Publishing Co., Inc., Lancaster PA (1987), p. 57.
17. L.R. Schmidt, "Biaxial Stretching of Heat-Softened Plastic Sheets", Ph.D. Dissertation, Univ. Colorado, Boulder CO (1972), p. 129.
18. C.J. Benning, *Plastic Foams*, Vol. 1, Wiley-Interscience, New York (1969), p. 86.
19. Anon., "Volara Vacuum Forming Guide", Voltek, Division of Sekisui America Corp., Lawrence MA (Jan 1984).
20. R.J. Crawford and S.K.L. Lui, "Prediction of Wall Thickness Distribution in Thermoformed Mouldings", *Euro. Polym. J.*, 18 (1982), pp. 699–705.
21. S. Timoshenko and J.N. Goodier, *Theory of Elasticity*, 3rd Ed., McGraw-Hill Book Co., New York (1968), p. 207.

22. J.G. Williams, *Stress Analysis of Polymers*, 2nd Ed., Ellis Harwood Ltd/Halsted Press, London (1980), p. 240.
23. J.L. Throne, *Thermoforming*, Carl Hanser Verlag, Munich (1987), Table 7.11, p. 201.
24. N. Rosenzweig, "Wall Thickness Distribution in Thermoforming", SPE ANTEC Tech. Papers, 29 (1983), pp. 478–482.
25. J.L. Throne, *Thermoforming*, 1st Ed., Carl Hanser Verlag, Munich (1987), Table 7.12, pp. 204–205.
26. H. Fukase, "Prediction of Wall Thickness Distribution in Blow Molded Articles", I.H.I. Engineering Review, 15:1 (Jan 1975). An English language copy of this paper is available from Hisahiko Fukase, Researcher, Machinery Department, Ishikawajima-Harima Heavy Industries Co., Ltd., Research Institute, 1, Shinnakaharamachi, Isogoku, Yokohama Japan.
27. J.L. Throne, "New Concepts in Thermforming", Polym.-Plast. Techn. Eng., 30 (1991), pp. 761–808.
28. J.L. Throne, "Guidelines for Thermoforming Part Wall Thickness", Polym.-Plast. Techn. Eng., 30 (1991), pp. 685–700, Figure 3.
29. J.L. Throne, "Guidelines for Thermoforming Part Wall Thickness", Polym.-Plast. Techn. Eng., 30 (1991), pp. 685–700, Figure 4.
30. J.L. Throne, "Guidelines for Thermoforming Part Wall Thickness", Polym.-Plast. Techn. Eng., 30 (1991), pp. 685–700, Figure 6.
31. J.L. Throne, "Computer-Aided Engineering for Thermoforming—The Latest Improvements and What's Coming Next", SPI Conference Proceedings, National Plastics Exposition (7 Jun 1994), Figure 5.
32. H.G. DeLorenzi and H.F. Nied, "Finite Element Simulation of Thermoforming and Blow Molding", Chapter 5, in A.I. Isayev., Ed., *Modeling of Polymer Processing*, Hanser Verlag, Munich (1991).
33. W.N. Song, F.A. Mirza, and J. Vlachopoulos, "Finite Element Analysis of Inflation of an Axisymmetric Sheet of Finite Thickness", J. Rheol., 25 (1991), pp. 93–102.
34. K. Kouba and J. Vlachopoulos, "T-FORMCAD: A Finite Element Software Package for Thermoforming and Blow Molding", Accuform Co., Ltd., and CAPPA-D, Dept. Chem. Eng., McMaster University, Hamilton ON, Canada (1993).
35. W. Song, "Large Deformation Finite Element Analysis for Polymer Forming Processes", Ph.D. Dissertation, McMaster University, Hamilton, Ontario CAN (1993).
36. K.H. Huebner, *The Finite Element Method for Engineers*, John Wiley & Sons, New York (1980), p. 6.
37. L.R.G. Treloar, "Stress-Strain Data for Vulcanized Rubber Under Various Types of Deformation", Trans. Faraday Soc., 40 (1944), pp. 59–70.
38. L.R.G. Treloar, "Strains in an Inflated Rubber Sheet, and the Mechanism of Bursting", Trans. Inst. Rubber Ind., 19 (1944), pp. 201–212.
39. J.L. Throne, "Modeling Plug-Assist Thermoforming", Adv. Polym. Tech., 9 (1989), pp. 309–320.
40. J.G. Williams and H. Ford, "Stress-Strain Relationships for Some Unreinforced Plastics", J. Mech. Engrg. Sci., 6 (1964), pp. 405–417.
41. J.L. Throne, "Some Design Guidelines for Plug Assists", SPE ANTEC Tech. Papers, 39 (1993), Figure 3, pp. 182–190.
42. J.L. Throne, "Some Design Guidelines for Plug Assists", SPE ANTEC Tech. Papers, 39 (1993), Figure 4, pp. 182–190.
43. W. Song, "Large Deformation Finite Element Analysis for Polymer Forming Processes", Ph.D. Dissertation, McMaster University, Hamilton, ON Canada (1993), Figure 6.9.
44. J.L. Throne, "Plug-Assist Thermoforming—A New Design Protocol for Rectangular Parts", Polym.-Plast. Techn. Eng., 30 (1991), pp. 685–701.
45. J.L. Throne, "Some Design Guidelines for Plug Assists", SPE ANTEC Tech. Papers, 39 (1993), Figure 5, pp. 182–190.
46. K. Kouba, O. Bartos, and J. Vlachopoulos, "Computer Simulation of Thermoforming in Complex Shapes", Polym. Eng. Sci., 32 (1992), pp. 699–704.

47. R.I. Tanner, *Engineering Rheology*, Clarendon Press, Oxford (1985), pp. 202–207.
48. J.L. Throne, "Plug-Assist Thermoforming—A New Design Protocol for Rectangular Parts", *Polym.-Plast. Tech., Eng.*, 30 (1991), pp. 685-701.
49. W. Song, "Large Deformation Finite Element Analysis for Polymer Forming Processes", Ph.D. Dissertation, McMaster University, Hamilton, ON Canada (1993), Figure 6.16.
50. J.L. Throne, "Effect of Recycle on Properties and Profits: Algorithms", *Adv. Proc. Tech.*, 7 (1987), pp. 347–360.
51. J.W. Shea, E.D. Nelson and R.R. Cammons, "The Effect of Recycling on the Properties of Injection Molded Polycarbonate", *SPE ANTEC Tech. Papers*, 21 (1975), pp. 614–617.
52. S.B. Driscoll, "Thermoplastic Resin Re grind Study", *SPE ANTEC Tech. Papers*, 23 (1977), pp. 536–538.
53. P. Basile, C. Jolicoeur and H.P. Schreiber, "Polymer Reprocessing: Properties of Polyethylene-Polyvinyl Chloride Mixtures", *SPE ANTEC Tech. Papers*, 26 (1980), pp. 475–477.
54. M. Heneczowski, "Weather Resistance of PS After Multiple Processing", *Kunststoffe*, 83 (1993), pp. 473–475.
55. M.A. Sheryshev, I.V. Zhoyolev and K.A. Salazkin, "Calculation of Wall Thickness of Articles Produced by Negative Vacuum Forming", *Soviet Plastics*, 7 (1969), Figure 2, pp. 30–34.
56. W.A. Nietzert, "Die Thermoformung von Kunststoff-Folien", *Plastverarbeiter*, 27: 5 (1976), Figure 17, pp. 244–249.
57. H. Oelze, "Verformen von PVC-Hartfolien", *Kunststoffe*, 47 (1957), Figure 17, pp. 9–14.
58. G.L. Beall, *TFI (Thermoforming Software)*, IDES, Inc., Laramie WY, 1990.
59. Anon., "Structural Adhesives for the Transportation Industry Worldwide", ITW Adhesive Systems, Farmington MI, Bulletin TG1 (Jan 1993).
60. G.L. Beall, "Solving the Plastic Product Design and Development Puzzle", Seminar, University of Wisconsin-Milwaukee, Milwaukee (18-22 Apr 1994).
61. R.C. Progelhof and J.L. Throne, *Polymer Engineering Principles: Properties, Processes, and Tests for Design*, Hanser Publishers, Munich (1993), Section 6.1.
62. R.A. Malloy, *Plastic Part Design for Injection Molding*, Hanser Publishers, Munich (1994).
63. B.S. Benjamin, *Structural Design with Plastics*, 2nd Ed., Van Nostrand Reinhold Co., New York (1982).
64. Crawford and Lui [20] call areal draw ratio "stretching ratio" or "stretch ratio".
65. W.L. Gheen, "Computer Aids to Thermoforming: Stretch Factor and Average Formed Thickness", *SPE ANTEC Tech. Papers*, 30 (1984), pp. 748–749.
66. L.R. Schmidt and J.F. Carley, "Biaxial Stretching of Heat-Softened Plastic Sheets: Experiments and Results", *Polym. Eng. Sci.*, 15 (1975), pp. 51-62, especially footnote, p. 60.
67. A Kobayashi, *Machining of Plastics*, McGraw-Hill Book Co., New York (1967), p. 44, Table 2.1.
68. A.S. Lodge and H.G. Howell, "Nonlinear Elastic Properties of Molten Plastics", *Nonlinear Elasticity, Symp. Proc. Phys. Soc.*, 76B (1974).
69. H. Chang and R.A. Daane, "Coefficients of Friction for Solid Polymers in Various Forms", *SPE ANTEC Tech. Papers*, 20 (1974), pp. 335–.
70. G.A. Taylor, "Finite Element Simulation of Thermoforming - Experiments and Analyses", *SPE ANTEC Tech. Papers*, 35 (1989), pp. 435-437, Figure 5.
71. C.M. Campbell, "Designing for Thermoforming", Materials Presented, Distributed at SPE Thermoforming Symposium & Workshop, Arlington TX (20 Mar 1984).
72. J.L. Throne, "Some Design Guidelines for Plug Assists", *SPE ANTEC Tech. Papers*, 39 (1993), pp. 182–190.
73. H. Voigt, "Lehrgang für Thermoformung", Paul Kiefel GmbH, 8228 Freilassing, Industriestrae 19 (Undated), p. 3.4.1. .pa
74. M.O. Lai and D.L. Holt, "Thickness Variation in the Thermoforming of Poly(methyl Methacrylate) and High-Impact Polystyrene Sheets", *J. Appl. Polym. Sci.*, 19 (1975), pp. 1805–1814.
75. A.M. Voskresenskii, Ya.C. Neiman and Y.V. Nikitin, "Kinetics of Cooling a Deformable Sheet Thermoplastic Blank During Vacuum Forming", *Plast. Massy* (Feb 1975), pp. 27–28.
76. M.A. Vilyaf, C.L. Moskovskii, Y.V. Nikitin, and V.I. Bichgalter, "Calculation of the Nonuniformity of Thickness of Cylindrical Vacuum Pneumatic Formed Products", *Plast. Massy* (May 1976), pp. 34–36.

77. Y.V. Nikitin and T.G. Shlyakhova, "Evaluation of the Moldability of Sheets Made of Impact-Resistant Polystyrene", *Plast. Massy* (Jan 1979), p. 55.
78. Y.V. Nikitin, T.G. Shlyakhova and H.M. Efremova, "Thermomechanical Analysis of Sheets Made of High-Impact Polystyrene", *Plast. Massy* (May 1982), pp. 42–43.
79. Y.V. Nikitin and T.G. Shlyakhova, "Effect of Properties of Impact-Resistant Polystyrene Sheets and Their Draw Ratio on the Properties of Thermoformed Parts", *Plast. Massy* (May 1983), pp. 32–39.
80. Y.V. Nikitin, T.G. Shlyakhova and E.A. Belova, "Effect of Cooling on Residual Stresses in Thermoformed Parts", *Plast. Massy* (Aug 1983), pp. 27–28.
81. Y.V. Nikitin, T.G. Shlyakhova and P.B. Chudinov, "Effect of the Properties of Sheet and Their Uniaxial Drawing Ratios on the Properties of Thermoformed Parts", *Plast. Massy* (Sep 1984), pp. 24–26.
82. Y.V. Nikitin, T.G. Shlyakhova, T.A. Burdeinaya and V.V. Scherbak, "Effects of the Stress State on Impact-Resistant PS Sheets and the Rate of Their Drawing on the Properties of Thermoformed Products", *Plast. Massy* (Aug 1986), pp. 30–32.
83. M.A. Scheryschew and I.K. Gawrilow, "Vakuumbildung von Formteilen aus Kautschukmischungen", *Plast. Kautschuk*, 25:2 (Feb 1978), pp. 95–98.
84. A.R. Ragab and S.A. Khorshied, "A Simplified Model for Prediction of Processing Time in Pressure Thermoforming", *Plast. Rubber Proc. Appl.*, 6 (1986), pp. 21–27.
85. C.J.S. Petrie and K. Ito, "Prediction of Wall Thickness of Blow Moulded Containers", *Plast. Rubber: Proc.*, 5 (1980), pp. 68–72.
86. J.L. Throne and M. Kmetz, "Computer-Aided Design in Thermoforming", *Plast. Eng.*, 45:9 (Sep 1989), pp. 35–38.
87. H. Fukase, A. Iwaaki, and T. Kunio, "A Method of Calculating the Wall Thickness Distribution in Blow Molded Articles", *SPE ANTEC Tech. Papers*, 24 (1978), pp. 650–652.
88. W.A. Neitzert and H.J. Schmidt, "Die Thermoformung von Kunststoff-Folien", *Plastverarbeiter* 17 (1966), pp. 493–498.
89. W.A. Neitzert and H.J. Schmidt, "Die Thermoformung von Kunststoff-Folien", *Plastverarbeiter* 18 (1967), pp. 316–322.
90. W.A. Neitzert and H.J. Schmidt, "Die Thermoformung von Kunststoff-Folien", *Plastverarbeiter* 18 (1967), pp. 537–541.
91. A. Höger, *Warmformen von Kunststoffen*, Carl Hanser Verlag, Munich (1971), p. 61.
92. J.L. Throne, *Thermoforming*, Carl Hanser Verlag, Munich (1986).

Appendix 7.I Draw Ratios for Truncated Cone

As shown in Fig. 7.95, a sheet that is partially drawn into a cone of slant height s , depth h and diameter d and cone angle β is divided into the frustum of a cone and a spherical cap. $R = d/2$, the cone radius at the rim. If r is the indeterminate radius at the bottom of the frustum, the frustum area is:

$$A_f = \pi(R + r)[(R - r)^2 + h_f^2]^{1/2} \quad (7.I.1)$$

h_f is related to h by:

$$h_f = h(1 - r/R) \quad (7.I.2)$$

and $h = R \tan \beta$. The area of the spherical cap is:

$$A_{cup} = 2\pi a \delta \quad (7.I.3)$$

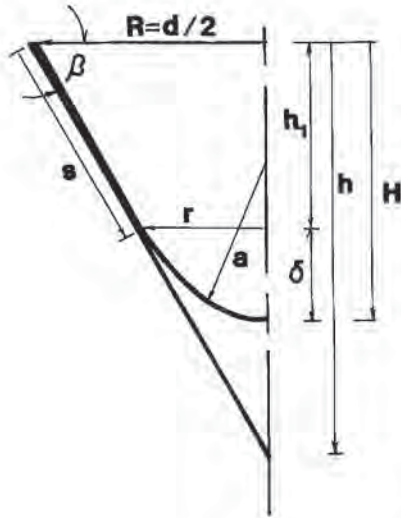


Figure 7.95 Geometric factors for draw-down into full right cone of angle

But $r^2 + \delta^2 = 2a\delta$. So:

$$A_{\text{cap}} = (\delta^2 + r^2) \quad (7.1.4)$$

Now $r = a \cos \beta$ and $\delta = a(1 - \sin \beta)$. Thus:

$$A_{\text{cap}} = 2\pi r^2 \cdot \left[\frac{1 - \sin \beta}{\cos^2 \beta} \right] \quad (7.1.5)$$

The total area, in terms of r , is:

$$A_{\text{total}} = \frac{\pi R^2}{\cos \beta} - \frac{\pi r^2}{\cos \beta} \cdot \left[1 - \frac{2(1 - \sin \beta)}{\cos \beta} \right] \quad (7.1.6)$$

Areal Draw Ratio

The areal draw ratio is:

$$Ra = \frac{A_{\text{total}}}{\pi R^2} = \left(\frac{1}{\cos \beta} \right) \cdot \left[1 - \left(\frac{r}{R} \right)^2 \left[1 - \frac{2(1 - \sin \beta)}{\cos \beta} \right] \right] \quad (7.1.7)$$

For full draw-down into $\beta = 60^\circ$ cone, $Ra \equiv 2$.

The relationship between r and H , the depth of the formed part, $H \leq h$, is:

$$r = \frac{(h - H) \cdot \cos \beta}{2 \sin \beta - 1} \quad (7.1.8)$$

The areal draw ratio, in terms of measured depth of draw, $H:D$, is:

$$Ra = \left(\frac{1}{\cos \beta} \right) \cdot \left\{ 1 - (\tan \beta - 2(H:D))^2 \cdot \left[\frac{\cos \beta}{2 \sin \beta - 1} \right]^2 \cdot \left[1 - \frac{2(1 - \sin \beta)}{\cos \beta} \right] \right\} \quad (7.1.9)$$

For a 60° cone:

$$Ra = 2\{1 - 0.2165[1.732 - 2(H:D)]^2\} \quad (7.I.10)$$

Linear Draw Ratio

The slant height s down the cone frustum is given as:

$$s^2 = (R - r)^2 + h_1^2 = (R - r)^2 + R^2 \tan^2 \beta (1 - r/R)^2 \quad (7.I.11)$$

$$s = (R - r)/\cos \beta \quad (7.I.12)$$

The distance across the cap is:

$$s' = a\alpha/2 \quad (7.I.13)$$

where α is the base half-angle in radian, $\alpha = \pi/2 - \beta'$. In terms of r :

$$s' = \frac{r\alpha}{2 \cos \beta} \quad (7.I.14)$$

The linear draw ratio, RL, is:

$$RL = \left(\frac{1}{2R}\right) \cdot \left[\frac{2(R - r)}{\cos \beta} + \frac{r\alpha}{2 \cos \beta} \right] \quad (7.I.15)$$

$$RL = \left(\frac{1}{\cos \beta}\right) \cdot \left\{ 1 - \left(\frac{r}{R}\right) \cdot \left[1 - \frac{(\pi/2 - \beta')}{4} \right] \right\} \quad (7.I.16)$$

For $\beta = 60^\circ$ cone:

$$RL = 2 \left[1 - 0.869 \left(\frac{r}{R}\right) \right] \quad (7.I.17)$$

RL = 2 for full draw, $r = R$.

In terms of measured depth of draw, H:D, RL is:

$$RL = \left(\frac{1}{\cos \beta}\right) \cdot \left\{ 1 - \left[1 - \frac{(\pi/2 - \beta')}{4} \right] \cdot (\tan \beta - 2(H:D)) \cdot \frac{\cos \beta}{2 \sin \beta - 1} \right\} \quad (7.I.18)$$

For 60° cone:

$$RL = 2\{1 - 0.594[1.732 - 2(H:D)]\} \quad (7.I.19)$$

Appendix 7.II Mechanical Property Loss in Regrind

Consider the simple regrind scheme in Fig. 7.96. The following assumptions are made:

- After each processing step, the mechanical property is X times that of the polymer property before processing.
- For each unit of polymer processed, Y units are regrind.
- A composite mechanical property is obtained from the properties of the virgin polymer and the regrind according to a linear law of mixtures.
- As a result, $0 \leq X \leq 1$ and $0 \leq Y \leq 1$.

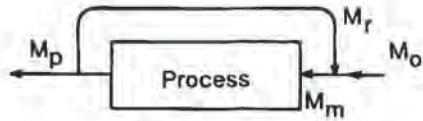


Figure 7.96 Schematic of steady-state recycle loop, including extrusion and thermoforming effects but ignoring regrind effects

The following definitions hold:

- M_o is the mechanical property of the virgin polymer.
- M_r is the mechanical property of the regrind.
- M_m is the mechanical property of the mixture.
- M_p is the mechanical property of the process polymer system.

For the first pass, there is no regrind, thus:

$$M_{p1} = X \cdot M_{m1} = X \cdot M_o \quad (7.II.1)$$

For the second pass:

$$M_{p2} = X \cdot M_{m2} \quad (7.II.2)$$

But:

$$M_{m2} = Y \cdot M_{r1} + (1 - Y) \cdot M_o \quad (7.II.3)$$

And:

$$M_{r1} = M_{p1} \quad (7.II.4)$$

Therefore:

$$M_{p2} = X[YX + (1 - Y)] \cdot M_o \quad (7.II.5)$$

For the third pass:

$$M_{p3} = X \cdot M_{m3} \quad (7.II.6)$$

But:

$$M_{m3} = Y \cdot M_{r2} + (1 - Y) \cdot M_o \quad (7.II.7)$$

And:

$$M_{r2} = M_{p2} \quad (7.II.8)$$

Therefore:

$$M_{p3} = [X^3Y^2 + X^2Y(1 - Y) + X(1 - Y)] \cdot M_o \quad (7.II.9)$$

For the N th pass:

$$M_{pN} = \left[(X - 1) \cdot \sum_{i=0}^{N-1} (XY)^i + 1 \right] \cdot M_o \quad (7.II.10)$$

But:

$$\sum_{i=0}^{n-1} ar^i = ar + ar^2 + ar^3 + \dots + ar^n = a \left(\frac{1 - r^n}{1 - r} \right) \quad (7.II.11)$$

Therefore, for the N th pass:

$$M_{p_N} = \left[1 - (1 - X) \cdot \frac{[1 - (XY)^{N-1}]}{1 - (XY)} \right] \cdot M_o \quad (7.II.12)$$

For an infinite number of cycles, $N \rightarrow \infty$:

$$\text{Since } (XY) < 1, \lim_{N \rightarrow \infty} (XY)^{N-1} \rightarrow 0 \quad (7.II.13)$$

And:

$$M_{p_\infty} = \left[1 - \frac{1 - X}{1 - XY} \right] \cdot M_o \quad (7.II.14)$$

For $X = 0.9$, $Y = 0.5$:

- After 1 pass, $M_{p_1}/M_o = 0.9$
- After 2 passes, $M_{p_2}/M_o = 0.855$
- After 3 passes, $M_{p_3}/M_o = 0.835$
- After 8 passes, $M_{p_8}/M_o = 0.8185$
- After 20 passes, $M_{p_{20}}/M_o = 0.8182$
- After ∞ passes, $M_p/M_o = 0.8182$

Thus, after three cycles, in this example, accuracy is within 2% of the limiting vales, which is usually well within experimental standard deviation.

8 Producing Sheet and Film

- 8.1 Introduction
- 8.2 Forming Thin Films
- 8.3 Forming Sheet
 - Single-Screw Extrusion
 - Filtering the Polymer
 - Flow Improvement Devices
 - Pressure and Temperature in Extruder
 - Sheet Die Concepts
 - Gage Thickness Monitoring and Control
 - Twin-Screw Extrusion
- 8.4 Roll Stacks
- 8.5 Sheet Trimming
- 8.6 Take-Off and Take-Up Rolls
- 8.7 Residence Time and Residence Time Distribution Through Extruder and Die
- 8.8 Drying
- 8.9 Producing Biaxially Oriented Sheet
- 8.10 Multilayer Sheet Formation
 - Coextrusion
 - Lamination
- 8.11 Sheet Quality and Quality Control
 - Sheet Dimension
 - Orientation
 - Sheet Squareness and Flatness
 - Moisture
 - Sheet Appearance
 - Annoyance Factors
 - Lamination Quality
- 8.12 References

8.1 Introduction

To produce their final products, injection molders, extruders and blow molders begin with polymer resin in the form of pellets or powders. Thermoformers produce their final products from sheet or film purchased from a *converter* or the processor who converts the polymer resin. The production of the sheet or film by extrusion or one of a handful of allied processes that impart shear and heat to the polymer resin adds economic and physical property penalties to the process. In addition, a substantial portion of the sheet or film is not formed into product and that portion must be returned to the converter for additional reprocessing. While the details of the conversion process are not of paramount importance to the thermoformer, the quality of the sheet or film is. The emphasis in this chapter, then, is on an understanding of those aspects of the conversion process that most affect the performance of the sheet as it passes through the thermoforming process:

- Thermal history,
- Shear history,
- Residence time in the conversion equipment,
- Techniques in drying,
- Aspects of the chill roll, such as:
 - Roll diameter,
 - Roll temperature, and
 - Roll texture,
- Bank buildup,
- Machine direction and cross-machine direction orientation,
- Methods of orienting sheet,
- Effect of processing on polymer morphology,
- Desirable molecular weight for extrusion v. that for thermoforming,
- Sheet gage measurement and control,
- Identification and sourcing of surface defects,
- And so on.

As a result, this chapter presents a general overview of the conversion process, with primary focus on single-screw extrusion through a sheeting die, the most common method of producing thermoformable sheet. The technical aspects of extrusion are given elsewhere¹.

¹ There are many sources of technical information on extrusion and extruder screw design. Some of these are:
 P.N. Richardson, *Introduction to Extrusion, Society of Plastics Engineers*, Greenwich CT (1974).
 J.L. White, *Twin Screw Extrusion: Technology and Principles*, Hanser Publishers, Munich (1991).
 R.T. Fenner, *Extruder Screw Design: Solutions to Polymer Melt Flow in Extrusion Equipment, Including Wire-Coating Dies*, Iliffe Books, London (1970).
 S. Levy and J.F. Carley, *Plastics Extrusion Technology Handbook*, 2nd Ed., Industrial Press, Inc., New York (1989).
 W. Michaeli, *Extrusion Dies: Design and Engineering Computations*, Hanser Publishers, Munich (1984).
 C. RauwendaaI, *Polymer Extrusion*, Hanser Publishers, Munich (1986).
 F. Hensen, Ed., *Plastics Extrusion Technology*, Hanser Publishers, Munich (1988).
 N.M. Bikales, Ed., *Extrusion and Other Plastics Operations*, Wiley-Interscience, New York (1971).